Stability and Hopf Bifurcation Analysis of Hopfield Neural Networks with a General Distribution of Delays

by

Raluca Jessop

A thesis
presented to the University of Waterloo
in fulfillment of the
thesis requirement for the degree of
Doctor of Philosophy
in
Applied Mathematics

Waterloo, Ontario, Canada, 2011

I hereby declare that I am the sole author of this thesis. This is a true copy of the thesis, including any required final revisions, as accepted by my examiners.

I understand that my thesis may be made electronically available to the public.

Abstract

We investigate the linear stability and perform the bifurcation analysis for Hopfield neural networks with a general distribution of delays, where the neurons are identical. We start by analyzing the scalar model and show what kind of information can be gained with only minimal information about the exact distribution of delays. We determine a mean delay and distribution independent stability region. We then illustrate a way of improving on this conservative result by approximating the true region of stability when the actual distribution is not known, but some moments or cumulants of the distribution are. We compare the approximate stability regions with the stability regions in the case of the uniform and gamma distributions. We show that, in general, the approximations improve as more moments or cumulants are used, and that the approximations using cumulants give better results than the ones using moments. Further, we extend these results to a network of n identical neurons, where we examine the stability of a symmetrical equilibrium point via the analysis of the characteristic equation both when the connection matrix is symmetric and when it is not. Finally, for the scalar model, we show under what conditions a Hopf bifurcation occurs and we use the centre manifold technique to determine the criticality of the bifurcation. When the kernel represents the gamma distribution with $p = 1$ and $p = 2$, we transform the delay differential equation into a system of ordinary differential equations and we compare the centre manifold computation to the one we obtain in the ordinary differential case.

Acknowledgements

I am extremely fortunate to have met my wonderful husband, Brent. Together we have an amazing boy Thomas and another baby on the way. I thank all three for the wonderful journey they brought me on and for inspiring me to be a better human being every day. I thank Brent for his love, care, protection, kindness and support. I thank Thomas for his love, tenderness, and giving us the opportunity to experience miracles.

This work would not have been possible without the guidance and support of my supervisor Sue Ann Campbell. I would like to thank her for her invaluable knowledge, kindness, patience and understanding.

I would like to offer my warm gratitude to my parents Silvia and Miki Amariei and my brother Horatiu Amariei for their love, immense help, encouragement and confidence.

I would like to express my sincere thanks to Helen Warren for her kindness and all of her help.

Dedication

I would like to dedicate this to my grandmother Elena Stefan.

Contents

List of Tables

List of Figures

Chapter 1

Introduction

In this thesis we investigate the linear stability and perform the bifurcation analysis for Hopfield neural networks with a general distribution of delays, where the neurons are identical. Hopfield neural networks are a particular type of an artificial neural network consisting of n coupled units, where each unit (or node) is connected to all other units. They have been popularized by the physicist John Hopfield [32, 33] who used them as content addressable memory systems. The Hopfield model has an energy function associated with it, where the units converge to states which are local minima in the energy function, i.e. if a state is a local minimum in the energy function it is a stable equilibrium for the network. The network converges to a state if it is given only part of the state, i.e. it is able to recover the entire memory from only a partial memory [28, 33, 62]. Therefore the Hopfield network provides a model for understanding human memory. Under certain conditions, the system can also be shown to exhibit a global attractor and in this case it can be used as a model for signal and image processing [22].

The Hopfield network can be improved by introducing time delays into the model to account for the time it takes for the signal to travel among the units or for the processing time at a given unit. Such an addition explained the instabilities of the equilibrium points of the system which occurred when implementing the model into real electrical circuits, which were not predicted by previous theory [47]. In this thesis we study Hopfield neural networks with distributed time delays which take into account the fact that the signal conduction and processing may not take exactly the same amount of time in every case. Thus the Hopfield model is further improved by accounting for the natural variability inherent in a physical or biological system.

In this thesis we focus on linear stability analysis for several reasons. The conditions found using linear stability analysis give the exact transition from stability to instability, i.e. we are able to determine the true boundary of stability where the equilibrium point loses stability. This means that we can derive delay dependent conditions for stability,

i.e. we are able to quantify how much delay the system can tolerate. Another reason is that more work has been done on Hopfield networks with distributed delay using Liapunov functions than linear stability analysis.

In the first section of this introductory chapter we present the underlying motivating factor of artificial neural networks, biological neurons. We review the structure of a neuron, the transmission of neural signals, and ways in which the communication between these biological neurons can be modeled. In the following section we define artificial neural networks and we give the physical interpretation behind the development of the Hopfield model. In the final section of this chapter we present Hopfield neural networks with time delays and give a literature review of Hopfield models with discrete and distributed delays.

1.1 Biology of Neurons

The human brain and the other parts of the nervous system are composed of nerve cells (neurons) and glial cells. The latter are supportive cells of the nervous system, and their main function consists in providing physical and functional support to neurons. Neurons are cells that are specialized for the reception, conduction, and transmission of electrochemical signals. There are 100 billion neurons and an estimated 100 trillion connections (synapses) among them [51]. They come in an incredible variety of shapes, sizes and properties, but share typical anatomical features as seen in Figure 1.1.

The cell body (soma) constitutes the metabolic centre and contains the cell's nucleus. Many extensions called dendrites branch out from the cell body and receive incoming synaptic signals from other neurons. A single long cylindrical fiber called the axon also projects from the cell body and branches out at its ends. The propagation of the electrochemical nerve signal is called an action potential. An action potential is a self-regenerating wave of electrochemical activity that allows a neuron to carry a signal over the length of the axon to the terminal branches, which form connections with adjacent neurons [51, 62].

Next we describe why there is an electric potential across the membrane of the axon, how it propagates, and ways it can be modeled. The axon membrane is made of two layers of lipid molecules separating the intracellular cytoplasm of the axon and the extracellular fluid, and of ionic channels (or pores), enzymes, pumps, and receptors. The pores act like gates in the lipid barrier through which substances can be transferred from one side to the other.

In the late 1940s a series of experiments carried out by Hodgkin and Huxley [30] and others proved the existence of an electrical potential across the axon membrane. In the resting state, the cytoplasm inside all neurons contains an ionic composition that makes the cell interior more negative in potential than the exterior of the cell. Such a voltage is

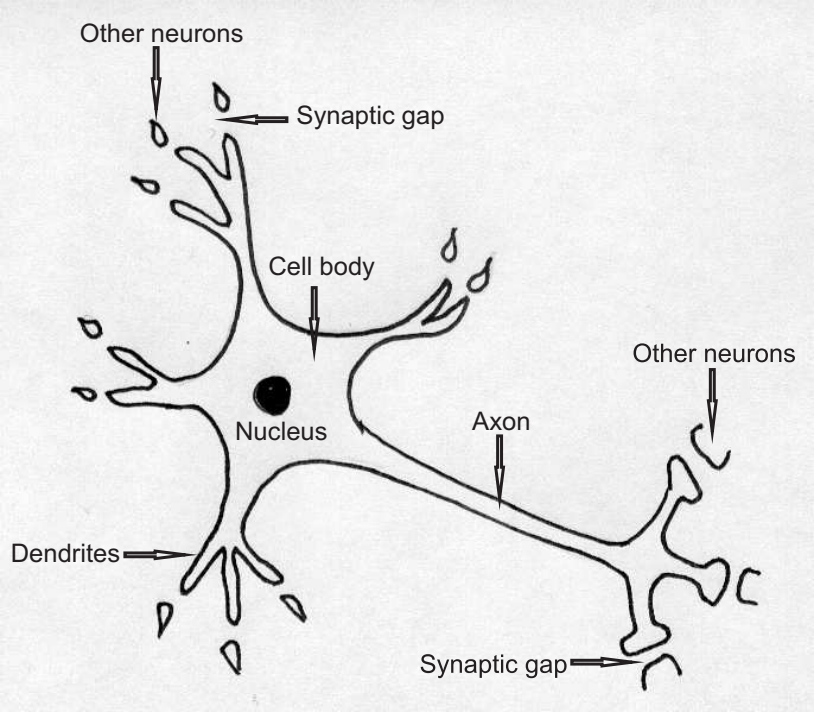

Figure 1.1: The anatomy of a neuron.

maintained at a metabolic expense by pumps located in the membrane. The two layers of lipids act like a thin insulator and thus the membrane of the axon has the property of capacitance, i.e. separation of charge. Therefore the membrane potential $V_m(t) = V_{\text{int}}(t) - V_{\text{ext}}(t)$ (difference between the intracellular and extracellular voltages) allows the capacitance C to build up a charge Q. By Faraday's Law we have

$$Q = CV_m.$$

When the voltage across the capacitor changes, a current will flow. The capacitive current I_C is obtained by differentiating the above equation with respect to time,

$$I_C(t) = C\frac{dV_m(t)}{dt}. \tag{1.1}$$

Charged ions (like Na^+, K^+, Ca^{2+}, or Cl^-) flow through the pores, which open or close in response to local conditions like the voltage across the excitable membrane (the resistance to the penetration of ions changes as the potential difference is changed). The starting point of the propagation of the action potential requires the integrated excitatory

inputs in the soma to be greater than a certain threshold voltage. If this threshold is surpassed, the sodium channels open letting Na^+ ions enter the cell. After a slight delay, the potassium channels open, letting K^+ ions exit the cell. The sodium pores then close in response to a decrease in the voltage difference, followed by the closing of the potassium channels. This process repeats and thus the spike-like signal is transported down the axon without attenuation or change in shape [16].

Hodgkin and Huxley [30] proposed an electric circuit model for an ionic channel which consists of a battery and a resistor in series. The battery models the force due to the difference in concentration of ions inside and outside the cell, and the resistor models the permeability of the channel to the specific ion. Then by Kirchhoff's Voltage Law, the voltage drop across the membrane is equal to the sum of the voltage drop across the battery (E_{ion}) and the voltage drop across the resistor:

$$V_m = E_{\text{ion}} + RI_{\text{ion}},$$

where I_{ion} is the current through the resistance R given by Ohm's Law. Thus

$$I_{\text{ion}}(t) = \frac{V_m(t) - E_{\text{ion}}(t)}{R}. \tag{1.2}$$

The cell is then modeled by a resistor-capacitor (RC) circuit (as seen in Figure 1.2) with a current source I_{ext}, representing the synaptic current or the applied current injected into the cell experimentally. Applying Kirchhoff's Current Law, we have $I_C + I_{\text{ion}} = I_{\text{ext}}$, and

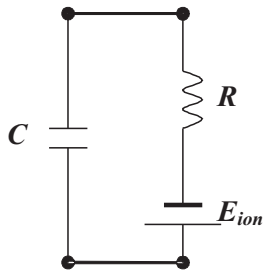

Figure 1.2: The RC circuit describing the current flow across the axon membrane.

from equation (1.1) we get

$$C\frac{dV_m(t)}{dt} = -I_{\text{ion}}(t) + I_{\text{ext}}(t). \tag{1.3}$$

Using (1.2) we then obtain

$$C\frac{dV_m(t)}{dt} = -\frac{1}{R}(V_m(t) - E_{\text{ion}}(t)) + I_{\text{ext}}(t).$$

We note that under certain conditions, membranes of some nerve cells do exhibit an RC circuit type of behaviour [38]. Equation (1.3) is similar to the first of the four differential equations in the Hodgkin and Huxley model, where I_{ion} is further expanded as a sum of the potassium, sodium and leak currents. The other three differential equations in the Hodgkin and Huxley model were chosen to fit the data and describe the dynamics of the closing and opening of the ionic channels.

To extend equation (1.3) to a network of n neurons, we let the external current coming into neuron k to be $I_{\text{ext}_k} = I_{\text{syn}_{k,j}} + I_{\text{app}_k}$, where $I_{\text{syn}_{k,j}}$ is the synaptic current coming from neuron j into neuron k, and I_{app_k} is the experimentally applied current to neuron k. Therefore we have

$$C_k \frac{dV_{m_k}}{dt} = -I_{\text{ion}_k} + \sum_{j=1, j\neq k}^{n} I_{\text{syn}_{k,j}} + I_{\text{app}_k}, \qquad k = 1, \ldots, n. \tag{1.4}$$

The synaptic current can be modeled by

$$I_{\text{syn}_{k,j}} = g_{\text{syn}_j}(V_{m_j})(V_{m_k} - V_{\text{syn}}), \tag{1.5}$$

where g_{syn_j} represents the synaptic conductance and depends on the presynaptic voltage V_{m_j}, and V_{syn} represents the synaptic reversal potential [39].

There are a multitude of mathematical models that characterize biological neurons and try to give insights into the processes that occur inside the neuron or to describe the communications among them. But we will finish reviewing the biological processes here. Next we will define artificial neural networks and develop a model that describes them.

1.2 Artificial Neural Networks

Artificial neural networks (or neural networks) are biologically motivated machines that are designed to perform tasks the same why the brain would perform a task or a function. Such networks are implemented using electronic components or simulated in software on a computer [62]. They are built to have nodes corresponding to neurons, and connections between them corresponding to the synapses. The architecture of these nodes and connections is inspired by the architecture of the biological nervous system.

Neural networks aspire to capture the following properties of the brain: i) capability of organizing neurons into ensembles that process specific kind of information, ii) connectivity, i.e. the ability of each neuron to connect to a large number of other neurons, iii) plasticity, i.e. the modification of the synaptic coupling, which represents the ability to learn and to adapt to the environment.

The benefits of a neural network are the ability to perform fast computations through its massively parallel distributed structure, the ability to learn and to generalize, i.e. the network produces reasonable outputs for inputs not encountered during training, and the ability to provide insight for the interpretation of neurobiological phenomena [28].

A model of a neuron (node) in the network is presented in Figure 1.3. An input signal

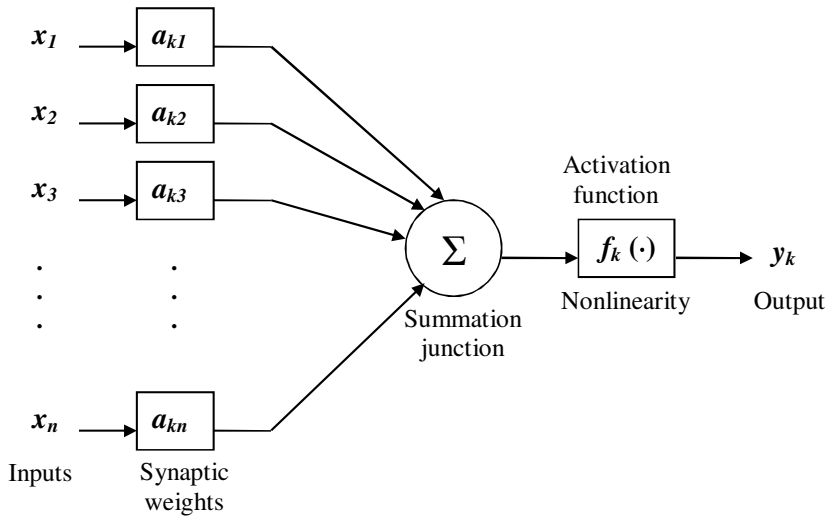

Figure 1.3: Spatial model of a neuron (node) in an artificial neural network proposed in [28].

$x_j, j = 1, \ldots, n$, at synapse j connected to neuron k is multiplied by the synaptic weight a_{kj}. This synaptic weight represents the strength of the connection and it is positive if it is excitatory or negative if it is inhibitory. The matrix $[a_{kj}]$ formed by the synaptic strengths is called the connection matrix. The summing junction is a linear combiner of all the input signals. The activation function $f_k, k = 1, \ldots, n$, is a nonlinear element that has the property of limiting the amplitude of the output signal y_k,

$$f_k\left(\sum_{j=1}^{n} a_{kj}x_j\right) = y_k, \qquad k = 1, \ldots, n. \tag{1.6}$$

The function $f_k, k = 1, \ldots, n$, models the property of nonlinearity of biological neurons. This function [14, 22, 33, 47] is usually taken to be monotonically increasing and differentiable on $(-\infty, \infty)$, satisfying

$$f_k(0) = 0, \qquad f_k'(v) \leq f_k'(0) \text{ for any } v \in \mathbb{R}, \qquad k = 1, \ldots, n, \tag{1.7}$$

and

$$\lim_{v \to \pm\infty} f_k(v) = \pm 1, \qquad k = 1, \ldots, n. \tag{1.8}$$

The most commonly used form is a sigmoidal-shaped function like the hyperbolic tangent function, $f_k(v) = \tanh(c_k v)$. By introducing and varying the parameter $c_k = f_k'(0)$, called the amplifier gain, we obtain different shapes of the tanh function as seen in Figure 1.4.

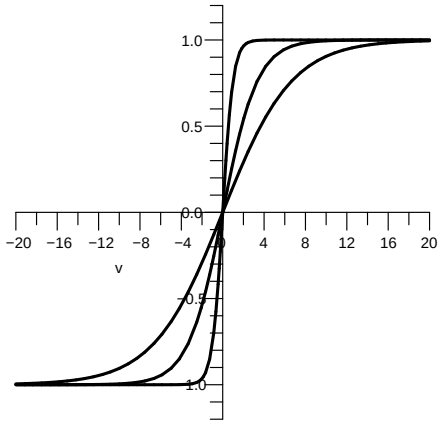

Figure 1.4: The activation function $f(v) = \tanh(cv)$, for different values of the amplifier gain, c. As c is increased, the activation function approaches the step function $f(v) = 1$ if $v > 0$, $f(v) = -1$ if $v < 0$.

An extension to the model in (1.6) is to take into account the temporal nature of the input data. One way of modeling the temporal behaviour is to represent each neuron as an RC circuit whose output then passes through a nonlinear element. In these terms, the inputs $x_j, j = 1, \ldots, n$, represent potentials and the synaptic weights a_{kj} denote conductances. The balancing equation for the electric currents flowing through neuron k is given by Kirchhoff's Current Law:

$$I_{C_k} + I_{R_k} = I_{\text{syn}_k} + I_{\text{app}_k}, \tag{1.9}$$

where I_{C_k} is the current through the capacitor, I_{R_k} is the current through the resistor, I_{app_k} is an exterior applied current, and I_{syn_k} is the synaptic current. The synaptic current is the sum of all the currents coming from all the other neurons,

$$I_{\text{syn}_k}(t) = \sum_{j=1}^{n} a_{kj} x_j(t), \tag{1.10}$$

as seen in Figure 1.5. Let the voltage across the RC circuit of neuron k be given by v_k. Then, by Faraday's Law, the capacitive current is

$$I_{C_k} = C_k \frac{dv_k(t)}{dt}, \tag{1.11}$$

where C_k is the capacitance of neuron k. The resistive current is given by Ohm's Law,

$$I_{R_k} = \frac{v_k(t)}{R_k}, \tag{1.12}$$

where R_k is the resistance of neuron k. After passing through the RC circuit, the current then passes through the nonlinear element, and thus the change in voltage across the nonlinear element is given by

$$f_k(v_k(t)) = x_k(t). \tag{1.13}$$

Substituting equations (1.10) – (1.13) into equation (1.9) we obtain the temporal extension of equation (1.6),

$$C_k \frac{dv_k(t)}{dt} = -\frac{v_k(t)}{R_k} + \sum_{j=1}^{n} a_{kj} f_j(v_j(t)) + I_{\mathrm{app}_k}(t), \qquad k = 1, \ldots, n. \tag{1.14}$$

This is depicted in Figure 1.5 and represents a system of n ordinary differential equations (ODEs). System (1.14) is referred to as the Hopfield neural network.

Let $v_k(t_0) = v_{0k}$, for $k = 1, \ldots, n$, be the initial conditions corresponding to (1.14). Since $f_k, k = 1, \ldots, n$, is chosen to be a bounded continuously differentiable function, all solutions are bounded and the right-hand side of (1.14) is C^1. Thus the initial value problem has a unique solution defined on $[t_0, \infty)$ [49].

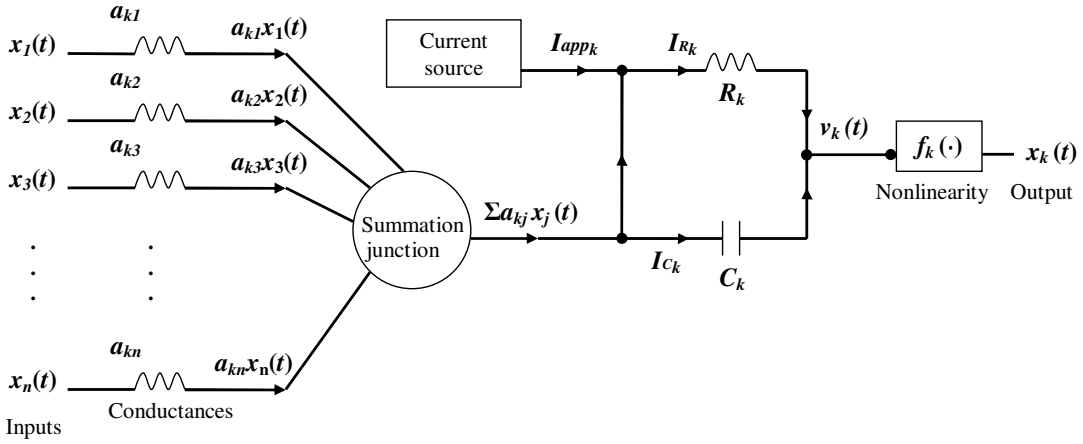

Figure 1.5: Representation of the Hopfield neural network (1.14) as an RC circuit. Arrows represent the direction of the electric current.

Using the energy function

$$E(v)(t) = -\frac{1}{2}\sum_{k=1}^{n}\sum_{j=1}^{n} a_{kj} v_k v_j + \sum_{k=1}^{n} \frac{1}{R_k} \int_0^{v_k} f_k^{-1}(v)\, dv - \sum_{k=1}^{n} I_{\mathrm{app}_k} v_k,$$

acting as the Liapunov function of the system, Hopfield [33] proved that when the connection matrix is symmetric ($a_{kj} = a_{jk}$), model (1.14) acts like a content-addressable memory, i.e. (1.14) is characterized by a set of stable equilibria. Initial points that are close to a particular equilibrium and far from others will converge to that nearby stable state. The location of a particular equilibrium point is thought of as the information of a particular memory. From a partial information about this memory (i.e. initial condition close enough to the fixed point) we are able to determine the complete memory.

In the next section we improve the model in (1.14) by introducing time delays to take into account the fact that it takes a certain amount of time for the signal to travel from neuron j to neuron k.

1.3 Hopfield Neural Network with Time Delays

In many biological and physical models, time delays play an important role. They arise for example due to age structure, gestation, maturation, or for neural networks, due to the delay in the propagation of the electrochemical signal among neurons. In the previous section we developed the Hopfield model (1.14), where we assumed that the communication between two neurons (or nodes) was instantaneous. In reality, it takes time for the signal to travel among neurons since axons have a certain length, and because of the processing of the signal at synaptic gaps [38]. Also, in electric circuits, the communication between two nodes is delayed due to the time it takes for the signal to travel through different elements.

To take these facts into account, System (1.14) can be transformed into a system of delay differential equations (DDEs),

$$C_k \frac{dv_k(t)}{dt} = -\frac{v_k(t)}{R_k} + \sum_{j=1}^{n} w_{kj} f_j(v_j(t - \tau_{kj})) + I_k, \qquad k = 1, \ldots, n, \tag{1.15}$$

where τ_{kj} represents the time it takes for the electric signal to travel from neuron j to neuron k. The above model is called a DDE with discrete delay, where the derivative of the state at time t depends on the value of the state at fixed prior times. We note that the formal definition of a DDE will be presented in Chapter 2, where we give an overview of delay differential equations.

In most applications, including neural networks, the time delays are not fixed. The delay in the signal transmission among neurons varies due to the multitude of axon sizes and shapes and due to intrinsic biological processes. Hence (1.14) can be represented as a DDE with distributed delay,

$$C_k \frac{dv_k(t)}{dt} = -\frac{v_k(t)}{R_k} + \sum_{j=1}^{n} w_{kj} f_j \left(\int_0^{\infty} v_j(t - u) g_{kj}(u)\, du \right) + I_k, \qquad k = 1, \ldots, n, \tag{1.16}$$

where the signal delay u from neuron j to neuron k occurs with a certain probability given by the kernel $g_{kj}(u)$. The distribution $g_{kj}(u)$ is a probability density function (p.d.f.) with mean delay $\tau_{kj} = \int_0^\infty u g_{kj}(u)\, du$. In the above model, the derivative of v_k at time t depends on the value of $v_j, j = 1, \ldots, n$, over the entire past interval $(-\infty, t]$.

We note that for given initial conditions, since the left-hand side of (1.15) and (1.16) is Lipschitz (as $f_k, k = 1, \ldots, n$, is chosen to be continuously differentiable), Theorem 2.3 from [26] guarantees the local existence and uniqueness of solutions of the above two systems.

In most neural models, time delays are assumed to be fixed (as in model (1.15)). In the next section we review results from the literature, where Hopfield networks with discrete delay are studied.

1.3.1 Hopfield Neural Networks with Discrete Delay

The stability and bifurcation of Hopfield models of the form (1.15) have been studied extensively and in this section we present a few previously obtained results. The addition of time delays to the Hopfield network is first introduced by Marcus and Westervelt [47] to explain instabilities of equilibria that occurred when implementing real electrical circuits, which were not predicted by previous theory. Their goal is to give sufficient conditions that guarantee the local stability of the trivial equilibrium, without requiring the connection matrix to be symmetric, assuming that the neurons are identical and that no exterior current is applied. With these assumptions, after scaling their parameters, the system becomes

$$x_k'(t) = -x_k(t) + \sum_{j=1}^{n} w_{kj} f(x_j(t-\tau)), \qquad k = 1, \ldots, n. \tag{1.17}$$

After linearization, the system decouples into n DDEs,

$$x_k'(t) = -x_k(t) + \beta z_k x_k(t-\tau), \qquad k = 1, \ldots, n,$$

where $\beta = f'(0)$ is the amplifier gain and z_k are the eigenvalues of the connection matrix $[w_{kj}]$. The characteristic equation also decouples into n equations, $(\lambda_k + 1)e^{\lambda_k \tau} = \beta z_k$, $k = 1, \ldots, n$. Therefore they obtain the delay independent region of stability for the origin in the complex plane as seen in Figure 1.6. We note that for $\tau = 0$ the stability region is the half plane to the left of the line $1/\beta$, and as $\tau \to \infty$ the stability region is given by the circle of radius $1/\beta$. They also analyze the delay dependent region of stability. They show that if $\tau < \tau_c$ (where $\tau_c = -\pi/\beta z_{\min}/2$ is the critical value for the delay) only fixed point attractors are observed, but if $\tau > \tau_c$ the system also exhibits oscillatory attractors. They conclude numerically that the basin of attraction for sustained oscillations decreases as the delay decreases.

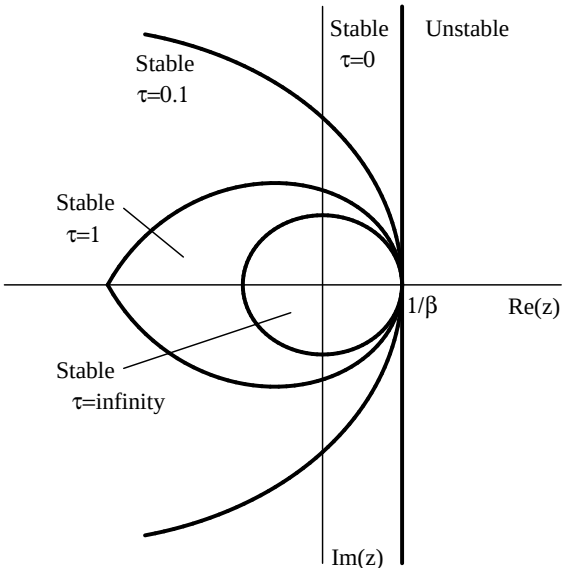

Figure 1.6: Linear delay independent region of stability of the trivial equilibrium of system (1.17) for different values of τ.

Gopalsamy and He [22] investigate the delay independent region of stability for the Hopfield network,

$$x_k'(t) = -b_k x_k(t) + \sum_{j=1}^{n} w_{kj} f_j(c_j x_j(t - \tau_{kj})) + I_k, \qquad k = 1, \ldots, n. \tag{1.18}$$

They provide sufficient conditions for the existence of a global attractor, without assuming that the connection matrix is symmetric, or that the neurons are identical. Using the Liapunov functional

$$V(x)(t) = \sum_{k=1}^{n} \left(|x_k(t)| + \sum_{j=1}^{n} |w_{kj}||c_j| \int_{t-\tau_{kj}}^{t} |x_j(u)|\, du \right)$$

they show that the unique equilibrium point x_k^* of (1.18) is globally asymptotically stable for each constant applied current I_k if

$$\max_{1 \le k \le n} \left[\frac{|c_k|}{b_k} \sum_{j=1}^{n} |w_{kj}| \right] < 1. \tag{1.19}$$

Under this condition, the Hopfield model (1.18) can be used in applications to signal and image processing, where the existence of a global attractor associated with a specific input is paramount.

Bélair et al. [5] analyze the Hopfield model (1.17) by depicting the connection matrix $[w_{kj}]$ as a signed directed graph. They define a network to be frustrated if the signed directed graph has a negative cycle. One of their main results requires a network not to be frustrated, in order for the delay induced instability of the trivial solution of (1.17) to be impossible. They analyze a frustrated network of three neurons with no self-connection ($w_{ii} = 0$) and show that the stability of the origin is lost giving rise to a Hopf bifurcation. Using the centre manifold technique, they show the Hopf bifurcation is supercritical.

Gopalsamy and Leung [23] analyze a system of two identical neurons with no self-feedback and show that if $w^2\beta_1\beta_2 > 1$, then the trivial solution of (1.17) (with $n = 2$) becomes unstable when $\tau > \tau_c$, where τ_c depends on the connection strength w and the amplifier gains β_1 and β_2. They also show that $\mathrm{Re}\,(d\lambda/d\tau)|_{\tau=\tau_c} > 0$, and thus prove that the transversality condition for the Hopf bifurcation to occur is satisfied. They calculate the amplitude of the periodic solution and show that the Hopf bifurcation is supercritical using perturbation theory.

Campbell et al. [11] analyze a ring of n identical neurons,

$$x_k'(t) = -x_k(t) + w_s f_s(x_k(t-\tau_s) + w[f(x_{k-1}(t-\tau)) + f(x_{k+1}(t-\tau))], \qquad k \mod n.$$

Here, the architecture of the network is simplified, since a neuron communicates with only its two nearest neighbors, but the self-connection delay (τ_s) differs from the delay between two distinct neurons (τ). They give delay independent and dependent conditions that guarantee the asymptotic stability of the trivial solution of the linearized system. Since the characteristic equation has two pairs of pure imaginary roots, they present conditions under which the above system undergoes an equivariant Hopf bifurcation. They show, using the centre manifold reduction, that all branches of the periodic solutions are either supercritical or all are subcritical.

In the next section we are going to look at previously obtained results for models where the delay is distributed.

1.3.2 Biological and Physical Models with Distributed Delay

Models with distributed delay take into account the fact that biological and physical events such as gestation, maturation, regeneration, recovery period from a disease, or signal conduction may not take exactly the same time in every case. Such models have been developed mostly in applications to population biology [15, 21, 42] and epidemiology [3, 8], and only recently to neural networks. The majority of these models use specific kernels, usually the uniform distribution or the gamma distribution with $p = 1$ (called the weak kernel) and $p = 2$ (called the strong kernel). The uniform distribution with mean delay τ is given by

$$g(u) = \begin{cases} \frac{1}{\rho\tau}, & \text{if } u \in \left[\tau\left(1-\frac{\rho}{2}\right), \tau\left(1+\frac{\rho}{2}\right)\right] \\ 0, & \text{otherwise,} \end{cases} \tag{1.20}$$

where parameter $\rho \in (0, 2]$ controls the width and height of the distribution. The gamma distribution with mean delay $\tau = p/a$ is given by

$$g_{a,p}(u) = \frac{u^{p-1}a^p e^{-au}}{\Gamma(p)}, \tag{1.21}$$

where parameters $a, p > 0$ control the shape of the distribution. These distributions will be discussed in more detail in Subsections 2.4.2 and 2.4.3. When p in (1.21) represents an integer then $\Gamma(p) = (p-1)!$ and a scalar equation with one gamma distributed delay can be shown to be equivalent to a system of $p+1$ ordinary differential equations. We present details about this reduction, often called the linear chain trick, in Section 2.5. We note that distributed delay models include the discrete delay models if we take the kernel to be the Dirac distribution. For example, if $g_{kj} = \delta(t-\tau_{kj})$, then system (1.16) with distributed delay becomes system (1.15) with discrete delay.

Thiel et al. [58] introduce distributed delay in three previously analyzed biological models and show that complex dynamics are abolished. They first extend a previously developed model that describes the dynamics of pyramidal cells in the hippocampus, where the delay is uniform distributed. The widening of the distribution (i.e. increasing ρ in (1.20)) causes the membrane voltage to oscillate with a regular period, abolishing irregular fluctuations. Further they analyze the Mackey-Glass model, which models the concentration of white blood cells, where again the delay is uniform distributed. They demonstrate that the previously observed aperiodic behaviour changes into regular fluctuations when the width of the distribution is sufficiently increased. Lastly they analyze the logistic equation with a gamma distributed delay and show that the wider the distribution, the lower the amplitude of the oscillations. As the variance of the distribution increases, the limit cycle is abolished, and the solutions approach a stable equilibrium. In all three examples, Thiel et al. conclude that the introduction of the distributed delay simplifies the behaviour of the system.

In [60, 61], Wolkowicz et al. study the global asymptotic behaviour of a chemostat model with a gamma distributed delay which describes the lag in the process of nutrient conversion. They show that the corresponding discrete delay model can be obtained as the limiting case of the distributed delay model. In other words, if in the limit p in (1.21) approaches infinity while the mean delay p/a is held fixed (which corresponds to the variance p/a^2 approaching zero), the results of the distributed delay model yield those for the corresponding system with discrete delay. They also note that changing the mean delay has a much larger effect on stability than changing the variance.

A general assumed principle is that a system with a distribution of delays is more stable than the same system with a discrete delay (this principle has not yet been proven). MacDonald [46] demonstrates that increasing the discrete delay τ in the linear scalar

model, $x'(t) = -ax(t) - bx(t-\tau)$, destabilizes the equilibrium point and it can never be restabilized. However, for the modified equation

$$x'(t) = -ax(t) - b\int_0^\infty g(u)x(t-u)\,du \tag{1.22}$$

with a gamma distributed delay, increasing the mean delay, $\tau = \int_0^\infty ug(u)\,du$, can also destabilize the equilibrium point, but it will always be restabilized for large enough τ, for any value of p. The above DDE represents the linearization of the scalar Hopfield model (1.16), which we consider in Chapter 3. Bernard et al. [7] have studied the stability of the trivial solution of (1.22) and concluded that the uniform and gamma distributed delays increase the stability region of the equilibrium point when compared to a discrete delay. More results supporting the principle that a model with distributed delay is more stable than one with discrete delay are cited below (see [4, 24, 36, 64]). In Chapter 4 we show that if in the limit the mean delay of a general distribution approaches infinity, the region of stability of the symmetric equilibrium point of the Hopfield model (1.16), where the neurons are identical, is always greater than the stability region of the corresponding model with discrete delay.

In practice, one is not able to determine the exact distribution of delays when trying to model real physical systems. Hence developing a theory for general kernels is very important. In this thesis we obtain linear stability and Hopf bifurcation results for Hopfield neural networks with a general distribution of delays. Next we give a review of the literature where results for distributed DEs with general kernels have been obtained. In the population biology literature there are several such papers. Faria and Oliveira [20] address the local and global stability of n-dimensional Lotka-Volterra system

$$x_k'(t) = r_k x_k(t)\left[1 - b_k x_k(t) - L_k(x_t)\right], \qquad k = 1, \ldots, n,$$

where $b_k \in \mathbb{R}$, $r_k > 0$ and $L_k : \mathcal{C} \to \mathbb{R}$ are linear bounded operators,

$$L_k(x_t) = \sum_{j=1}^{n} l_{kj} \int_{-\tau}^{0} (x_j)_t(\theta)\,d\eta_{kj}(\theta),$$

for some $l_{kj} \in \mathbb{R}$ and η_{kj} are normalized functions of bounded variations. Using matrix theory, they give conditions on the interaction coefficients of the system that guarantee asymptotic stability, independent of the distribution functions η_{kj}.

Ruan [53] considers Hutchinson's equation with distributed delay,

$$\dot{x}(t) = rx(t)\left[1 - \frac{1}{K}\int_0^\infty x(t-u)g(u)\,du\right],$$

which models a population of insects, where the delay represents the time between egg laying and hatching. He shows that if the mean delay is less than $1/r$ the equilibrium point $x^* = K$ is asymptotically stable, for any distribution of delays $g(u)$.

Using averaging theory, Atay [4] studies the stability of functional differential equations near a Hopf bifurcation under delayed feedback of the form

$$\dot{x}(t) = Lx_t + \epsilon g(x_t;\epsilon) + \epsilon\kappa f(x_t;\epsilon), \qquad \text{where } x_t \in C([-\tau,0],\mathbb{R}^n.)$$

He shows that when the delays act towards destabilizing the system, the discrete delay is locally the most destabilizing among distributions having the same mean delay. He also obtains this result globally for distributions that are symmetrically distributed about their mean.

Jirsa and Ding [36] analyze an $n \times n$ linear system with a common delay,

$$\dot{x}_i = -x_i + \sum_{j=1}^{N} a_{ij} \int_0^\infty f(\tau,d)x_j(t-\tau)d\tau,$$

where d represents the width of the distribution f. They show that if $f(\tau,d)$ is a p.d.f. which is positive definite then the trivial solution of the system becomes less unstable as d increases, i.e. the discrete delay (for which $d = 0$) is the most destabilizing.

In [7], Bernard et al. obtain stability results of the trivial equilibrium of the scalar equation (1.22) where the kernel is arbitrary. They find the sufficient condition on the mean delay,

$$E < \frac{\pi(1+a/b)}{c\sqrt{b^2-a^2}}, \qquad b > |a|, \tag{1.23}$$

where $E = \int_{\tau_{\min}}^\infty ug(u)\,du$ and $c = \sup\{c|\cos(x) = 1 - cx/\pi, x > 0\} \approx 2.2764$, such that the trivial solution of (1.22) is asymptotically stable. They also obtain stronger conditions on E when the distribution is symmetric about the mean, and when it is positively skewed. For the symmetric distribution case, they show that the region of stability of the distributed delay model is always greater than the region of stability of the corresponding delay model since their sufficient condition is

$$E < \frac{\arccos(-a/b)}{\sqrt{b^2-a^2}}, \qquad b > |a|, \tag{1.24}$$

which represents the true boundary of stability for the corresponding model with one fixed delay E. We note that in their paper they consider general distributions which have nonzero minimum delay, i.e. are defined on $[\tau^{\min}, 0)$, where $\tau^{\min} > 0$ represents the minimum delay.

For the uniform distribution, this can be achieved naturally by incorporating the constraint $\rho < 2$. The gamma distribution can be reformulated to achieve this as follows,

$$g(u) = \begin{cases} 0, & \text{for } 0 \leq u < \tau^{\min} \\ \frac{a^p}{\Gamma(p)}(u-\tau^{\min})^{p-1}e^{-a(u-\tau^{\min})}, & \text{for } \tau^{\min} \leq u. \end{cases}$$

Distributions with nonzero minimum delay are called delay distributions with a gap, while if $\tau^{\min} = 0$, they are called delay distributions without a gap [46]. We note that in this thesis we only consider delay distributions without a gap. In applications, using delay distributions with a gap describes the fact that the probability of having zero delay is extremely small. For example, a situation where the minimum delay must be strictly greater than zero occurs when modeling agricultural commodity markets. In this type of models the delay is related to the biological constraints (gestation plus growth period) where $\tau^{\min} > 0$ represents the finite minimum time that must elapse before a decision to alter production is translated into an actual change in supply [6].

In [1], Adimy et al. study a model describing blood cell production in the bone marrow. They work with general kernels defined on $[\underline{\tau}, \overline{\tau}]$, where $\underline{\tau}$ and $\overline{\tau}$ represent the minimum and maximum delays, respectively. By constructing a Liapunov functional, they show that the trivial equilibrium is globally asymptotically stable if it is the only equilibrium. They also determine conditions for a Hopf bifurcation at the nontrivial equilibrium point to occur for any general distribution of delays. They verify the criticality of the bifurcation numerically.

Yuan and Bélair [64] perform the stability and Hopf bifurcation analysis for the generic scalar DDE

$$\dot{x}(t) = F\left(x(t), \int_{\tau^{\min}}^{\infty} x(t-\tau)k(\tau)\,d\tau\right),$$

where the distribution $k(\tau)$ is defined on $[\tau^{\min}, 0)$. They obtain a conservative region of stability for the above model with a general distribution of delays. When the kernel represents the uniform and gamma distributions, they determine sufficient conditions for the linear stability of the equilibrium point of the above DDE. For the gamma distribution, their sufficient condition gives a larger stability region than the one of the corresponding model with a discrete delay for any $\tau^{\min} \geq 0$. Whereas, for the uniform distribution, their sufficient condition gives a larger stability region than the one of the corresponding model with a discrete delay when $\tau^{\min} = 0$ or when $\tau^{\min} > 0$ with the restriction that the ratio $\tau^{\min}/\rho$ is small enough (where ρ represents the width of the distribution). For a general delay distribution with a gap, they determine the direction of the Hopf bifurcation and the stability of the periodic solution using the Liapunov-Schmidt method, which was proposed by Stech in [56]. They apply their results to a model for the control of granulopoiesis and to a model of white blood cell production. We note that in Chapter 5 of this thesis we propose a method of determining the direction of the Hopf bifurcation and the stability

of the periodic solution for the scalar Hopfield model with a general distribution of delays (without a gap) using the centre manifold technique.

We now go back to neural models and present a few results for the Hopfield networks with distributed delay. We first note that the work of Faria and Oliveira [20] discussed above can be viewed as the linearization of a Hopfield-type neural network about an equilibrium point. Liao et al. [43] consider a two-neuron neural network with distributed delay,

$$x_1'(t) = -x_1(t) + a_1 f\left[x_2(t) - w_2 \int_0^\infty g(u) x_2(t-u)\, du\right],$$
$$x_2'(t) = -x_2(t) + a_2 f\left[x_1(t) - w_1 \int_0^\infty g(u) x_1(t-u)\, du\right],$$

where the kernel g represents a gamma distribution with $p = 1$. Parameter a_i corresponds to the range of the potential variable x_i, and w_i measures the inhibitory influence of the past history, $i = 1, 2$. They study the linear stability of the above system using the Routh-Hurwitz criterion. They prove the existence of a Hopf bifurcation at a critical value of the mean delay, which acts as a bifurcation parameter. They find the periodic solution and determine its stability using perturbation theory.

In [54], Ruan and Filfil study a two-neuron neural network with discrete and distributed delay,

$$\frac{1}{a_{10}} x_1'(t) + x_1(t) = F\left[f_1 + c_{12} x_2(t-\sigma_{12}) + b_{11} \int_{-\infty}^t x_1(\tau) K_{11}(t-\tau)\, d\tau\right],$$
$$\frac{1}{a_{20}} x_2'(t) + x_2(t) = F\left[f_2 + c_{21} x_1(t-\sigma_{21}) + b_{22} \int_{-\infty}^t x_2(\tau) K_{22}(t-\tau)\, d\tau\right],$$

where the kernel again represents a gamma distribution with $p = 1$. The discrete delays describe the neural interaction history, while the distributed delays describe the neural feedback. Using the linear chain trick they transform the above system into a system of four DEs which only exhibit discrete delays. They give conditions under which the equilibrium point is locally asymptotically stable and also under which a Hopf bifurcation occurs. They verify their results numerically and show that the behaviour of the system is governed by the discrete delays.

The previously mentioned paper by Gopalsamy and He [22] investigates the global delay independent region of stability for the Hopfield network with distributed delay,

$$x_k'(t) = -b_k x_k(t) + \sum_{j=1}^n w_{kj} f_j\left(c_j \int_0^\infty g_{kj}(u) x_j(t-u)\, du\right) + I_k, \qquad k = 1, \ldots, n, \quad (1.25)$$

where $b_k > 0$ and the kernel g_{kj} is a general gamma distribution of the form (1.21). They use a Liapunov functional similar to the one in the discrete case,

$$V(x)(t) = \sum_{k=1}^{n} \left(|x_k(t) - x_k^*| + \sum_{j=1}^{n} |w_{kj}||c_j| \int_0^\infty g_{kj}(u) \left(\int_{t-u}^{t} |x_j(s) - x_k^*| \, ds \right) du \right),$$

where x_k^* is the unique equilibrium point of (1.25). They prove that if (1.19) is satisfied, then the fixed point is globally asymptotically stable for each constant applied current I_k.

In his Master's Thesis, Grégoire-Lacoste [24] investigates the global stability of the unique equilibrium point of a Hopfield neural network with distributed delay. He also performs local stability analysis to determine the boundary of stability of the equilibrium point for the uniform, exponential, triangular, and gamma distributions. The results are compared to the results of the corresponding system with a fixed delay. It is observed that if the equilibrium point is stable for a system with discrete delay τ, it remains stable when the delay is replaced by any of the studied distributions with mean delay τ. Also for all the considered distributions, the region of stability of the equilibrium point of the model with distributed delay is greater than the stability region of the equilibrium point of the corresponding discrete delay model.

Chen [12] considers the neural network with a general distribution of delays,

$$x_i'(t) = -f_i(x_i(t)) + \sum_{j=1}^{n} a_{ij} \int_{-\infty}^{t} K_{ij}(t-s) g_j(x_j(s)) \, ds + I_i, \qquad k = 1, \ldots, n, \tag{1.26}$$

where $f_i, i = 1, \ldots, n$, is differentiable, $g_i, i = 1, \ldots, n$, is globally Lipschitz with Lipschitz constant k_i, and the kernel K_{ij} is arbitrary. The Hopfield network can be seen as a special case of the above equation. Using matrix theory and constructing the Liapunov functional,

$$V(y)(t) = \sum_{i=1}^{n} \xi_i \left\{ |y_i(t)| + \sum_{j=1}^{n} k_j |a_{ij}| \int_0^\infty K_{ij}(s) \left(\int_{t-s}^{t} |y_j(\tau)| \, d\tau \right) ds \right\},$$

he proves the existence, uniqueness and global asymptotic stability of the equilibrium point of (1.26).

In Chapters 3 and 4 of this thesis, we study the stability of hyperbolic equilibrium points, where the stability of the trivial equilibrium of the corresponding linearized system determines the stability of the equilibrium point of the nonlinear system. An advantage of using linearization is that the conditions found using the linear stability analysis give the exact transition from stability to instability, i.e. we are able to determine the true boundary of stability where the equilibrium point loses stability. Since part of this method consists of analyzing the roots of the characteristic equation, a disadvantage of using this

approach is that sometimes it is necessary to place certain assumptions on the model in order to simplify the expression for the characteristic equation. Another method of showing an equilibrium point is stable is constructing a suitable Liapunov function and using it to determine sufficient conditions for stability. In this case the true boundary of stability is not determined explicitly, only a conservative region of stability is found which guarantees the stability of the equilibrium point under specific conditions on the parameters in the system. An advantage of using Liapunov functions is that they can be applied to more general systems and thus the obtained conditions give stronger results. Disadvantages of using this method include the fact that Liapunov functions are difficult to obtain in practice, give only conservative stability results, and are usually used to prove the global stability of a unique equilibrium point. The difficulties of the Liapunov function method are increased when a system has multiple equilibrium points, where it might be necessary to find a different Liapunov function for each equilibrium point. In Chapter 6 we compare our results obtained using the linearization method with the results obtained in [22] using the Liapunov approach.

In the next chapter we give an overview of DDEs with emphasis on systems with distributed delay. We present the definition, existence and uniqueness theorems and show how to arrive at the characteristic equation associated with the system. We also discuss in more detail the Dirac, uniform and gamma distributions.

Chapter 2

Delay Differential Equations - An Overview

In this chapter we present an overview of delay differential equations. We first give the formal definition, present the initial value problem and state existence and uniqueness theorems. For the rest of the chapter, we then focus on delay differential equations with one distributed delay, showing how to arrive at the characteristic equation. We finish the chapter by discussing the uniform and gamma distributions, and show how a scalar delay differential equation with a gamma distributed delay can be transformed into a system of ordinary differential equations.

2.1 Definition, Initial Value Problem, Existence and Uniqueness Theorems

A delay differential equation is a differential equation where the highest order derivative only occurs with one value of the argument, and this argument is not less than the argument of the unknown function and its lower order derivatives appearing in the equation. For example,

$$x'(t) = x^2(t-1) + x(t)$$

is a delay differential equation, while

$$x'(t-5) = x^3(t) - x^4(t)$$

is not.

More formally, for $r > 0$, let $\mathcal{C} = C([-r, 0], \mathbb{R}^n)$ be the Banach space of continuous functions mapping the interval $[-r, 0]$ into $\mathbb{R}^n$. We designate the norm on this space to be

$$||\boldsymbol{\phi}||_r = \sup_{-r \leq \theta \leq 0} ||\boldsymbol{\phi}(\theta)||,$$

where $||\cdot||$ is the Euclidean norm on $\mathbb{R}^n$. If $\boldsymbol{x}$ is a function defined at least on $[t-r, t]$ with values in $\mathbb{R}^n$, we define a new function $\boldsymbol{x}_t \in \mathcal{C}$ by

$$\boldsymbol{x}_t(\theta) = \boldsymbol{x}(t+\theta), \qquad \text{for } -r \leq \theta \leq 0.$$

For $D \subseteq \mathbb{R}^n$, let $\mathcal{C}_D = C([-r, 0], D)$ be the set of continuous functions mapping $[-r, 0]$ into D.

Definition 1 *If $J \subseteq \mathbb{R}$, $\boldsymbol{f} : J \times \mathcal{C}_D \to \mathbb{R}^n$ is a given function and "$\cdot$" represents the right-hand derivative, then we say that the relation*

$$\dot{\boldsymbol{x}}(t) = \boldsymbol{f}(t, \boldsymbol{x}_t) \tag{2.1}$$

is a delay differential equation on $J \times \mathcal{C}_D$.

We note that the right-hand derivative of a function $x(t) : \mathbb{R} \to \mathbb{R}$ is given by

$$\limsup_{h \to 0^+} \frac{x(t+h) - x(t)}{h}.$$

For a given $t_0 \in J$ and $\phi_0 \in \mathcal{C}_D$, the initial value problem (IVP) associated with the DDE in (2.1) is

$$\begin{cases} \dot{\boldsymbol{x}}(t) = \boldsymbol{f}(t, \boldsymbol{x}_t), & t > t_0 \\ \boldsymbol{x}(t) = \boldsymbol{\phi}_0(t - t_0), & t_0 - r \leq t \leq t_0, \end{cases} \tag{2.2}$$

i.e. the initial condition at t_0 must specify $\boldsymbol{x}$ for the whole past interval, $t \in [t_0 - r, t_0]$. The function $\boldsymbol{\phi}_0$ is called the initial function, t_0 the initial instant, and $[t_0 - r, t_0]$ the initial set. We note that $\boldsymbol{\phi}_0$ is a known continuous function, which does not necessarily satisfy the DDE. Thus the solutions might not be differentiable at $t = t_0$.

Equation (2.1) is a general type of equation and includes:
(i) ODEs when $r = 0$,

$$\dot{\boldsymbol{x}}(t) = \boldsymbol{f}(t, \boldsymbol{x}(t)),$$

(ii) DDEs with discrete delays, for example

$$\dot{\boldsymbol{x}}(t) = \boldsymbol{f}(t, \boldsymbol{x}(t), \boldsymbol{x}(t - r_1), \ldots, \boldsymbol{x}(t - r_n)), \qquad \text{where } r = \max_{1 \leq i \leq n} r_i,$$

(iii) or DDEs with distributed delay,

$$\dot{\boldsymbol{x}}(t) = \int_{-r}^{0} \boldsymbol{f}(t, \theta, \boldsymbol{x}(t+\theta))\, d\theta.$$

In this case, the delay can be infinite, i.e.

$$\dot{\boldsymbol{x}}(t) = \int_{-\infty}^{0} \boldsymbol{f}(t, \theta, \boldsymbol{x}(t+\theta))\, d\theta,$$

and thus the initial condition becomes $\boldsymbol{x}(t) = \boldsymbol{\phi}_0(t - t_0)$ for $t \in (-\infty, t_0]$.

Next, we formally define the solution of a DDE.

Definition 2 *A function $\boldsymbol{x}(t)$ is a solution of equation (2.1) on $[t_0 - r, \beta)$ if there are $t_0, \beta \in \mathbb{R}$ with $\beta > t_0$ such that $\boldsymbol{x} \in C([t_0 - r, \beta), D), [t_0, \beta) \subset J$, and $\boldsymbol{x}(t)$ satisfies equation (2.1) for $t \in [t_0, \beta)$.*

We note that a function $\boldsymbol{x}(t)$ is a solution to the IVP (2.2) on $[t_0 - r, \beta)$ if $\boldsymbol{x}(t)$ is a solution of equation (2.1) and $\boldsymbol{x}_{t_0} = \boldsymbol{\phi}_0$.

As in the case of ODEs, finding a solution to the IVP (2.2) is equivalent to solving the corresponding integral equation,

$$\begin{cases} \boldsymbol{x}_{t_0} = \boldsymbol{\phi}_0 \\ \boldsymbol{x}(t) = \boldsymbol{\phi}_0(0) + \int_{t_0}^{t} \boldsymbol{f}(s, \boldsymbol{x}_s)\, ds, \qquad t_0 \le t < \beta. \end{cases}$$

Before presenting existence and uniqueness theorems, we need the following definition.

Definition 3 *Let $\boldsymbol{f} : J \times \mathcal{C}_D \to \mathbb{R}^n$ and let $S \subset J \times \mathcal{C}_D$. Then $\boldsymbol{f}$ is Lipschitz on S if there exists $L \ge 0$ such that*

$$||\boldsymbol{f}(t, \boldsymbol{\phi}) - \boldsymbol{f}(t, \boldsymbol{\psi})|| \le L\, ||\boldsymbol{\phi} - \boldsymbol{\psi}||_r\,,$$

whenever $(t, \boldsymbol{\phi})$ and $(t, \boldsymbol{\psi}) \in S$.

The existence, uniqueness, continuation of solutions, and continuous dependence theorems are very similar to the ones corresponding to ordinary differential equations. We next state the local existence and uniqueness theorems for DDEs with finite delay. Their proofs can be found in Section 2.2 in [26] and will not be reproduced here.

Theorem 1 *(Local Existence) Suppose Ω is an open subset in $\mathbb{R} \times \mathcal{C}$. Let $\boldsymbol{f} : \Omega \to \mathbb{R}^n$ be continuous on its domain. If $(t_0, \boldsymbol{\phi}_0) \in \Omega$, then there is a solution of the IVP (2.2) passing through $(t_0, \boldsymbol{\phi}_0)$ that exists on $[t_0 - r, t_0 + \delta)$ for some $\delta > 0$.*

Theorem 2 *(Uniqueness) Suppose Ω is an open subset in $\mathbb{R} \times \mathcal{C}$. Let $\boldsymbol{f} : \Omega \to \mathbb{R}^n$ be continuous and Lipschitz on each compact set in Ω. If $(t_0, \boldsymbol{\phi}_0) \in \Omega$, then there is a unique solution of the IVP (2.2) passing through $(t_0, \boldsymbol{\phi}_0)$.*

In the case of DDEs with infinite delay, Kolmanovskii and Myshkis [40] have stated and proved an existence and uniqueness theorem (Theorem 2.3 in Chapter 3) by imposing some restrictions on the metric space $C((-\infty, 0], \mathbb{R}^n)$. We consider the IVP

$$\begin{cases} \dot{\boldsymbol{x}}(t) = \boldsymbol{f}(t, \boldsymbol{x}_t), & t > t_0 \\ \boldsymbol{x}_{t_0}(\theta) = \boldsymbol{\phi}_0(\theta), & -\infty < \theta \leq 0. \end{cases} \tag{2.3}$$

Since $C((-\infty, 0], \mathbb{R}^n)$ is not a complete metric space, one must regulate the behaviour of the considered functions as $t \to -\infty$ by indicating an appropriate subset $K \subseteq C((-\infty, 0], \mathbb{R}^n)$ which is [40]. Some examples of K are [40]:
(1) the Banach space of functions $\boldsymbol{\psi} \in C((-\infty, 0], \mathbb{R}^n)$ such that $e^{pt}\boldsymbol{\psi}(t)$ is bounded and uniformly continuous, with the norm

$$||\boldsymbol{\psi}||_K = \sup_{-\infty < t \leq 0} e^{pt} ||\boldsymbol{\psi}(t)||,$$

where p is fixed;
(2) the Banach space of the same functions as in (1), with $p = 0$ for which

$$||\boldsymbol{\psi}||_K = \sup_{-\infty < t \leq 0} ||\boldsymbol{\psi}(t)|| + \int_{-\infty}^{0} ||\boldsymbol{\psi}(t)||\, dt < \infty;$$

(3) the space $C((-\infty, 0], \mathbb{R}^n)$ equipped with the metric

$$d_K(\boldsymbol{u}_1, \boldsymbol{u}_2) = \sum_{i=1}^{\infty} \frac{1}{2^i} \frac{||(\boldsymbol{u}_1 - \boldsymbol{u}_2)|_{[-i,0]}||}{1 + ||(\boldsymbol{u}_1 - \boldsymbol{u}_2)|_{[-i,0]}||}.$$

We now state the theorem of existence and uniqueness for DDEs with infinite delay whose proof can be found in [40, page 103].

Theorem 3 *(Existence and Uniqueness for DDEs with infinite delay)*
*Let $\boldsymbol{\phi}_0 \in K$, the functional $\boldsymbol{f} : [t_0, \infty) \times K \to \mathbb{R}^n$ be continuous and for any $(t, \boldsymbol{\psi}) \in [t_0, \infty) \times K$ there are $\epsilon, L > 0$ for which the inequality $||\boldsymbol{f}(t + \sigma, \boldsymbol{\psi}_1) - \boldsymbol{f}(t + \sigma, \boldsymbol{\psi}_2)|| \leq L||\boldsymbol{\psi}_1 - \boldsymbol{\psi}_2||_K$ is valid if $\sigma \in (0, \epsilon), \boldsymbol{\psi}_i \in K, (\boldsymbol{\psi}_i)_{-\sigma} = \boldsymbol{\psi}, \max\limits_{-\sigma \leq \theta \leq 0} ||\boldsymbol{\psi}_i(\theta) - \boldsymbol{\psi}_i(0)|| < \epsilon, i = 1, 2.$
Then there is a $t_{\phi_0} \in (t_0, \infty]$ such that*
(a) there exists a solution $\boldsymbol{x}$ of (2.3) on the interval $[t_0, t_{\phi_0})$;
(b) on any interval $[t_0, t_1] \subset [t_0, t_{\phi_0})$ this solution is unique.

In the next section we look in greater detail at DDEs with a distribution of delays. In the following sections, we will discuss equilibrium points, linearization and the characteristic equation associated with these type of equations.

2.2 DDEs with Distributed Delay

For the rest of the chapter we will restrict our discussion to DDEs with one distributed delay of the form,

$$\dot{\boldsymbol{x}}(t) = \int_0^\infty \boldsymbol{f}(\boldsymbol{x}(t), \boldsymbol{x}(t-u))g(u)\,du, \tag{2.4}$$

where $f : \mathbb{R}^n \times \mathbb{R}^n \to \mathbb{R}^n$. Here the delay u occurs with a certain probability given by the kernel $g(u)$, which is a p.d.f. Let us look at the formal definition of a p.d.f. [31].

Definition 4 *Let U denote a random variable of the continuous type on a one-dimensional space $\mathbb{S}$, which consists of an interval or a union of intervals. Let a function $g(u)$ be nonnegative such that*

$$\int_{\mathbb{S}} g(u)\,du = 1.$$

Whenever a probability set function $P(S), S \subset \mathbb{S}$, can be expressed in terms of such a $g(u)$ by

$$P(S) = Prob(U \in S) = \int_S g(u)\,du,$$

then $g(u)$ is called a p.d.f. of U.

In our case, we only consider p.d.f.'s defined on $\mathbb{S} \subseteq [0, \infty)$, since these particular ones give rise to DDEs (by Definition 1). In other words, for equation (2.4) to be a DDE, the kernel $g(u)$ must equal zero for $u < 0$. We note that equation (2.4) also encompasses DDEs with finite distributed delay, when $\mathbb{S}$ is a finite interval or a union of finite intervals, or when $g(u)$ is zero outside a finite interval. Since $g(u) = 0$ for $u \notin \mathbb{S}$, by the above definition we have

$$\int_0^\infty g(u)\,du = 1. \tag{2.5}$$

The mean value (in our case, mean delay) of the p.d.f. $g(u)$ is given by

$$\tau = \int_0^\infty ug(u)\,du. \tag{2.6}$$

The kernel $g(u)$ is usually taken in the literature to be the uniform or gamma distributions, which will be discussed in more detail in Subsections 2.4.2 and 2.4.3. We note that if $g(u)$ represents the Dirac distribution, which is characterized by the following two properties

$$\delta(u) = \begin{cases} 0, & \text{for} \quad u \neq 0 \\ \text{“infinite”}, & \text{for} \quad u = 0 \end{cases}$$

and

$$\int_{-\infty}^{\infty} f(u)\delta(u)\,du = f(0),$$

then we recover the corresponding ODE system,

$$\dot{\boldsymbol{x}}(t) = \int_0^{\infty} \boldsymbol{f}(\boldsymbol{x}(t), \boldsymbol{x}(t-u))\delta(u)\,du = \boldsymbol{f}(\boldsymbol{x}(t), \boldsymbol{x}(t)). \tag{2.7}$$

Also, if $g(u)$ represents the Dirac distribution τ units shifted to the right, which has the two properties

$$\delta(u-\tau) = \begin{cases} 0, & \text{for} \quad u \neq \tau \\ \text{“infinite”}, & \text{for} \quad u = \tau \end{cases}$$

and

$$\int_{-\infty}^{\infty} f(u)\delta(u-\tau)\,du = f(\tau), \tag{2.8}$$

then system (2.4) becomes a DDE system with one discrete delay τ,

$$\dot{\boldsymbol{x}}(t) = \int_0^{\infty} \boldsymbol{f}(\boldsymbol{x}(t), \boldsymbol{x}(t-u))\delta(u-\tau)\,du = \boldsymbol{f}(\boldsymbol{x}(t), \boldsymbol{x}(t-\tau)), \tag{2.9}$$

by property (2.8). Therefore model (2.4) encompasses the corresponding ODE model and also the model with one discrete delay, if the kernel is chosen to be the Dirac distribution.

In Chapters 3 and 4 we study the dependence of the linear stability of the equilibrium points on the mean delay. Thus we want to transform equation (2.4) so that the mean delay appears explicitly. First we note that as $\tau \to 0$, then the distribution $g(u)$ approaches the Dirac distribution $\delta(u)$, since $g(u)$ is nonzero on $(0, \infty)$ and thus, as the mean delay approaches 0, the entire weight of the distribution gets compressed closer and closer to $u = 0$. Hence as $\tau \to 0$, we recover the non-delayed model (2.7). Having dealt with the case $\tau = 0$, we now restrict to the case $\tau > 0$ (which, biologically, is the most interesting case). Making the change of variables $s = t/\tau, v = u/\tau$, system (2.4) becomes

$$\frac{d\boldsymbol{x}}{ds}\frac{ds}{dt} = \frac{1}{\tau}\frac{d\boldsymbol{x}}{ds} = \int_0^{\infty} \boldsymbol{f}(\boldsymbol{x}(\tau s), \boldsymbol{x}(\tau s - \tau v))g(\tau v)\tau\,dv.$$

We let “$'$” denote the right-hand derivative with respect to s and we define

$$\hat{g}(v) = \tau g(\tau v), \tag{2.10}$$

then (2.4) becomes equivalent to

$$\boldsymbol{x}'(s) = \tau \int_0^{\infty} \boldsymbol{f}(\boldsymbol{x}(s), \boldsymbol{x}(s-v))\hat{g}(v)\,dv. \tag{2.11}$$

The new distribution $\hat{g}(v)$ is still a p.d.f. since

$$\int_0^\infty \hat{g}(v)\,dv = \int_0^\infty \tau g(\tau v)\,dv \overset{u=\tau v}{=} \int_0^\infty \tau g(u)\frac{1}{\tau}\,du = \int_0^\infty g(u)du = 1, \tag{2.12}$$

by property (2.5), with mean value

$$\int_0^\infty v\hat{g}(v)\,dv = \int_0^\infty \tau v g(\tau v)\,dv \overset{u=\tau v}{=} \int_0^\infty ug(u)\frac{1}{\tau}\,du = \frac{1}{\tau}\int_0^\infty ug(u)\,du = \frac{1}{\tau}\tau = 1, \tag{2.13}$$

by (2.6). Therefore $\hat{g}(v)$ has mean delay 1 and we will call it the normalized distribution.

In the next section we will discuss the equilibrium points of (2.11), we show how to obtain the linear system associated with (2.11) and compute the characteristic equation.

2.3 Equilibria, Linearization, Characteristic Equation

In Chapters 3 and 4 we analyze the linear stability of the equilibrium points of models with distributed delay via the characteristic equation. The stability of the equilibrium points depends on whether the characteristic equation has negative, positive or zero roots. The goal of this section is to show how to arrive at an expression for the characteristic equation associated with the general system (2.11).

To start, we note that an equilibrium point of the corresponding nondelayed model

$$\boldsymbol{x'}(s) = \tau \boldsymbol{f}(\boldsymbol{x}(s), \boldsymbol{x}(s)) \tag{2.14}$$

satisfies

$$0 = \boldsymbol{f}(\boldsymbol{x}^*, \boldsymbol{x}^*).$$

An equilibrium point of (2.11) is a constant solution $\boldsymbol{x}(s) = \boldsymbol{x}^*$ for all $s \in \mathbb{R}$ and satisfies

$$0 = \int_0^\infty \boldsymbol{f}(\boldsymbol{x}^*, \boldsymbol{x}^*)\hat{g}(v)\,dv = \boldsymbol{f}(\boldsymbol{x}^*, \boldsymbol{x}^*)\int_0^\infty \hat{g}(v)\,dv = \boldsymbol{f}(\boldsymbol{x}^*, \boldsymbol{x}^*),$$

by property (2.12). Hence the equilibrium points are not altered by the inclusion of delay.

Since system (2.11) is autonomous, i.e. of the form $\boldsymbol{x'}(s) = \boldsymbol{f}(\boldsymbol{x}_s)$, without loss of generality, we take the initial instant from now on to be $s_0 = 0$. Then, given the initial function $\phi_0 \in C[(-\infty, 0], \mathbb{R}^n]$, we can define the IVP associated with DDE (2.11) to be

$$\begin{cases} \boldsymbol{x'}(s) = \tau \int_0^\infty \boldsymbol{f}(\boldsymbol{x}(s), \boldsymbol{x}(s-v))\hat{g}(v)\,dv, & s > 0 \\ \boldsymbol{x}(s) = \boldsymbol{\phi}_0(s), & s \le 0. \end{cases} \tag{2.15}$$

We are now ready to define the concepts of stability, instability and asymptotic stability of an equilibrium point of the above IVP [15].

Definition 5 *If $\boldsymbol{x}^*$ is an equilibrium solution of (2.15) on $\mathbb{R}^n$, then it is called stable if given any $\epsilon > 0$ there exists a corresponding $\delta = \delta(\epsilon) > 0$ such that $||\boldsymbol{\phi}_0(s) - \boldsymbol{x}^*|| < \delta$ for all $s \leq 0$ implies that any solution of (2.15) exists on $\mathbb{R}^n$ and satisfies $||\boldsymbol{x}(s) - \boldsymbol{x}^*|| < \epsilon$ for all $s > 0$. Otherwise, $\boldsymbol{x}^*$ is said to be unstable.*

If an equilibrium solution $\boldsymbol{x}^*$ of (2.15) is stable and in addition there exists a constant $\delta_0 > 0$ such that $||\boldsymbol{\phi}_0(s) - \boldsymbol{x}^*|| < \delta_0$ for all $s \leq 0$ implies that $||\boldsymbol{x}(s) - \boldsymbol{x}^*|| \to 0$ as $s \to +\infty$, then x^* is called asymptotically stable.

Next we linearize system (2.11) about the equilibrium point $\boldsymbol{x}^*$. Let $\boldsymbol{y}(s) = \boldsymbol{x}(s) - \boldsymbol{x}^*$ and since $\boldsymbol{f}(\boldsymbol{x}^*, \boldsymbol{x}^*) = \boldsymbol{0}$, by Taylor's Theorem we have

$$\begin{aligned} \boldsymbol{f}(\boldsymbol{x}, \boldsymbol{x}_s) &= \boldsymbol{f}(\boldsymbol{x}^*, \boldsymbol{x}^*) + \boldsymbol{A}(\boldsymbol{x}(s) - \boldsymbol{x}^*) + \boldsymbol{A}_s(\boldsymbol{x}(s-v) - \boldsymbol{x}^*) + \text{ h.o.t.} \\ &= \boldsymbol{A}\boldsymbol{y}(s) + \boldsymbol{A}_s\boldsymbol{y}(s-v) + \text{ h.o.t. ,} \end{aligned}$$

where "h.o.t. " stands for "higher order terms", $\boldsymbol{A}$ is an $n \times n$ matrix representing the Jacobian matrix with respect to the first argument of $\boldsymbol{f}$ evaluated at $(\boldsymbol{x}^*, \boldsymbol{x}^*)$,

$$\boldsymbol{A} = \left(\begin{array}{cccc} \dfrac{\partial f_1}{\partial x_1} & \dfrac{\partial f_1}{\partial x_2} & \cdots & \dfrac{\partial f_1}{\partial x_n} \\ \dfrac{\partial f_2}{\partial x_1} & \dfrac{\partial f_2}{\partial x_2} & \cdots & \dfrac{\partial f_2}{\partial x_n} \\ \vdots & \vdots & \vdots & \vdots \\ \dfrac{\partial f_n}{\partial x_1} & \dfrac{\partial f_n}{\partial x_2} & \cdots & \dfrac{\partial f_n}{\partial x_n} \end{array} \right) \Bigg|_{(\boldsymbol{x}^*, \boldsymbol{x}^*)}$$

and $\boldsymbol{A}_s$ is an $n \times n$ matrix representing the Jacobian matrix with respect to the second argument of $\boldsymbol{f}$ evaluated at $(\boldsymbol{x}^*, \boldsymbol{x}^*)$,

$$\boldsymbol{A}_s = \left(\begin{array}{cccc} \dfrac{\partial f_1}{\partial (x_s)_1} & \dfrac{\partial f_1}{\partial (x_s)_2} & \cdots & \dfrac{\partial f_1}{\partial (x_s)_n} \\ \dfrac{\partial f_2}{\partial (x_s)_1} & \dfrac{\partial f_2}{\partial (x_s)_2} & \cdots & \dfrac{\partial f_2}{\partial (x_s)_n} \\ \vdots & \vdots & \vdots & \vdots \\ \dfrac{\partial f_n}{\partial (x_s)_1} & \dfrac{\partial f_n}{\partial (x_s)_2} & \cdots & \dfrac{\partial f_n}{\partial (x_s)_n} \end{array} \right) \Bigg|_{(\boldsymbol{x}^*, \boldsymbol{x}^*)}$$

where $\partial f_i / \partial (x_s)_j, i, j = 1, \ldots, n$, represents the derivative of f_i with respect to the j^{th} component of the second argument.

Therefore we call the linear system

$$\boldsymbol{y}'(s) = \tau \boldsymbol{A}\boldsymbol{y}(s) + \tau \boldsymbol{A}_s \int_0^\infty \boldsymbol{y}(s-v)\hat{g}(v)\, dv \tag{2.16}$$

the linearization of (2.11) about $\boldsymbol{x}^*$. We now show how to obtain the characteristic equation associated with (2.16), which will give conditions under which the trivial solution of (2.16) is asymptotically stable. We let the solutions of (2.16) to be of the form $\boldsymbol{y}(s) = e^{\lambda s}\boldsymbol{C}$, where $\boldsymbol{C}$ is a nontrivial constant vector, then

$$\lambda e^{\lambda s}\boldsymbol{C} = \tau \boldsymbol{A} e^{\lambda s}\boldsymbol{C} + \tau \boldsymbol{A}_s \int_0^\infty e^{\lambda(s-v)}\boldsymbol{C}\hat{g}(v)\,dv.$$

This is equivalent to

$$\left(\lambda \boldsymbol{I} - \tau \boldsymbol{A} - \tau \boldsymbol{A}_s \int_0^\infty e^{-\lambda v}\hat{g}(v)\,dv\right)\boldsymbol{C} = \boldsymbol{0}.$$

Since $\boldsymbol{C} \neq \boldsymbol{0}$, in order to solve the above system, we impose that the determinant of the matrix inside the brackets to be zero. Hence, we obtain the characteristic equation to be

$$\Delta(\lambda) = \det\left(\lambda \boldsymbol{I} - \tau \boldsymbol{A} - \tau \boldsymbol{A}_s \int_0^\infty e^{-\lambda v}\hat{g}(v)\,dv\right) = 0. \tag{2.17}$$

We can also write the above characteristic equation in terms of the Laplace transform of $\hat{g}(v)$, but first let us define the Laplace transform and look into conditions that guarantee its existence.

Definition 6 *Let $f(t)$ be a function on $[0,\infty)$. The Laplace transform of f is the function F defined by the integral [52]*

$$F(s) = \mathscr{L}(f(t)) = \int_0^\infty e^{-st} f(t)\,dt.$$

The domain of $F(s)$ is all the values of s for which the limit

$$\lim_{N\to\infty} \int_0^N e^{-st} f(t)\,dt$$

exists.

A function $f(t)$ is said to be of exponential order α if there exist positive constants T and M such that $|f(t)| \leq Me^{\alpha T}$, for all $t \geq T$. The following theorem guarantees the existence of the transform, provided the function $f(t)$ does not grow faster than an exponential function of the form $Me^{\alpha T}$ (Theorem 2, Section 7.2 in [52]).

Theorem 4 *If $f(t)$ is piecewise continuous on $[0,\infty)$ and of exponential order α, then its Laplace transform $F(s)$ exists for all $s > \alpha$.*

We next state a property of Laplace transforms which will be used in Section 2.4.3:

$$\text{If } F(s) = \mathscr{L}(f(t)) \text{ then } F^{(n)}(s) = \mathscr{L}((-1)^n t^n f(t)), \tag{2.18}$$

where the superscript (n) represents the n^{th} derivative of F with respect to s [52].

By Definition 6, the Laplace transform of $\hat{g}(v)$ is

$$\hat{G}(\lambda) = \mathscr{L}(\hat{g}(v)) = \int_0^\infty e^{-\lambda v}\hat{g}(v)\,dv.$$

Therefore we can rewrite the characteristic equation (2.17) as

$$\Delta(\lambda) = \det\left(\lambda \boldsymbol{I} - \tau \boldsymbol{A} - \tau \boldsymbol{A}_s \hat{G}(\lambda)\right) = 0. \tag{2.19}$$

For the linear system (2.16), it has been proven [29] that its trivial solution is asymptotically stable if and only if all the roots of the corresponding characteristic equation have negative real parts.

To see under what conditions the asymptotic stability of the trivial solution of the linear system (2.16) guarantees the asymptotic stability of the equilibrium point of (2.11), we need the following definition [26]:

Definition 7 *We say that $x = 0$ is a hyperbolic equilibrium point of* (2.16) *if none of the roots of the characteristic equation* (2.17) *have zero real part.*

If $x = 0$ is a hyperbolic equilibrium point of (2.16), then the asymptotic stability or instability of x^* as a solution of (2.11) is guaranteed by that of the trivial solution of the linearized system (2.16) [45].

In chapters 3 and 4, we will investigate the stability region of equilibrium points of DDEs with a general distribution of delays via the analysis of the characteristic equation. We will also approximate this region of stability when the distribution is unknown, and verify our results by comparing our approximations to the true region of stability of DDEs with uniform and gamma distributed delay. Thus, in the next section we will have a closer look at these two distributions.

2.4 Distributions

Before presenting the uniform and the gamma distributions, we will give an overview of the moments and cumulants of a distribution, which will be needed in Chapters 3 and 4 for approximating the linear stability region of a model with a general distribution of delays. We note that in all our computations we will be using the normalized distribution $\hat{g}(v)$.

Definition 8 *The n^{th} raw moment (or n^{th} moment about zero) of a distribution $\hat{g}$ is the expected value of v^n,*

$$m_n = E[v^n] = \int_0^\infty v^n \hat{g}(v)\, dv, \tag{2.20}$$

where E is the expectation operator.

We can easily see, by (2.12) and (2.13), that $m_0 = m_1 = 1$ and that $m_n > 0$ for all n. The first moment, m_1, represents the mean of the distribution. The variance of the distribution is given by

$$\sigma^2 = E[(v - m_1)^2] = E[v^2 - 2m_1 v + m_1^2],$$

and since E is a linear operator we have

$$\begin{aligned} \sigma^2 &= E[v^2] - 2m_1 E[v] + m_1^2 \\ &= m_2 - 2m_1^2 + m_1^2 \\ &= m_2 - m_1^2. \end{aligned}$$

Therefore the second moment is related to the variance of the distribution via $m_2 = \sigma^2 + 1$. The ratio $E[(v - m_1)^3]/\sigma^3$ is used as a measure of the lopsidedness of the distribution, i.e. skewed to the right or to the left. Thus the third moment is related to the skewness of the distribution [31].

The moments can also be defined using the moment-cumulant generating function,

$$M(t) = E[e^{itv}] = \int_0^\infty e^{itv} \hat{g}(v)\, dv. \tag{2.21}$$

Then, the moments m_n are given by [50]

$$\frac{d^n}{dt^n} M(t)\bigg|_{t=0} = i^n m_n. \tag{2.22}$$

From (2.22) we have

$$\begin{aligned} M(0) &= m_0 = 1, \\ M'(0) &= i m_1 = i, \\ M''(0) &= i^2 m_2, \\ M'''(0) &= i^3 m_3, \end{aligned} \tag{2.23}$$

and so on.

Instead of using the moments of a distribution, sometimes it is preferable to use the cumulants.

Definition 9 *The cumulants, κ_n, of a distribution $\hat{g}$ are given by [50]*

$$\left.\frac{d^n}{dt^n}\ln M(t)\right|_{t=0} = i^n\kappa_n, \tag{2.24}$$

where $M(t)$ is the moment-cumulant generating function, as defined in (2.21)*.*

We easily see that $\kappa_0 = \ln M(0) = \ln 1 = 0$. There is a direct relationship between the moments and the cumulants of a distribution. Let us calculate the first three cumulants. From (2.24), we have that

$$i\kappa_1 = \left.\frac{d\ln M(t)}{dt}\right|_{t=0} = \left.\frac{M'(t)}{M(t)}\right|_{t=0} = \frac{M'(0)}{M(0)} = i \tag{2.25}$$

from the first two equations in (2.23). For the second cumulant we get

$$\begin{aligned} i^2\kappa_2 &= \left.\frac{d^2\ln M(t)}{dt^2}\right|_{t=0} \\ &= \left.\frac{d}{dt}\left(\frac{M'(t)}{M(t)}\right)\right|_{t=0} \\ &= \left.\frac{M''(t)M(t)-[M'(t)]^2}{M^2(t)}\right|_{t=0} \\ &= \frac{M''(0)M(0)-[M'(0)]^2}{M^2(0)} \\ &= i^2\left(m_2-1\right) \end{aligned} \tag{2.26}$$

from the first three equations in (2.23). For the third cumulant we have

$$\begin{aligned} i^3\kappa_3 &= \left.\frac{d^3\ln M(t)}{dt^3}\right|_{t=0} \\ &= \left.\frac{d}{dt}\left(\frac{M''(t)M(t)-(M'(t))^2}{M^2(t)}\right)\right|_{t=0} \\ &= \frac{M'''(0)(M(0))^3-3(M(0))^2M'(0)M''(0)+2M(0)(M'(0))^3}{(M(0))^4} \\ &= i^3\left(m_3-3m_2+2\right) \end{aligned} \tag{2.27}$$

from (2.23). Therefore, from (2.25) – (2.27) we have

$$\begin{aligned} \kappa_1 &= 1, \\ \kappa_2 &= m_2-1, \\ \kappa_3 &= m_3-3m_2+2. \end{aligned} \tag{2.28}$$

We note that the first cumulant represents the mean value, the second cumulant is the variance of the distribution, and the third cumulant is related to the skewness of the distribution.

To obtain a general recursive formula for the n^{th} cumulant in terms of the first n moments, we use Faá di Bruno's formula [37],

$$\frac{d^n}{dt^n} f(g(t)) = \sum \frac{n!}{r_1! r_2! \cdots r_n!} f^{(r_1+r_2+\cdots+r_n)}(g(t)) \prod_{j=1}^{n} \left(\frac{g^{(j)}(t)}{j!} \right)^{r_j},$$

where the sum is over all n-tuples of nonnegative integers $(r_1, r_2, \ldots, r_n)$ satisfying the constraint

$$1 \cdot r_1 + 2 \cdot r_2 + \cdots + n \cdot r_n = n. \tag{2.29}$$

From (2.24), we see that in our case, $g(t) = M(t)$, and $f(t) = \ln(t)$ with its n^{th} derivative given by

$$f^{(n)}(t) = \frac{(-1)^{n-1}(n-1)!}{t^n}.$$

Using this and Faá di Bruno's formula, equation (2.24) becomes

$$\begin{aligned} i^n \kappa_n &= \sum \frac{n!}{r_1! r_2! \cdots r_n!} \frac{(-1)^{r_1+r_2+\cdots+r_n-1}(r_1+r_2+\cdots+r_n-1)!}{(M(t))^n} \prod_{j=1}^{n} \left(\frac{M^{(j)}(t)}{j!} \right)^{r_j} \Bigg|_{t=0} \\ &= \sum \frac{n!}{r_1! r_2! \cdots r_n!} \frac{(-1)^{r_1+r_2+\cdots+r_n-1}(r_1+r_2+\cdots+r_n-1)!}{(M(0))^n} \prod_{j=1}^{n} \left(\frac{M^{(j)}(0)}{j!} \right)^{r_j} \\ &= \sum \frac{(-1)^{r_1+r_2+\cdots+r_n-1}(r_1+r_2+\cdots+r_n-1)! n!}{r_1! r_2! \cdots r_n!} \prod_{j=1}^{n} \left(\frac{i^j m_j}{j!} \right)^{r_j}, \end{aligned}$$

where we used (2.22). We notice that

$$\prod_{j=1}^{n} i^{j r_j} = i^{\sum_{j=1}^{n} j r_j} = i^n,$$

by (2.29). Therefore the n^{th} cumulant is given by

$$\kappa_n = \sum \frac{(-1)^{r_1+r_2+\cdots+r_n-1}(r_1+r_2+\cdots+r_n-1)! n!}{r_1! r_2! \cdots r_n!} \prod_{j=1}^{n} \left(\frac{m_j}{j!} \right)^{r_j}.$$

where the sum is over all n-tuples of nonnegative integers $(r_1, r_2, \ldots, r_n)$ satisfying (2.29). To exemplify the above formula, we use it to determine the third cumulant. For $n = 3$, we

have $(r_1, r_2, r_3) \in \{(3,0,0),(1,1,0),(0,0,1)\}$. Therefore

$$\begin{aligned}\kappa_3 &= \frac{2!3!}{3!}\left(\frac{m_1}{1!}\right)^3 - \frac{3!}{1!1!}\left(\frac{m_1}{1!}\right)\left(\frac{m_2}{2!}\right) + \frac{3!}{1!}\left(\frac{m_3}{3!}\right) \\ &= 2(m_1)^3 - 3m_1m_2 + m_3 \\ &= 2 - 3m_2 + m_3,\end{aligned}$$

which is exactly the expression we derived in (2.27).

In the next three subsections we give the definitions of the Dirac, uniform and gamma distributions, we then compute their Laplace transforms, moments and cumulants.

2.4.1 The Dirac Distribution

As presented in Section 2.2, the Dirac distribution τ units shifted to the right is characterized by the following two properties

$$g(u) = \delta(u-\tau) = \begin{cases} 0, & \text{for} \quad u \neq \tau \\ \text{“infinite”}, & \text{for} \quad u = \tau \end{cases}$$

and

$$\int_{-\infty}^{\infty} f(u)\delta(u-\tau)\,du = f(\tau).$$

By Definition 6, the Laplace transform of the Dirac distribution is given by

$$\mathscr{L}(g(u)) = \int_0^{\infty} e^{-\lambda u}\delta(u-\tau)\,du = e^{-\lambda\tau}.$$

The normalized distribution is given by

$$\hat{g}(v) = \tau g(\tau v) = \tau\delta(\tau v - \tau). \tag{2.30}$$

Using (2.21), we compute the moment-cumulant generating function,

$$M(t) = \int_0^{\infty} e^{itv}\hat{g}(v)\,dv = \int_0^{\infty} e^{itv}\tau\delta(\tau v-\tau)\,dv \overset{v=u/\tau}{=} \int_0^{\infty} e^{itu/\tau}\tau\delta(u-\tau)\frac{1}{\tau}\,du = e^{it}.$$

From here we get that

$$\frac{d^n}{dt^n}M(t) = i^n e^{it}.$$

Using (2.22), the moments are then given by $m_n = 1$ for all $n = 0, 1, 2, \ldots$. Further, we have that $\ln M(t) = it$ and thus

$$\frac{d}{dt}\ln M(t) = i \qquad \Rightarrow \qquad \frac{d^n}{dt^n}\ln M(t) = 0 \text{ for all } n = 2, 3, \ldots.$$

Therefore, from (2.24), we have that $\kappa_1 = 1$ and $\kappa_n = 0$ for all $n \neq 1$.

2.4.2 The Uniform Distribution

The general uniform distribution with mean delay τ is given by

$$g(u) = \begin{cases} \frac{1}{\rho\tau}, & \text{if } u \in \left[\tau\left(1-\frac{\rho}{2}\right), \tau\left(1+\frac{\rho}{2}\right)\right] \\ 0, & \text{elsewhere,} \end{cases}$$

where $0 < \rho \leq 2$. The parameter ρ controls the width and height of the distribution. Figure 2.1 shows examples of this distribution for different values of ρ, but having the same mean delay, $\tau = 2$. As ρ decreases the width of the distribution decreases and the height increases. Hence, as $\rho \to 0$, the uniform distribution becomes the Dirac distribution, $\delta(u-\tau)$. Hence we have

$$\lim_{\rho\to 0}\int_0^\infty \boldsymbol{f}(\boldsymbol{x}(t), \boldsymbol{x}(t-u))g(u)\,du = \int_0^\infty \boldsymbol{f}(\boldsymbol{x}(t), \boldsymbol{x}(t-u))\delta(u-\tau)\,du = \boldsymbol{f}(\boldsymbol{x}(t), \boldsymbol{x}(t-\tau)),$$

i.e. as ρ becomes smaller and smaller, the DDE in (2.4) with a uniform distribution of delays (with mean delay τ) approaches the DDE with one discrete delay τ (equation (2.9)).

Using Definition 6, we obtain the Laplace transform of $g(u)$,

$$\mathscr{L}(g(u)) = \int_{\tau(1-\rho/2)}^{\tau(1+\rho/2)} \frac{e^{-\lambda u}}{\rho\tau}\,du = -\frac{e^{-\lambda u}}{\rho\tau\lambda}\Big|_{u=\tau(1+\rho/2)}^{u=\tau(1+\rho/2)} = \frac{1}{\rho\tau\lambda}[e^{-\tau\lambda(1-\rho/2)} - e^{-\tau\lambda(1+\rho/2)}].$$

If we let $\rho \to 0$, we get

$$\lim_{\rho\to 0}\mathscr{L}(g(u)) = \lim_{\rho\to 0}\frac{1}{\tau\lambda}\left[\frac{\tau\lambda}{2}e^{-\tau\lambda(1-\rho/2)} + \frac{\tau\lambda}{2}e^{-\tau\lambda(1+\rho/2)}\right] = e^{-\tau\lambda},$$

which is exactly the Laplace transform of $\delta(u-\tau)$. Thus, as expected, we obtain that

$$\lim_{\rho\to 0}\mathscr{L}(g(u)) = \mathscr{L}(\delta(u-\tau)).$$

By (2.10), the normalized distribution becomes

$$\hat{g}(v) = \begin{cases} \frac{1}{\rho}, & \text{if } v \in [1-\frac{\rho}{2}, 1+\frac{\rho}{2}] \\ 0, & \text{elsewhere.} \end{cases} \tag{2.31}$$

As seen in Section 2.3, the Laplace transform of $\hat{g}(v)$ is needed when determining the characteristic equation and thus we compute it here,

$$\hat{G}(\lambda) = \mathscr{L}(\hat{g}(v)) = \int_{1-\frac{\rho}{2}}^{1+\frac{\rho}{2}} \frac{e^{-\lambda v}}{\rho}\,dv = -\frac{e^{-\lambda v}}{\rho\lambda}\Big|_{v=1-\rho/2}^{v=1+\rho/2} = \frac{1}{\rho\lambda}[e^{-\lambda(1-\rho/2)} - e^{-\lambda(1+\rho/2)}]. \tag{2.32}$$

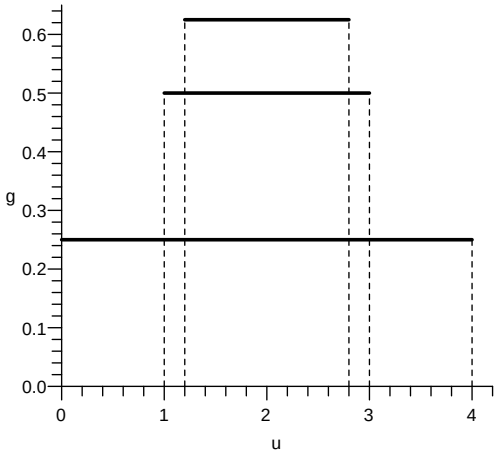

Figure 2.1: The uniform distribution for $\rho = 0.8, 1, 2$ and mean delay $\tau = 2$.

From the definition in (2.20), the moments are given by

$$\begin{aligned} m_n &= \int_0^\infty v^n \hat{g}(v)\, dv = \frac{1}{\rho} \int_{1-\rho/2}^{1+\rho/2} v^n\, dv \\ &= \frac{1}{(n+1)\rho} \left[\left(1 + \frac{\rho}{2}\right)^{n+1} - \left(1 - \frac{\rho}{2}\right)^{n+1} \right]. \end{aligned} \tag{2.33}$$

Using this and the expression in (2.28), we compute the first few moments and cumulants for $\rho = 2$, $\rho = 1$ and $\rho = 4/5$, as shown in Table 2.1. These will be useful in Chapters 3 and 4 when approximating the region of stability of the equilibrium points of systems with uniform distributed delay.

We note that the third cumulant is always zero for any ρ,

$$\kappa_3 = \frac{1}{4\rho} \left[\left(1 + \frac{\rho}{2}\right)^4 - \left(1 - \frac{\rho}{2}\right)^4 \right] - \frac{1}{\rho} \left[\left(1 + \frac{\rho}{2}\right)^3 - \left(1 - \frac{\rho}{2}\right)^3 \right] + 2 = 0, \tag{2.34}$$

Table 2.1: Moments and cumulants of the uniform distribution.

ρ	m_0	m_1	m_2	m_3	κ_0	κ_1	κ_2	κ_3
2	1	1	4/3	2	0	1	1/3	0
1	1	1	13/12	5/4	0	1	1/12	0
4/5	1	1	79/75	29/25	0	1	4/75	0

where we substituted (2.33) (with $n = 2$ and $n = 3$) into (2.28).

In the next subsection we discuss the gamma distribution: its definition, Laplace transform, moments and cumulants.

2.4.3 The Gamma Distribution

The gamma distribution is given by

$$g(u) = \frac{u^{p-1}a^p e^{-au}}{\Gamma(p)},$$

where $a, p \geq 0$ are parameters determining the shape of the distribution. Γ is the gamma function defined by $\Gamma(0) = 1$ and $\Gamma(p+1) = p\Gamma(p)$. We will only consider p in the gamma distribution to be a positive integer and in this case $\Gamma(p) = (p-1)!$. We note that the gamma distribution is defined on the infinite interval $[0, \infty)$. We mention that for $p = 1$ the gamma distribution becomes the exponential distribution, $g(u) = ae^{-au}$.

To compute the mean delay of the gamma distribution, we first show by induction that for any nonnegative integer α we have

$$\int_0^\infty w^\alpha e^{-\beta w}\, dw = \frac{\alpha!}{\beta^{\alpha+1}}. \tag{2.35}$$

For $\alpha = 0$ we have

$$\int_0^\infty w^0 e^{-\beta w}\, dw = -\frac{e^{-\beta w}}{\beta}\bigg|_0^\infty = 0 + \frac{1}{\beta} = \frac{0!}{\beta}. \tag{2.36}$$

We assume (2.35) is true. Integrating by parts with $u = w^{\alpha+1}$ and $dv = e^{-\beta w}dw$, we have

$$\begin{aligned}\int_0^\infty w^{\alpha+1} e^{-\beta w}\, dw &= -\frac{w^{\alpha+1}e^{-\beta w}}{\beta}\bigg|_0^\infty - \int_0^\infty -\frac{(\alpha+1)w^\alpha e^{-\beta w}}{\beta}\, dw \\ &= 0 + \frac{\alpha+1}{\beta}\frac{\alpha!}{\beta^{\alpha+1}} \\ &= \frac{(\alpha+1)!}{\beta^{\alpha+2}}. \end{aligned} \tag{2.37}$$

From (2.35), (2.36) and (2.37), we conclude that the statement in (2.35) is true. Therefore using (2.35), the mean delay becomes

$$\tau = \int_0^\infty ug(u)\,du = \int_0^\infty \frac{u^p a^p e^{-au}}{(p-1)!}\,du = \frac{a^p}{(p-1)!}\frac{p!}{a^{p+1}} = \frac{p}{a}.$$

The gamma distribution for a fixed value of the mean delay $\tau = 2$, for $p = 1, 2, 4$, and 8 is shown in Figure 2.2. As p increases, the peak becomes narrower and the position of the

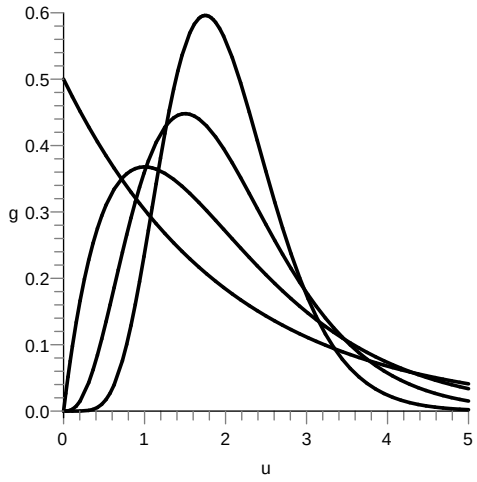

Figure 2.2: The gamma distribution for $p = 1, 2, 4, 8$ and mean delay $\tau = 2$.

maximum tends to $u = \tau = 2$. We see from Figure 2.2 that as p becomes larger and larger, the gamma distribution approaches the Dirac distribution, $\delta(u - \tau)$. Therefore we have

$$\lim_{p\to\infty} \int_0^\infty \boldsymbol{f}(\boldsymbol{x}(t), \boldsymbol{x}(t-u))g(u)\,du = \int_0^\infty \boldsymbol{f}(\boldsymbol{x}(t), \boldsymbol{x}(t-u))\delta(u-\tau)\,du = \boldsymbol{f}(\boldsymbol{x}(t), \boldsymbol{x}(t-\tau)),$$

i.e. as p becomes larger and larger, the DDE in (2.4) with a gamma distribution of delays (with mean delay τ) approaches the DDE with one discrete delay τ (equation (2.9)).

We next compute the Laplace transform of the gamma distribution. Let $f(u) = e^{-au}$, then

$$\begin{aligned} F(\lambda) &= \mathscr{L}(e^{-au}) = (\lambda + a)^{-1}, \\ F'(\lambda) &= -(\lambda + a)^{-2}, \\ F''(\lambda) &= 2(\lambda + a)^{-3}, \\ F'''(\lambda) &= -6(\lambda + a)^{-4}, \end{aligned}$$

and so on. In general we have

$$\begin{aligned} F^{(p-1)}(\lambda) &= (-1)^{p-1}(p-1)!(\lambda + a)^{-p} \\ &= \mathscr{L}((-1)^{p-1}u^{p-1}e^{-au}), \end{aligned}$$

by property (2.18). Multiplying both sides by $a^p/(p-1)!$, we obtain the Laplace transform of the gamma distribution,

$$\mathscr{L}\left(\frac{u^{p-1}a^p e^{-au}}{(p-1)!}\right) = \left(\frac{a}{\lambda + a}\right)^p. \tag{2.38}$$

We substitute $a = p/\tau$ into (2.38) to obtain the Laplace transform in terms of the mean delay τ,

$$\mathscr{L}(g(u)) = \left(\frac{p/\tau}{\lambda + p/\tau}\right)^p = \left(\frac{\lambda + p/\tau}{p/\tau}\right)^{-p} = \left(1 + \frac{\lambda\tau}{p}\right)^{-p}.$$

Letting $p \to \infty$ with τ fixed, we have

$$\lim_{p\to\infty} \mathscr{L}(g(u)) = \lim_{p\to\infty} \left(1 + \frac{\lambda\tau}{p}\right)^{-p} \overset{n=p/(\lambda\tau)}{=} \left[\lim_{n\to\infty} \left(1 + \frac{1}{n}\right)^n\right]^{-\lambda\tau} = e^{-\lambda\tau},$$

which is the Laplace transform of $\delta(u-\tau)$. Hence, as in the case of the uniform distribution, we have that

$$\lim_{p\to\infty} \mathscr{L}(g(u)) = \mathscr{L}(\delta(u - \tau)).$$

By (2.10), the normalized distribution is given by

$$\hat{g}(v) = \tau g(\tau v) = \frac{(\tau\, a)^p v^{p-1} e^{-a\tau v}}{(p-1)!} = \frac{p^p v^{p-1} e^{-pv}}{(p-1)!}, \tag{2.39}$$

with the n^{th} moment given by

$$m_n = \int_0^\infty v^n \hat{g}(v)\, dv = \frac{p^p}{(p-1)!} \int_0^\infty v^{n+p-1} e^{-pv}\, dv = \frac{p^p}{(p-1)!} \frac{(n+p-1)!}{p^{n+p}},$$

by (2.35). Therefore the n^{th} moment of the gamma distribution is

$$m_n = p^{-n}\frac{(n+p-1)!}{(p-1)!}. \tag{2.40}$$

Using this and (2.28), we obtain the first few moments and cumulants for $p = 3$, $p = 4$ and $p = 5$, which are shown in Table 2.2. These will be used in the next two chapters when approximating the linear stability of the equilibrium points of DDEs with a gamma distributed delay.

Table 2.2: Moments and cumulants of the gamma distribution.

p	m_0	m_1	m_2	m_3	κ_0	κ_1	κ_2	κ_3
3	1	1	4/3	20/9	0	1	1/3	2/9
4	1	1	5/4	15/8	0	1	1/4	1/8
5	1	1	6/5	42/25	0	1	1/5	2/25

The Laplace transform of the normalized gamma distribution is computed in a very similar way to the procedure used in obtaining (2.38),

$$\hat{G}(\lambda) = \mathscr{L}(\hat{g}(v)) = \left(\frac{p}{\lambda+p}\right)^p. \tag{2.41}$$

The uniform and gamma distributions are the most used distributions in models with distributed delay. In the next subsection we show how one can transform a p.d.f. defined on the whole real axis into one that is defined only on the positive real axis, and thus could be used in systems with distributed delay.

2.4.4 Other Distributions

As seen in the last two subsections, the uniform and gamma distributions are only defined on the positive real axis, making them the most frequently used distributions in the literature of DDEs with distributed delay. As mentioned at the beginning of Section 2.2, only distributions defined on the positive real axis give rise to DDEs. In this subsection we show through a particular example how one can transform a p.d.f. defined on the whole real axis into one that is defined only on the positive real axis. We examine the Gaussian distribution (also referred to as the normal distribution) and scale it so that its integral from $[0, \infty)$ is equal to 1. The Gaussian distribution is given by

$$\text{Gaussian}(u) = \frac{1}{\sigma\sqrt{2\pi}}\exp\left[-\frac{(u-\tau)^2}{2\sigma^2}\right], \tag{2.42}$$

defined on $(-\infty, \infty)$, where τ represents its mean value and σ its standard deviation. Our scaled Gaussian distribution defined on $[0, \infty)$ is

$$g(u) = K \exp\left[-\frac{(u-\tau)^2}{2\sigma^2}\right], \tag{2.43}$$

where K (to be determined) is the scaling factor such that

$$\int_0^\infty g(u) = \int_0^\infty K \exp\left[-\frac{(u-\tau)^2}{2\sigma^2}\right] = 1. \tag{2.44}$$

To find K, we will make use of the following identity

$$\int_0^\infty e^{-w^2/2}\, dw = \sqrt{\frac{\pi}{2}}, \tag{2.45}$$

and of the error function given by $\operatorname{erf}(x) = 2\int_0^x e^{-t^2}\, dt/\sqrt{\pi}$, which is equivalent to

$$\operatorname{erf}\left(\frac{x}{\sqrt{2}}\right) = \sqrt{\frac{2}{\pi}} \int_0^{x\sqrt{2}} e^{-w^2/2}\, dw, \tag{2.46}$$

where we made the change of variables $w = t\sqrt{2}$ for the error function to be consistent with the expression in (2.45). We let $y = (u-\tau)/\sigma$ and thus (2.44) becomes

$$\begin{aligned}
1 &= K \int_{-\tau/\sigma}^\infty e^{-y^2/2}\sigma\, dy \\
&= K\sigma \left(\int_{-\tau/\sigma}^0 e^{-y^2/2}\, dy + \int_0^\infty e^{-y^2/2}\, dy \right) \\
&= K\sigma\sqrt{\frac{\pi}{2}} \left(\sqrt{\frac{2}{\pi}} \int_0^{\tau/\sigma} e^{-y^2/2}\, dy + 1 \right) \\
&= K\sigma\sqrt{\frac{\pi}{2}} \left(\operatorname{erf}\left(\frac{\tau}{\sigma\sqrt{2}}\right) + 1 \right),
\end{aligned}$$

by (2.45) and (2.46). Therefore the scaling factor is given by

$$K = \frac{\sqrt{2}}{\sigma\sqrt{\pi}\left[\operatorname{erf}\left(\tau/(\sigma\sqrt{2})\right) + 1\right]}.$$

And thus the scaled Gaussian distribution defined on $[0, \infty)$ is given by

$$g(u) = \frac{\sqrt{2}}{\sigma\sqrt{\pi}\left[\operatorname{erf}\left(\tau/(\sigma\sqrt{2})\right) + 1\right]} \exp\left[-\frac{(u-\tau)^2}{2\sigma^2}\right].$$

By (2.10), our normalized Gaussian distribution then becomes

$$\hat{g}(v) = \tau g(\tau v) = \tau K \exp\left[-\frac{\tau^2(v-1)^2}{2\sigma^2}\right] = \hat{K}\exp\left[-\frac{(v-1)^2}{2\hat{\sigma}^2}\right],$$

with mean 1 and standard deviation $\hat{\sigma} = \sigma/\tau$, where

$$\hat{K} = \frac{\sqrt{2}}{\hat{\sigma}\sqrt{\pi}\left[\operatorname{erf}\left(1/(\hat{\sigma}\sqrt{2})\right)+1\right]}. \tag{2.47}$$

We next compute $\hat{G}(\lambda) = \mathscr{L}(\hat{g}(v))$, the Laplace transform of $\hat{g}(v)$,

$$\begin{aligned}
\hat{G}(\lambda) &= \hat{K}\int_0^\infty \exp[-\lambda v]\exp\left[-\frac{(v-1)^2}{2\hat{\sigma}^2}\right]\,dv \\
&= \hat{K}\int_0^\infty \exp\left[-\frac{v^2-2v+1+2\hat{\sigma}^2\lambda v}{2\hat{\sigma}^2}\right]\,dv \\
&= \hat{K}\int_0^\infty \exp\left[-\frac{(v-1+\hat{\sigma}^2\lambda)^2-\hat{\sigma}^4\lambda^2+2\hat{\sigma}^2\lambda}{2\hat{\sigma}^2}\right]\,dv \\
&= \hat{K}\exp\left[\frac{\hat{\sigma}^2\lambda^2}{2}-\lambda\right]\int_0^\infty \exp\left[-\frac{(v-1+\hat{\sigma}^2\lambda)^2}{2\hat{\sigma}^2}\right]\,dv \\
&= \hat{K}\hat{\sigma}\exp\left[\frac{\hat{\sigma}^2\lambda^2}{2}-\lambda\right]\int_{(\hat{\sigma}^2\lambda-1)/\hat{\sigma}}^\infty e^{-w^2/2}\,dw.
\end{aligned} \tag{2.48}$$

where we made the change of variables $w = (v-1+\hat{\sigma}^2\lambda)/\hat{\sigma}$. When $\hat{\sigma}^2\lambda - 1 \geq 0$, equation (2.48) becomes

$$\begin{aligned}
\hat{G}(\lambda) &= \hat{K}\hat{\sigma}e^{\hat{\sigma}^2\lambda^2/2-\lambda}\left(\int_0^\infty e^{-w^2/2}\,dw - \int_0^{(\hat{\sigma}^2\lambda-1)/\hat{\sigma}} e^{-w^2/2}\,dw\right) \\
&= \hat{K}\hat{\sigma}e^{\hat{\sigma}^2\lambda^2/2-\lambda}\sqrt{\frac{\pi}{2}}\left[1-\operatorname{erf}\left(\frac{\hat{\sigma}^2\lambda-1}{\sqrt{2}\hat{\sigma}}\right)\right],
\end{aligned} \tag{2.49}$$

using (2.45) and (2.46). When $\hat{\sigma}^2\lambda - 1 < 0$, equation (2.48) becomes

$$\begin{aligned}
\hat{G}(\lambda) &= \hat{K}\hat{\sigma}e^{\hat{\sigma}^2\lambda^2/2-\lambda}\left(\int_0^\infty e^{-w^2/2}\,dw + \int_{(\hat{\sigma}^2\lambda-1)/\hat{\sigma}}^0 e^{-w^2/2}\,dw\right) \\
&= \hat{K}\hat{\sigma}e^{\hat{\sigma}^2\lambda^2/2-\lambda}\left(\int_0^\infty e^{-w^2/2}\,dw + \int_0^{(1-\hat{\sigma}^2\lambda)/\hat{\sigma}} e^{-w^2/2}\,dw\right) \\
&= \hat{K}\hat{\sigma}e^{\hat{\sigma}^2\lambda^2/2-\lambda}\sqrt{\frac{\pi}{2}}\left[1+\operatorname{erf}\left(\frac{1-\hat{\sigma}^2\lambda}{\sqrt{2}\hat{\sigma}}\right)\right],
\end{aligned} \tag{2.50}$$

From (2.47)–(2.50) and using the fact that the error function is an odd function, we obtain the Laplace transform of $\hat{g}(v)$,

$$\hat{G}(\lambda) = \frac{e^{\hat{\sigma}^2\lambda^2/2-\lambda}}{\operatorname{erf}\left(1/(\hat{\sigma}\sqrt{2})\right)+1}\left[1+\operatorname{erf}\left(\frac{1-\hat{\sigma}^2\lambda}{\hat{\sigma}\sqrt{2}}\right)\right]. \tag{2.51}$$

The moment-cumulant generating function can be determined in a similar way to the procedure we used in obtaining (2.51). But since the computations for determining the stability region would be too tedious using the cumbersome expression in (2.51), we refrain from using the scaled Gaussian distribution in later chapters, and only use the uniform and gamma distributions to verify our results for DDEs with a general distribution of delays.

In the final section of this chapter, we present a method of transforming a scalar DDE with a gamma distributed delay into a system of ODEs. This is a good way of verifying the results obtained for DDEs with distributed delay, and also we will use this reduction in Chapter 5 to check whether the computation of the centre manifold of a scalar DDE is performed correctly.

2.5 The Linear Chain Trick

A scalar DDE with a gamma distributed delay can be shown to be equivalent to a system of $p+1$ ODEs. This transformation is called the linear chain trick [45, 46]. Such an approach may seem attractive as the model can then be analyzed using the theoretical and numerical methods for ODEs. However, it will only be practical if p is a small integer, while real data may call for much larger and/or noninteger p. This can be seen in a paper by Yan [63], where data for the pre-symptomatic infectious period in an outbreak of mumps was fit by a gamma distribution with $p = 70$.

We present the linear chain trick reduction by considering the scalar Hopfield model

$$\frac{dx(s)}{ds} = -\alpha\tau x(s) + w\tau\int_0^\infty f\left(x(s-v)\right)\hat{g}_p(v)\,dv + c\tau, \tag{2.52}$$

$$\text{with initial condition } x(s) = \phi_0(s), \text{ for } s \in (-\infty, 0], \tag{2.53}$$

where $\hat{g}_p(v)$ represents the normalized gamma distribution given in (2.39). The above equation with $p = 1$ and $p = 2$ is used in Chapter 5 to verify whether the general calculation of the centre manifold for any distribution is consistent with these two particular cases.

First we do a change of variables, $t = s - v$, then equation (2.52) becomes

$$\frac{dx(s)}{ds} = -\alpha\tau x(s) + w\tau\int_{-\infty}^{s} f\left(x(t)\right)\hat{g}_p(s-t)\,dt + c\tau. \tag{2.54}$$

To transform equation (2.54) into a system of ODEs, let

$$x_0(s) = x(s) \tag{2.55}$$

$$x_q(s) = \int_{-\infty}^{s} f(x(t))\hat{g}_q(s-t)\,dt, \qquad q = 1, \ldots, p, \tag{2.56}$$

where

$$\hat{g}_q(s-t) = \frac{(\tau\, a)^q (s-t)^{q-1} e^{-a\tau(s-t)}}{(q-1)!} = \frac{p^q (s-t)^{q-1} e^{-p(s-t)}}{(q-1)!}, \tag{2.57}$$

since the mean delay is $\tau = p/a$. We note that $\lim_{v\to\infty} \hat{g}_q(v) = 0$ and

$$\hat{g}_q(0) = \begin{cases} p, & \text{if } q = 1, \\ 0, & \text{if } q > 1. \end{cases} \tag{2.58}$$

Substituting (2.55) and (2.56) into (2.54), we obtain

$$\frac{dx_0(s)}{ds} = -\alpha\tau x_0(s) + w\tau x_p(s) + c\tau. \tag{2.59}$$

Next, we take the derivative of $x_q(s)$ with respect to s using Leibniz Rule,

$$\frac{dx_q(s)}{ds} = \int_{-\infty}^{s} f(x(t)) \frac{\partial \hat{g}_q(s-t)}{\partial s}\,dt + f(x(s))\hat{g}_q(0). \tag{2.60}$$

We consider two cases.

Case 1: $\mathbf{q = 1}$

From (2.58) and (2.57) we have $\hat{g}_1(0) = p$ and $\hat{g}_1(t-s) = pe^{-p(s-t)}$, and thus

$$\frac{\partial \hat{g}_1(s-t)}{\partial s} = -p^2 e^{-p(s-t)} = -p\hat{g}_1(s-t).$$

Therefore, using (2.55) and (2.56), equation (2.60) becomes

$$\frac{dx_1(s)}{ds} = -\int_{-\infty}^{s} f(x(t)) p\hat{g}_1(t-s)\,dt + pf(x(s)) = p[f(x_0(s)) - x_1(s)]. \tag{2.61}$$

Case 2: $\mathbf{q > 1}$

From (2.58) we have $\hat{g}_q(0) = 0$. From (2.57) we obtain,

$$\begin{aligned} \frac{\partial \hat{g}_q(s-t)}{\partial s} &= \frac{p^q (q-1)(s-t)^{q-2} e^{-p(s-t)}}{(q-1)!} + \frac{-pp^q (s-t)^{q-1} e^{-p(s-t)}}{(q-1)!} \\ &= p\left[\frac{p^{q-1}(s-t)^{q-2} e^{-p(s-t)}}{(q-2)!} - \frac{p^q (s-t)^{q-1} e^{-p(s-t)}}{(q-1)!}\right] \\ &= p[\hat{g}_{q-1}(s-t) - \hat{g}_q(s-t)]. \end{aligned}$$

Using (2.56), equation (2.60) becomes

$$\frac{dx_q(s)}{ds} = \int_{-\infty}^{s} f(x(t))p[\hat{g}_{q-1}(s-t) - \hat{g}_q(s-t)]\,dt = p[x_{q-1}(s) - x_q(s)]. \tag{2.62}$$

From (2.59), (2.61) and (2.62) we obtain the system of ODEs

$$\begin{cases} x_0'(s) = -\alpha\tau x_0(s) + w\tau x_p(s) + c\tau \\ x_1'(s) = p[f(x_0(s)) - x_1(s)] \\ x_q'(s) = p[x_{q-1}(s) - x_q(s)], \qquad \text{for } q = 2, \ldots, p. \end{cases} \tag{2.63}$$

From (2.53), (2.55) and (2.56), the initial conditions for this ODE system are

$$\begin{aligned} &x_0(0) = x(0) = \phi_0(0), \\ &x_q(0) = \int_{-\infty}^{0} f(x(t))\hat{g}_q(0-t)\,dt = \int_0^{\infty} f(\phi_0(-t))\hat{g}_q(t)\,dt, \qquad \text{for } q = 1, \ldots, p. \end{aligned}$$

We note that in the engineering literature when $p = 1$, system (2.63) is called a model with a first order lag, and when $p = 2$ it is called model with a second order lag.

To verify whether (2.52) and (2.63) are equivalent in terms of their linear stability, we next compare their characteristic equations. Let x^* be an equilibrium point of (2.52), i.e.

$$0 = -\alpha\tau x^* + w\tau f(x^*) + c\tau.$$

Letting $y(s) = x(s) - x^*$ and using the above identity, the linearized equation corresponding to (2.52) becomes

$$y'(s) = -\alpha\tau y(s) + \beta\tau \int_0^{\infty} y(s-v)\hat{g}_p(v)\,dv,$$

where $\beta = wf'(x^*)$. This is the scalar version of (2.16) and by (2.19), its characteristic equation is given by

$$\Delta_{\mathrm{DDE}}(\lambda) = \lambda + \alpha\tau - \beta\tau\mathscr{L}(\hat{g}(v)).$$

Since $\hat{g}(v)$ represents the normalized gamma distribution, by (2.41) the characteristic equation becomes

$$\Delta_{\mathrm{DDE}}(\lambda) = \lambda + \alpha\tau - \beta\tau\left(\frac{p}{\lambda + p}\right)^p = 0. \tag{2.64}$$

Now we turn to the ODE system (2.63). Let $(x_0^*, x_1^*, \ldots, x_p^*)$ be an equilibrium point satisfying

$$\begin{cases} 0 = -\alpha\tau x_0^* + w\tau x_p^* + c\tau \\ 0 = p[f(x_0^*) - x_1^*] \\ 0 = p[x_{q-1}^* - x_q^*], \qquad \text{for } q = 2, \ldots, p. \end{cases}$$

Letting $y_q(s) = x_q(s) - x_q^*, q = 0, \ldots, p$, and using the above equations, the linearized ODE system becomes

$$\begin{cases} y_0'(s) = -\alpha\tau y_0(s) + w\tau y_p(s) \\ y_1'(s) = p[\bar{\beta} y_0(s) - y_1(s)] \\ y_q'(s) = p[y_{q-1}(s) - y_q(s)], \qquad \text{for } q = 2, \ldots, p. \end{cases},$$

where $\bar{\beta} = f'(x_0^*) = \beta/w$. The above linear system can be written as $\boldsymbol{y}'(s) = \boldsymbol{A}\boldsymbol{y}(s)$, where $\boldsymbol{y} = [y_0, y_1, \ldots, y_p]^T$ and $\boldsymbol{A}$ is a $(p+1) \times (p+1)-$matrix of the form

$$\boldsymbol{A} = \begin{pmatrix} -\alpha\tau & 0 & 0 & \ldots & w\tau \\ p\bar{\beta} & -p & 0 & \ldots & 0 \\ 0 & p & -p & \ldots & 0 \\ \vdots & \vdots & \ddots & \vdots & \vdots \\ 0 & 0 & \ldots & p & -p \end{pmatrix}.$$

Therefore the characteristic equation corresponding to the ODE system is given by

$$\Delta_{\text{ODE}}(\lambda) = \det(\lambda \boldsymbol{I} - \boldsymbol{A}) = \begin{vmatrix} \lambda + \alpha\tau & 0 & 0 & \ldots & -w\tau \\ -p\bar{\beta} & \lambda + p & 0 & \ldots & 0 \\ 0 & -p & \lambda + p & \ldots & 0 \\ \vdots & \vdots & \ddots & \vdots & \vdots \\ 0 & 0 & \ldots & -p & \lambda + p \end{vmatrix}.$$

Expanding the determinant over the first row, we get

$$\Delta_{\text{ODE}}(\lambda) = (\lambda + \alpha\tau) \begin{vmatrix} \lambda + p & 0 & \ldots & 0 \\ -p & \lambda + p & \ldots & 0 \\ \vdots & \vdots & \ddots & \vdots \\ 0 & 0 & -p & \lambda + p \end{vmatrix} + (-1)^{p+1} w\tau \begin{vmatrix} -p\bar{\beta} & \lambda + p & \ldots & 0 \\ 0 & -p & \lambda + p \ldots & 0 \\ \vdots & \vdots & \ddots & \vdots \\ 0 & 0 & \ldots & -p \end{vmatrix}.$$

Since the above two matrices are lower and upper triangular, respectively, we obtain

$$\Delta_{\text{ODE}}(\lambda) = (\lambda + \alpha\tau)(\lambda + p)^p + (-1)^{p+1} w\tau\bar{\beta}(-p)^p = (\lambda + \alpha\tau)(\lambda + p)^p - \beta\tau p^p = 0,$$

which has the same zeros as the characteristic equation (2.64) corresponding to the DDE (2.52). Therefore (2.52) and (2.63) are indeed equivalent in terms of linear stability.

In the next chapter, we will analyze the scalar DDE of the form (2.11) with a general distribution of delays in terms of its linear stability. We will develop a method of approximating the stability by using only the first few moments or cumulants of the distribution.

Chapter 3

Stability of the Scalar DDE with Distributed Delay

In this chapter we investigate the linear stability of the equilibrium points of the scalar DDE of the form (2.11) with one distributed delay via analysis of the characteristic equation. First we show what can be determined without choosing a particular distribution, or with minimal information about a distribution. Next we illustrate a way of approximating the region of stability when the actual distribution is not known, but some moments or cumulants of the distribution are. Finally, we compare the approximate stability regions with the stability regions for the uniform and gamma distributions and show that the approximations using cumulants give better results than the ones using moments. The results of this chapter have been already published in [10], but will be presented here in greater detail.

3.1 Distribution Independent Results

In this chapter we consider the scalar DDE,

$$\dot{x}(t) = \int_0^\infty f(x(t), x(t-u))g(u)\,du. \tag{3.1}$$

where the kernel $g(u)$ is a p.d.f. with mean delay $\tau > 0$. Since we will study the dependence of the linear stability of the equilibrium point on the mean delay, we transform the above equation so that the mean delay appears explicitly, as presented in Section 2.2,

$$x'(s) = \tau \int_0^\infty f(x(s), x(s-v))\hat{g}(v)\,dv, \tag{3.2}$$

where the scaled kernel $\hat{g}(v)$ is given in (2.10) and has mean delay 1.

We assume that the DDE (3.2) has an equilibrium point x^*, i.e.

$$0 = \tau \int_0^\infty f(x^*, x^*)\hat{g}(v)\, dv = f(x^*, x^*),$$

by (2.12). We let $y(s) = x(s) - x^*$ and linearizing (3.2) about x^*, as presented in Section (2.3), we obtain the scalar version of equation (2.16),

$$y'(s) = -\alpha y(s) + \beta \int_0^\infty y(s - v)\hat{g}(v)\, dv, \tag{3.3}$$

where $-\alpha$ is the derivative of f with respect to its first argument, and β is the derivative of f with respect to its second argument. We note that when $\alpha > 0$, (3.3) represents the linearization of the scalar Hopfield model we developed in Chapter 1. Thus, we chose the minus sign in front of α in order for model (3.3) to be consistent with system (1.16).

Setting $y(s) = ce^{\lambda s}$, we derive the characteristic equation

$$\Delta(\lambda) = \lambda + \alpha\tau - \beta\tau \int_0^\infty e^{-\lambda v}\hat{g}(v)\, dv = 0, \tag{3.4}$$

which represents the scalar version of (2.17). Using Definition 6, this can also be written as

$$\Delta(\lambda) = \lambda + \alpha\tau - \beta\tau\hat{G}(\lambda) = 0,$$

where $\hat{G}(\lambda)$ is the Laplace transform of $\hat{g}(v)$.

Changes of stability of the equilibrium point will take place when the characteristic equation has a root with zero real part. In the following we will describe where in the parameter space such changes may occur, and hence determine the region of stability of the equilibrium point. We will consider the parameter α as fixed and describe the stability region in the $\beta,\ \tau$ parameter space for the two cases: $\alpha > 0$ and $\alpha < 0$.

In the study of systems with discrete delays, it is common to describe the delay independent stability region. Such results give a conservative estimate of the stability region which is useful if one is unable to accurately estimate the time delay in the system. In this section we will formulate similar results for equation (3.2). In particular we will give one result which is independent of all aspects of the distribution and one which is independent of all aspects save the mean delay. This latter may be especially useful as the mean delay is often all one may be able to estimate for a particular system.

Before presenting our results, we state Rouché's Theorem [13] from Complex Variable Theory, which will be used to prove our first result. Its proof can be found in [13, page 313] and we will not reproduce it here. We present it as a lemma:

Lemma 1 *(Rouché) Let two functions $f_1(z)$ and $f_2(z)$ be analytic on and inside a simple closed contour C and assume that they do not reduce to zero at any point of C.*
If $|f_2(z)| < |f_1(z)|$ on C, then the functions $f_1(z)$ and $f_1(z) + f_2(z)$ have the same number of zeros inside the region bounded by C.

We now state and prove our first result which will help locate the region of stability of the equilibrium point.

Theorem 5 *Assume that $\hat{G}(\lambda)$ is analytic in $\mathrm{Re}(\lambda) \geq 0$, i.e. in the right-half complex plane. If $0 < |\beta| < \alpha$ then the characteristic equation has no roots with positive real part. If $0 < |\beta| < -\alpha$ then the characteristic equation has one root with positive real part.*

Proof. Let $f_1(\lambda) = \lambda + \alpha\tau$ and $f_2(\lambda) = -\beta\tau\hat{G}(\lambda)$, and consider the contour in the complex plane, $C = C_1 \cup C_2$, given by

$$C_1 : \ \lambda = Re^{i\theta}, \ -\frac{\pi}{2} \leq \theta \leq \frac{\pi}{2}$$

$$C_2 : \ \lambda = iy, \ -R \leq y \leq R,$$

where R is a positive real number. On C_1 we have $f_1(\lambda) = Re^{i\theta} + \alpha\tau$, thus

$$\begin{aligned} |f_1(\lambda)| &= |R\cos\theta + iR\sin\theta + \alpha\tau| \\ &= \sqrt{(R\cos\theta + \alpha\tau)^2 + R^2\sin^2\theta} \\ &= \sqrt{R^2 + \alpha^2\tau^2 + 2R\alpha\tau\cos\theta} \end{aligned}$$

But $R\alpha\tau\cos\theta \geq -|R\alpha\tau\cos\theta| = -R|\alpha|\tau|\cos\theta| \geq -R|\alpha|\tau$, and thus we have

$$|f_1(\lambda)| \geq \sqrt{R^2 + \alpha^2\tau^2 - 2R|\alpha|\tau} = \sqrt{(R - |\alpha|\tau)^2} = |R - |\alpha|\tau|. \tag{3.5}$$

Now, $f_2(\lambda) = -\beta\tau\hat{G}(Re^{i\theta})$. Thus

$$\begin{aligned} |f_2(\lambda)| &= \left| -\beta\tau \int_0^\infty e^{-Re^{i\theta}v}\hat{g}(v)\,dv \right| \\ &\leq |\beta|\tau \int_0^\infty |e^{-Re^{i\theta}v}|\hat{g}(v)\,dv, \end{aligned}$$

since $\hat{g}(v)$ is nonnegative. But

$$|e^{-Re^{i\theta}v}| = |e^{-Rv\cos\theta - iRv\sin\theta}| = e^{-Rv\cos\theta} \leq 1,$$

since $Rv\cos\theta \geq 0$ for $\theta \in [-\pi/2, \pi/2]$. Therefore

$$|f_2(\lambda)| \leq |\beta|\tau \int_0^\infty \hat{g}(v)\, dv = |\beta|\tau, \tag{3.6}$$

using the fact that $\hat{g}(v)$ is a p.d.f. From (3.5) and (3.6) we have that on C_1, $|f_1(\lambda)| > |f_2(\lambda)|$ for R sufficiently large.
On C_2, $f_1(\lambda) = iy + \alpha\tau$, therefore

$$|f_1(\lambda)| = |iy + \alpha\tau| = \sqrt{\alpha^2\tau^2 + y^2} \geq |\alpha|\tau. \tag{3.7}$$

Further $f_2(\lambda) = -\beta\tau\hat{G}(iy)$, thus

$$|f_2(\lambda)| = |-\beta\tau \int_0^\infty e^{-iyv}\hat{g}(v)\, dv| \leq |\beta|\tau \int_0^\infty |e^{-iyv}|\hat{g}(v)\, dv = |\beta|\tau. \tag{3.8}$$

Thus from (3.7) and (3.8) we have that on C_2, $|f_1(\lambda)| > |f_2(\lambda)|$ if $|\alpha| > |\beta|$.
Further, note that if $\alpha \neq 0$, and $\beta \neq 0$ then both f_1 and f_2 do not reduce to zero anywhere on C. Hence by Lemma 1, if $|\alpha| > |\beta| > 0$ and R is sufficiently large then $f_1(\lambda)$ and $\Delta(\lambda) = f_1(\lambda) + f_2(\lambda)$ have the same number of zeros inside C. Let $R \to \infty$ then $f_1(\lambda)$ and $\Delta(\lambda)$ have the same number of zeros with $\mathrm{Re}(\lambda) > 0$. Now $f_1(\lambda)$ has just one zero at $\lambda = -\alpha\tau$. Therefore, if $\alpha > 0$, $\Delta(\lambda)$ has no zeros in the right-half complex plane, and if $\alpha < 0$, $\Delta(\lambda)$ has one zero in the right-half complex plane. The results follow. □

From this theorem, we can conclude that the trivial solution of equation (3.3) (and hence the equilibrium point of equation (3.2)) is locally asymptotically stable if $\alpha > 0$ and $|\beta| < \alpha$ and unstable if $\alpha < 0$ and $|\beta| < -\alpha$.

We can next determine a region in the parameter space where the equilibrium point is unstable for any distribution $\hat{g}(v)$. The proof of the following result is similar to the proof of Theorem 3.1 in [1].

Theorem 6 *The equilibrium point of* (3.2) *is unstable when* $\beta > \alpha$.

Proof. Note that we only need to consider the case when $\beta > |\alpha|$, since from Theorem 5 we already have instability for $\alpha < \beta < -\alpha$ when $\alpha < 0$. We focus on the real roots of the characteristic equation (3.4), hence we assume $\Delta(\lambda) : \mathbb{R} \to \mathbb{R}$. Now

$$\frac{d\Delta(\lambda)}{d\lambda} = 1 + \beta\tau \int_0^\infty ve^{-\lambda v}\hat{g}(v)\, dv > 0, \tag{3.9}$$

since $\beta > 0$. Thus $\Delta(\lambda)$ is a strictly increasing function. For $\lambda = 0$ we have

$$\Delta(0) = \tau(\alpha - \beta) < 0,$$

since $\beta > \alpha$. If $\lambda \geq 0$ then $|e^{-\lambda v}| \leq 1$, and thus the integral term is bounded,

$$\int_0^\infty e^{-\lambda v}\hat{g}(v)\,dv \leq \left|\int_0^\infty e^{-\lambda v}\hat{g}(v)\,dv\right| \leq \int_0^\infty |e^{-\lambda v}|\hat{g}(v)\,dv \leq \int_0^\infty \hat{g}(v)\,dv = 1.$$

It follows that

$$\lim_{\lambda\to+\infty} \Delta(\lambda) = +\infty.$$

Since $\Delta(\lambda)$ is continuous, we conclude that $\Delta(\lambda)$ has a unique real root which is positive, i.e. the characteristic equation has at least one root with positive real part. The result follows. □

Some additional information about the stability region may be obtained from the characteristic equation (3.4). First note that the characteristic equation has a zero root if $\alpha - \beta = 0$, for any distribution. For $\alpha > 0$, from Theorems 5 and 6, stability is gained as this line is crossed by decreasing the parameter β, and thus the line $\beta = \alpha$ forms part of the boundary of the stability region. For $\alpha < 0$ we need to determine how the eigenvalue changes as this line is crossed in the parameter space. We will focus on varying the parameter β, the analysis for the variation of α is similar.

To begin, we note that from $\Delta(\lambda) = 0$ we have

$$\frac{d\Delta}{d\beta} = \frac{\partial\Delta}{\partial\beta} + \frac{\partial\Delta}{\partial\lambda}\frac{d\lambda}{d\beta} = 0,$$

and therefore

$$\frac{d\mathrm{Re}(\lambda)}{d\beta} = \mathrm{Re}\left(\frac{d\lambda}{d\beta}\right) = -\mathrm{Re}\left(\frac{\partial\Delta}{\partial\beta}\Big/\frac{\partial\Delta}{\partial\lambda}\right). \tag{3.10}$$

In particular, we need to evaluate this when $\lambda = 0$, i.e. along the line $\beta = \alpha$,

$$\begin{aligned}\left.\frac{d\mathrm{Re}(\lambda)}{d\beta}\right|_{\lambda=0,\ \beta=\alpha} &= -\mathrm{Re}\left(\left.\frac{\partial\Delta}{\partial\beta}\Big/\frac{\partial\Delta}{\partial\lambda}\right|_{\lambda=0,\beta=\alpha}\right)\\ &= -\mathrm{Re}\left(\left.\frac{-\tau\int_0^\infty e^{-\lambda v}\hat{g}(v)\,dv}{1+\beta\tau\int_0^\infty ve^{-\lambda v}\hat{g}(v)\,dv}\right|_{\lambda=0,\beta=\alpha}\right)\\ &= \frac{\tau}{1+\alpha\tau},\end{aligned}$$

since $\hat{g}(v)$ is a p.d.f. with mean delay 1. From this it is easy to conclude that

$$\frac{d\mathrm{Re}(\lambda)}{d\beta} \lesseqgtr 0 \text{ along the line } \beta = \alpha, \text{ with } \alpha < 0 \text{ and } \tau \lesseqgtr -\frac{1}{\alpha}. \tag{3.11}$$

It follows that for $\alpha < 0$ and $\tau < -1/\alpha$, the equilibrium point becomes stable as β is decreased through the line $\beta = \alpha$. Hence, for $\alpha < 0$ the line segment $\beta = \alpha$, $\tau < -1/\alpha$ forms part of the stability boundary.

We also note that from (2.13) and (3.9) we have

$$\left.\frac{d\Delta(\lambda)}{d\lambda}\right|_{\beta=\alpha,\ \tau=-1/\alpha} = 1 - \int_0^\infty v\hat{g}(v)\,dv = 0,$$

since the point $(\alpha, -1/\alpha)$ is on the line $\beta = \alpha$ corresponding to the characteristic equation having one zero root (i.e. $\lambda = 0$). Thus the point $(\alpha, -1/\alpha)$ is always a double zero root of the characteristic equation for any distribution.

To further define the boundary of stability, we need to determine where the characteristic equation has a pair of pure imaginary roots, $\pm i\omega$. This occurs when we set $\lambda = i\omega, \omega > 0$ in the characteristic equation (3.4), i.e.,

$$i\omega + \alpha\tau - \beta\tau \int_0^\infty e^{-i\omega v}\hat{g}(v)\,dv = 0. \tag{3.12}$$

Separating this into real and imaginary parts, we find that for the characteristic equation to have a pair of pure imaginary roots, the parameters must satisfy the following equations

$$\begin{array}{rcl} \alpha\tau &=& \beta\tau \int_0^\infty \cos(\omega v)\,\hat{g}(v)\,dv \stackrel{\text{def}}{=} \beta\tau C(\omega), \\ -\omega &=& \beta\tau \int_0^\infty \sin(\omega v)\,\hat{g}(v)\,dv \stackrel{\text{def}}{=} \beta\tau S(\omega). \end{array} \tag{3.13}$$

Fixing α, we can formally define curves, parameterized by ω, in the $\beta\tau$-plane along which the equations in (3.13) are satisfied. These curves are given by

$$\beta = \frac{\alpha}{C(\omega)}, \qquad \tau = -\frac{\omega C(\omega)}{\alpha S(\omega)}, \tag{3.14}$$

for all $\omega > 0$ such that $C(\omega)$ and $S(\omega)$ are nonzero. The values of ω such that $C(\omega) = 0$ or $S(\omega) = 0$ define discontinuities in the curves and do not correspond to roots of the characteristic equation (3.12). In the light of Theorems 5 and 6, the curves in (3.14) that form part of the stability boundary must lie in the region $\beta \le -|\alpha|$.

To obtain explicit expressions for the curves given in (3.14), we need to evaluate $C(\omega)$ and $S(\omega)$ which requires knowledge of the distribution $\hat{g}(v)$. We can, however, determine how the number of eigenvalues changes as one crosses one of these curves. Taking the derivative of τ in (3.14) with respect to ω we obtain

$$\frac{d\tau}{d\omega} = -\frac{1}{\alpha S(\omega)}\left(C(\omega) + \omega\frac{C'(\omega)S(\omega) - S'(\omega)C(\omega)}{S(\omega)}\right). \tag{3.15}$$

From equations (3.12) and (3.13), the characteristic equation when $\lambda = i\omega$ can be written as

$$0 = \Delta(i\omega) = i\omega + \alpha\tau - \beta\tau\left(C(\omega) - iS(\omega)\right) \tag{3.16}$$
$$= \alpha\tau - \beta\tau C(\omega) + i[\omega + \beta\tau S(\omega)] \tag{3.17}$$
$$= U(\omega) + iV(\omega). \tag{3.18}$$

Using this, we compute the rate of change of the real part of λ with respect to β. From (3.16) we have

$$\frac{\partial\Delta}{\partial\beta} = -\tau C(\omega) + i\tau S(\omega).$$

Since λ is a complex number, from (3.17) and (3.18) we get

$$\frac{\partial\Delta}{\partial\lambda} = \frac{dV}{d\omega} - i\frac{dU}{d\omega} = 1 + \beta\tau S'(\omega) + i\beta\tau C'(\omega).$$

Substituting these into (3.10) and evaluating the expression along the curves where $\lambda = i\omega$, we get

$$\begin{aligned}
\left.\frac{d\mathrm{Re}(\lambda)}{d\beta}\right|_{\lambda=i\omega} &= -\mathrm{Re}\left(\frac{\partial\Delta}{\partial\beta}\Big/\left.\frac{\partial\Delta}{\partial\lambda}\right|_{\lambda=i\omega}\right) \\
&= -\mathrm{Re}\left(\frac{-\tau(C(\omega) - iS(\omega))}{1 + \beta\tau S'(\omega) + i\beta\tau C'(\omega)}\right) \\
&= \tau\mathrm{Re}\left(\frac{C(\omega) - iS(\omega)}{(1 + \beta\tau S'(\omega)) + i\beta\tau C'(\omega)}\right) \\
&= \frac{\tau}{H^2(\omega)}\left(C(\omega) + \beta\tau C(\omega)S'(\omega) - \beta\tau S(\omega)C'(\omega)\right) \\
&= \frac{\tau}{H^2(\omega)}\left(C(\omega) + \omega\frac{C'(\omega)S(\omega) - S'(\omega)C(\omega)}{S(\omega)}\right),
\end{aligned} \tag{3.19}$$

where $H^2(\omega) = (1 + \beta\tau S'(\omega))^2 + (\beta\tau C'(\omega))^2$ is a positive function of ω and we have used $\beta\tau = -\omega/S(\omega)$ from (3.14). Comparing (3.19) with (3.15) we obtain

$$\left.\frac{d\mathrm{Re}(\lambda)}{d\beta}\right|_{\lambda=i\omega} = \frac{\alpha}{\beta}\frac{\omega}{H^2(\omega)}\frac{d\tau}{d\omega}, \tag{3.20}$$

since $\tau S(\omega) = -\omega/\beta$, again from (3.14). Thus whether the number of eigenvalues with positive real part is increasing or decreasing as β is increased through a point on one of the curves defined by (3.14) depends on the sign of α and whether τ is an increasing or decreasing function of ω at that point (since the curves in (3.14) only form part of the stability boundary for β negative).

We can also obtain the following distribution independent results.

Theorem 7 *Under the conditions of Theorem 5, the equilibrium point of* (3.2) *is locally asymptotically stable in the following regions of parameter space*

$$(1)\ |\beta| < \alpha$$
$$(2)\ \beta \leq -|\alpha|\ \textit{and}\ 0 < \tau < -\frac{1}{\beta}.$$

Proof. Result (1) follows from Theorem 5 and the subsequent discussion. To see (2), consider equations (3.13). From the first equation, we have

$$\left|\frac{\alpha}{\beta}\right| \leq \int_0^\infty |\cos(\omega v)|\hat{g}(v)\,dv \leq \int_0^\infty \hat{g}(v)\,dv = 1.$$

While from the second equation, we have

$$\left|-\frac{1}{\beta\tau}\right| \leq \int_0^\infty \left|\frac{\sin(\omega v)}{\omega v}\right| v\hat{g}(v)\,dv \leq \int_0^\infty v\hat{g}(v)\,dv = 1.$$

Thus equations (3.13) have a solution only if $|\beta| \geq |\alpha|$ and $\tau \geq 1/|\beta|$. In particular, for $\beta < 0$ this means the system cannot have pure imaginary roots if $\beta \leq -|\alpha|$ and $\tau < -1/\beta$ and hence for this range of β, the stability cannot change. Result (2) follows. □

We note that, in the case $\alpha > 0$, the second result of this theorem is similar to Theorem 9 in [53], although we have proven it in a different way.

The results of Theorems 6 and 7 are illustrated in Figure 3.1.

Theorem 7 describes the region of stability of the equilibrium point with either no knowledge of the distribution of delays or knowledge of only the first moment of the distribution, i.e. the mean delay, τ. From the proof of Theorem 7, it is clear that the curves given by equations (3.14) must lie outside the stability region described by the theorem. Thus this region is only a conservative estimate of the full region in the parameter space where the equilibrium point is stable. In the next section we will show how one may improve this approximation by using more information from the distribution. We note that it is only necessary to consider $\beta \leq -|\alpha|$, given the results of Theorems 6 and 7.

3.2 Approximating the Boundary of the Stability Region

In practice, we may not know the exact distribution of delays in a system, however, we may be able to determine some statistical properties of the distribution. In the following we

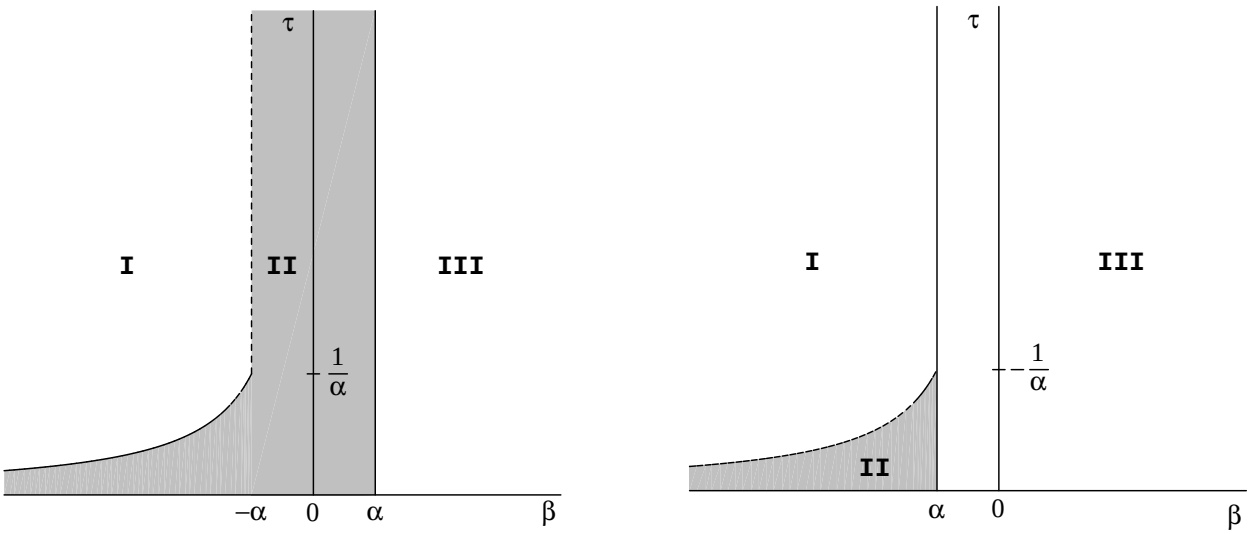

(a) $\alpha > 0$ (b) $\alpha < 0$

Figure 3.1: Illustration of the distribution independent stability results described by Theorems 6 and 7. (I) No distribution independent stability results are known for this region. (II) Region of stability described by Theorem 7. (III) Region of instability described by Theorem 6.

show how to approximate the true boundary of stability, using only the first few moments or cumulants of the distribution. In the previous section, we established that the boundary of the stability region (in the $\beta\tau$-plane) consists of all or part of the line $\beta = \alpha$ and the curve(s) defined parametrically by equations (3.14) for $\beta \leq -|\alpha|$. In this section, we shall show how partial knowledge of the distribution, $\hat{g}(v)$, can allow us to approximate these latter curves.

3.2.1 Approximations using Moments

In this subsection we present a method of approximating $C(\omega)$ and $S(\omega)$ given in (3.13) in terms of the moments of $\hat{g}(v)$. Thus we show how we can determine curves in the $\beta\tau$-plane that approximate the curves in (3.14), which form part of the true stability boundary.

We start by expanding the moment-cumulant generating function $M(t)$ given in (2.21) in its Taylor series about $t = 0$,

$$M(t) = \int_0^\infty e^{itv}\hat{g}(v)\,dv = \sum_{n=0}^{\infty} \frac{d^n}{dt^n}M(t)\bigg|_{t=0} \frac{t^n}{n!} = \sum_{n=0}^{\infty} i^n m_n \frac{t^n}{n!}, \tag{3.21}$$

using (2.22). The radius of convergence of the above series is given by [48]

$$R = \limsup_{n\to\infty} \left| \frac{m_n}{n!}\frac{(n+1)!}{m_{n+1}} \right| = \limsup_{n\to\infty} \frac{(n+1)m_n}{m_{n+1}}.$$

If the above limit exists, the series in (3.21) converges for $|t| < R$.

Substituting $t = -\omega$ into (3.21), we can then relate the integral term in the characteristic equation (3.12) to the moments of $\hat{g}(v)$ as follows,

$$\begin{aligned}
\int_0^\infty e^{-i\omega v}\hat{g}(v)\,dv &= \sum_{n=0}^{\infty}(-1)^n i^n m_n \frac{\omega^n}{n!} \\
&= m_0 - im_1\omega + i^2 m_2\frac{\omega^2}{2!} - i^3 m_3\frac{\omega^3}{3!} + i^4 m_4\frac{\omega^4}{4!} - i^5 m_5\frac{\omega^5}{5!} + \cdots \\
&= m_0 - im_1\omega - m_2\frac{\omega^2}{2!} + im_3\frac{\omega^3}{3!} + m_4\frac{\omega^4}{4!} - im_5\frac{\omega^5}{5!} - \cdots \\
&= \left(m_0 - m_2\frac{\omega^2}{2!} + m_4\frac{\omega^4}{4!} - \cdots\right) - i\left(m_1\omega - m_3\frac{\omega^3}{3!} + m_5\frac{\omega^5}{5!} - \cdots\right) \\
&= \sum_{n=0}^{\infty}\frac{(-1)^n\omega^{2n}}{(2n)!}m_{2n} - i\sum_{n=0}^{\infty}\frac{(-1)^n\omega^{2n+1}}{(2n+1)!}m_{2n+1}.
\end{aligned} \tag{3.22}$$

From the definitions of $C(\omega)$ and $S(\omega)$ in (3.13), we have

$$\begin{aligned}
C(\omega) &= \mathrm{Re}\left(\int_0^\infty e^{-i\omega v}\hat{g}(v)\,dv\right), \\
S(\omega) &= -\mathrm{Im}\left(\int_0^\infty e^{-i\omega v}\hat{g}(v)\,dv\right).
\end{aligned} \tag{3.23}$$

Using this and (3.22), we obtain

$$\begin{aligned} C(\omega) &= \sum_{n=0}^{\infty} \frac{(-1)^n \omega^{2n}}{(2n)!} m_{2n}, \\ S(\omega) &= \sum_{n=0}^{\infty} \frac{(-1)^n \omega^{2n+1}}{(2n+1)!} m_{2n+1}. \end{aligned} \tag{3.24}$$

The radius of convergence of the series for $C(\omega)$ is given by

$$R_C = \limsup_{n\to\infty} \left| \frac{m_{2n}}{(2n)!} \frac{(2n+2)!}{m_{2n+2}} \right| = \limsup_{n\to\infty} \frac{(2n+1)(2n+2)m_{2n}}{m_{2n+2}},$$

and for $S(\omega)$ is given by

$$R_S = \limsup_{n\to\infty} \left| \frac{m_{2n+1}}{(2n+1)!} \frac{(2n+3)!}{m_{2n+3}} \right| = \limsup_{n\to\infty} \frac{(2n+2)(2n+3)m_{2n+1}}{m_{2n+3}}.$$

Truncating the series for $C(\omega)$ in (3.24) up to M terms and the series for $S(\omega)$ up to N terms, we obtain the following approximations for $C(\omega)$ and $S(\omega)$ in terms of the moments,

$$C(\omega) \approx \sum_{n=0}^{M} \frac{(-1)^n \omega^{2n}}{(2n)!} m_{2n} \qquad \text{and} \qquad S(\omega) \approx \sum_{n=0}^{N} \frac{(-1)^n \omega^{2n+1}}{(2n+1)!} m_{2n+1}. \tag{3.25}$$

Thus we define approximation (M, N) as the approximation for $C(\omega)$ and $S(\omega)$ if we use the first M terms in the series for $C(\omega)$ and the first N terms in the series for $S(\omega)$. We note that these approximations should improve as ω approaches 0 or as M and N increase. We note that the above approximations will only be useful for $\omega < \bar{R}$, where $\bar{R} = \min\{R_C, R_S\}$.

For example, in the case of the gamma distribution, substituting the expression for the moments given in (2.40), we obtain

$$\begin{aligned} R_C &= \limsup_{n\to\infty} \frac{(2n+1)(2n+2)}{p^{-2}(2n+p)(2n+p+1)} = p^2, \\ R_S &= \limsup_{n\to\infty} \frac{(2n+2)(2n+3)}{p^{-2}(2n+p+1)(2n+p+2)} = p^2. \end{aligned}$$

Thus for the gamma distribution, the approximations are only useful for $\omega < p^2$.

For the uniform distribution, we first rewrite the expressions for the moments given in (2.33) as

$$m_n = \frac{\left(1+\frac{\rho}{2}\right)^{n+1}(1-K^{n+1})}{(n+1)\rho}, \text{ where } K = \frac{1-\rho/2}{1+\rho/2}, \text{ and } K \in [0,1).$$

Therefore we have

$$\begin{aligned} R_C &= \limsup_{n\to\infty} \frac{(2n+1)(2n+2)\left(1+\frac{\rho}{2}\right)^{2n+1}(1-K^{2n+1})}{(2n+1)\rho} \frac{(2n+3)\rho}{\left(1+\frac{\rho}{2}\right)^{2n+3}(1-K^{2n+3})} \\ &= \limsup_{n\to\infty} \frac{(2n+2)(2n+3)}{\left(1+\frac{\rho}{2}\right)^{2}} \\ &= \infty, \end{aligned}$$

and

$$\begin{aligned} R_S &= \limsup_{n\to\infty} \frac{(2n+2)(2n+3)\left(1+\frac{\rho}{2}\right)^{2n+2}(1-K^{2n+2})}{(2n+2)\rho} \frac{(2n+4)\rho}{\left(1+\frac{\rho}{2}\right)^{2n+4}(1-K^{2n+4})} \\ &= \limsup_{n\to\infty} \frac{(2n+3)(2n+4)}{\left(1+\frac{\rho}{2}\right)^{2}} \\ &= \infty. \end{aligned}$$

Since both R_C and R_S approach infinity in the case of the uniform distribution, the two series in (3.24) converge for any $\omega > 0$.

In the case of the Dirac distribution, from Section 2.4.1 we have that $m_n = 1$ for all $n = 0, 1, 2, \ldots$. Substituting this into (3.24), we get that $C(\omega) = \cos(\omega)$ and $S(\omega) = \sin(\omega)$. As for the uniform distribution, the two radii of convergence approach infinity, and therefore the approximations are defined for any $\omega > 0$. Next, we substitute (2.30) into (3.23) to get

$$\begin{aligned} C(\omega) &= \mathrm{Re}\left(\int_0^\infty e^{-i\omega v}\tau\delta(\tau v - \tau)\,dv\right) \\ &= \mathrm{Re}\left(\int_0^\infty e^{-i\omega u/\tau}\tau\delta(u-\tau)\frac{1}{\tau}\,du\right) \qquad (\text{where } u = \tau v) \\ &= \mathrm{Re}\left(e^{-i\omega\tau/\tau}\right) \qquad (\text{by property (2.8)}) \\ &= \mathrm{Re}\left(e^{-i\omega}\right) \\ &= \cos(\omega). \end{aligned}$$

Similarly we get $S(\omega) = -\mathrm{Im}\left(e^{-i\omega}\right) = \sin(\omega)$. Therefore, for the Dirac distribution, the approximations using moments in (3.25) represent the truncated Taylor series expansions for $C(\omega)$ and $S(\omega)$. When all the moments are substituted, we then recover the exact expression for $C(\omega)$ and $S(\omega)$ given in (3.23).

When the distribution is not known, but with knowledge of some moments of $\hat{g}(v)$, we may obtain an approximation for the curve(s) in (3.14). The results for different cases are summarized in Table 3.1, where we used the fact that $m_0 = m_1 = 1$.

Table 3.1: Approximations using moments for $C(\omega)$, $S(\omega)$ and equations (3.14), where M and N relate to the number of terms used in the summation for $C(\omega)$ and $S(\omega)$, respectively.

(M,N)	$C(\omega)$	$S(\omega)$	β	τ
$(0,0)$	1	ω	α	$-\dfrac{1}{\alpha}$
$(0,1)$	1	$\omega - \dfrac{m_3}{6}\omega^3$	α	$\dfrac{6}{\alpha(m_3\omega^2-6)}$
$(1,0)$	$1-\dfrac{m_2}{2}\omega^2$	ω	$\dfrac{2\alpha}{2-m_2\omega^2}$	$\dfrac{m_2\omega^2-2}{2\alpha}$
$(1,1)$	$1-\dfrac{m_2}{2}\omega^2$	$\omega - \dfrac{m_3}{6}\omega^3$	$\dfrac{2\alpha}{2-m_2\omega^2}$	$\dfrac{3(m_2\omega^2-2)}{\alpha(6-m_3\omega^2)}$

In particular, we see that approximation $(0,0)$ is just the single point $(\alpha, -1/\alpha)$ in the $\beta\tau$-plane, which corresponds to the characteristic equation having a double zero root. Since $\tau > 0$, this approximation exists only for $\alpha < 0$. For both positive or negative α, this approximation predicts that the region of stability is the entire half plane to the left of the line $\beta = \alpha$.

When $\alpha > 0$, approximation $(0,1)$ represents the line $\beta = \alpha$ and thus it predicts no stability region. When $\alpha < 0$, since $m_3 > 0$ (by the definition in (2.20)), we have

$$1 - \frac{m_3\omega^2}{6} \leq 1 \qquad \text{or} \qquad \frac{6}{6 - m_3\omega^2} \geq 1, \text{ for } \omega \geq \sqrt{\frac{6}{m_3}}.$$

Multiplying by $-1/\alpha$ we get

$$\tau = \frac{6}{\alpha(m_3\omega^2 - 6)} \geq -\frac{1}{\alpha}.$$

Hence, when $\alpha < 0$, approximation $(0,1)$ represents the line $\beta = \alpha$ with $\tau \geq -1/\alpha$. Therefore for negative α, this approximation predicts the region below the horizontal line $\tau = -1/\alpha$ and to the left of the vertical line $\beta = \alpha$ is stable, whereas the region above the horizontal line $\tau = -1/\alpha$ and to the left of the vertical line $\beta = \alpha$ is unstable.

For approximation $(1,0)$, from the expression for β in Table 3.1 we obtain

$$\omega^2 = \frac{2}{m_2}\left(1 - \frac{\alpha}{\beta}\right). \tag{3.26}$$

Thus in the $\beta\tau$-plane, approximation $(1,0)$ using moments is given by

$$\tau^m_{(1,0)} = -\frac{1}{\beta}, \qquad \omega = \sqrt{\frac{2}{m_2}\left(1 - \frac{\alpha}{\beta}\right)}, \tag{3.27}$$

where, for $\alpha < 0$ we require $\beta \leq \alpha$ in order for ω to be defined. We note that approximation $(1,0)$ always underestimates the region of stability. For $\beta \leq -|\alpha|$, this approximation recovers the results of Theorem 7. For $\beta > -\alpha$ ($\alpha > 0$) the curve enters the region of distribution independent stability and thus gives a worse estimate than Theorem 7.

For approximation $(1,1)$, we substitute (3.26) and $m_2\omega - 2 = -2\alpha/\beta$ into the expression for τ to obtain

$$\tau = -\frac{6\alpha/\beta}{\alpha[6 - 2m_3(\beta-\alpha)/(m_2\beta)]} = -\frac{1}{\beta - \frac{m_3}{3m_2}(\beta-\alpha)} = -\frac{1}{\left(1 - \frac{m_3}{3m_2}\right)\beta + \frac{m_3}{3m_2}\alpha}.$$

Therefore in the $\beta\tau$-plane, approximation $(1,1)$ using moments is given by

$$\tau^m_{(1,1)} = -\frac{1}{\left(1 - \frac{m_3}{3m_2}\right)\beta + \frac{m_3}{3m_2}\alpha}, \qquad \omega = \sqrt{\frac{2}{m_2}\left(1 - \frac{\alpha}{\beta}\right)}, \tag{3.28}$$

where, again for $\alpha < 0$, we require $\beta \leq \alpha$ in order for ω to be defined. Approximation $(1,1)$ is a hyperbola with a vertical asymptote at $\beta = \nu\alpha/(\nu-1)$, where $\nu = m_3/(3m_2) > 0$ (since the moments are positive). The relationship between approximation $(1,1)$ and the results of Theorem 7 will depend on the value of ν, and hence on the moments of the particular distribution. However, for large β, we can say that if $\nu < 1$ then

$$1 \leq \frac{1}{1 - \nu + \nu\alpha/\beta},$$

since $\nu\alpha/\beta \to 0$ as $\beta \to \infty$. Dividing the above inequality by $-\beta$ we get that

$$\tau^m_{(1,0)} = -\frac{1}{\beta} \leq -\frac{1}{(1-\nu)\beta + \nu\alpha} = \tau^m_{(1,1)},$$

Therefore if $\nu < 1$, then for large β, approximation $(1,1)$ always lies above approximation $(1,0)$.

For $\alpha > 0$, the curve in (3.28) enters the region $\beta < |\alpha|$ if its vertical asymptote is to the right of the line $\beta = -\alpha$, i.e. if

$$\frac{\nu\alpha}{\nu - 1} > -\alpha \quad \Leftrightarrow \quad \frac{\nu}{1-\nu} < 1.$$

Thus, for $\alpha > 0$, the curve given by approximation $(1,1)$ enters the region of distribution-independent stability if $\nu \in (0, 1/2) \cup (1, \infty)$.

In the next subsection we approximate the boundary of stability where $\lambda = i\omega$ using the cumulants of $\hat{g}(v)$.

3.2.2 Approximations using Cumulants

In this subsection we approximate the curves in (3.14), which form part of the true boundary of stability of the equilibrium of (3.2), using the first few cumulants of $\hat{g}(v)$. We start by expanding $\ln M(t)$ in its Taylor series around zero,

$$\ln M(t) = \sum_{n=0}^{\infty} \frac{d^n}{dt^n} \ln M(t)\bigg|_{t=0} \frac{t^n}{n!} = \sum_{n=0}^{\infty} i^n \kappa_n \frac{t^n}{n!},$$

by (2.24). Exponentiating and using (2.21), we get

$$\int_0^{\infty} e^{itv} \hat{g}(v)\, dv = \exp\left[\sum_{n=0}^{\infty} i^n \kappa_n \frac{t^n}{n!}\right],$$

We then substitute $t = -\omega$ into this to obtain a relationship between the integral term in the characteristic equation (3.12) and the cumulants of $\hat{g}(v)$,

$$\begin{aligned}
\int_0^{\infty} e^{-i\omega v} \hat{g}(v)\, dv &= \exp\left[\sum_{n=0}^{\infty} (-1)^n i^n \kappa_n \frac{\omega^n}{n!}\right] \\
&= \exp\left[\sum_{n=0}^{\infty} \frac{(-1)^n \omega^{2n}}{(2n)!} \kappa_{2n} - i \sum_{n=0}^{\infty} \frac{(-1)^n \omega^{2n+1}}{(2n+1)!} \kappa_{2n+1}\right] \\
&= \exp\left[\sum_{n=0}^{\infty} \frac{(-1)^n \omega^{2n}}{(2n)!} \kappa_{2n}\right] \cos\left[\sum_{n=0}^{\infty} \frac{(-1)^n \omega^{2n+1}}{(2n+1)!} \kappa_{2n+1}\right] \\
&\quad - i \exp\left[\sum_{n=0}^{\infty} \frac{(-1)^n \omega^{2n}}{(2n)!} \kappa_{2n}\right] \sin\left[\sum_{n=0}^{\infty} \frac{(-1)^n \omega^{2n+1}}{(2n+1)!} \kappa_{2n+1}\right].
\end{aligned}$$

Using (3.23), we then obtain

$$\begin{aligned}
C(\omega) &= \exp\left[\sum_{n=0}^{\infty} \frac{(-1)^n \omega^{2n}}{(2n)!} \kappa_{2n}\right] \cos\left[\sum_{n=0}^{\infty} \frac{(-1)^n \omega^{2n+1}}{(2n+1)!} \kappa_{2n+1}\right], \\
S(\omega) &= \exp\left[\sum_{n=0}^{\infty} \frac{(-1)^n \omega^{2n}}{(2n)!} \kappa_{2n}\right] \sin\left[\sum_{n=0}^{\infty} \frac{(-1)^n \omega^{2n+1}}{(2n+1)!} \kappa_{2n+1}\right].
\end{aligned} \tag{3.29}$$

The radius of convergence of the series inside the exponential function is given by

$$R_1 = \limsup_{n\to\infty} \left| \frac{\kappa_{2n}}{(2n)!} \frac{(2n+2)!}{\kappa_{2n+2}} \right| = \limsup_{n\to\infty} \frac{(2n+1)(2n+2)\kappa_{2n}}{\kappa_{2n+2}},$$

Table 3.2: Approximations using cumulants for $C(\omega)$, $S(\omega)$ and equations (3.14), where M is the numbers of terms used in the sum inside the exponential function in (3.30), and N is the numbers of terms used in the sum inside the sine and cosine functions in (3.30).

(M,N)	$C(\omega)$	$S(\omega)$	β	τ
$(0,0)$	$\cos(\omega)$	$\sin(\omega)$	$\dfrac{\alpha}{\cos(\omega)}$	$-\dfrac{\omega\cos(\omega)}{\alpha\sin(\omega)}$
$(0,1)$	$\cos\left(\omega-\frac{\kappa_3}{6}\omega^3\right)$	$\sin\left(\omega-\frac{\kappa_3}{6}\omega^3\right)$	$\dfrac{\alpha}{\cos\left(\omega-\frac{\kappa_3\omega^3}{6}\right)}$	$-\dfrac{\omega\cos\left(\omega-\frac{\kappa_3\omega^3}{6}\right)}{\alpha\sin\left(\omega-\frac{\kappa_3\omega^3}{6}\right)}$
$(1,0)$	$\dfrac{\cos(\omega)}{\exp\left(\frac{\kappa_2}{2}\omega^2\right)}$	$\dfrac{\sin(\omega)}{\exp\left(\frac{\kappa_2}{2}\omega^2\right)}$	$\dfrac{\alpha\exp\left(\frac{\kappa_2\omega^2}{2}\right)}{\cos(\omega)}$	$-\dfrac{\omega\cos(\omega)}{\alpha\sin(\omega)}$
$(1,1)$	$\dfrac{\cos\left(\omega-\frac{\kappa_3\omega^3}{6}\right)}{\exp\left(\frac{\kappa_2}{2}\omega^2\right)}$	$\dfrac{\sin\left(\omega-\frac{\kappa_3\omega^3}{6}\right)}{\exp\left(\frac{\kappa_2}{2}\omega^2\right)}$	$\dfrac{\alpha\exp\left(\frac{\kappa_2\omega^2}{2}\right)}{\cos\left(\omega-\frac{\kappa_3\omega^3}{6}\right)}$	$-\dfrac{\omega\cos\left(\omega-\frac{\kappa_3\omega^3}{6}\right)}{\alpha\sin\left(\omega-\frac{\kappa_3\omega^3}{6}\right)}$

and the radius of convergence of the series inside the cosine and sine functions is given by

$$R_2 = \limsup_{n\to\infty}\left|\frac{\kappa_{2n+1}}{(2n+1)!}\frac{(2n+3)!}{\kappa_{2n+3}}\right| = \limsup_{n\to\infty}\frac{(2n+2)(2n+3)\kappa_{2n+1}}{\kappa_{2n+3}}.$$

By truncating the sum inside the exponential function up to M terms and the sums inside the sine and cosine functions up to N terms in (3.29), we obtain the following approximations for $C(\omega)$ and $S(\omega)$ in terms of cumulants,

$$\begin{aligned} C(\omega) &\approx \exp\left[\sum_{n=0}^{M}\frac{(-1)^n\omega^{2n}}{(2n)!}\kappa_{2n}\right]\cos\left[\sum_{n=0}^{N}\frac{(-1)^n\omega^{2n+1}}{(2n+1)!}\kappa_{2n+1}\right], \\ S(\omega) &\approx \exp\left[\sum_{n=0}^{M}\frac{(-1)^n\omega^{2n}}{(2n)!}\kappa_{2n}\right]\sin\left[\sum_{n=0}^{N}\frac{(-1)^n\omega^{2n+1}}{(2n+1)!}\kappa_{2n+1}\right]. \end{aligned} \tag{3.30}$$

We note that these approximations are only useful for $\omega < \hat{R}$, where $\hat{R} = \min\{R_1, R_2\}$. The first four approximations using cumulants can be seen in Table 3.2, where we used the fact that $\kappa_0 = 0$ and $\kappa_1 = 1$.

In the previous subsection, we showed that when the kernel is a Dirac distribution,

$$C(\omega) = \cos(\omega) \qquad \text{and} \qquad S(\omega) = \sin(\omega). \tag{3.31}$$

These are exactly the values for $C(\omega)$ and $S(\omega)$ from the first row of Table 3.2 and thus approximation $(0,0)$ using cumulants recovers the results for the corresponding equation

with one fixed delay τ, i.e. model (3.1) where $g(u) = \delta(u - \tau)$,

$$\dot{x}(t) = \int_0^\infty f(x(t), x(t-u))\delta(u-\tau)\,du = f(x(t), x(t-\tau)). \tag{3.32}$$

We also note that, since from Section 2.4.1 we have that $\kappa_n = 0$ for all $n = 2, 3, \ldots$, all approximations using cumulants for the Dirac distribution are the same and equal to approximation $(0, 0)$. Substituting (3.31) into (3.13), we have

$$\begin{aligned} \alpha\tau &= \beta\tau\cos(\omega), \\ -\omega &= \beta\tau\sin(\omega). \end{aligned}$$

From the first equation we have that

$$\omega = \arccos(\alpha/\beta) + 2j\pi, \qquad j \in \mathbb{Z}, \tag{3.33}$$

with the restriction $\beta < -|\alpha|$ in order for the arccosine function to be defined. Squaring and adding the two equations we get $\alpha^2\tau^2 + \omega^2 = \beta^2\tau^2$. Solving for τ and substituting (3.33) we obtain approximation $(0, 0)$ to be

$$\tau^\kappa_{(0,0)} = \frac{1}{\sqrt{\beta^2 - \alpha^2}} \arccos\left(\frac{\alpha}{\beta}\right), \qquad \beta < -|\alpha|. \tag{3.34}$$

In the above expression we have used (3.33) with $j = 0$ in order for the curve in (3.34) to be in the second quadrant and the closest to the β-axis, i.e. we chose the curve that forms part of the boundary of the stability region. We note that since the above curve is only defined for $\beta < -|\alpha|$, it never enters the distribution independent region of stability, $|\beta| < \alpha$ described by result (1) of Theorem 7. For $\alpha > 0$, $-1 < \alpha/\beta < 0$ and thus $\arccos(\alpha/\beta) > \pi/2 > 1$. Therefore

$$\tau^m_{(1,0)} = -\frac{1}{\beta} \leq \frac{1}{\sqrt{\beta^2 - \alpha^2}} < \frac{1}{\sqrt{\beta^2 - \alpha^2}} \arccos\left(\frac{\alpha}{\beta}\right) = \tau^\kappa_{(0,0)}.$$

Hence, for $\alpha > 0$, we can conclude that approximation $(0, 0)$ using cumulants always lies above approximation $(1, 0)$ using moments. We also notice that

$$\lim_{\beta\to-\alpha^-} \tau^\kappa_{(0,0)} = \frac{\pi}{0^+} = +\infty, \tag{3.35}$$

i.e. the curve described by (3.34) with $\alpha > 0$ has a vertical asymptote at $\beta = -\alpha$. For $\alpha < 0$, we have that

$$\begin{aligned} \lim_{\beta\to\alpha^-} \tau^\kappa_{(0,0)} &= \lim_{\beta\to\alpha^-} -\frac{1}{\sqrt{1 - \alpha^2/\beta^2}} \left(-\frac{\alpha}{\beta^2}\right) \frac{2\sqrt{\beta^2 - \alpha^2}}{2\beta} \\ &= \lim_{\beta\to\alpha^-} \frac{-\beta}{\sqrt{\beta^2 - \alpha^2}} \frac{\alpha}{\beta^2} \frac{\sqrt{\beta^2 - \alpha^2}}{\beta} \\ &= -\frac{1}{\alpha}. \end{aligned}$$

Thus when $\alpha < 0$, we can only conclude that approximation $(0,0)$ using cumulants approaches $-1/\alpha$ as $\beta \to \alpha^-$. We note that for distributions symmetric around their mean (like the uniform distribution for example), by Theorem 4.0.5 from [7], approximation $(0,0)$ using cumulants represents a conservative boundary of stability, i.e. if $\tau < \tau^{\kappa}_{(0,0)}$ then the equilibrium point x^* of (3.2) is locally asymptotically stable.

For approximation $(0,1)$, we substitute the values of $C(\omega)$ and $S(\omega)$ from Table 3.2 into (3.13) to get

$$\begin{array}{rcl} \alpha\tau & = & \beta\tau\cos\left(\omega - \frac{\kappa_3}{6}\omega^3\right), \\ -\omega & = & \beta\tau\sin\left(\omega - \frac{\kappa_3}{6}\omega^3\right). \end{array} \tag{3.36}$$

Squaring and adding the two equations we have $\alpha^2\tau^2 + \omega^2 = \beta^2\tau^2$, and thus

$$\omega = \tau\sqrt{\beta^2 - \alpha^2}. \tag{3.37}$$

From the first equation in (3.36), we get

$$\frac{\kappa_3}{6}\omega^3 - \omega + \arccos\left(\frac{\alpha}{\beta}\right) = 0.$$

Substituting (3.37), we obtain a third degree equation for $\tau^{\kappa}_{(0,1)}$,

$$[\tau^{\kappa}_{(0,1)}]^3\frac{\kappa_3}{6}(\beta^2 - \alpha^2)\sqrt{\beta^2 - \alpha^2} - \tau^{\kappa}_{(0,1)}\sqrt{\beta^2 - \alpha^2} + \arccos\left(\frac{\alpha}{\beta}\right) = 0.$$

Since the explicit expression for $\tau^{\kappa}_{(0,1)}$ would be too cumbersome, we can only conclude that $\tau^{\kappa}_{(0,1)}$ is undefined at $\beta = -|\alpha|$, but we cannot make any comparisons between approximation $(0,1)$ and the other approximations.

For approximation $(1,0)$, using the fact that $\cos(\omega) = \alpha\exp\left(\frac{\kappa_2\omega^2}{2}\right)/\beta$ and substituting this into the value for τ from Table 3.2, we get

$$\tau^{\kappa}_{(1,0)} = -\frac{\omega e^{\kappa_2\omega^2/2}}{\beta\sin(\omega)},$$

where for $\alpha > 0$ we require $\omega \in (\pi/2, \pi)$ and for $\alpha < 0$ we require $\omega \in (0, \pi/2)$ in order to obtain the curve closest to the τ-axis. But as seen in (2.28), the second cumulant represents the variance of a distribution, i.e. $\kappa_2 = \sigma^2$, where σ is the standard deviation, and thus κ_2 is always nonnegative. Thus we have that $e^{\kappa_2\omega^2/2} \geq 1$. Also, since ω is in either $(0, \pi/2)$ or $(\pi/2, \pi)$ we have that $\omega/\sin(\omega) > 1$. Therefore,

$$\tau^{m}_{(1,0)} = -\frac{1}{\beta} < -\frac{\omega e^{\kappa_2\omega^2/2}}{\beta\sin(\omega)} = \tau^{\kappa}_{(1,0)},$$

i.e. approximation $(1,0)$ using cumulants always lies above approximation $(1,0)$ using moments.

We cannot make any general comparisons between approximation $(1,1)$ using cumulants and the other approximations, but we will see in Sections 3.3 and 3.4 how this approximation behaves for specific distributions (uniform and gamma) and how it compares to the other approximations in those particular cases.

We note that in practice, the cumulants of a distribution are as easy or difficult to compute as its moments, due to the recursive relationship between cumulants and moments (see equation (2.28)). An advantage of choosing to work with cumulants is that they are more reliable numerically. We expect to see better numerical results with the approximations using cumulants since the truncation of the expansion occurs inside the exponential, sine and cosine functions (see (3.30)), whereas in the approximations using moments, the truncation occurs inside a polynomial (see (3.25)).

In the following two sections we apply the approximations using moments and cumulants to specific distributions and compare them to the true boundary of stability.

3.3 Verifying the Approximations for the Uniform Distribution

In this section we will apply the approximation procedures we derived in the previous section to the uniform distribution, thus determining approximations for the boundary of the region of stability. We will then compare these approximations with the true boundary derived from the characteristic equation.

The normalized uniform distribution as given in (2.31) is

$$\hat{g}(v) = \begin{cases} \frac{1}{\rho}, & \text{if } v \in [1-\frac{\rho}{2}, 1+\frac{\rho}{2}] \\ 0, & \text{elsewhere.} \end{cases}$$

We will look at three different cases: $\rho = 2$, $\rho = 1$, and $\rho = 4/5$. Substituting the values for the moments given in Table 2.1 into Table 3.1, we obtain the corresponding approximations using moments for β and τ as seen in Table 3.3. These approximations represent curves in the $\beta\tau$-plane parameterized by ω. For the moment approximations, we can actually eliminate ω and have τ as a function of β, as seen at the end of Subsection 3.2.1.

All four approximations using moments can be seen in Figures 3.2 – 3.4. Approximation $(0,0)$ using moments represents the point $(\alpha, -1/\alpha)$ when $\alpha < 0$. Approximation $(0,1)$ using moments represents the line $\beta = \alpha$, with the restriction $\tau \geq -1/\alpha$ for $\alpha < 0$.

Table 3.3: Approximations using moments for equations (3.14) when the kernel represents a uniform distribution with $\rho = 2$, $\rho = 1$, and $\rho = 4/5$.

	$\rho = 2$		$\rho = 1$		$\rho = 4/5$	
(M, N)	β	τ	β	τ	β	τ
$(0,0)$	α	$-\frac{1}{\alpha}$	α	$-\frac{1}{\alpha}$	α	$-\frac{1}{\alpha}$
$(0,1)$	α	$\frac{3}{\alpha(\omega^2-3)}$	α	$\frac{24}{\alpha(5\omega^2-24)}$	α	$\frac{150}{\alpha(29\omega^2-150)}$
$(1,0)$	$\frac{3\alpha}{3-2\omega^2}$	$\frac{2\omega^2-3}{3\alpha}$	$\frac{24\alpha}{24-13\omega^2}$	$\frac{13\omega^2-24}{24\alpha}$	$\frac{150\alpha}{150-79\omega^2}$	$\frac{79\omega^2-150}{150\alpha}$
$(1,1)$	$\frac{3\alpha}{3-2\omega^2}$	$\frac{2\omega^2-3}{\alpha(3-\omega^2)}$	$\frac{24\alpha}{24-13\omega^2}$	$\frac{13\omega^2-24}{\alpha(24-5\omega^2)}$	$\frac{150\alpha}{150-79\omega^2}$	$\frac{79\omega^2-150}{\alpha(150-29\omega^2)}$

From (3.27), approximation $(1,0)$ using moments represents the curve $\tau = -1/\beta$, with the restriction $\beta \leq \alpha$ for $\alpha < 0$, and corresponds to the dotted curve in Figures 3.2 – 3.4. When $\alpha > 0$, approximation $(1,0)$ enters the distribution independent stability region $|\beta| < \alpha$ at $\beta = -\alpha, \tau = 1/\alpha$.

From (3.28), approximation $(1,1)$ using moments is given by

$$\rho = 2: \qquad \tau = -\frac{2}{\beta+\alpha}, \qquad \omega = \sqrt{\frac{3}{2}\left(1-\frac{\alpha}{\beta}\right)},$$

$$\rho = 1: \qquad \tau = -\frac{13}{8\beta+5\alpha}, \qquad \omega = \sqrt{\frac{24}{13}\left(1-\frac{\alpha}{\beta}\right)},$$

$$\rho = \frac{4}{5}: \qquad \tau = -\frac{79}{50\beta+29\alpha}, \qquad \omega = \sqrt{\frac{150}{79}\left(1-\frac{\alpha}{\beta}\right)},$$

with again the restriction $\beta \leq \alpha$ for $\alpha < 0$. Approximation $(1,1)$ using moments is depicted as the dashed black curve in Figures 3.2 – 3.4. We note that when $\alpha > 0$, for $\rho = 2$ approximation $(1,1)$ has a vertical asymptote at $\beta = -\alpha$, and thus never enters the distribution independent stability region, whereas for $\rho = 1$ and $\rho = 4/5$, it enters the region $|\beta| < \alpha$ when $\tau = 13/(3\alpha)$ and $\tau = 79/(21\alpha)$, respectively.

Since the third cumulant is always zero for any ρ as seen in (2.34), from Table 3.2 we see that approximation $(0,1)$ using cumulants is identical to approximation $(0,0)$ using cumulants, and approximation $(1,0)$ using cumulants is identical to approximation $(1,1)$ using cumulants. Substituting the values for the cumulants given in Table 2.1 into Table 3.2,

we obtain the corresponding approximations using cumulants as seen in Table 3.4. These approximations represent curves in the $\beta\tau$-plane parameterized by ω. Approximation $(0,0)$ (and thus $(0,1)$) using cumulants corresponds to the curve depicted by crosses, and approximation $(1,0)$ (and thus $(1,1)$) using cumulants corresponds to the curve depicted by circles in Figures 3.2 – 3.4. From (3.35), we know that for $\alpha > 0$ approximation $(0,0)$ (and in this case also $(0,1)$) using cumulants has a vertical asymptote at $\beta = -\alpha$ and thus never enters the distribution independent stability region $|\beta| < \alpha$.

Table 3.4: Approximations using cumulants for equations (3.14) when the kernel represents a uniform distribution with $\rho = 2$, $\rho = 1$, and $\rho = 4/5$. Approximation $(0,1)$ using cumulants is identical to approximation $(0,0)$ using cumulants, and approximation $(1,1)$ using cumulants is identical to approximation $(1,0)$ using cumulants.

	$\rho = 2$		$\rho = 1$		$\rho = 4/5$	
(M,N)	β	τ	β	τ	β	τ
$(0,0)$	$\dfrac{\alpha}{\cos(\omega)}$	$-\dfrac{\omega\cos(\omega)}{\alpha\sin(\omega)}$	$\dfrac{\alpha}{\cos(\omega)}$	$-\dfrac{\omega\cos(\omega)}{\alpha\sin(\omega)}$	$\dfrac{\alpha}{\cos(\omega)}$	$-\dfrac{\omega\cos(\omega)}{\alpha\sin(\omega)}$
$(1,0)$	$\dfrac{\alpha\exp\left(\frac{\omega^2}{6}\right)}{\cos(\omega)}$	$-\dfrac{\omega\cos(\omega)}{\alpha\sin(\omega)}$	$\dfrac{\alpha\exp\left(\frac{\omega^2}{24}\right)}{\cos(\omega)}$	$-\dfrac{\omega\cos(\omega)}{\alpha\sin(\omega)}$	$\dfrac{\alpha\exp\left(\frac{2\omega^2}{75}\right)}{\cos(\omega)}$	$-\dfrac{\omega\cos(\omega)}{\alpha\sin(\omega)}$

We now turn to the exact representation of the curves where the characteristic equation has a pair of pure imaginary roots. Since our scalar equation with uniform distributed delay is similar to the linearization of the delay equation used by Adimy et al. [2] to represent the dynamics of a pluripotent stem cell population, the computations that follow are similar to those found in [2]. From the definitions for $C(\omega)$ and $S(\omega)$ in (3.13) we have

$$\begin{aligned} C(\omega) &= \frac{1}{\rho}\int_{1-\rho/2}^{1+\rho/2}\cos(\omega v)\,dv = \frac{2\cos(\omega)\sin(\rho\omega/2)}{\rho\omega}, \\ S(\omega) &= \frac{1}{\rho}\int_{1-\rho/2}^{1+\rho/2}\sin(\omega v)\,dv = \frac{2\sin(\omega)\sin(\rho\omega/2)}{\rho\omega}. \end{aligned} \tag{3.38}$$

Substituting these into equations (3.14), we see that the curves are defined (parametrically in terms of ω) by

$$\beta = \frac{\alpha\rho\omega}{2\cos(\omega)\sin(\rho\omega/2)}, \qquad \tau = -\frac{\omega\cos(\omega)}{\alpha\sin(\omega)}. \tag{3.39}$$

Due to the singularities at $\omega = k\pi, \omega = (2k+1)\pi/2$ and $\omega = 2k\pi/\rho$ for $k = 0, 1, \ldots$, these equations define multiple curves in the $\beta\tau$-plane. To determine which curve(s) form part

of the stability boundary we analyze the rate of change of the real part of the eigenvalues as one of the curves is crossed, using the formula (3.20) derived in the Section (3.1). Since τ in (3.39) does not depend on ρ, we can determine the sign of $d\mathrm{Re}(\lambda)/(d\beta)|_{\lambda=i\omega}$ in (3.20) for any ρ.

First, we compute the derivative τ from (3.39) with respect to ω,

$$\frac{d\tau}{d\omega} = -\frac{\cos(\omega)}{\alpha\sin(\omega)} - \frac{\omega}{\alpha}\frac{\left(-\sin^2(\omega) - \cos^2(\omega)\right)}{\sin^2(\omega)} = -\frac{\cos(\omega)}{\alpha\sin(\omega)} + \frac{\omega}{\alpha\sin^2(\omega)}.$$

When $\alpha > 0$, from (3.39) we need only to consider ω values such that $\cos(\omega)/\sin(\omega) < 0$, and thus

$$\frac{d\tau}{d\omega} = \frac{1}{\alpha}\left(-\frac{\cos(\omega)}{\sin(\omega)} + \frac{\omega}{\sin^2(\omega)}\right) > 0.$$

When $\alpha < 0$, we rewrite the derivative as

$$\frac{d\tau}{d\omega} = \frac{1}{\alpha\sin^2(\omega)}(\omega - \sin(\omega)\cos(\omega)).$$

But we only consider values of ω such that $\cos(\omega)/\sin(\omega) > 0$ in this case, therefore

$$\frac{\sin(\omega)\cos(\omega)}{\omega} = \left|\frac{\sin(\omega)\cos(\omega)}{\omega}\right| = \left|\frac{\sin(\omega)}{\omega}\right||\cos(\omega)| < 1.$$

Thus $\omega - \sin(\omega)\cos(\omega) > 0$ and $\frac{d\tau}{d\omega} < 0$. We therefore determine that $\alpha\frac{d\tau}{d\omega} > 0$, for any value of α. Using this and the fact that we only consider $\beta < 0$, we conclude from (3.20) that

$$\left.\frac{d\mathrm{Re}(\lambda)}{d\beta}\right|_{\lambda=i\omega} < 0.$$

In other words, the real part of λ decreases (increases) as β increases (decreases), as the curves where $\lambda = i\omega$ are crossed. It follows from this computation that the boundary of the stability region is formed by the curve closest to the τ axis.

For $\rho = 2$, the parametric equations in (3.39) become

$$\beta = \frac{\alpha\omega}{\cos(\omega)\sin(\omega)}, \qquad \tau = -\frac{\omega\cos(\omega)}{\alpha\sin(\omega)}. \tag{3.40}$$

Due to the singularities at $\omega = k\pi$ and $\omega = (2k+1)\pi/2$ for $k = 0, 1, \ldots$, these equations define multiple curves in the $\beta\tau$-plane, which lie either in the second or fourth quadrant. Since we are interested in $\tau > 0$, the only curves of interest are those in the second quadrant.

For $\alpha > 0$, the curve forming the boundary of the stability region is defined by equation (3.40) with with $\omega \in [\frac{\pi}{2}, \pi]$. Some simple properties of this curve are as follows. Since

$$\lim_{\omega \to \frac{\pi}{2}^+} \beta = \frac{\alpha\pi/2}{\cos(\pi/2)\sin(\pi/2)} = -\infty,$$
$$\lim_{\omega \to \frac{\pi}{2}^+} \tau = -\frac{\pi/2\cos(\pi/2)}{\alpha\sin(\pi/2)} = 0.$$

the curve has a horizontal asymptote, $\tau = 0$, as ω approaches $\pi/2$ from the right. Further we have that

$$\lim_{\omega \to \pi^-} \beta = \frac{\alpha\pi}{\cos(\pi)\sin(\pi)} = -\infty,$$
$$\lim_{\omega \to \pi^-} \tau = -\frac{\pi\cos(\pi)}{\alpha\sin(\pi)} = +\infty.$$

But we notice that substituting $\sin(\omega) = \alpha\omega/(\beta\cos(\omega))$ from the first equation in (3.40) into the second equation, we get

$$\tau = -\frac{\beta\cos^2(\omega)}{\alpha^2},$$

and therefore,

$$\lim_{\omega \to \pi^-} \tau = -\frac{\beta}{\alpha^2}.$$

Hence the curve forming the boundary of stability has an oblique asymptote, $\tau = -\beta/\alpha^2$, which is approached as $\omega \to \pi^-$. This curve corresponds to the solid black line in Figure 3.2(a). We note that stability is always recovered when τ is sufficiently large, i.e. for $\tau > -\beta/\alpha^2$.

For $\alpha < 0$, the curve forming the boundary of the stability region is defined by equation (3.40) with $\omega \in [0, \frac{\pi}{2}]$. Since

$$\lim_{\omega \to 0^+} \beta = \lim_{\omega \to 0^+} \frac{\alpha}{-\sin^2(\omega) + \cos^2(\omega)} = \alpha,$$
$$\lim_{\omega \to 0^+} \tau = -\frac{\cos(\omega) - \omega\sin(\omega)}{\alpha\cos(\omega)} = -\frac{1}{\alpha},$$

the curve approaches the point $(\beta, \tau) = (\alpha, -1/\alpha)$ as $\omega \to 0^+$. We also have that

$$\lim_{\omega \to \frac{\pi}{2}^-} \beta = \frac{\alpha\pi/2}{\cos(\pi/2)\sin(\pi/2)} = -\infty,$$
$$\lim_{\omega \to \frac{\pi}{2}^-} \tau = -\frac{\pi/2\cos(\pi/2)}{\alpha\sin(\pi/2)} = 0.$$

Thus the curve has a horizontal asymptote, $\tau = 0$, as ω approaches $\pi/2$ from the left. This curve corresponds to the solid black curve in Figure 3.2(b). In this case, stability is lost as soon as τ crosses the solid black curve.

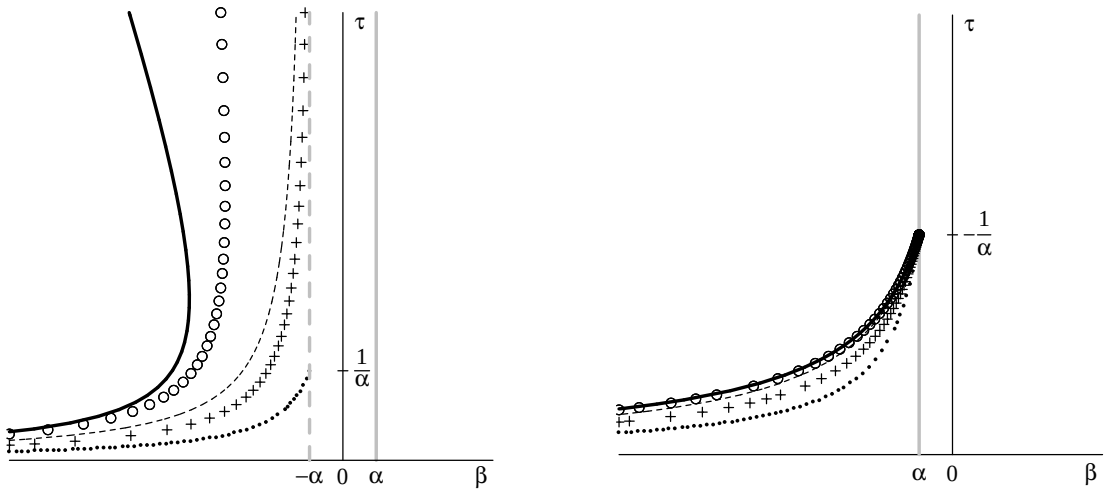

(a) $\alpha > 0$ (b) $\alpha < 0$

Figure 3.2: Stability region for the uniform distribution with $\rho = 2$. The region of distribution independent stability lies between the solid and dashed gray lines when $\alpha > 0$. The true region of stability lies between the solid gray line and the solid black curve which is defined by equations (3.40). The approximations using moments are defined in Table 3.3: approximation $(0, 0)$ using moments predicts that the region of stability is the entire half plane to the left of the line $\beta = \alpha$, approximation $(0, 1)$ using moments predicts no stability region for $\alpha > 0$, whereas for $\alpha < 0$, it predicts the region below $\tau = -1/\alpha$ and to the left of $\beta = \alpha$ to be stable, approximation $(1, 0)$ using moments corresponds to the dotted curve, and approximation $(1, 1)$ using moments corresponds to the dashed black curve. The approximations using cumulants are defined in Table 3.4: approximations $(0, 0)$ and $(1, 0)$ using cumulants correspond to the curves depicted by the black crosses and black circles, respectively. Approximation $(0, 1)$ using cumulants is identical to approximation $(0, 0)$, and approximation $(1, 0)$ using cumulants is identical to approximation $(1, 1)$.

For $\rho = 1$, the parametric equations in (3.39) are given by

$$\beta = \frac{\alpha\omega}{2\cos(\omega)\sin(\omega/2)}, \qquad \tau = -\frac{\omega\cos(\omega)}{\alpha\sin(\omega)}. \tag{3.41}$$

These equations define multiple curves in the $\beta\tau$-plane with singularities at $\omega = k\pi$ and $\omega = (2k+1)\pi/2$ for $k = 0, 1, \ldots$. For $\alpha < 0$ the closest curve to the τ axis is defined by equation (3.41) with $\omega \in [0, \frac{\pi}{2}]$ and for $\alpha > 0$ with $\omega \in [\frac{\pi}{2}, \pi]$. Properties of these curves are obtain in a similar way to the case $\rho = 2$. For $\alpha < 0$, the curve approaches the point $(\beta, \tau) = (\alpha, -1/\alpha)$ as $\omega \to 0$. For $\alpha > 0$, the curve has a vertical asymptote at $\beta = -\alpha\pi/2$, which is approached as $\omega \to \pi^-$, since

$$\lim_{\omega\to\pi^-} \beta = \frac{\alpha\pi}{2\cos(\pi)\sin(\pi/2)} = -\frac{\alpha\pi}{2},$$
$$\lim_{\omega\to\pi^-} \tau = -\frac{\pi\cos(\pi)}{\alpha\sin(\pi)} = +\infty.$$

For any α, the curves in (3.41) have a horizontal asymptote, $\tau = 0$, which is approached as $\omega \to \pi/2$. The curves forming the stability boundary correspond to the solid black lines in Figure 3.3. We note that for $\alpha > 0$, if $-\alpha\pi/2 < \beta < \alpha$ then stability is always recovered when τ is sufficiently large, but for $\alpha < 0$ stability is lost as soon as τ crosses the solid black curve.

For $\rho = 4/5$, the parametric equations in (3.39) become

$$\beta = \frac{2\alpha\omega}{5\cos(\omega)\sin(2\omega/5)}, \qquad \tau = -\frac{\omega\cos(\omega)}{\alpha\sin(\omega)}. \tag{3.42}$$

These equations define multiple curves in the $\beta\tau$-plane with singularities at $\omega = k\pi$ and $\omega = (2k+1)\pi/2$ for $k = 0, 1, \ldots$. For $\alpha < 0$ the curve closest to the τ axis is defined by equation (3.42) with $\omega \in [0, \frac{\pi}{2}]$ and for $\alpha > 0$ with $\omega \in [\frac{\pi}{2}, \pi]$. For $\alpha < 0$, the curve approaches the point $(\beta, \tau) = (\alpha, -1/\alpha)$ as $\omega \to 0$. For $\alpha > 0$ we have that

$$\lim_{\omega\to\pi^-} \beta = \frac{2\alpha\pi}{5\cos(\pi)\sin(2\pi/5)} = -\frac{2\alpha\pi}{5\sin(2\pi/5)},$$
$$\lim_{\omega\to\pi^-} \tau = -\frac{\pi\cos(\pi)}{\alpha\sin(\pi)} = +\infty.$$

Thus the curve have a vertical asymptote at $\beta = -2\alpha\pi/(5\sin(2\pi/5))$, which is approached as $\omega \to \pi^-$. For any α, the curves in (3.42) have a horizontal asymptote, $\tau = 0$, which is approached as $\omega \to \pi/2$. The curves which form the boundary of stability correspond to the solid black lines in Figure 3.4. We note that for $\alpha > 0$, if $-2\alpha\pi/(5\sin(2\pi/5)) < \beta < \alpha$ then stability is always recovered when τ is sufficiently large, but for $\alpha < 0$ stability is lost as soon as τ crosses the solid black curve.

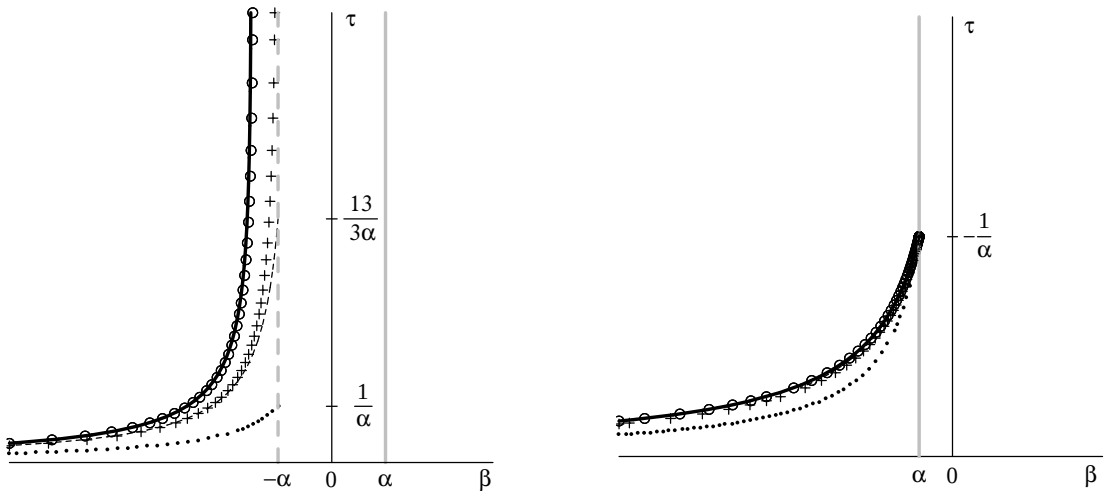

(a) $\alpha > 0$ (b) $\alpha < 0$

Figure 3.3: Stability region for the uniform distribution with $\rho = 1$. The region of distribution independent stability lies between the solid and dashed gray lines when $\alpha > 0$. The true region of stability lies between the solid gray line and the solid black curve which is defined by equations (3.41). The approximations using moments are defined in Table 3.3: approximation $(0, 0)$ using moments predicts that the region of stability is the entire half plane to the left of the line $\beta = \alpha$, approximation $(0, 1)$ using moments predicts no stability region for $\alpha > 0$, whereas for $\alpha < 0$, it predicts the region below $\tau = -1/\alpha$ and to the left of $\beta = \alpha$ to be stable, approximation $(1, 0)$ using moments corresponds to the dotted curve, and approximation $(1, 1)$ using moments corresponds to the dashed black curve. The approximations using cumulants are defined in Table 3.4: approximations $(0, 0)$ and $(1, 0)$ using cumulants correspond to the curves depicted by the black crosses and black circles, respectively. Approximation $(0, 1)$ using cumulants is identical to approximation $(0, 0)$, and approximation $(1, 0)$ using cumulants is identical to approximation $(1, 1)$.

Comparing the approximations with the true boundary of the stability region in Figures 3.2 – 3.4 we can make several conclusions. The approximations using cumulants give better results than those using moments. No approximation using cumulants enters the

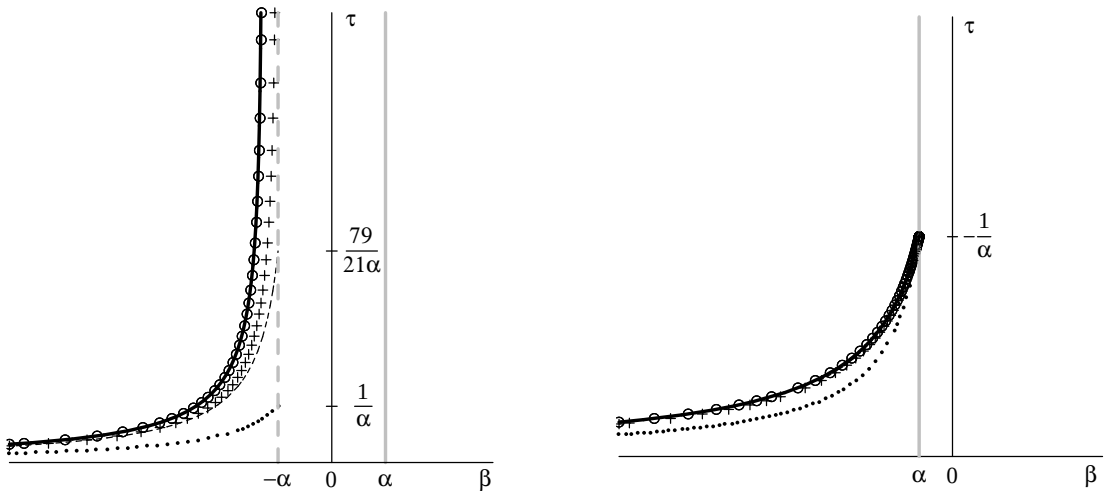

(a) $\alpha > 0$ (b) $\alpha < 0$

Figure 3.4: Stability region for the uniform distribution with $\rho = 4/5$. The region of distribution independent stability lies between the solid and dashed gray lines when $\alpha > 0$. The true region of stability lies between the solid gray line and the solid black curve which is defined by equations (3.42). The approximations using moments are defined in Table 3.3: approximation $(0, 0)$ using moments predicts that the region of stability is the entire half plane to the left of the line $\beta = \alpha$, approximation $(0, 1)$ using moments predicts no stability region for $\alpha > 0$, whereas for $\alpha < 0$, it predicts the region below $\tau = -1/\alpha$ and to the left of $\beta = \alpha$ to be stable, approximation $(1, 0)$ using moments corresponds to the dotted curve, and approximation $(1, 1)$ using moments corresponds to the dashed black curve. The approximations using cumulants are defined in Table 3.4: approximations $(0, 0)$ and $(1, 0)$ using cumulants correspond to the curves depicted by the black crosses and black circles, respectively. Approximation $(0, 1)$ using cumulants is identical to approximation $(0, 0)$, and approximation $(1, 0)$ using cumulants is identical to approximation $(1, 1)$.

distribution independent region. We note that the approximations using cumulants from Table 3.4 recover the exact expression for τ in (3.39). All approximations seem to improve as the number of moments or cumulants used increases. This corresponds to increasing N

and M in the approximations for $C(\omega)$ and $S(\omega)$ so is as expected. For negative α, all approximations and the exact boundary of stability pass through or approach the point $(\beta, \tau) = (\alpha, -1/\alpha)$. In this case all approximations are close to the exact boundary of stability and seem to give better results than for positive α. For $\alpha > 0$ all approximations are better for large negative β. This is expected for the moment approximations (see (3.27) and (3.28)) and approximation $(0, 0)$ using cumulants (see (3.33)), since larger negative β implies smaller ω. We also note that the approximate stability regions are always conservative, i.e. they underestimate the region of of stability.

3.4 Verifying the Approximations for the Gamma Distribution

In this section we will apply the approximation procedures we derived in Subsections 3.2.1 and 3.2.2 to the gamma distribution, thus determining approximations for the boundary of the region of stability. We will then compare these approximations with the true boundary of stability derived from the characteristic equation.

Recall that the normalized gamma distribution as given in (2.39) is

$$\hat{g}(v) = \frac{p^p v^{p-1} e^{-pv}}{(p-1)!}.$$

We will look at three different cases: $p = 3$, $p = 4$, and $p = 5$. We leave out the $p = 1$ and $p = 2$ cases, since their $(1, 1)$ approximation using cumulants predicts a much larger stability region with boundaries that are off the graph. Substituting the values for the moments given in Table 2.2 into Table 3.1, we obtain the corresponding approximations using moments as seen in Table 3.5. The approximate curves in Table 3.5 are curve in the $\beta\tau$-plane parameterized by ω. All four approximations using moments can be seen in Figures 3.5 – 3.7. Approximation $(0, 0)$ using moments represents the point $(\alpha, -1/\alpha), (\alpha < 0)$. Approximation $(0, 1)$ using moments represents the line $\beta = \alpha$, with the restriction $\tau \geq -1/\alpha$, for $\alpha < 0$. Approximation $(1, 0)$ using moments corresponds to the dotted curve and represents the curve $\tau \geq -1/\beta$ with the restriction $\beta \leq \alpha$ for $\alpha < 0$. Approximation

Table 3.5: Approximations using moments for equations (3.14) when the kernel represents a gamma distribution with $p = 3$, $p = 4$, and $p = 5$.

	$p = 3$		$p = 4$		$p = 5$	
(M, N)	β	τ	β	τ	β	τ
$(0,0)$	α	$-\dfrac{1}{\alpha}$	α	$-\dfrac{1}{\alpha}$	α	$-\dfrac{1}{\alpha}$
$(0,1)$	α	$\dfrac{54}{\alpha(20\omega^2 - 54)}$	α	$\dfrac{16}{\alpha(5\omega^2 - 16)}$	α	$\dfrac{25}{\alpha(7\omega^2 - 25)}$
$(1,0)$	$\dfrac{3\alpha}{3 - 2\omega^2}$	$\dfrac{2\omega^2 - 3}{3\alpha}$	$\dfrac{8\alpha}{8 - 5\omega^2}$	$\dfrac{5\omega^2 - 8}{8\alpha}$	$\dfrac{5\alpha}{5 - 3\omega^2}$	$\dfrac{3\omega^2 - 5}{5\alpha}$
$(1,1)$	$\dfrac{3\alpha}{3 - 2\omega^2}$	$\dfrac{9(2\omega^2 - 3)}{\alpha(27 - 10\omega^2)}$	$\dfrac{8\alpha}{8 - 5\omega^2}$	$\dfrac{2(5\omega^2 - 8)}{\alpha(16 - 5\omega^2)}$	$\dfrac{5\alpha}{5 - 3\omega^2}$	$\dfrac{5(3\omega^2 - 5)}{\alpha(25 - 7\omega^2)}$

$(1,1)$ using moments is depicted as the dashed black curve and is given by

$$p = 3: \qquad \tau = -\frac{9}{4\beta + 5\alpha}, \qquad \omega = \sqrt{\frac{3}{2}\left(1 - \frac{\alpha}{\beta}\right)},$$

$$p = 4: \qquad \tau = -\frac{2}{\beta + \alpha}, \qquad \omega = \sqrt{\frac{8}{5}\left(1 - \frac{\alpha}{\beta}\right)},$$

$$p = 5: \qquad \tau = -\frac{15}{8\beta + 7\alpha}, \qquad \omega = \sqrt{\frac{5}{3}\left(1 - \frac{\alpha}{\beta}\right)},$$

with again the restriction $\beta \leq \alpha$ for $\alpha < 0$. We note that when $\alpha > 0$, for $p = 3$ approximation $(1,1)$ has a vertical asymptote at $\beta = -5\alpha/4$ and for $p = 4$ approximation $(1,1)$ has a vertical asymptote at $\beta = -\alpha$ and thus it never enters the distribution independent stability region, whereas for $p = 5$ approximation $(1,1)$ enters the region $|\beta| < \alpha$ when $\tau = 15/\alpha$.

Next, we substitute the values for the cumulants given in Table 2.2 into Table 3.2 to obtain the corresponding approximations using cumulants as seen in Tables 3.6 – 3.8. Figures 3.5 – 3.7 show the four approximations using cumulants: approximation $(0,0)$ corresponds to the curve depicted by black crosses, approximation $(0,1)$ corresponds to the curve depicted by gray crosses, approximation $(1,0)$ corresponds to the curve depicted by black circles, and approximation $(1,1)$ corresponds to the curve depicted by gray circles. From (3.35), for $\alpha > 0$ approximation $(0,0)$ using cumulants has a vertical asymptote at $\beta = -\alpha$ and thus never enters the distribution independent stability region $|\beta| < \alpha$.

We now turn to the exact representation of the curves where the characteristic equation has a pair of pure imaginary roots. We start by determining the exact expressions for $C(\omega)$

Table 3.6: Approximations using cumulants for equations (3.14) when the kernel represents a gamma distribution with $p = 3$.

(M, N)	β	τ
$(0,0)$	$\dfrac{\alpha}{\cos(\omega)}$	$-\dfrac{\omega\cos(\omega)}{\alpha\sin(\omega)}$
$(0,1)$	$\dfrac{\alpha}{\cos\left(\omega-\omega^3/27\right)}$	$-\dfrac{\omega\cos\left(\omega-\omega^3/27\right)}{\alpha\sin\left(\omega-\omega^3/27\right)}$
$(1,0)$	$\dfrac{\alpha\exp\left(\omega^2/6\right)}{\cos(\omega)}$	$-\dfrac{\omega\cos(\omega)}{\alpha\sin(\omega)}$
$(1,1)$	$\dfrac{\alpha\exp\left(\omega^2/6\right)}{\cos\left(\omega-\omega^3/27\right)}$	$-\dfrac{\omega\cos\left(\omega-\omega^3/27\right)}{\alpha\sin\left(\omega-\omega^3/27\right)}$

Table 3.7: Approximations using cumulants for equations (3.14) when the kernel represents a gamma distribution with $p = 4$.

(M, N)	β	τ
$(0,0)$	$\dfrac{\alpha}{\cos(\omega)}$	$-\dfrac{\omega\cos(\omega)}{\alpha\sin(\omega)}$
$(0,1)$	$\dfrac{\alpha}{\cos\left(\omega-\omega^3/48\right)}$	$-\dfrac{\omega\cos\left(\omega-\omega^3/48\right)}{\alpha\sin\left(\omega-\omega^3/48\right)}$
$(1,0)$	$\dfrac{\alpha\exp\left(\omega^2/8\right)}{\cos(\omega)}$	$-\dfrac{\omega\cos(\omega)}{\alpha\sin(\omega)}$
$(1,1)$	$\dfrac{\alpha\exp\left(\omega^2/8\right)}{\cos\left(\omega-\omega^3/48\right)}$	$-\dfrac{\omega\cos\left(\omega-\omega^3/48\right)}{\alpha\sin\left(\omega-\omega^3/48\right)}$

and $S(\omega)$. From (3.23) we have that

$$\begin{aligned} C(\omega) &= \mathrm{Re}\left(\int_0^\infty \hat{g}(v)e^{-i\omega v}\,dv\right) \\ &= \mathrm{Re}\left(\frac{p^p}{(p-1)!}\int_0^\infty v^{p-1}e^{-(p+i\omega)v}\,dv\right) \\ &= \mathrm{Re}\left(\frac{p^p}{(p-1)!}\frac{(p-1)!}{(p+i\omega)^p}\right) \\ &= \mathrm{Re}\left(\frac{p^p(p-i\omega)^p}{(p^2+\omega^2)^p}\right) \\ &= \left(\frac{p}{p^2+\omega^2}\right)^p \mathrm{Re}\left(p-i\omega\right)^p, \end{aligned} \tag{3.43}$$

Table 3.8: Approximations using cumulants for equations (3.14) when the kernel represents a gamma distribution with $p = 5$.

(M, N)	β	τ
$(0,0)$	$\dfrac{\alpha}{\cos(\omega)}$	$-\dfrac{\omega\cos(\omega)}{\alpha\sin(\omega)}$
$(0,1)$	$\dfrac{\alpha}{\cos\left(\omega-\omega^3/75\right)}$	$-\dfrac{\omega\cos\left(\omega-\omega^3/75\right)}{\alpha\sin\left(\omega-\omega^3/75\right)}$
$(1,0)$	$\dfrac{\alpha\exp\left(\omega^2/10\right)}{\cos(\omega)}$	$-\dfrac{\omega\cos(\omega)}{\alpha\sin(\omega)}$
$(1,1)$	$\dfrac{\alpha\exp\left(\omega^2/10\right)}{\cos\left(\omega-\omega^3/75\right)}$	$-\dfrac{\omega\cos\left(\omega-\omega^3/75\right)}{\alpha\sin\left(\omega-\omega^3/75\right)}$

where we used identity (2.35). Similarly we obtain,

$$S(\omega) = -\left(\frac{p}{p^2+\omega^2}\right)^p \operatorname{Im}\left(p - i\omega\right)^p. \tag{3.44}$$

We note that for the remaining of this section all the computations and simplifications are done using the symbolic algebra language Maple$^{\text{TM}}$.

For $p = 3$ we have,

$$C(\omega) = \frac{243(3-\omega^2)}{(9+\omega^2)^3} \qquad \text{and} \qquad S(\omega) = \frac{27\omega(27-\omega^2)}{(9+\omega^2)^3}. \tag{3.45}$$

Using these we can get expressions for β and τ parameterized by ω, but in this case we can actually obtain an expression for β as a function of τ. We start by substituting (3.45) into (3.13) to obtain

$$\alpha(9+\omega^2)^3 = 243\beta(3-\omega^2), \tag{3.46}$$

$$-\omega(9+\omega^2)^3 = 27\beta\tau\omega(27-\omega^2). \tag{3.47}$$

From (3.47) we have that $(9+\omega^2)^3 = 27\beta\tau(\omega^2-27)$. Using this into (3.46) we obtain an equation in ω^2, which does not depend on β,

$$\alpha\tau(\omega^2-27) = 9(3-\omega^2) \qquad \Rightarrow \qquad \omega^2 = \frac{27(\alpha\tau+1)}{\alpha\tau+9}.$$

We substitute the expression for ω^2 into (3.46) to obtain β as a function of τ,

$$\beta = -\frac{8(\alpha\tau+3)^3}{\tau(\alpha\tau+9)^2} \tag{3.48}$$

For $\alpha > 0$, ω is defined for all $\tau \geq 0$ and the curve lies in the second quadrant with a horizontal asymptote at $\tau = 0$ and a vertical asymptote at $\beta = -8\alpha$, since

$$\lim_{\tau \to 0^+} \beta = -\frac{216}{0^+} = -\infty,$$
$$\lim_{\tau \to +\infty} \beta = -8\alpha.$$

For $\alpha < 0$, ω is defined for $\tau \leq -1/\alpha$ which corresponds to $\beta \leq \alpha$, or $\tau > -9/\alpha$ which corresponds to $\beta > -8\alpha$. However, as noted above, we only consider curves where β is negative, and thus only the portion of the curve with $\tau \leq -1/\alpha$ will form part of the stability boundary. This curve has a horizontal asymptote at $\tau = 0$.

Next, we analyze the rate of change of the real part of the eigenvalues as the curve in (3.48) is crossed, using the formula (3.20). We start by differentiating (3.45),

$$C'(\omega) = \frac{927\omega(\omega^2 - 9)}{(\omega^2 + 9)^4} \qquad \text{and} \qquad S'(\omega) = \frac{81(\omega^4 - 54\omega^2 + 81)}{(\omega^2 + 9)^4}.$$

Substituting these and (3.45) into (3.15), after simplifying, we obtain

$$\frac{d\tau}{d\omega} = \frac{432\omega}{\alpha(\omega^2 - 27)^2}.$$

Therefore (3.20) becomes

$$\left.\frac{d\mathrm{Re}(\lambda)}{d\beta}\right|_{\lambda = i\omega} = \frac{432\omega^2}{\beta(\omega^2 - 27)^2 H^2(\omega)} < 0,$$

since $\beta < 0$. Thus the real part of λ decreases (increases) as β increases (decreases), as the curve where $\lambda = i\omega$ is crossed.

The region of stability for $p = 3$ can be seen in Figure 3.5. For $\alpha > 0$ the equilibrium point is locally asymptotically stable when

$$\beta < \alpha \text{ and } \beta > -\frac{8(\alpha\tau + 3)^3}{\tau(\alpha\tau + 9)^2}.$$

For $\alpha < 0$ the equilibrium point is locally asymptotically stable when

$$\beta < \alpha \text{ and } \beta > -\frac{8(\alpha\tau + 3)^3}{\tau(\alpha\tau + 9)^2} \text{ with } \tau < -1/\alpha,$$

i.e., τ is underneath the solid black curve as seen in Figure 3.5. We note that for $\alpha > 0$, if $-8\alpha < \beta < \alpha$ then stability is always recovered when τ is sufficiently large, but for $\alpha < 0$ stability is lost as soon as τ crosses the solid black curve.

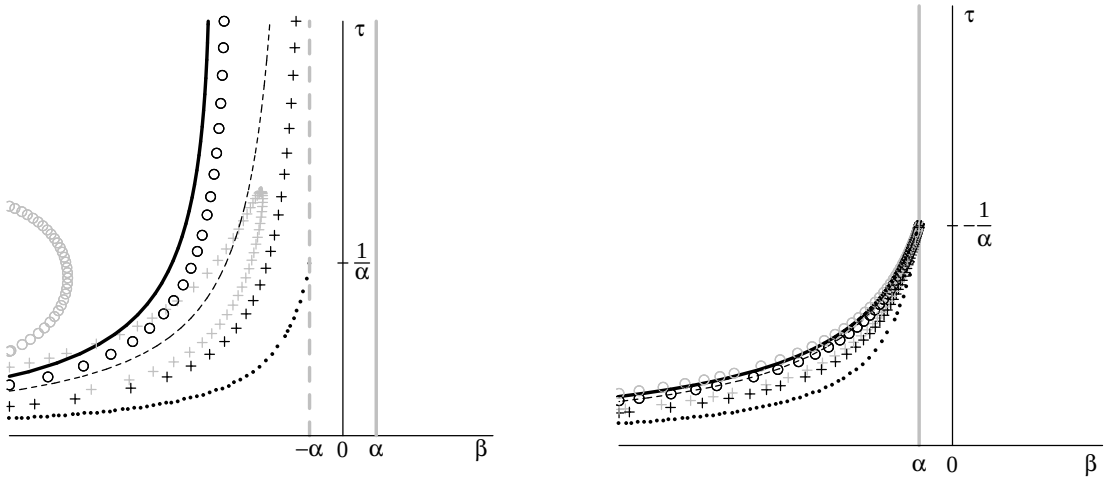

(a) $\alpha > 0$ (b) $\alpha < 0$

Figure 3.5: Stability region for the gamma distribution with $p = 3$. The region of distribution independent stability lies between the solid and dashed gray lines when $\alpha > 0$. The true region of stability lies between the solid gray line and the solid black curve which is defined by equations (3.48). The approximations using moments are defined in Table 3.5: approximation $(0, 0)$ using moments predicts that the region of stability is the entire half plane to the left of the line $\beta = \alpha$, approximation $(0, 1)$ using moments predicts no stability region for $\alpha > 0$, whereas for $\alpha < 0$, it predicts the region below $\tau = -1/\alpha$ and to the left of $\beta = \alpha$ to be stable, approximation $(1, 0)$ using moments corresponds to the dotted curve, and approximation $(1, 1)$ using moments corresponds to the dashed black curve. The approximations using cumulants are defined in Table 3.6: approximations $(0, 0)$, $(0, 1)$, $(1, 0)$ and $(1, 1)$ using cumulants correspond to the curves depicted by the black crosses, gray crosses, black circles and gray circles, respectively.

For $p = 4$, from (3.43) and (3.44) we have

$$C(\omega) = \frac{256(\omega^4 - 96\omega^2 + 256)}{(16 + \omega^2)^4} \qquad \text{and} \qquad S(\omega) = \frac{4096\omega(16 - \omega^2)}{(16 + \omega^2)^4}. \tag{3.49}$$

Substituting these into (3.13) we get

$$\alpha(16+\omega^2)^4 = 256\beta(\omega^4 - 96\omega^2 + 256), \tag{3.50}$$
$$-\omega(16+\omega^2)^4 = 4096\beta\tau\omega(16-\omega^2). \tag{3.51}$$

From (3.51) we have that $(16+\omega^2)^4 = 4096\beta\tau(\omega^2-16)$. Using this into (3.50) we obtain an equation in ω^2,

$$16\alpha\tau(\omega^2-16) = \omega^4 - 96\omega^2 + 256.$$

We solve for ω^2 to get

$$\omega_\pm^2 = 8(\alpha\tau + 6 \pm \sqrt{\alpha^2\tau^2 + 8\alpha\tau + 32}).$$

We substitute the expression for $\omega_\pm^2$ into (3.50) to obtain $\beta_\pm$ as a function of τ,

$$\beta_\pm = \frac{(\alpha\tau + 8 \pm \sqrt{\alpha^2\tau^2 + 8\alpha\tau + 32})^4}{8\tau(\alpha\tau + 4 \pm \sqrt{\alpha^2\tau^2 + 8\alpha\tau + 32})}$$

We first show that β_+ is always positive by proving that $A = \alpha\tau+4+\sqrt{\alpha^2\tau^2 + 8\alpha\tau + 32} > 0$ for any $\tau > 0$. When $\alpha\tau + 4 > 0$, obviously $A > 0$. When $\alpha\tau + 4 < 0$, we have $(\alpha\tau+4)^2 < (\alpha\tau+4)^2 + 16$. Taking the square root on both sides we get

$$-(\alpha\tau+4) < \sqrt{(\alpha\tau+4)^2 + 16},$$

which is equivalent to

$$\alpha\tau + 4 > -\sqrt{\alpha^2\tau^2 + 8\alpha\tau + 32},$$

i.e. $A > 0$. In both cases we get that β_+ is positive, and hence the curve given by β_+ will not form part of the stability boundary as a consequence of Theorems 6 and 7. Therefore, in what follows we only consider β_-, which we rename $\beta_- = \beta$,

$$\beta = \frac{(\alpha\tau + 8 - \sqrt{\alpha^2\tau^2 + 8\alpha\tau + 32})^4}{8\tau(\alpha\tau + 4 - \sqrt{\alpha^2\tau^2 + 8\alpha\tau + 32})}. \tag{3.52}$$

For $\alpha > 0$, we have that $\alpha\tau + 6 > 0$. In order for ω_- to be defined, we impose that

$$\alpha\tau + 6 \geq \sqrt{\alpha^2\tau^2 + 8\alpha\tau + 32}.$$

Squaring both sides we get $\alpha^2\tau^2 + 12\alpha\tau + 36 \geq \alpha^2\tau^2 + 8\alpha\tau + 32$. This is equivalent to $\alpha\tau + 1 \geq 0$, which is always true and hence ω_- is defined for all $\tau > 0$. The curve in (3.52) has a horizontal asymptote at $\tau = 0$, since

$$\lim_{\tau\to 0^+} \beta = \frac{(8-4\sqrt{2})^4}{8(0^+)(4-4\sqrt{2})} = -\infty.$$

Next we investigate whether it has a vertical asymptote by rationalizing both the numerator and the denominator in (3.52),

$$\begin{aligned}\lim_{\tau\to+\infty}\beta &= \lim_{\tau\to+\infty}\frac{(\alpha\tau+8-\sqrt{\alpha^2\tau^2+8\alpha\tau+32})^4}{8\tau(\alpha\tau+4-\sqrt{\alpha^2\tau^2+8\alpha\tau+32})}\frac{(\alpha\tau+8+\sqrt{\alpha^2\tau^2+8\alpha\tau+32})^4}{(\alpha\tau+8+\sqrt{\alpha^2\tau^2+8\alpha\tau+32})^4}\\ &\quad\times\frac{\alpha\tau+4+\sqrt{\alpha^2\tau^2+8\alpha\tau+32}}{\alpha\tau+4+\sqrt{\alpha^2\tau^2+8\alpha\tau+32}}\\ &= \lim_{\tau\to+\infty}-\frac{(32+8\alpha\tau)^4(\alpha\tau+4+\sqrt{\alpha^2\tau^2+8\alpha\tau+32})}{128\tau(\alpha\tau+8+\sqrt{\alpha^2\tau^2+8\alpha\tau+32})^4}\\ &= -\frac{(8\alpha)^4(2\alpha)}{128(2\alpha)^4}\\ &= -4\alpha.\end{aligned}$$

Thus the curve in (3.52) has a vertical asymptote at $\beta=-4\alpha$.

For $\alpha<0$, we must have $\alpha\tau+6>0$, otherwise $\omega_-<0$. We further impose $\alpha\tau+6\geq\sqrt{\alpha^2\tau^2+8\alpha\tau+32}$, which is equivalent to $\alpha\tau+1\geq 0$. Therefore ω_- is defined only for $\tau\leq -1/\alpha$ which corresponds to $\beta\leq\alpha$. This curve has a horizontal asymptote at $\tau=0$.

Next, we investigate how the real part of λ changes as we cross the curve in (3.52). We start by differentiating $C(\omega)$ and $S(\omega)$ in (3.49),

$$C'(\omega)=-\frac{1024\omega(\omega^4-160\omega^2+1280)}{(\omega^2+15)^5}\qquad\text{and}\qquad S'(\omega)=\frac{4096(5\omega^4-160\omega^2+256)}{(\omega^2+16)^5}.$$

Substituting these and (3.49) into (3.15), after simplifying, we obtain

$$\frac{d\tau}{d\omega}=\frac{\omega(\omega^4-32\omega^2+1280)}{8\alpha(\omega^2-16)^2}.$$

Therefore (3.20) becomes

$$\left.\frac{d\mathrm{Re}(\lambda)}{d\beta}\right|_{\lambda=i\omega}=\frac{\omega^2(\omega^4-32\omega^2+1280)}{8\beta(\omega^2-16)^2H^2(\omega)}<0,$$

since $\beta<0$. Thus the real part of λ decreases (increases) as β increases (decreases), as the curves where $\lambda=i\omega$ are crossed. The region of stability for $p=4$ can be as seen in Figure 3.6. For $\alpha>0$ the equilibrium point is locally asymptotically stable when

$$\beta<\alpha\text{ and }\beta>\frac{(\alpha\tau+8-\sqrt{\alpha^2\tau^2+8\alpha\tau+32})^4}{8\tau(\alpha\tau+4-\sqrt{\alpha^2\tau^2+8\alpha\tau+32})}.$$

For $\alpha < 0$ the equilibrium point is locally asymptotically stable when

$$\beta < \alpha \text{ and } \beta > \frac{(\alpha\tau + 8 - \sqrt{\alpha^2\tau^2 + 8\alpha\tau + 32})^4}{8\tau(\alpha\tau + 4 - \sqrt{\alpha^2\tau^2 + 8\alpha\tau + 32})} \text{ with } \tau < -1/\alpha,$$

i.e., τ is underneath the solid black curve as seen in Figure 3.6. We note that for $\alpha > 0$, if $-4\alpha < \beta < \alpha$ then stability is always recovered when τ is sufficiently large, but for $\alpha < 0$ stability is lost as soon as τ crosses the solid black curve.

For $p = 5$, from (3.43) and (3.44) we have

$$C(\omega) = \frac{78125(\omega^4 - 50\omega^2 + 125)}{(25 + \omega^2)^5} \qquad \text{and} \qquad S(\omega) = \frac{3125\omega(\omega^4 - 250\omega^2 + 3125)}{(25 + \omega^2)^5}. \quad (3.53)$$

Substituting these into (3.13) we get

$$\alpha(25 + \omega^2)^5 = 78125\beta(\omega^4 - 50\omega^2 + 125), \quad (3.54)$$

$$-\omega(25 + \omega^2)^5 = 3125\beta\tau\omega(\omega^4 - 250\omega^2 + 3125). \quad (3.55)$$

From (3.55) we have that $(25+\omega^2)^5 = -3125\beta\tau(\omega^4 - 250\omega^2 + 3125)$. Using this into (3.54) we obtain an equation in ω^2,

$$-\alpha\tau(\omega^4 - 250\omega^2 + 3125) = 25(\omega^4 - 50\omega^2 + 125).$$

We solve for ω^2 to get

$$\omega_\pm^2 = \frac{25(5\alpha\tau + 25 \pm 2\sqrt{5\alpha^2\tau^2 + 30\alpha\tau + 125})}{\alpha\tau + 25}.$$

We then use this to obtain from (3.54) an expression of β in terms of τ. Similarly to the case $p = 4$, we show that when using ω_+, we have that $\beta > 0$ and hence it cannot form part of the stability boundary. When substituting ω_-, we obtain,

$$\beta = \frac{2(3\alpha\tau + 25 - \sqrt{5\alpha^2\tau^2 + 30\alpha\tau + 125})^5}{\tau(\alpha\tau + 25)^3(11\alpha\tau + 25 - 5\sqrt{5\alpha^2\tau^2 + 30\alpha\tau + 125})}. \quad (3.56)$$

For $\alpha > 0$, we have that $\alpha\tau + 5 > 0$ and $\alpha\tau + 25 > 0$. We next impose that

$$5(\alpha\tau + 5) \geq 2\sqrt{5\alpha^2\tau^2 + 30\alpha\tau + 125}.$$

Squaring both sides and simplifying we get $\alpha^2\tau^2 + 26\alpha\tau + 25 > 0$, which is always true and hence ω is defined for all $\tau > 0$. The curve in (3.52) has a horizontal asymptote at $\tau = 0$, since

$$\lim_{\tau \to 0^+} \beta = \frac{2(25 - 4\sqrt{5})^5}{25^3(0^+)(25 - 25\sqrt{5})} = -\infty.$$

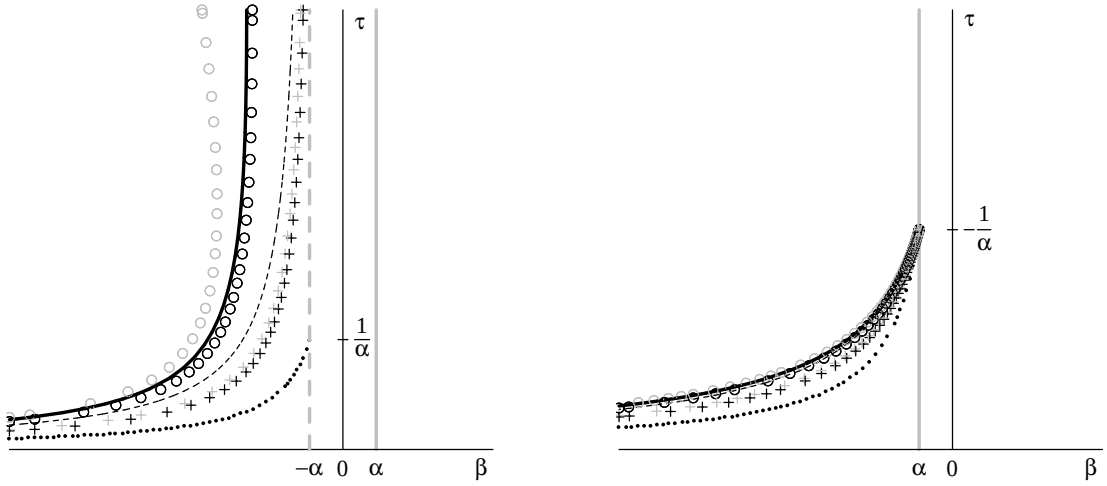

(a) $\alpha > 0$ (b) $\alpha < 0$

Figure 3.6: Stability region for the gamma distribution with $p = 4$. The region of distribution independent stability lies between the solid and dashed gray lines when $\alpha > 0$. The true region of stability lies between the solid gray line and the solid black curve which is defined by equations (3.52). The approximations using moments are defined in Table 3.5: approximation $(0, 0)$ using moments predicts that the region of stability is the entire half plane to the left of the line $\beta = \alpha$, approximation $(0, 1)$ using moments predicts no stability region for $\alpha > 0$, whereas for $\alpha < 0$, it predicts the region below $\tau = -1/\alpha$ and to the left of $\beta = \alpha$ to be stable, approximation $(1, 0)$ using moments corresponds to the dotted curve, and approximation $(1, 1)$ using moments corresponds to the dashed black curve. The approximations using cumulants are defined in Table 3.7: approximations $(0, 0)$, $(0, 1)$, $(1, 0)$ and $(1, 1)$ using cumulants correspond to the curves depicted by the black crosses, gray crosses, black circles and gray circles, respectively.

Rationalizing both the numerator and the denominator in (3.56) similarly to the case $p = 4$,

we obtain

$$\lim_{\tau\to+\infty}\beta = -\frac{512(11+5\sqrt{5})}{(3+\sqrt{5})^5}\alpha \approx -2.89\alpha.$$

Thus the curve in (3.56) has a vertical asymptote at $\beta \approx -2.89\alpha$.

For $\alpha < 0$, when $\alpha\tau + 5 < 0$, we must impose $\alpha\tau + 25 < 0$, i.e. $\tau > -25/\tau$, otherwise $\omega_-^2 < 0$. In this case we have $3\alpha\tau + 25 < 0$ and $11\alpha\tau + 25 < 0$ and thus β in (3.56) is always negative. This curve has a horizontal asymptote at $\tau = -25/\alpha$ as $\beta \to -\infty$, and a vertical asymptote $\beta = 0$ as $\tau \to \infty$. When $\alpha\tau + 5 > 0$, we have $\alpha\tau + 25 > 0$. We impose

$$5\alpha\tau + 25 > 2\sqrt{5\alpha^2\tau^2 + 30\alpha\tau + 125},$$

which is equivalent to

$$(\alpha\tau + 1)(\alpha\tau + 25) > 0.$$

Since $\alpha\tau + 25 > 0$, we must have $\alpha\tau + 1 > 0$, i.e. $\tau \leq -1/\alpha$. In summary, ω is defined for $\tau \leq -1/\alpha$ or $\tau > -25/\alpha$. This curve has a horizontal asymptote at $\tau = 0$ as $\beta \to -\infty$. In the $\beta\tau$-plane, we only consider the curve with $\tau \leq -1/\alpha$ which corresponds to $\beta \leq \alpha$, since it is closer to the β-axis and thus it will form part of the stability boundary.

Next, we investigate how the real part of λ changes as we cross these lines. We differentiate $C(\omega)$ and $S(\omega)$ in (3.53) to obtain

$$C'(\omega) = -\frac{156250\omega(3\omega^4 - 250\omega^2 + 1875)}{(\omega^2+25)^6},$$
$$S'(\omega) = -\frac{15625(\omega^6 - 375\omega^4 + 9375\omega^2 - 15625)}{(\omega^2+25)^6}.$$

Substituting these and (3.53) into (3.15), after simplifying, we have

$$\frac{d\tau}{d\omega} = \frac{10000\omega(\omega^4 - 30\omega^2 + 625)}{\alpha(\omega^4 - 250\omega^2 + 3125)^2}.$$

Therefore (3.20) becomes

$$\left.\frac{d\mathrm{Re}(\lambda)}{d\beta}\right|_{\lambda=i\omega} = \frac{10000\omega^2(\omega^4 - 30\omega^2 + 625)}{\beta(\omega^4 - 250\omega^2 + 3125)^2 H^2(\omega)} < 0,$$

since $\beta < 0$. Thus the real part of λ decreases (increases) as β increases (decreases), as the curves where $\lambda = i\omega$ are crossed. The region of stability for $p = 5$ can be as seen in Figure 3.7. For $\alpha > 0$ the equilibrium point is locally asymptotically stable when

$$\beta < \alpha \text{ and } \beta > \frac{2(3\alpha\tau + 25 - \sqrt{5\alpha^2\tau^2 + 30\alpha\tau + 125})^5}{\tau(\alpha\tau+25)^3(11\alpha\tau + 25 - 5\sqrt{5\alpha^2\tau^2 + 30\alpha\tau + 125})}.$$

For $\alpha < 0$ the equilibrium point is locally asymptotically stable when

$$\beta < \alpha \text{ and } \beta > \frac{2(3\alpha\tau + 25 - \sqrt{5\alpha^2\tau^2 + 30\alpha\tau + 125})^5}{\tau(\alpha\tau + 25)^3(11\alpha\tau + 25 - 5\sqrt{5\alpha^2\tau^2 + 30\alpha\tau + 125})} \text{ with } \tau < -1/\alpha,$$

i.e., τ is underneath the solid black curve as seen in Figure 3.7. We note that for $\alpha > 0$, if $-2.89\alpha < \beta < \alpha$ then stability is always recovered when τ is sufficiently large, but for $\alpha < 0$ stability is lost as soon as τ crosses the solid black curve.

We next compare the approximations to the true boundary of stability in Figures 3.5 – 3.7. The approximations using cumulants give better results than those using moments. No approximation using cumulants enters the distribution independent region. We note that the approximate stability regions are always conservative (i.e. they underestimate the region of stability), except for the approximate stability region predicted by approximation $(1, 1)$ using cumulants, which predicts a larger stability region than the actual one. Not all approximations improve as the number of moments or cumulants used increases: in all cases, approximation $(1, 1)$ using cumulants gives a worse estimate than approximation $(1, 0)$ using cumulants. Also, for $p = 3$, approximation $(0, 1)$ using cumulants gives a worse estimate than approximation $(0, 0)$ using cumulants. For negative α, all approximations and the exact boundary of stability pass through or approach the point $(\beta, \tau) = (\alpha, -1/\alpha)$. In this case all approximations are close to the exact boundary of stability and seem to give better results than for positive α. For $\alpha > 0$ all approximations are better for large negative β. This is expected for the moment approximations (see (3.27) and (3.28)) and approximation $(0, 0)$ using cumulants (see (3.33)), since larger negative β implies smaller ω. In all cases, approximation $(1, 0)$ using cumulants gives the best estimate of the true boundary of stability.

In the next chapter we expand the results in this chapter by applying them to an $n \times n$ Hopfield network. We analyze the linear stability of the symmetric equilibrium of system (1.16) when the neurons are identical. We determine the distribution independent region of stability and approximate the boundary of stability using the first few moments or cumulants of a distribution.

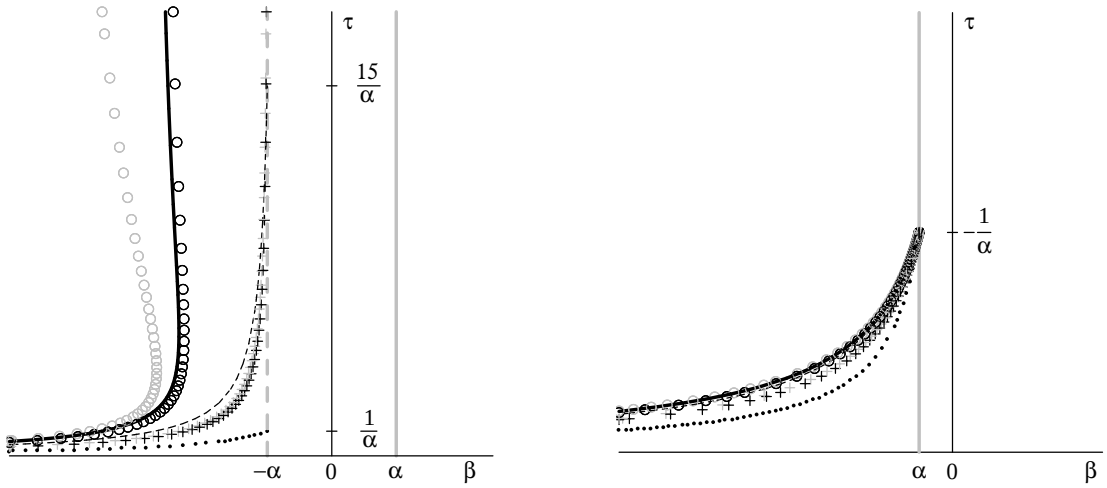

(a) $\alpha > 0$ (b) $\alpha < 0$

Figure 3.7: Stability region for the gamma distribution with $p = 5$. The region of distribution independent stability lies between the solid and dashed gray lines when $\alpha > 0$. The true region of stability lies between the solid gray line and the solid black curve which is defined by equations (3.56). The approximations using moments are defined in Table 3.5: approximation $(0, 0)$ using moments predicts that the region of stability is the entire half plane to the left of the line $\beta = \alpha$, approximation $(0, 1)$ using moments predicts no stability region for $\alpha > 0$, whereas for $\alpha < 0$, it predicts the region below $\tau = -1/\alpha$ and to the left of $\beta = \alpha$ to be stable, approximation $(1, 0)$ using moments corresponds to the dotted curve, and approximation $(1, 1)$ using moments corresponds to the dashed black curve. The approximations using cumulants are defined in Table 3.8: approximations $(0, 0)$, $(0, 1)$, $(1, 0)$ and $(1, 1)$ using cumulants correspond to the curves depicted by the black crosses, gray crosses, black circles and gray circles, respectively.

Chapter 4

Stability of the Hopfield Neural Network with Distributed Delay

In this chapter, we analyze the linear stability of the neural network (1.16) when the neurons are identical, where the kernel $g(u)$ represents a general distribution. We determine the distribution independent region of stability and try to improve on this conservative result by approximating the boundary of stability using the first few moments or cumulants of the distribution. We are able to also show that as the mean delay τ of the distribution becomes larger and larger, the stability region of the network with a distributed delay is less conservative than the corresponding system with one fixed delay τ. Hence we are able to partially prove the conjecture that a system with distributions of delays is more stable than the corresponding one with a fixed delay. The results of this chapter have been already published in [35], but will be presented here in greater detail.

We start by dividing system (1.16) by C_k and assuming that the injected current is constant, we obtain

$$\dot{v}_k(t) = -\alpha_k v_k(t) + \sum_{j=1}^{n} w_{kj} \int_0^\infty f_j(v_j(t-u)) g_{kj}(u)\, du + F_k, \qquad k = 1, \ldots, n, \tag{4.1}$$

where $\alpha_k = 1/(R_k C_k), w_{kj} = a_{kj}/C_k$, and $F_k = I_k/C_k$.

For the rest of the chapter, in order to simplify our calculations we shall assume that all neurons are identical, hence $\alpha_k \equiv \alpha, f_k(v_j) \equiv f(v_j)$, and $g_{kj}(u) \equiv g(u)$ for all $k, j = 1, \ldots, n$. Then the above model is reduced to

$$\dot{v}_k(t) = -\alpha v_k(t) + \sum_{j=1}^{n} w_{kj} \int_0^\infty f(v_j(t-u)) g(u)\, du + F_k, \qquad k = 1, \ldots, n. \tag{4.2}$$

We note that α is always positive since it represents the inverse of the product between the resistance and capacitance. We next transform the above system so that the mean delay τ of the distribution $g(u)$ appears explicitly. As noted in Section 2.2, when $\tau \to 0$ we recover the non-delayed model

$$\dot{v}_k(t) = -\alpha v_k(t) + \sum_{j=1}^{n} w_{kj} f(v_j(t)) + F_k, \qquad k = 1, \ldots, n. \tag{4.3}$$

For $\tau > 0$ we make the change of variables $s = t/\tau, v = u/\tau$ and thus by (2.11), system (4.2) becomes

$$v_k'(s) = -\alpha\tau v_k(s) + \tau \sum_{j=1}^{n} w_{kj} \int_0^\infty f(v_j(s-v))\hat{g}(v)\, dv + \tau F_k, \qquad k = 1, \ldots, n, \tag{4.4}$$

where "$'$" represents the right-hand derivative with respect to s, and the normalized distribution $\hat{g}(v)$ is given in (2.10).

In the following, in order to further simplify our calculations, we investigate the linear stability of the symmetric equilibrium point $\boldsymbol{v}^* = (v^*, v^*, \ldots, v^*)^T$ of the above model. System (4.4) possesses a symmetric equilibrium point, $\boldsymbol{v}^* = (v^*, v^*, \ldots, v^*)^T$, if the following equations are satisfied

$$\alpha v^* - F_k = \left(\sum_{j=1}^{n} w_{kj} \right) f(v^*), \qquad k = 1, \ldots, n. \tag{4.5}$$

Given the properties of f in (1.7) and (1.8), we can always guarantee the existence of such an equilibrium by either adjusting the external inputs for a particular connection matrix, or by adjusting the connection strengths when particular external inputs are applied. In particular, if $F_k = 0$, $k = 1, 2, \ldots, n$ the system admits the trivial equilibrium point, $\boldsymbol{v}^* = \mathbf{0}$.

Let $y_k(s) = v_k(s) - v^*$ and $\beta = f'(v^*)$. We note that, since f is monotonically increasing, β is nonnegative. We next expand $f(v_j)$ into its Taylor series around $v_j = v^*$,

$$f(v_j) = f(v^*) + f'(v^*)(v_j - v^*) + \text{ h.o.t. } = f(v^*) + \beta y_j + \text{ h.o.t.}$$

From (4.4) we have

$$y_k'(s) = -\alpha\tau y_k(s) - \alpha\tau v^* + \tau \sum_{j=1}^{n} w_{kj} \int_0^\infty [f(v^*) + \beta y_j(s-v) + \text{ h.o.t. }]\hat{g}(v)\, dv + \tau F_k.$$

Using (2.12) and (4.5), we then obtain the linearization of (4.4) about $\boldsymbol{v}^*$,

$$y_k'(s) = -\alpha\tau y_k(s) + \beta\tau \sum_{j=1}^{n} w_{kj} \int_0^\infty y_j(s-v)\hat{g}(v)\,dv, \qquad k = 1, \ldots, n. \tag{4.6}$$

In order to analyze the linear stability of the trivial solution of (4.6), we compute the characteristic equation associated with the above system. To do so, it is easier to look at the analogous vector form of (4.6),

$$\boldsymbol{y'}(s) = -\alpha\tau \boldsymbol{y}(s) + \beta\tau \boldsymbol{W} \int_0^\infty \boldsymbol{y}(s-v)\hat{g}(v)\,dv, \tag{4.7}$$

where $\boldsymbol{y} = (y_1, \ldots, y_n)^T$ and $\boldsymbol{W}$ is an $n \times n$ matrix with the $(kj)^{\text{th}}$ entry given by w_{kj}. Let $z_k, k = 1, \ldots, n$, be the eigenvalues of $\boldsymbol{W}$, then there exists a matrix $\boldsymbol{P}$ such that $\boldsymbol{W} = \boldsymbol{P}\boldsymbol{E}\boldsymbol{P}^{-1}$ [34]. Matrix $\boldsymbol{E}$ is an upper triangular matrix in Jordan canonical form, and the columns of $\boldsymbol{P}$ are the n generalized eigenvectors associated with the eigenvalues z_k. Thus $\boldsymbol{E} = \boldsymbol{D} + \boldsymbol{N}$, where $\boldsymbol{D}$ is a diagonal matrix with z_k as its diagonal elements, and $\boldsymbol{N}$ is a nilpotent matrix with zeros on the main diagonal, and zeros and/or ones on the upper off-diagonal, i.e.

$$\boldsymbol{E} = \begin{bmatrix} z_1 & * & 0 & \cdots & 0 \\ 0 & z_2 & * & \cdots & 0 \\ \vdots & & \ddots & \ddots & \vdots \\ & & & \ddots & * \\ 0 & & \cdots & 0 & z_n \end{bmatrix}, \tag{4.8}$$

where $*$ represents 0 or 1. With the change of variables $\boldsymbol{y} = \boldsymbol{P}\boldsymbol{x}$, equation (4.7) becomes

$$\boldsymbol{P}\boldsymbol{x'}(s) = -\alpha\tau \boldsymbol{P}\boldsymbol{x}(s) + \beta\tau \boldsymbol{P}\boldsymbol{E}\boldsymbol{P}^{-1} \int_0^\infty \boldsymbol{P}\boldsymbol{x}(s-v)\hat{g}(v)\,dv.$$

We multiply the above equation by $\boldsymbol{P}^{-1}$ to obtain

$$\boldsymbol{x'}(s) = -\alpha\tau \boldsymbol{x}(s) + \beta\tau \boldsymbol{E} \int_0^\infty \boldsymbol{x}(s-v)\hat{g}(v)\,dv.$$

Substituting $\boldsymbol{x} = e^{\lambda s}\boldsymbol{C}$ and letting $\hat{G}(v)$ represent the Laplace transform of $\hat{g}(v)$ as given in Definition 6, we have

$$\left[(\lambda + \alpha\tau)\boldsymbol{I} - \beta\tau \hat{G}(v)\boldsymbol{E}\right] \boldsymbol{C} = 0,$$

where $\boldsymbol{I}$ represents the $n \times n$ identity matrix. To obtain the characteristic matrix, we set the determinant of the coefficient matrix equal to zero, and using (4.8) we then have

$$\Delta(\lambda) = \det \left[(\lambda + \alpha\tau)\boldsymbol{I} - \beta\tau\hat{G}(v) \begin{bmatrix} z_1 & * & 0 & \cdots & 0 \\ 0 & z_2 & * & \cdots & 0 \\ \vdots & & \ddots & \ddots & \vdots \\ & & & \ddots & * \\ 0 & & \cdots & 0 & z_n \end{bmatrix} \right] = 0.$$

We notice that the coefficient matrix is upper triangular, and therefore the characteristic equation becomes,

$$\begin{aligned} 0 &= \Delta(\lambda) \\ &= \prod_{k=1}^{n} \Delta_k(\lambda) \\ &= \prod_{k=1}^{n} \left(\lambda + \alpha\tau - \beta\tau z_k \hat{G}(v) \right) \\ &= \prod_{k=1}^{n} \left(\lambda + \alpha\tau - \beta\tau z_k \int_0^\infty e^{-\lambda v} \hat{g}(v)\, dv \right). \end{aligned} \tag{4.9}$$

Since the characteristic equation is a product of the $\Delta_k(\lambda)$'s, λ is a root of $\Delta(\lambda)$ if and only if it is a root of $\Delta_k(\lambda)$ for some k. Therefore, the linear stability of (4.6) may be determined by studying the roots of $\Delta_k(\lambda)$, $k = 1, \ldots, n$. In Section 4.1 we will do this by assuming that the connection matrix $\boldsymbol{W}$ is symmetric, i.e. all its eigenvalues z_k are real [34]. In Section 4.2, we consider the case when $\boldsymbol{W}$ is not symmetric, i.e. its eigenvalues may be complex.

4.1 Connection Matrix with Real Eigenvalues

In this section we assume that the eigenvalues of the connection matrix $\boldsymbol{W}$ are real, i.e. $z_k \in \mathbb{R}$ for all $k = 1, \ldots, n$. We start by describing the distribution independent region of stability, which we present in the following subsection. Then in the following subsection, we improve on this conservative result by approximating the region of stability using the first few moments or cumulants of a distribution.

4.1.1 Distribution Independent Results

In this subsection we will give one result which is independent of all aspects of the distribution and one which is independent of all aspects save the mean delay. The main results of this subsection generalize to n dimensions the theorems presented in Chapter 3 for the scalar case.

Changes of stability of the equilibrium point of (4.6) will take place when the characteristic equation (4.9) has a root with zero real part. In the following we determine where in the parameter space such changes may occur, and hence describe the stability region in the $z\tau$-plane, which represents the common region of stability of all regions of stability in the $z_k\tau$-planes for $k = 1, \ldots, n$. In other words, the stability in the $z\tau$-plane guarantees stability in any of the $z_k\tau$-planes, $k = 1, \ldots, n$.

As for the scalar case, we start by locating the region of stability of the equilibrium point using Lemma 1 (Rouché).

Theorem 8 *Assume that $\hat{G}(\lambda)$ is analytic in $\mathrm{Re}(\lambda) \geq 0$, i.e. in the right-half complex plane. If $0 < |z_k| < \alpha/\beta$ for each $k = 1, \ldots, n$, then the characteristic equation has no roots with positive real part.*

Proof. Let $h(\lambda) = \lambda + \alpha\tau$ and $f_k(\lambda) = -\beta\tau z_k \hat{G}(\lambda)$, $k = 1, \ldots, n$. We again consider the contour in the complex plane, $C = C_1 \cup C_2$, given by

$$C_1 : \ \lambda = Re^{i\theta}, \ -\frac{\pi}{2} \leq \theta \leq \frac{\pi}{2}$$

$$C_2 : \ \lambda = iy, \ -R \leq y \leq R,$$

where R is a positive real number.

Similarly to the proof of Theorem 5, we show that on C_1, $|h(\lambda)| > |f_k(\lambda)|$ for each $k = 1, \ldots, n$, if R sufficiently large. Since $\alpha > 0$ and $\beta \geq 0$, on C_2 we have that $|h(\lambda)| > |f_k(\lambda)|$ if $\alpha > \beta|z_k|$ for each $k = 1, \ldots, n$.

Further, if $\beta \neq 0$ and $z_k \neq 0$ for $k = 1, \ldots, n$, then h and f_k, $k = 1, \ldots, n$, do not reduce to zero anywhere on C. Hence by Lemma 1, if $\alpha/\beta > |z_k| > 0$ for each $k = 1, \ldots, n$, and R is sufficiently large then $h(\lambda)$ and $\Delta_k(\lambda) = h(\lambda) + f_k(\lambda)$, $k = 1, \ldots, n$, have the same number of zeros inside C. Let $R \to \infty$ then $h(\lambda)$ and $\Delta_k(\lambda)$ have the same number of zeros with $\mathrm{Re}(\lambda) > 0$. Since α is positive, $h(\lambda)$ and thus $\Delta_k(\lambda)$ have no zeros in the right-half complex plane. Therefore the characteristic equation $\Delta(\lambda) = \prod_{k=1}^{n} \Delta_k(\lambda)$ has no roots with positive real part. □

The next result determines a region in the parameter space where the equilibrium point is unstable for any distribution $\hat{g}(v)$.

Theorem 9 *The equilibrium point $\boldsymbol{v}^*$ of (4.4) is unstable if at least one z_k, $k = 1, \ldots, n$, satisfies $z_k > \alpha/\beta$.*

Proof. We first pick one z_r for which we have $z_r > \alpha/\beta$. We next investigate the real roots of $\Delta_r(\lambda)$ and thus we assume $\Delta_r(\lambda) : \mathbb{R} \to \mathbb{R}$. Similarly to the proof of Theorem 6, we show that $\Delta_r(\lambda)$ has a unique real root which is positive. Therefore the characteristic equation $\Delta(\lambda) = \prod_{k=1}^{n} \Delta_k(\lambda)$ has at least one root with positive real part. The result follows. □

Note that for any distribution, the characteristic equation has a zero root (or zero roots) if for at least one k, $z_k = \alpha/\beta$. From Theorem 8, we have that the equilibrium point $\boldsymbol{v}^*$ of (4.4) is locally asymptotically stable if $|z_k| < \alpha/\beta$, i.e. if all z_k, $k = 1, \ldots, n$, are inside the region $|z| < \alpha/\beta$ in the $z\tau$-plane. From Theorem 9, we have that $\boldsymbol{v}^*$ is unstable if at least one z_k, $k = 1, \ldots, n$, is in the region $z > \alpha/\beta$ in the $z\tau$-plane. Therefore stability is gained as the line $z = \alpha/\beta$ is crossed by decreasing z, and thus this line forms part of the boundary of the stability region.

To further define the boundary of stability, we need to determine where the characteristic equation has a pair of pure imaginary roots, $\lambda = \pm i\omega$. We consider the most generic case: suppose that for one k, $\Delta_k(\lambda)$ has a pair of pure imaginary roots, i.e.

$$\Delta_k(i\omega) = i\omega + \alpha\tau - \beta\tau z_k \int_0^\infty e^{-i\omega v} \hat{g}(v)\, dv = 0. \tag{4.10}$$

Separating this into real and imaginary parts we find

$$\begin{array}{rcl} \alpha\tau & = & \beta\tau z_k \int_0^\infty \cos(\omega v)\, \hat{g}(v)\, dv \stackrel{\text{def}}{=} \beta\tau z_k C(\omega), \\ -\omega & = & \beta\tau z_k \int_0^\infty \sin(\omega v)\, \hat{g}(v)\, dv \stackrel{\text{def}}{=} \beta\tau z_k S(\omega). \end{array} \tag{4.11}$$

Consider

$$z = \frac{\alpha}{\beta C(\omega)}, \qquad \tau = -\frac{\omega C(\omega)}{\alpha S(\omega)}, \tag{4.12}$$

for all $\omega > 0$ such that $C(\omega)$ and $S(\omega)$ are nonzero. Equations (4.12) represent curves in the $z\tau$-plane parameterized by ω. We then choose the curve which is the closest to the τ-axis. If all $z_k, k = 1, \ldots, n$, lie below this curve then the equilibrium point of (4.6) is stable. Hence the curve described by (4.12) and closest to the τ-axis forms part of the boundary of stability. In the light of Theorems 8 and 9, the curves in (4.12) which form part of the stability boundary must lie in the region $z \leq -\alpha/\beta$.

We next determine whether the real part of the eigenvalue increases or decreases as we cross the lines in (4.12). As in (3.15), taking the derivative of τ in (4.12) with respect to ω we obtain

$$\frac{d\tau}{d\omega} = -\frac{1}{\alpha S(\omega)} \left(C(\omega) + \omega \frac{C'(\omega)S(\omega) - S'(\omega)C(\omega)}{S(\omega)} \right). \tag{4.13}$$

Using the definitions of $C(\omega)$ and $S(\omega)$ from (4.11), we rewrite (4.10) as

$$\begin{aligned} 0 = \Delta_k(i\omega) &= i\omega + \alpha\tau - \beta\tau z_k \left(C(\omega) - iS(\omega)\right) \\ &= \alpha\tau - \beta\tau z_k C(\omega) + i[\omega + \beta\tau z_k S(\omega)] \\ &= U_k(\omega) + iV_k(\omega) \end{aligned} \tag{4.14}$$

Next we compute the rate of change of the real part of λ with respect to z_k. Since

$$\Delta(\lambda) = \Delta_k(\lambda) \prod_{\substack{r=1 \\ r\neq k}}^{n} \Delta_r(\lambda),$$

we have that

$$\left.\frac{\partial \Delta}{\partial z_k}\right|_{\lambda=i\omega} = -\beta\tau \left[C(\omega) - iS(\omega)\right] \prod_{\substack{r=1 \\ r\neq k}}^{n} \left(i\omega + \alpha\tau - \beta\tau z_r \left(C(\omega) - iS(\omega)\right)\right).$$

and

$$\begin{aligned} \left.\frac{\partial \Delta}{\partial \lambda}\right|_{\lambda=i\omega} &= \left.\frac{\partial \Delta_k}{\partial \lambda}\right|_{\lambda=i\omega} \prod_{\substack{r=1 \\ r\neq k}}^{n} \Delta_r(i\omega) + \sum_{\substack{l=1 \\ l\neq k}}^{n} \Delta_k(i\omega) \left.\frac{\partial \Delta_l}{\partial \lambda}\right|_{\lambda=i\omega} \prod_{\substack{r=1 \\ r\neq k,l}}^{n} \Delta_r(i\omega) \\ &= \left.\frac{\partial \Delta_k}{\partial \lambda}\right|_{\lambda=i\omega} \prod_{\substack{r=1 \\ r\neq k}}^{n} \Delta_r(i\omega), \end{aligned}$$

where we used the fact that $\Delta_k(i\omega) = 0$. Since λ is a complex number, from (4.14) we get

$$\begin{aligned} \left.\frac{\partial \Delta}{\partial \lambda}\right|_{\lambda=i\omega} &= \left(\frac{dV_k}{d\omega} - i\frac{dU_k}{d\omega}\right) \prod_{\substack{r=1 \\ r\neq k}}^{n} \Delta_r(i\omega) \\ &= \left[1 + \beta\tau z_k \left(S'(\omega) + iC'(\omega)\right)\right] \prod_{\substack{r=1 \\ r\neq k}}^{n} \left(i\omega + \alpha\tau - \beta\tau z_r \left(C(\omega) - iS(\omega)\right)\right). \end{aligned}$$

Similarly to (3.10), we then have

$$\begin{aligned} \left.\frac{d\mathrm{Re}(\lambda)}{dz_k}\right|_{\lambda=i\omega} &= -\mathrm{Re}\left(\frac{\partial \Delta}{\partial z_k} \Big/ \left.\frac{\partial \Delta}{\partial \lambda}\right|_{\lambda=i\omega}\right) \\ &= -\mathrm{Re}\left(\frac{-\beta\tau(C(\omega) - iS(\omega))}{1 + \beta\tau z_k (S'(\omega) + iC'(\omega))}\right). \end{aligned}$$

And thus, as in (3.19), we obtain

$$\left.\frac{d\mathrm{Re}(\lambda)}{dz_k}\right|_{\lambda=i\omega} = \frac{\beta\tau}{H^2(\omega)}\left(C(\omega) + \omega\frac{C'(\omega)S(\omega) - S'(\omega)C(\omega)}{S(\omega)}\right), \tag{4.15}$$

where $H^2(\omega) = (1+\beta\tau z_k S'(\omega))^2 + (\beta\tau z_k C'(\omega))^2$ is a positive function of ω and we have used that $\beta\tau z_k = -\omega/S(\omega)$ from (4.11). Comparing (4.15) to (4.13) we see that

$$\left.\frac{d\mathrm{Re}(\lambda)}{dz_k}\right|_{\lambda=i\omega} = -\frac{\beta\tau}{H^2(\omega)}\alpha S(\omega)\frac{d\tau}{d\omega} = \frac{\alpha}{z_k}\frac{\omega}{H^2(\omega)}\frac{d\tau}{d\omega},$$

where we used the fact that $\beta = \alpha/(z_k C(\omega))$ from the first equation in (4.11), and $\alpha\tau S(\omega) = -\omega C(\omega)$ from the second equation in (4.12). Thus whether the number of eigenvalues with positive real part is increasing or decreasing as z_k is increased through a point on one of the curves defined by (4.12) depends on the sign of z_k and whether τ is an increasing or decreasing function of ω at that point.

We can also obtain the following distribution independent result. Its proof is similar to the proof of Theorem 7.

Theorem 10 *Assume that $\hat{G}(\lambda)$ is analytic in $\mathrm{Re}(\lambda) \geq 0$. Then the equilibrium point $\boldsymbol{v}^*$ of (4.4) is locally asymptotically stable if, for each $k = 1, \ldots, n$, either*

$$(1)\ |z_k| < \frac{\alpha}{\beta},$$

or

$$(2)\ -\frac{1}{\beta\tau} < z_k \leq -\frac{\alpha}{\beta}.$$

Theorem 10 describes the region of stability of the equilibrium point with either no knowledge of the distribution of delays or knowledge of only the first moment of the distribution, i.e. the mean delay, τ. We note that if all $z_k, k = 1, \ldots, n$, satisfy the condition in (1), then the equilibrium $\boldsymbol{v}^*$ of (4.4) is locally asymptotically stable for any value of the mean delay τ and for all distributions $\hat{g}(v)$. We call this the distribution independent stability region.

The results of Theorems 9 and 10 are illustrated in Figure 4.1. The stability region in the shaded area is a conservative result and is independent of the distribution, save the mean delay.

In practice the results of Theorem 10 are useful only if one is able to compute $\beta = f'(v^*)$. This might not be trivial since one has to solve the nonlinear system (4.5). But since we know from (1.7) that $\beta \leq f'(0) = \gamma$, we can use this to obtain the following corollary to Theorem 10.

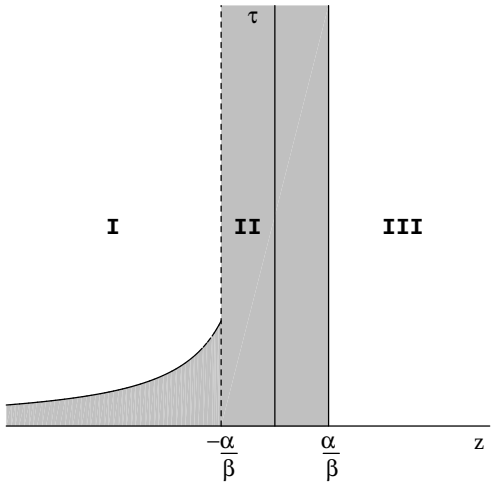

Figure 4.1: Illustration of the distribution independent stability results described by Theorems 9 and 10. (I) No distribution independent stability results are known for this region. (II) Region of stability described by Theorem 10: all z_k's must lie to the right of the curve $-1/(\beta\tau)$ and be less than $-\alpha/\beta$, or have norm less than α/β. (III) Region of instability described by Theorem 9: at least one of the z_k's must be greater than α/β.

Corollary 1 *Assume that* $\hat{G}(\lambda)$ *is analytic in* $\mathrm{Re}(\lambda) \geq 0$. *Then the equilibrium point* $\boldsymbol{v}^*$ *of* (4.2) *is locally asymptotically stable if, for each* $k = 1, \ldots, n$, *either*

$$(1)\ |z_k| < \frac{\alpha}{\gamma},$$

or

$$(2)\ -\frac{1}{\gamma\tau} < z_k \leq -\frac{\alpha}{\gamma}.$$

The results of the above corollary and their comparison to Theorem 10 are presented in Figure 4.2. Since $\beta \leq \gamma$, it is clear that the stability result presented in Corollary 1 is more conservative than the result of Theorem 10, but it might be more useful in practice since one only needs to know the neuron gain, $\gamma = f'(0)$.

To further characterize the stability region we need to use information from the distribution. In the next subsection we will show how one may find a better approximation to the region of stability than that given by Theorem 10 (shaded area in Figure 4.1) by using the first few moments or cumulants of the distribution. We note that it is only necessary to consider $z_k < -\alpha/\beta$, given the results of Theorems 8 and 9.

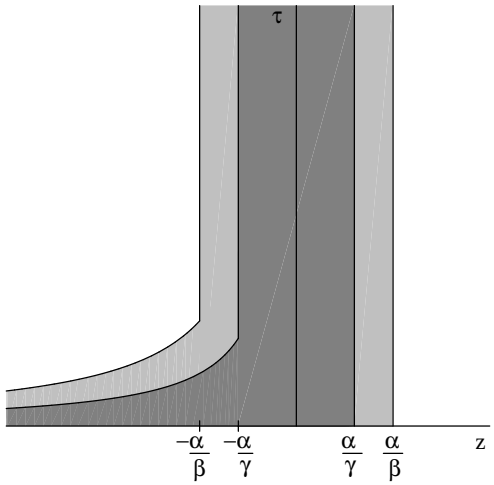

Figure 4.2: Comparison between the stability results described by Corollary 1 and the ones presented in Theorem 10. The stability region guaranteed by Corollary 1 (the dark gray region) is more conservative than the one guaranteed by Theorem 10 (the light gray region), but it is easier to obtain since it is only dependent on the neuron gain γ.

4.1.2 Approximating the Boundary of the Stability Region

In the following we apply the approximation procedure we developed in Chapter 3 in order to find a better estimate for the true boundary of stability than the conservative one described in the previous subsection in Theorem 10.

Recall that the boundary of the stability region in the $z\tau$-plane consists the line $z = \alpha/\beta$ and the curve(s) defined parametrically by equations (4.12) for $z \leq -\alpha/\beta$. In this subsection, we approximate these latter curves the same way we approximated the curves in (3.14). The computations are very similar to the ones in Subsections 3.2.1 and 3.2.2 and thus we do not replicate them here.

As described in Subsection 3.2.1, we obtain the approximations using moments for the curve(s) in (4.12), as seen in Table 4.1. Approximation $(0, 0)$ using moments does not exist since we only consider $\tau > 0$, i.e. this approximation predicts that the stability region is the entire half plane to the left of $z_k = \alpha/\beta$. Approximation $(0, 1)$ using moments represents the line $z_k = \alpha/\beta$, i.e. this approximation predicts that there is no stability

Table 4.1: Approximations using moments for $C(\omega)$, $S(\omega)$ and equations (4.12), where M and N relate to the number of terms used in the summation for $C(\omega)$ and $S(\omega)$, respectively.

(M,N)	$C(\omega)$	$S(\omega)$	z_k	τ
$(0,0)$	1	ω	$\dfrac{\alpha}{\beta}$	$-\dfrac{1}{\alpha}$
$(0,1)$	1	$\omega - \dfrac{m_3}{6}\omega^3$	$\dfrac{\alpha}{\beta}$	$\dfrac{6}{\alpha(m_3\omega^2-6)}$
$(1,0)$	$1-\dfrac{m_2}{2}\omega^2$	ω	$\dfrac{2\alpha}{\beta(2-m_2\omega^2)}$	$\dfrac{m_2\omega^2-2}{2\alpha}$
$(1,1)$	$1-\dfrac{m_2}{2}\omega^2$	$\omega - \dfrac{m_3}{6}\omega^3$	$\dfrac{2\alpha}{\beta(2-m_2\omega^2)}$	$\dfrac{3(m_2\omega^2-2)}{\alpha(6-m_3\omega^2)}$

region. Approximation $(1,0)$ using moments is given by

$$\tau^m_{(1,0)} = -\frac{1}{\beta z_k}, \qquad \omega = \sqrt{\frac{2}{m_2}\left(1-\frac{\alpha}{\beta z_k}\right)}. \tag{4.16}$$

The above approximation always underestimates the region of stability. For $z_k \leq -\alpha/\beta$, it recovers the results of Theorem 10. For $z_k > -\alpha/\beta$ the curve enters the region of distribution independent stability and thus gives a worse estimate than Theorem 10. Approximation $(1,1)$ using moments is given by

$$\tau^m_{(1,1)} = -\frac{1}{\left(1-\frac{m_3}{3m_2}\right)\beta z_k + \frac{m_3}{3m_2}\alpha}, \qquad \omega = \sqrt{\frac{2}{m_2}\left(1-\frac{\alpha}{\beta z_k}\right)}. \tag{4.17}$$

The above approximation is a hyperbola with a vertical asymptote at $z_k = \nu\alpha/(\beta(\nu-1))$, where $\nu = m_3/(3m_2) > 0$. The relationship between approximation $(1,1)$ using moments and the results of Theorem 10 will depend on the value of ν, and hence on the moments of the particular distribution. As shown in Subsection 3.2.1, for large z_k, we can say that if $\nu < 1$ then approximation $(1,1)$ using moments always lies above approximation $(1,0)$ using moments. Also, the curve in (4.17) enters the region of distribution-independent stability if $\nu \in (0,1/2) \cup (1,\infty)$.

Next, as described in Subsection 3.2.2, we determine the approximations using cumulants for the curve(s) in (4.12), as seen in Table 4.2. Recall that approximation $(0,0)$ using cumulants recovers the results for the corresponding equation with one fixed delay τ, i.e. model (4.2) where $g(u) = \delta(u-\tau)$. This approximation is given by

$$\tau^\kappa_{(0,0)} = \frac{1}{\sqrt{\beta^2 z_k^2 - \alpha^2}} \arccos\left(\frac{\alpha}{\beta z_k}\right), \qquad z_k < -\alpha/\beta. \tag{4.18}$$

Table 4.2: Approximations using cumulants for $C(\omega)$, $S(\omega)$ and equations (4.12), where M is the numbers of terms used in the sum inside the exponential function in (3.30), and N is the numbers of terms used in the sum inside the sine and cosine functions in (3.30).

(M,N)	$C(\omega)$	$S(\omega)$	z_k	τ
$(0,0)$	$\cos(\omega)$	$\sin(\omega)$	$\dfrac{\alpha}{\beta\cos(\omega)}$	$-\dfrac{\omega\cos(\omega)}{\alpha\sin(\omega)}$
$(0,1)$	$\cos\left(\omega-\frac{\kappa_3}{6}\omega^3\right)$	$\sin\left(\omega-\frac{\kappa_3}{6}\omega^3\right)$	$\dfrac{\alpha}{\beta\cos\left(\omega-\frac{\kappa_3\omega^3}{6}\right)}$	$-\dfrac{\omega\cos\left(\omega-\frac{\kappa_3\omega^3}{6}\right)}{\alpha\sin\left(\omega-\frac{\kappa_3\omega^3}{6}\right)}$
$(1,0)$	$\dfrac{\cos(\omega)}{\exp\left(\frac{\kappa_2}{2}\omega^2\right)}$	$\dfrac{\sin(\omega)}{\exp\left(\frac{\kappa_2}{2}\omega^2\right)}$	$\dfrac{\alpha\exp\left(\frac{\kappa_2\omega^2}{2}\right)}{\beta\cos(\omega)}$	$-\dfrac{\omega\cos(\omega)}{\alpha\sin(\omega)}$
$(1,1)$	$\dfrac{\cos\left(\omega-\frac{\kappa_3\omega^3}{6}\right)}{\exp\left(\frac{\kappa_2}{2}\omega^2\right)}$	$\dfrac{\sin\left(\omega-\frac{\kappa_3\omega^3}{6}\right)}{\exp\left(\frac{\kappa_2}{2}\omega^2\right)}$	$\dfrac{\alpha\exp\left(\frac{\kappa_2\omega^2}{2}\right)}{\beta\cos\left(\omega-\frac{\kappa_3\omega^3}{6}\right)}$	$-\dfrac{\omega\cos\left(\omega-\frac{\kappa_3\omega^3}{6}\right)}{\alpha\sin\left(\omega-\frac{\kappa_3\omega^3}{6}\right)}$

Since $\arccos(\alpha/(\beta z_k)) > 1$ for $z_k < -\alpha/\beta$, from (4.16) and (4.18), we can conclude that approximation $(0,0)$ using cumulants always lies above approximation $(1,0)$ using moments. Also, the curve in (4.18) has a vertical asymptote at $z_k = -\alpha/\beta$ and thus it never enters the distribution independent region of stability, $|z_k| < \alpha/\beta$ described by result (1) of Theorem 10. For approximation $(1,0)$ using cumulants, from Table 4.2, we get

$$\tau^{\kappa}_{(1,0)} = -\frac{\omega e^{\kappa_2\omega^2/2}}{\beta z_k \sin(\omega)},$$

where $\omega \in (\pi/2, \pi)$ in order to obtain the curve closest to the τ-axis. Since $\kappa_2 \geq 0$ and $\omega/\sin(\omega) > 1$, we have

$$\tau^{m}_{(1,0)} = -\frac{1}{\beta z_k} < -\frac{\omega e^{\kappa_2\omega^2/2}}{\beta z_k \sin(\omega)} = \tau^{\kappa}_{(1,0)},$$

i.e. approximation $(1,0)$ using cumulants always lies above approximation $(1,0)$ using moments.

We cannot make any general comparisons between approximations $(0,1)$ and $(1,1)$ using cumulants and the other approximations, but we will see in the following subsections how these approximations behave for specific distributions (uniform and gamma) and how they compare to the other approximations in those particular cases.

4.1.3 Verifying the Approximations for the Uniform Distribution

In this subsection we apply the approximation procedure we derived in the previous subsection to the uniform distribution. We compare these estimates for the boundary of stability to the true boundary of stability. We again look at the three cases: $\rho = 2$, $\rho = 1$, and $\rho = 4/5$.

Substituting (3.38) into equations (4.12), we obtain the true boundary of stability in the $z\tau$-plane, as shown by the black solid curve in Figures 4.3 and 4.4(a) (detail on how these curves are obtained is presented in Section 3.3). Thus the true region of stability lies between the solid gray line and the solid black curve, where the region of distribution independent stability lies between the solid and dashed gray lines. If all the $z_k, k = 1, \ldots, n$, lie between the solid gray line and the solid black curve, then the equilibrium point $\boldsymbol{v}^*$ of (4.4) (where $\hat{g}(v)$ is given in (2.31)) is locally asymptotically stable.

Substituting the values for the moments from Table 2.1 into the expressions for z_k and τ from Table 4.1, we get the approximations using moments as seen in Figures 4.3 and 4.4(a). Approximation $(0, 0)$ using moments does not exist. Approximation $(0, 1)$ using moments represents the line $z_k = \alpha/\beta$. Approximation $(1, 0)$ using moments represents the dotted curve and enters the distribution independent stability region $|z_k| < \alpha/\beta$ at $z_k = -\alpha/\beta, \tau = 1/\alpha$. Approximation $(1, 1)$ using moments is depicted as the dashed black curve. For $\rho = 2$ it has a vertical asymptote at $z_k = -\alpha/\beta$, and thus it never enters the distribution independent stability region, whereas for $\rho = 1$ and $\rho = 4/5$, it enters the region $|z_k| < \alpha/\beta$ when $\tau = 13/(3\alpha)$ and $\tau = 79/(21\alpha)$, respectively.

The approximations using cumulants are obtained by substituting the values for the cumulants from Table 2.1 into the expressions for z_k and τ from Table 4.2, as seen in Figures 4.3 and 4.4(a). Since the third cumulant is zero by (2.34), approximation $(0, 1)$ is identical to approximation $(0, 0)$, and approximation $(1, 1)$ is identical to approximation $(1, 0)$. Approximation $(0, 0)$ (and thus $(0, 1)$) using cumulants corresponds to the curve depicted by crosses, and approximation $(1, 0)$ (and thus $(1, 1)$) using cumulants corresponds to the curve depicted by circles. Approximation $(0, 0)$ (and in this case also $(0, 1)$) using cumulants has a vertical asymptote at $z_k = -\alpha/\beta$ and thus never enters the distribution independent stability region $|z_k| < \alpha/\beta$.

The conclusions about the approximations and their comparison to the true region of stability are the same as the ones we made at the end of Section 3.3.

4.1.4 Verifying the Approximations for the Gamma Distribution

In this subsection we will apply the approximations to the gamma distribution and compare these estimates to the true boundary of stability derived from the characteristic equation. We again look at the three different cases: $p = 3$, $p = 4$, and $p = 5$.

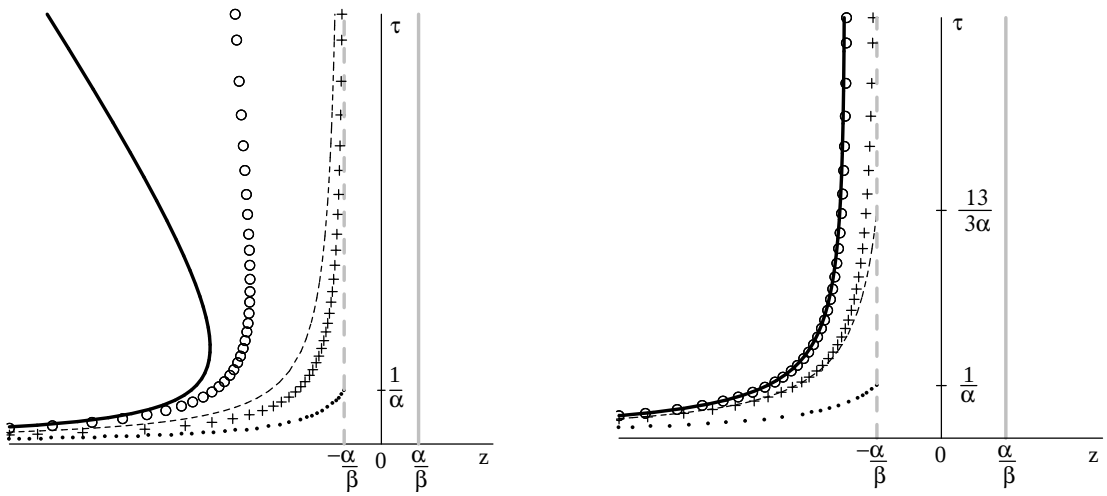

(a) Uniform, $\rho = 2$

(b) Uniform, $\rho = 1$

Figure 4.3: Stability region for the uniform distribution with $\rho = 2$ and $\rho = 1$. The region of distribution independent stability lies between the solid and dashed gray lines. The true region of stability lies between the solid gray line and the solid black curve: if all $z_k, k = 1, \ldots, n$, lie in this region, then the equilibrium $\boldsymbol{v}^*$ of (4.4) is locally asymptotically stable. Approximation $(0, 0)$ using moments predicts that the region of stability is the entire half plane to the left of the line $z_k = \alpha/\beta$, approximation $(0, 1)$ using moments predicts no stability region, approximation $(1, 0)$ using moments corresponds to the dotted curve, and approximation $(1, 1)$ using moments corresponds to the dashed black curve. Approximation $(0, 0)$ (and thus $(0, 1)$) using cumulants corresponds to the curve depicted by crosses. Approximation $(1, 0)$ (and thus $(1, 1)$) using cumulants corresponds to the curve depicted by circles.

Substituting (3.43) and (3.44) into equations (4.12), we obtain the true boundary of stability in the $z\tau$-plane, as shown by the black solid curve in Figures 4.4(b) and 4.5 (detail on how these curves are obtained is presented in Section 3.4). Thus the true region of stability lies between the solid gray line and the solid black curve, where the region of distribution independent stability lies between the solid and dashed gray lines. If all the $z_k, k = 1, \ldots, n$, lie between the solid gray line and the solid black curve, then the equilibrium point $\boldsymbol{v}^*$ of (4.4) (where $\hat{g}(v)$ is given in (2.39)) is locally asymptotically stable.

Substituting the values for the moments from Table 2.2 into the expressions for z_k and

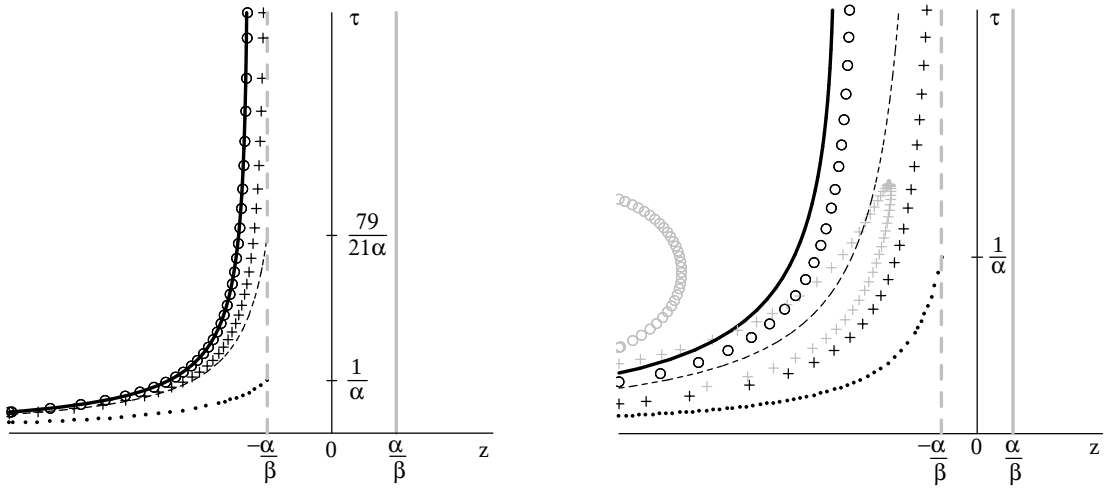

(a) Uniform, $\rho = 4/5$

(b) Gamma, $p = 3$

Figure 4.4: Stability region for the uniform distribution with $\rho = 4/5$ and for the gamma distribution with $p = 3$. The region of distribution independent stability lies between the solid and dashed gray lines. The true region of stability lies between the solid gray line and the solid black curve: if all $z_k, k = 1, \ldots, n$, lie in this region, then the equilibrium $\boldsymbol{v}^*$ of (4.4) is locally asymptotically stable. Approximation $(0, 0)$ using moments predicts that the region of stability is the entire half plane to the left of the line $z_k = \alpha/\beta$, approximation $(0, 1)$ using moments predicts no stability region, approximation $(1, 0)$ using moments corresponds to the dotted curve, and approximation $(1, 1)$ using moments corresponds to the dashed black curve. Approximations $(0, 0)$, $(0, 1)$, $(1, 0)$ and $(1, 1)$ using cumulants correspond to the curves depicted by black crosses, gray crosses, black circles and gray circles, respectively. In the case of the uniform distribution, approximation $(0, 0)$ using cumulants is identical to approximation $(0, 1)$, and approximation $(1, 0)$ using cumulants is identical to approximation $(1, 1)$.

τ from Table 4.1, we get the approximations using moments as seen in Figures 4.4(b) and 4.5 . Approximation $(0, 0)$ using moments does not exist. Approximation $(0, 1)$ using moments represents the line $z_k = \alpha/\beta$. Approximation $(1, 0)$ using moments represents the dotted curve and enters the distribution independent stability region $|z_k| < \alpha/\beta$ at $z_k = -\alpha/\beta, \tau = 1/\alpha$. Approximation $(1, 1)$ using moments is depicted as the dashed black curve. For $p = 3$ approximation $(1, 1)$ using moments has a vertical asymptote at $\beta = -5\alpha/4$ and for $p = 4$ it has a vertical asymptote at $\beta = -\alpha$, and thus they never

enter the distribution independent stability region, whereas for $p = 5$ it enters the region $|\beta| < \alpha$ when $\tau = 15/\alpha$.

The approximations using cumulants are obtained by substituting the values for the cumulants from Table 2.2 into the expressions for z_k and τ from Table 4.2, as seen in Figures 4.4(b) and 4.5. Approximation $(0, 0)$ corresponds to the curve depicted by black crosses, approximation $(0, 1)$ corresponds to the curve depicted by gray crosses, approximation $(1, 0)$ corresponds to the curve depicted by black circles, and approximation $(1, 1)$ corresponds to the curve depicted by gray circles. Approximation $(0, 0)$ using cumulants has a vertical asymptote at $z_k = -\alpha/\beta$ and thus never enters the distribution independent stability region $|z_k| < \alpha/\beta$.

The conclusion about the approximations and their comparison to the true region of stability are the same as the ones we made at the end of Section 3.4.

4.2 Connection Matrix with Complex Eigenvalues

In this section we analyze the stability of the equilibrium point $\boldsymbol{v}^*$ of (4.4), for a general interconnection matrix $\boldsymbol{W}$. In this case, the eigenvalues of $\boldsymbol{W}$ can be complex, $z_k = a_k + ib_k$, with $a_k, b_k \in \mathbb{R}$. We will determine conditions on these eigenvalues, in terms of the model parameters α, β and τ, that guarantee that the equilibrium point is locally asymptotically stable.

With definition of z_k above, the characteristic equation (4.9) becomes

$$0 = \Delta(\lambda) = \prod_{k=1}^{n} \Delta_k(\lambda) = \prod_{k=1}^{n} \left(\lambda + \alpha\tau - \beta\tau(a_k + ib_k) \int_0^\infty e^{-\lambda v} \hat{g}(v)\, dv \right), \tag{4.19}$$

where $\alpha, \beta, \tau > 0$. To determine the stability region we need to determine conditions such that all roots of (4.19) have negative real parts.

Theorem 11 *In the limit $\tau \to 0$, the equilibrium point $\boldsymbol{v}^*$ of (4.4) is locally asymptotically stable if $a_k < \alpha/\beta$ for each $k = 1, 2, \ldots, n$.*

Proof. As mentioned at the beginning of the chapter, when $\tau \to 0$, model (4.2) approaches the non-delayed model (4.3). We obtain the characteristic equation corresponding to (4.3) the same way we obtained (4.19),

$$0 = \prod_{k=1}^{n} (\lambda + \alpha - \beta(a_k + ib_k)).$$

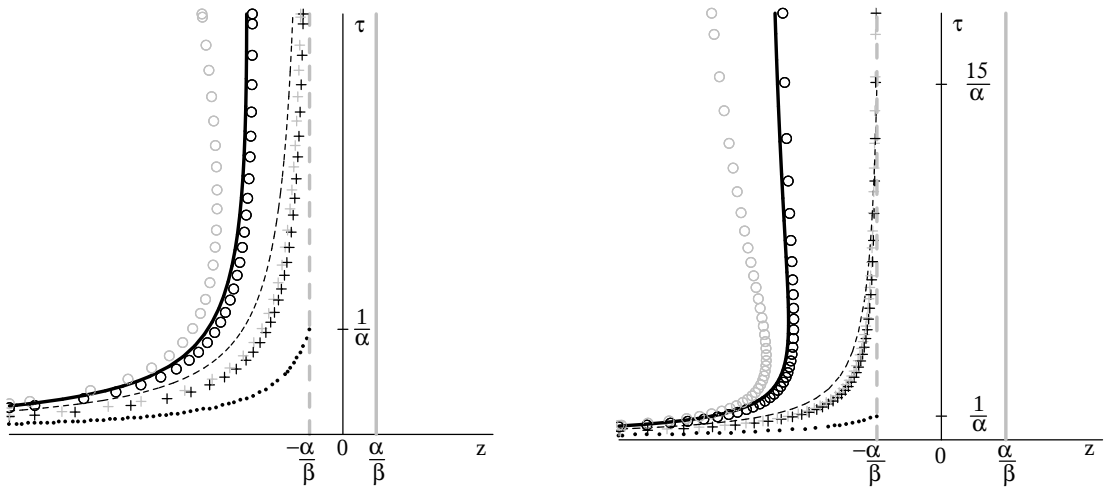

(a) Gamma, $p = 4$

(b) Gamma, $p = 5$

Figure 4.5: Stability region for the gamma distribution with $p = 4$ and $p = 5$. The region of distribution independent stability lies between the solid and dashed gray lines. The true region of stability lies between the solid gray line and the solid black curve: if all $z_k, k = 1, \ldots, n$, lie in this region, then the equilibrium $\boldsymbol{v}^*$ of (4.4) is locally asymptotically stable. Approximation $(0, 0)$ using moments predicts that the region of stability is the entire half plane to the left of the line $z_k = \alpha/\beta$, approximation $(0, 1)$ using moments predicts no stability region, approximation $(1, 0)$ using moments corresponds to the dotted curve, and approximation $(1, 1)$ using moments corresponds to the dashed black curve. Approximations $(0, 0)$, $(0, 1)$, $(1, 0)$ and $(1, 1)$ using cumulants correspond to the curves depicted by black crosses, gray crosses, black circles and gray circles, respectively.

Thus all roots of the characteristic equation have negative real parts if $a_k < \alpha/\beta$ for $k = 1, 2, \ldots, n$. The result follows. □

We next consider the case $\tau > 0$. We will study the roots of (4.19) by considering the roots of each factor, $\Delta_k(\lambda)$. If $b_k = 0$, from Section 4.1, we know that when $|a_k| < \alpha/\beta$ then all roots of $\Delta_k(\lambda)$ have negative real parts. Further, a standard result [41, 57] indicates that as the coefficients of $\Delta_k(\lambda)$ are varied, the number of roots with positive real parts can only change by a root passing through the imaginary axis. Now $\lambda = 0$ is a root of $\Delta_k(\lambda)$ only when $a_k = \alpha/\beta$ and $b_k = 0$. Further, using the definitions of $C(\omega)$ and $S(\omega)$ in

(4.11), $\lambda = i\omega, \omega > 0$, is a root of $\Delta_k(\lambda)$ when $a_k, b_k, \alpha, \beta, \tau$ satisfy the following equation

$$0 = \Delta_k(i\omega) = i\omega + \alpha\tau - \beta\tau(a_k + ib_k)\left(C(\omega) - iS(\omega)\right). \tag{4.20}$$

Separating (4.20) into the real and imaginary parts we obtain

$$\begin{aligned} \alpha\tau &= \beta\tau a_k C(\omega) + \beta\tau b_k S(\omega), \\ -\omega &= \beta\tau a_k S(\omega) - \beta\tau b_k C(\omega). \end{aligned} \tag{4.21}$$

To analyze these equations we need the following basic properties of $C(\omega)$ and $S(\omega)$.

Lemma 2 *Let $C(\omega)$ and $S(\omega)$ be defined as in (4.11). Then $C(0) = 1$, $S(0) = 0$, $C'(0) = 0$, $S'(0) = 1$ and $C^2(\omega) + S^2(\omega) \leq 1$ for any distribution.*

Proof. The first four results follow directly from the definitions of $C(\omega)$ and $S(\omega)$ in (4.11),

$$\begin{aligned} C(0) &= \int_0^\infty \cos(0)\hat{g}(v)\,dv = 1, \\ S(0) &= \int_0^\infty \sin(0)\hat{g}(v)\,dv = 0, \\ C'(0) &= \int_0^\infty -v\sin(0)\hat{g}(v)\,dv = 0, \\ S'(0) &= \int_0^\infty v\cos(0)\hat{g}(v)\,dv = 1, \end{aligned}$$

where we used properties (2.12) and (2.13). For the last result, note that

$$\begin{aligned} C^2(\omega) &= \left(\int_0^\infty \cos(\omega v)\,\hat{g}(v)\,dv\right)^2 \\ &= \int_0^\infty \cos(\omega v)\,\hat{g}(v)\,dv \int_0^\infty \cos(\omega w)\,\hat{g}(w)\,dw \\ &= \int_0^\infty \cos(\omega v)\,\hat{g}(v) \int_0^\infty \cos(\omega w)\,\hat{g}(w)\,dw\,dv \\ &= \int_0^\infty \int_0^\infty \cos(\omega v)\,\cos(\omega w)\,\hat{g}(v)\hat{g}(w)\,dw\,dv. \end{aligned}$$

Similarly,

$$S^2(\omega) = \int_0^\infty \int_0^\infty \sin(\omega v)\,\sin(\omega w)\,\hat{g}(v)\hat{g}(w)\,dw\,dv.$$

Adding the two expressions we get

$$\begin{aligned}
C^2(\omega) + S^2(\omega) &= \int_0^\infty \int_0^\infty [\cos(\omega v)\, \cos(\omega w) + \sin(\omega v)\, \sin(\omega w)]\, \hat{g}(v)\hat{g}(w)\, dw\, dv \\
&= \int_0^\infty \int_0^\infty \cos(\omega v - \omega w)\, \hat{g}(v)\hat{g}(w)\, dw\, dv \\
&\leq \left| \int_0^\infty \int_0^\infty \cos(\omega v - \omega w)\, \hat{g}(v)\hat{g}(w)\, dw\, dv \right| \\
&\leq \int_0^\infty \int_0^\infty |\cos(\omega v - \omega w)|\ \hat{g}(v)\hat{g}(w)\, dw\, dv \\
&\leq \int_0^\infty \int_0^\infty \hat{g}(v)\hat{g}(w)\, dw\, dv \\
&= \int_0^\infty \hat{g}(v)\, dv \int_0^\infty \hat{g}(w)\, dw \\
&= 1. \qquad \square
\end{aligned}$$

Now we can obtain extensions of result (1) of Theorem 10 and its corollary to the case when the eigenvalues of the connection matrix are complex.

Theorem 12 *The equilibrium point* $\boldsymbol{v}^*$ *of* (4.4) *is locally asymptotically stable if* $|z_k| < \alpha/\beta$*, for each* $k = 1, 2, \ldots, n$*.*

Proof. Squaring and adding equations (4.21) we obtain

$$\begin{aligned}
\alpha^2\tau^2 + \omega^2 &= \beta^2\tau^2 a_k^2 C^2(\omega) + \beta^2\tau^2 b_k^2 S^2(\omega) + 2\beta^2\tau^2 a_k b_k C(\omega) S^2(\omega) \\
&\quad + \beta^2\tau^2 a_k^2 S^2(\omega) + \beta^2\tau^2 b_k^2 C^2(\omega) - 2\beta^2\tau^2 a_k b_k C(\omega) S^2(\omega) \\
&= \beta^2\tau^2 a_k^2 (C^2(\omega) + S^2(\omega)) + \beta^2\tau^2 b_k^2 (C^2(\omega) + S^2(\omega)) \\
&= \beta^2\tau^2 (C^2(\omega) + S^2(\omega))(a_k^2 + b_k^2).
\end{aligned}$$

Therefore the magnitude of z_k is given by

$$|z_k| = \sqrt{a_k^2 + b_k^2} = \frac{\sqrt{\alpha^2\tau^2 + \omega^2}}{\beta\tau\sqrt{C^2(\omega) + S^2(\omega)}}.$$

Then by the last result of Lemma 2, a necessary condition on the magnitude of z_k for a pure imaginary root of $\Delta_k(\lambda)$ to exist is

$$|z_k| \geq \frac{\sqrt{\alpha^2\tau^2 + \omega^2}}{\beta\tau} \geq \frac{\alpha}{\beta}. \tag{4.22}$$

Clearly this cannot be satisfied if $|z_k| < \alpha/\beta$, so the result follows. $\square$

Theorem 12 represents the distribution independent stability region, since if all $z_k, k = 1, \ldots, n$, have magnitude less than α/β, then equilibrium point $\boldsymbol{v}^*$ of (4.4) is locally asymptotically stable for any distribution $\hat{g}(v)$. We note that this region is the delay independent region of stability of the corresponding model with one fixed delay τ, i.e. model (4.2) where $g(u) = \delta(u - \tau)$.

As mentioned in Section 4.1, $\beta = f'(v^*)$ might be difficult to compute in practice, but using the fact that $\beta \leq \gamma$, we can obtain the following corollary to the above theorem.

Corollary 2 *The equilibrium point $\boldsymbol{v}^*$ of (4.4) is locally asymptotically stable if $|z_k| < \alpha/\gamma$, for each $k = 1, 2, \ldots, n$.*

These conditions are easier to check, since we only require knowledge of the neuron gain $\gamma = f'(0)$.

To get more precise conditions for stability, we solve for a_k and b_k from (4.21),

$$\begin{aligned} a_k &= \frac{\tau\alpha C(\omega) - \omega S(\omega)}{\beta\tau(C^2(\omega) + S^2(\omega))}, \\ b_k &= \frac{\tau\alpha S(\omega) + \omega C(\omega)}{\beta\tau(C^2(\omega) + S^2(\omega))}. \end{aligned} \tag{4.23}$$

For fixed α, β and τ, system (4.23) represents a curve in the complex plane parameterized by $\omega > 0$. But $\lambda = -i\omega, \omega > 0$, is also a root of $\Delta_k(\lambda)$, and in this case $a_k, b_k, \alpha, \beta, \tau$ satisfy the equation

$$0 = \Delta_k(-i\omega) = -i\omega + \alpha\tau - \beta\tau(a_k + ib_k)\left(C(\omega) + iS(\omega)\right).$$

Separating into the real and imaginary parts we obtain

$$\begin{aligned} \alpha\tau &= \beta\tau a_k C(\omega) - \beta\tau b_k S(\omega), \\ -\omega &= \beta\tau a_k S(\omega) + \beta\tau b_k C(\omega). \end{aligned}$$

Solving for a_k and b_k, we have

$$\begin{aligned} a_k &= \frac{\tau\alpha C(\omega) - \omega S(\omega)}{\beta\tau(C^2(\omega) + S^2(\omega))} \\ b_k &= -\frac{\tau\alpha S(\omega) + \omega C(\omega)}{\beta\tau(C^2(\omega) + S^2(\omega))}. \end{aligned} \tag{4.24}$$

Therefore the curve in (4.24) is symmetric to the curve in (4.23) about $b_k = 0$. Thus, the two systems (4.23) and (4.24) can be represented by one system,

$$\begin{aligned} a_k &= \frac{\tau\alpha C(\omega) - \omega S(\omega)}{\beta\tau(C^2(\omega) + S^2(\omega))} \stackrel{\text{def}}{=} R(\omega), \\ b_k &= \frac{\tau\alpha S(\omega) + \omega C(\omega)}{\beta\tau(C^2(\omega) + S^2(\omega))} \stackrel{\text{def}}{=} I(\omega), \end{aligned} \tag{4.25}$$

if we let $\omega \in \mathbb{R}$. As shown above, the curve represented in (4.25) is symmetric about $b_k = 0$. When $\omega = 0$, this curve passes through the point $(\alpha/\beta, 0)$ with infinite slope, since

$$\begin{aligned} \left.\frac{da_k}{d\omega}\right|_{\omega=0} &= \left.\frac{(\tau\alpha C'(\omega) - S(\omega) - \omega S'\omega)\beta\tau(C^2(\omega) + S^2(\omega))}{\beta^2\tau^2(C^2(\omega) + S^2(\omega))^2}\right|_{\omega=0} \\ &\quad - \left.\frac{(\tau\alpha C(\omega) - \omega S(\omega))\beta\tau(2C(\omega)C'(\omega) + 2S(\omega)S'(\omega))}{\beta^2\tau^2(C^2(\omega) + S^2(\omega))^2}\right|_{\omega=0} \\ &= 0, \end{aligned}$$

where we used the fact that $C'(0) = S(0) = 0$ from Lemma 2, and thus

$$\frac{da_k}{db_k} = \frac{da_k}{d\omega}\frac{d\omega}{db_k} = 0.$$

From (4.22), we also have that points on the curve in (4.25) lie on or outside the circle $a_k^2 + b_k^2 = \alpha^2/\beta^2$.

Let $\bar{\omega}$ be the smallest positive value such that $I(\bar{\omega}) = 0$. If $I(\omega) \neq 0$ for $\omega \neq 0$, then let $\bar{\omega} = \infty$. Then we have the following distribution dependent result.

Theorem 13 *Let α, β and τ be fixed. The equilibrium point $\boldsymbol{v}^*$ of (4.4) is locally asymptotically stable if for each $k = 1, 2, \ldots, n$ the point (a_k, b_k) lies inside the curve $(R(\omega), I(\omega))$, $\omega \in [-\bar{\omega}, \bar{\omega}]$ where $R(\omega)$ and $I(\omega)$ are defined by (4.25) and*

$$M(\omega) = \sqrt{R^2(\omega) + I^2(\omega)} = \frac{\sqrt{\alpha^2\tau^2 + \omega^2}}{\beta\tau\sqrt{C^2(\omega) + S^2(\omega)}}, \qquad \text{for } \omega \in [0, \bar{\omega}], \tag{4.26}$$

is an increasing function of ω.

Proof. From Theorem 12, all roots of $\Delta_k(\lambda)$ have negative real parts if $|z_k| < \alpha/\beta$. For fixed α, β and τ, this corresponds to the point (a_k, b_k) lying inside the circle $a_k^2 + b_k^2 = \alpha^2/\beta^2$. As discussed above, if a_k and b_k are moved outside this circle the number of roots of $\Delta_k(\lambda)$ with positive real parts can only change if there is root with zero real part for some values of a_k and b_k.

Condition (4.26) avoids the anomaly of the curve $(R(\omega), I(\omega)),\ \omega \in [0, \bar{\omega}]$ spiraling back on itself, since it imposes that the magnitude of the points on this curve to be an increasing function of ω. From this and the properties of the curve $(R(\omega), I(\omega)),\ \omega \in [-\bar{\omega}, \bar{\omega}]$ discussed above, a root with zero real part will occur when $a_k = R(\omega), b_k = I(\omega)$ for some $\omega \in [-\bar{\omega}, \bar{\omega}]$. The result follows. □

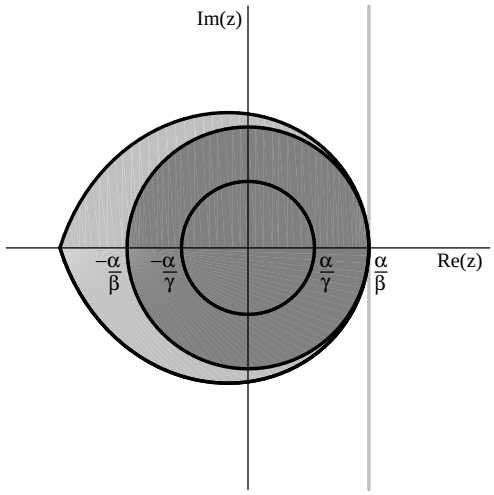

Figure 4.6: Illustration of the stability region described by Theorems 11 – 13 and Corollary 2. The region to the left of the grey line is the stability region for $\tau \to 0$. If all eigenvalues of the connection matrix lie inside the dark gray disk with boundary $|z_k| = \alpha/\beta$, then the equilibrium point $\boldsymbol{v}^*$ of (4.4) is stable for any mean delay or any distribution. The actual stability region (the light gray tear drop region) will depend on the particular distribution and the value of the mean delay τ. The region inside the smaller circle of radius α/γ also guarantees stability for any mean delay and any distribution; it is more conservative, but it is easier to obtain, since it only requires knowledge of the neuron gain $\gamma = f'(0)$.

The results of Theorems 12, 13 and Corollary 2 are depicted in Figure 4.6. As in [47], we represent the condition given by each theorem by a region in the complex plane such that if all the $z_k, k = 1, 2, \ldots, n$, lie inside this region then the condition is satisfied. We will refer to this region as the stability region of the equilibrium point $\boldsymbol{v}^*$ of (4.4). The region to the left of the grey line is the stability region for $\tau \to 0$ given by Theorem 11. The distribution independent region of stability (for $\tau > 0$) is shown in dark gray. The larger circle shows the result of Theorem 12 and the smaller one that of Corollary 2. The actual stability region (light grey) described by Theorem 13 encompasses this conservative

region. Its shape depends on the particular distribution and the value of the mean delay.

As mentioned in Chapter 1, a commonly held belief is that a system with a distribution of delays is more stable than the same system with a fixed delay [4, 7, 24, 36, 46, 64]. The following shows this is true for our system, for large enough mean delay.

Theorem 14 *In the limit $\tau \to \infty$, the stability region of the equilibrium $\boldsymbol{v}^*$ of (4.4) with the Dirac distribution (i.e. a fixed delay) lies inside or is the same as the stability region of the equilibrium $\boldsymbol{v}^*$ of (4.4) with any other distribution.*

Proof. From Theorem 13 the stability region of the equilibrium point for any distribution is the region in the complex plane enclosed by the curve $(R(\omega), I(\omega)),\ \omega \in [-\bar{\omega}, \bar{\omega}]$ where $R(\omega)$ and $I(\omega)$ are defined by (4.25). In the limit $\tau \to \infty$, this curve is given by $(R_\infty(\omega), I_\infty(\omega)),\ \omega \in [-\bar{\omega}, \bar{\omega}]$ where $R_\infty(\omega)$ and $I_\infty(\omega)$ are defined by

$$R_\infty(\omega) = \lim_{\tau\to\infty} R(\omega) = \frac{\alpha C(\omega)}{\beta(C^2(\omega) + S^2(\omega))},$$
$$I_\infty(\omega) = \lim_{\tau\to\infty} I(\omega) = \frac{\alpha S(\omega)}{\beta(C^2(\omega) + S^2(\omega))}.$$

For the case of a Dirac distribution, i.e. a fixed delay, the stability region is as defined above, with $C(\omega) = \cos(\omega)$ and $S(\omega) = \sin(\omega)$. As $\tau \to \infty$ this region becomes the circle $|z_k| = \alpha/\beta$. The result then follows from the fact that

$$R_\infty(\omega)^2 + I_\infty(\omega)^2 = \frac{\alpha^2}{\beta^2(C^2(\omega) + S^2(\omega))} \geq \frac{\alpha^2}{\beta^2},$$

by the last result of Lemma 2. □

We note that the behaviour of the stability region as the mean delay τ varies can be quite different for different distributions. As presented in [47], the size of the region of stability of the model with fixed delay decreases monotonically as τ increases. As $\tau \to \infty$, the stability region approaches the delay independent region of stability, $|z_k| < \alpha/\beta$. For the model with other distributions, we do not necessarily have this uniform convergence as the mean delay becomes larger and larger. For example, for the gamma distribution with $p = 3$, there exists a particular value of the mean delay, $\tau = \tau_c$, such that if all eigenvalues of the connection matrix are inside the tear drop region given by

$$|z_k| = \frac{\sqrt{\alpha^2\tau_c^2 + \omega^2}}{\beta\tau_c\sqrt{C^2(\omega) + S^2(\omega)}}, \tag{4.27}$$

then the equilibrium point is locally asymptotically stable for any value of the mean delay. But unlike the model with fixed delay, the value of τ_c is not infinity. This is depicted in

Figure 4.7(a). As τ increases the region of stability decreases until it reaches a minimum stability region at $\tau = \tau_c$, represented by the inner-most black curve. For $\tau > \tau_c$, the region of stability increases until it reaches the stability region for $\tau \to \infty$, depicted by the outer gray curve. Hence stability can be regained as we increase the mean delay, which cannot be achieved for the model with fixed delay. For real eigenvalues of the connection matrix, the value of τ_c corresponds to the maximum of the boundary of stability. As seen in Figure 4.7(b), at this maximum, the boundary of stability has a vertical slope (depicted as the dash black line) and if all $z_k, k = 1, \ldots, n$, are to the right of this line and less than α/β, then the equilibrium point is stable for any value of the mean delay. If any of the z_k's are located to the left of the vertical line, the stability can be regained for sufficiently large τ.

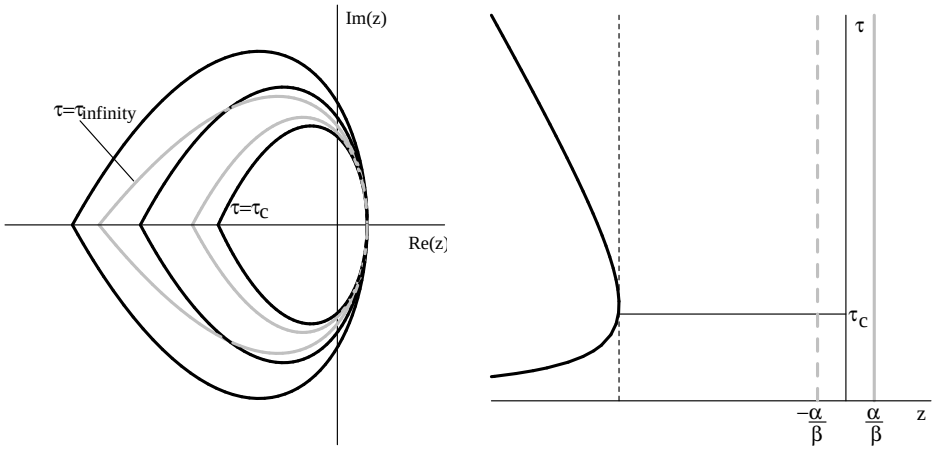

(a) Complex z_k's (b) Real z_k's

Figure 4.7: (a) As τ increases, the region of stability decreases until it reaches a minimum stability region at $\tau = \tau_c$, represented by the inner-most black curve. For $\tau > \tau_c$, the region of stability increases until it reaches the stability region for $\tau \to \infty$, depicted by the outer gray curve. Thus if all $z_k, k = 1, \ldots, n$, are inside the boundary corresponding to $\tau = \tau_c$, the equilibrium point is stable for any value of the mean delay. (b) For real eigenvalues of the connection matrix, the value of τ_c corresponds to the maximum on the boundary of stability (i.e. where the curve has a vertical slope in the $z\tau$-plane). Thus in the region between the dash black and solid gray lines, the equilibrium is stable for any value of the mean delay.

We illustrate our results with an example, where we analyze a three dimensional network with a particular connection matrix. We investigate the stability region of the equilibrium point of the nonlinear model in (4.2) with $n = 3$ and of its corresponding model with a fixed delay as we vary β. We perform the numerical simulations using the XPPAUT package [17].

Example. Consider the connection matrix

$$\boldsymbol{W} = \begin{bmatrix} 0 & 1 & 0 \\ -65/64 & 0 & 1/16 \\ 65/64 & 1 & 0 \end{bmatrix}$$

with eigenvalues $z_1 = 1/4, z_{2,3} = -1/8 \pm i$. We let $\alpha = 1$ and $F_k = 0$ for $k = 1, 2, 3$, and $\tau = 3$ (this value of τ is in fact the critical value of the mean delay, i.e. if the three eigenvalues of $\boldsymbol{W}$ are inside the region given by (4.27) with $\tau_c = 3$, then the equilibrium point is stable for any value of the mean delay). We let $g(u)$ to represent the gamma distribution with $p = 3$ and the signal function to be $f(v) = \tanh(\beta v)$. We compare the stability region of the equilibrium point of the three dimensional nonlinear model in (4.2) to the stability region of the equilibrium point of the corresponding model with a fixed delay $\tau = 3$.

For $\beta = 0.5$ the three eigenvalues of the connection matrix lie within the boundary of stability for the distributed delay model (the solid black curve) and also within the boundary of stability for the model with one fixed delay (the curve depicted by crosses), as seen in Figure 4.8(a). In this case, the three eigenvalues of $\boldsymbol{W}$ also lie inside the delay and distribution independent region of stability (the gray circle), hence Theorem 12 or Theorem 13 predicts that the equilibrium point of the model for both distributed and fixed delay is stable. This is seen in Figures 4.8(b) and (c), where all neurons converge to the steady state solution.

For $\beta = 1.2$ the three eigenvalues of the connection matrix lie within the boundary of stability for the distributed delay model (the solid black curve), but two of them lie outside the boundary of stability for the fixed delay model (the curve depicted by crosses), as seen in Figure 4.9(a). Thus Theorem 13 predicts that the equilibrium of the distributed delay model is stable, but cannot predict anything about the stability of the equilibrium of the fixed delay model. Figure 4.9(b) shows the neurons in the distributed delay model converging to the steady state solution, whereas the neurons in the fixed delay model oscillate, as seen in Figure 4.9(c).

For $\beta = 1.5$ the three eigenvalues of the connection matrix lie outside both the boundary of stability for the distributed and fixed delay models, as seen in Figure 4.10(a). Thus Theorem 13 cannot be applied to predict anything about the stability of the equilibrium point of the two models. Figures 4.10(b) and (c) show the three neurons oscillating for both the distributed and fixed delay models.

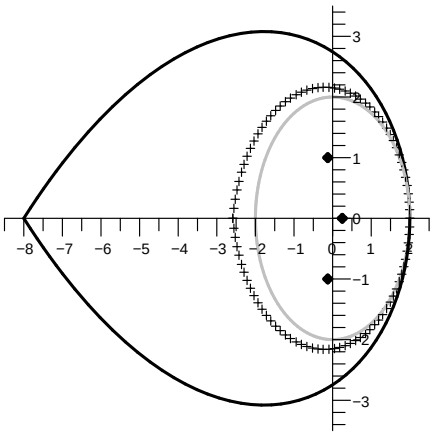

(a) $\beta = 0.5$ ($\tau = 3, \alpha = 1$)

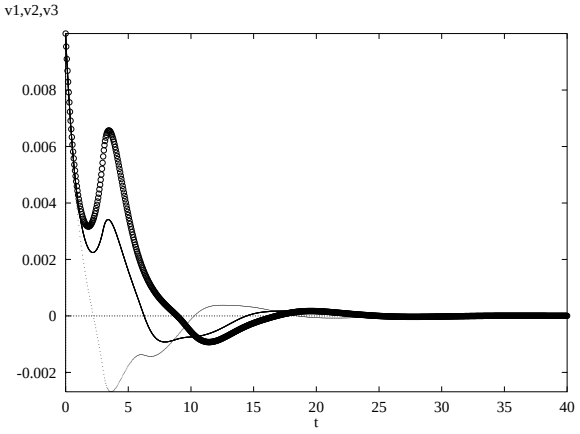

(b) Distributed delay (gamma, $p = 3$)

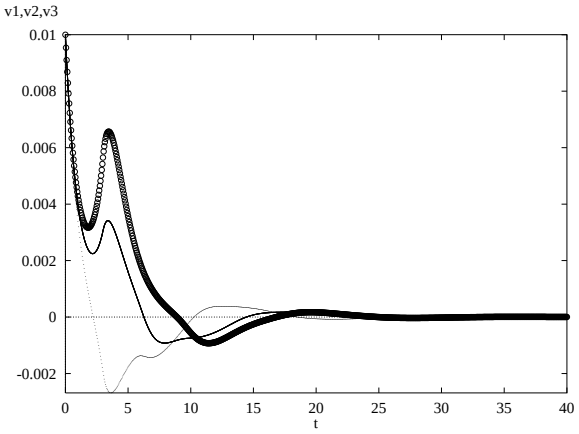

(c) Fixed delay

Figure 4.8: (a) The stability boundary of the distributed delay model is given by the black curve and of the model with fixed delay by the curve depicted by crosses. The gray circle represents the delay and distribution independent region of stability given by Theorem 12. The eigenvalues of the connection matrix are plotted as dots. Theorem 12 or Theorem 13 predicts that, for $\beta = 0.5$, the equilibrium of the model is stable for both distributed and fixed delay. This is confirmed by numerical simulations: all three neurons converge to the steady state solution in the model with (b) distributed and (c) fixed delay.

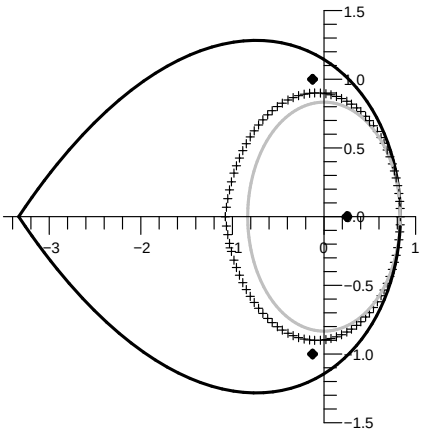

(a) $\beta = 1.2$ ($\tau = 3, \alpha = 1$)

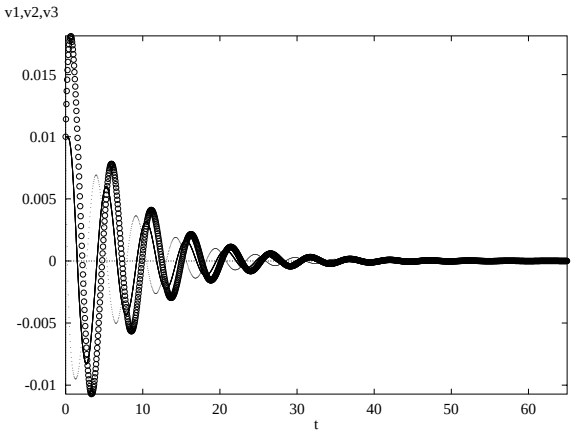

(b) Distributed delay (gamma, $p = 3$)

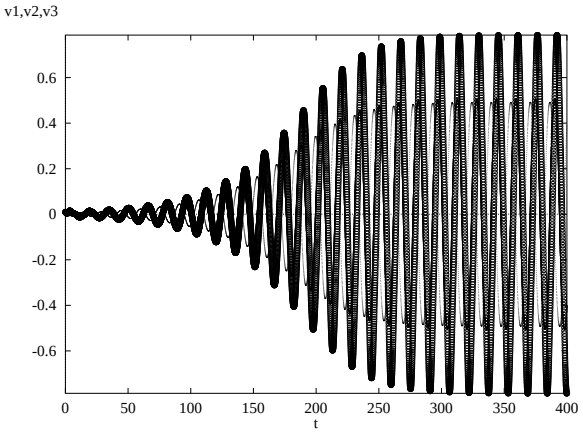

(c) Fixed delay

Figure 4.9: (a) The stability boundary of the distributed delay model is given by the black curve and of the fixed delay model by the curve depicted by crosses. The gray circle represents the delay and distribution independent region of stability given by Theorem 12. The eigenvalues of the connection matrix are plotted as dots. Theorem 13 predicts that, for $\beta = 1.2$, the equilibrium of the distributed delay model is stable, but cannot predict anything about the stability of the equilibrium point of the fixed delay model. This is confirmed by numerical simulations: (b) all three neurons in the distributed delay model converge to the steady state solution; (c) all three neurons in the fixed delay model oscillate.

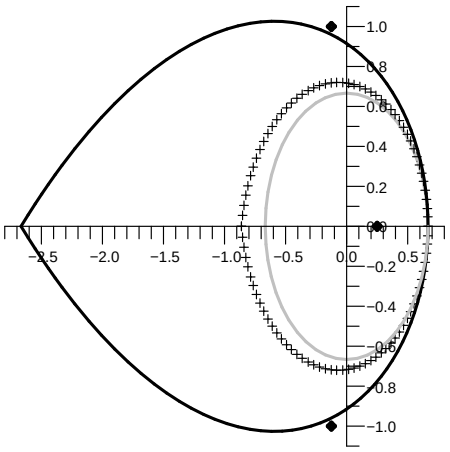

(a) $\beta = 1.5$ ($\tau = 3, \alpha = 1$)

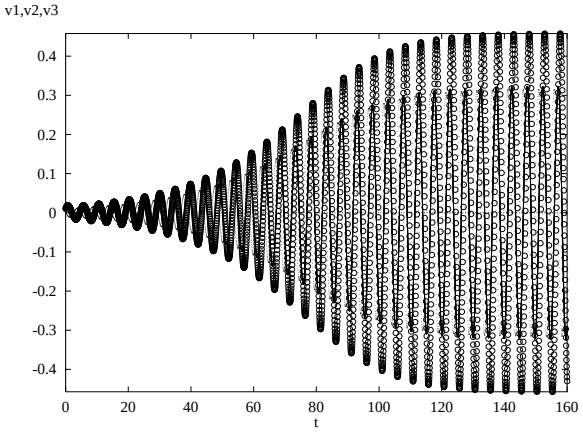

(b) Distributed delay(gamma, $p = 3$)

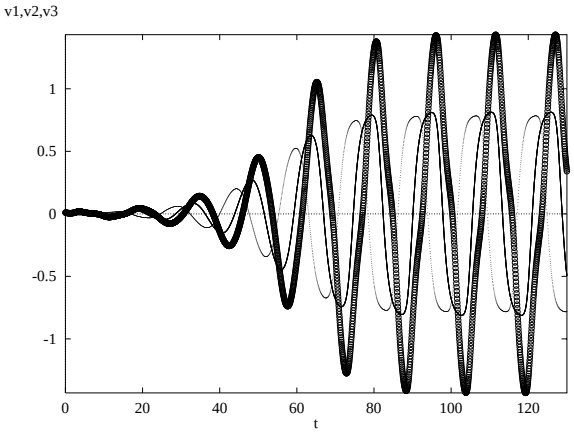

(c) Fixed delay

Figure 4.10: (a) The stability boundary of the distributed delay model is given by the black curve and of the model with fixed delay by the curve depicted by crosses. The gray circle represents the delay and distribution independent region of stability given by Theorem 12. The eigenvalues of the connection matrix are plotted as dots. For $\beta = 1.8$, Theorem 12 cannot be applied to predict the stability of the equilibrium point of the distributed and fixed delay models. This is confirmed by numerical simulations: all three neurons in the (b) distributed and (c) fixed delay models oscillate.

We note that for $\beta = 1.5$, the stability of the equilibrium point of the distributed delay model can be recovered by increasing the mean delay. As τ is increased beyond the critical value $\tau_c = 3$, the boundary of the stability region becomes larger and eventually encompasses the three eigenvalues, as seen in Figure 4.11(a). When $\tau = 20$, Theorem 13 predicts that the equilibrium of the distributed delay model is stable. On the other hand, for the fixed delay model, as τ becomes larger, the boundary of the stability region becomes smaller and thus the stability of the equilibrium point can never be recovered. Figure 4.11(b) shows the neurons in the distributed delay model converging to the steady state solution, whereas the neurons in the fixed delay model oscillate, as seen in Figure 4.11(c). □

In the next subsections we obtain approximations for the boundary of the stability region, $(R(\omega), I(\omega))$, $\omega \in [-\bar{\omega}, \bar{\omega}]$, using the approximations for $C(\omega)$ and $S(\omega)$ derived in Subsection 4.1.2. We then compare these approximations with the exact boundary of stability in the case of the uniform and gamma distributions.

4.2.1 Approximating the Boundary of the Stability Region

In the following we apply the approximation procedure we developed in Chapter 3 in order to find a better estimate for the true boundary of stability than the conservative one described by Theorem 12. We note that in this subsection, all the computations and simplifications are done using the symbolic algebra language Maple™.

From Theorem 13, we have that the boundary of stability is given by the curve $(R(\omega), I(\omega))$, $\omega \in [-\bar{\omega}, \bar{\omega}]$ where $R(\omega)$ and $I(\omega)$ are defined by (4.25). The boundary of stability can thus be approximated by substituting the approximations for $C(\omega)$ and $S(\omega)$ from Tables 4.1 and 4.2 into (4.25).

In particular, approximation $(0, 0)$ using moments is given by

$$\left|z^m_{(0,0)}\right| = \frac{\sqrt{\alpha^2\tau^2 + \omega^2}}{\beta\tau\sqrt{\omega^2 + 1}}.$$

Thus points on the above curve lie on or outside the circle $a_k^2 + b_k^2 = \alpha^2/\beta^2$ if

$$\frac{\alpha^2\tau^2 + \omega^2}{\beta^2\tau^2(\omega^2 + 1)} \geq \frac{\alpha^2}{\beta^2},$$

which is equivalent to $\tau \leq 1/\alpha$. Therefore, for $\tau > 1/\alpha$ approximation $(0, 0)$ using moments gives a worse estimate than Theorem 12.

We cannot make any general comparisons between the other approximations using moments and Theorem 12, but we will see in the following two subsections how these approximations behave in the case of the uniform and gamma distributions.

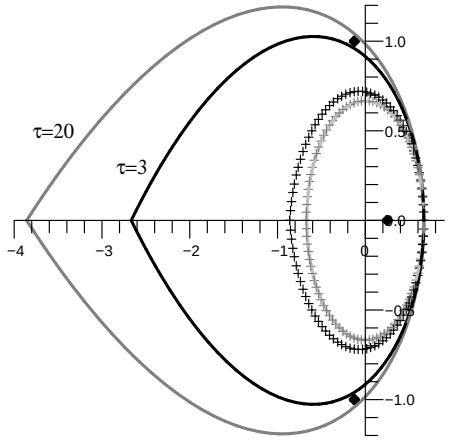

(a) $\beta = 1.5$ ($\tau = 20, \alpha = 1$)

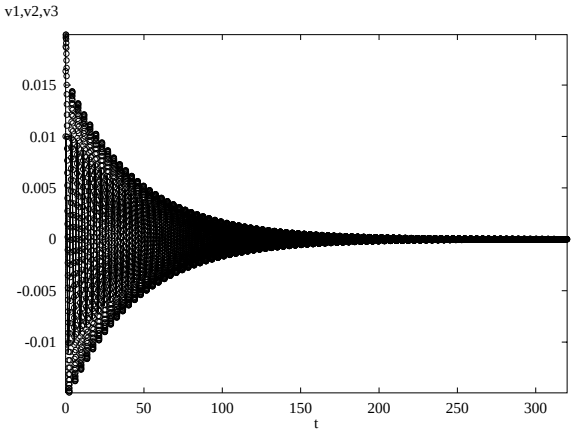

(b) Distributed delay (gamma, $p = 3$)

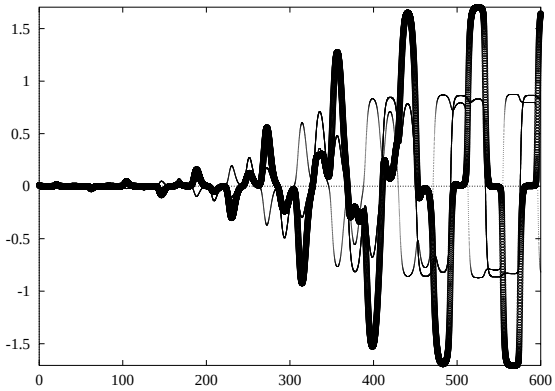

(c) Fixed delay

Figure 4.11: (a) For the distributed delay model, the boundary of the stability when $\tau = 20$ is represented by the dark gray curve, and for $\tau = 3$ by the black curve. When $\tau = 20$, the boundary of stability is larger than the one when $\tau = 3$, encompassing the three eigenvalues of $\boldsymbol{W}$, and hence the stability of the equilibrium point of the distributed delay model is recovered by increasing the delay. For the fixed delay model, the boundary of the stability when $\tau = 20$ is represented by the gray crosses, and for $\tau = 3$ by the black crosses. When $\tau = 20$, the boundary of stability is smaller than the one when $\tau = 3$, thus the stability of the equilibrium point of the fixed delay model is never recovered by increasing the delay. This is confirmed by numerical simulations: when $\tau = 20$, (b) all three neurons in the distributed delay model converge to the steady state solution; (c) all three neurons in the fixed delay model oscillate.

Points on the curves defined by approximations $(0,0)$ and $(0,1)$ using cumulants have magnitudes given by

$$\left|z^{\kappa}_{(0,0)}\right| = \left|z^{\kappa}_{(0,1)}\right| = \frac{\sqrt{\alpha^2\tau^2+\omega^2}}{\beta\tau}.$$

Thus

$$\left|z^{\kappa}_{(0,0)}\right|^2 = \left|z^{\kappa}_{(0,1)}\right|^2 \geq \frac{\alpha^2}{\beta^2}.$$

Points on the curves defined by approximations $(1,0)$ and $(1,1)$ using cumulants have magnitudes given by

$$\left|z^{\kappa}_{(1,1)}\right| = \left|z^{\kappa}_{(1,0)}\right| = \frac{e^{\kappa_2\omega^2/2}\sqrt{\alpha^2\tau^2+\omega^2}}{\beta\tau}.$$

Since κ_2 is always positive, we again have that

$$\left|z^{\kappa}_{(1,0)}\right|^2 = \left|z^{\kappa}_{(1,1)}\right|^2 \geq \frac{\alpha^2}{\beta^2}.$$

Therefore all four approximations using cumulants lie outside the circle $a_k^2 + b_k^2 = \alpha^2/\beta^2$, i.e. outside the distribution independent stability region described by Theorem 12.

In the following two subsections we apply the approximations using moments and cumulants to specific distributions and compare them to the true boundary of stability. Since the curve represented in (4.25) is symmetric about $b_k = 0$, we will only graph the approximations and the true region of stability in the upper half complex plane, i.e. for $\omega > 0$.

4.2.2 Verifying the approximations for the Uniform Distribution

In this subsection we compare the approximations using moments and cumulants to the true boundary of stability of the equilibrium point $\boldsymbol{v}^*$ of (4.4) when $\hat{g}(v)$ represents the normalized uniform distribution in (2.31). We again look at the three cases: $\rho = 2$, $\rho = 1$, and $\rho = 4/5$.

We substitute the values for the moments from Table 2.1 into the expressions for $C(\omega)$ and $S(\omega)$ from Table 4.1, and then we use these into (4.25) to obtain approximations to $R(\omega)$ and $I(\omega)$, thus determining the approximate stability boundary using moments. The first four approximations using moments are illustrated in Figures 4.12 and 4.13(a): approximations $(0,0)$, $(0,1)$, $(1,0)$ and $(1,1)$ using moments are represented by the dotted gray curve, dashed gray curve, dotted black curve, and dashed black curve, respectively.

We substitute the values for the cumulants from Table 2.1 into the expressions for $C(\omega)$ and $S(\omega)$ from Table 4.2, and then we use these into (4.25) to obtain approximations to $R(\omega)$ and $I(\omega)$, thus determining the approximate stability boundary using cumulants.

The first four approximations using cumulants are illustrated in Figures 4.12 and 4.13(a). Since by (2.34), $\kappa_3 = 0$, we again have that approximation $(0,0)$ using cumulants is identical to approximation $(0,1)$ and is represented by the curve depicted by crosses. Also, approximation $(1,0)$ using cumulants is identical to approximation $(1,1)$ and is represented by the curve depicted by circles.

We next determine the true boundary of stability. From (3.38) we obtain

$$C^2(\omega) + S^2(\omega) = \frac{4}{\rho^2\omega^2}\sin^2\left(\frac{\rho\omega}{2}\right).$$

Substituting this and (3.38) into (4.25) we obtain

$$\begin{aligned} a_k &= \frac{\rho\omega\left(\tau\alpha\cos(\omega) - \omega\sin(\omega)\right)}{2\beta\tau\sin\left(\omega\rho/2\right)} = R(\omega), \\ b_k &= \frac{\rho\omega\left(\tau\alpha\sin(\omega) + \omega\cos(\omega)\right)}{2\beta\tau\sin\left(\omega\rho/2\right)} = I(\omega). \end{aligned} \tag{4.28}$$

The above curve is represented by the solid black line in Figures 4.12 and 4.13(a). From the figures we can see that the magnitude of points on the this curve is an increasing function of ω, for $\omega \in [0, \bar{\omega}]$, where $\bar{\omega}$ is the smallest positive ω such that $I(\omega) = 0$. In order to apply Theorem 13, we show this analytically, i.e. we show $M'(\omega) > 0$, where $M(\omega)$ is given in (4.26). For any distribution, we have

$$M'(\omega) = \frac{\omega(C^2(\omega) + S^2(\omega)) - (\alpha^2\tau^2 + \omega^2)(C(\omega)C'(\omega) + S(\omega)S'(\omega))}{\beta\tau(\alpha^2\tau^2 + \omega^2)(C^2(\omega) + S^2(\omega))^{3/2}}.$$

Thus a sufficient condition to guarantee $M'(\omega) > 0$ is to show that

$$N(\omega) = C(\omega)C'(\omega) + S(\omega)S'(\omega) < 0. \tag{4.29}$$

For the uniform distribution, we first differentiate (3.38) to obtain

$$\begin{aligned} C'(\omega) &= \frac{\rho\omega\cos(\omega)\cos(\rho\omega/2) - 2\sin(\rho\omega/2)(\sin(\omega) + \cos(\omega))}{\rho\omega^2}, \\ S'(\omega) &= \frac{\rho\omega\sin(\omega)\cos(\rho\omega/2) - 2\sin(\rho\omega/2)(\sin(\omega) - \cos(\omega))}{\rho\omega^2}. \end{aligned}$$

Substituting this and (3.38) into the expression for $N(\omega)$ and simplifying, we get

$$N(\omega) = \frac{2\sin(\rho\omega/2)[\rho\omega\cos(\rho\omega/2) - 2\sin(\rho\omega/2)]}{\rho^2\omega^3}.$$

The sign of $\sin(\rho\omega/2)$ and $\cos(\rho\omega/2)$ in the above expression will depend on what interval the angle $\rho\omega/2$ belongs to. The parameter values used to generate Figures 4.12 and 4.13(a)

are $\alpha = 2, \beta = 2$ and $\tau = 1/2$. For these specific values we get $\bar{\omega} = 2.03$. Therefore we have that $\rho\omega/2 \in [0, \rho\bar{\omega}/2] \subset [0, \pi)$. If $\rho\omega/2 \in [\pi/2, \pi)$, then clearly $N(\omega) < 0$. For $\rho\omega/2 \in [0, \pi/2)$, we have that $\tan(\rho\omega/2) > \rho\omega/2$, or $\rho\omega - 2\tan(\rho\omega/2) < 0$, which is equivalent to $\rho\omega\cos(\rho\omega/2) - 2\sin(\rho\omega/2) < 0$. From this we again conclude that $N(\omega) < 0$. Therefore, by Theorem 13, the curve in (4.28) represents the true boundary of stability, i.e. if all $z_k, k = 1, \ldots, n$, lie inside this curve, then the equilibrium point $\boldsymbol{v}^*$ of (4.4) is locally asymptotically stable.

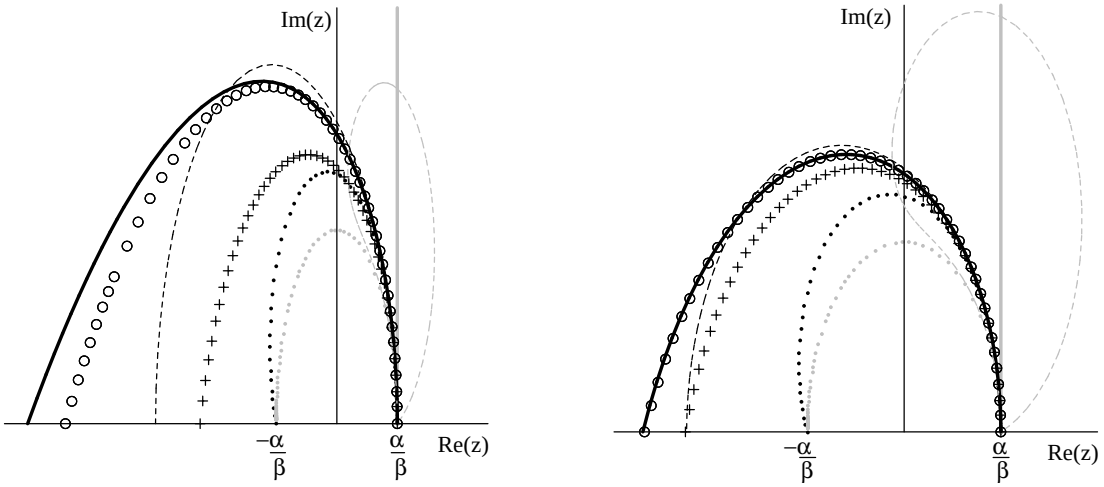

(a) Uniform, $\rho = 2$

(b) Uniform, $\rho = 1$

Figure 4.12: Stability region for the uniform distribution with $\rho = 2$ and $\rho = 1$ when $\tau = 1/2$. The true region of stability lies between the solid black curve and the real-axis. Without delay, the stability region lies to the left of the solid gray line. Approximations $(0, 0)$, $(0, 1)$, $(1, 0)$ and $(1, 1)$ using moments are represented by the dotted gray curve, dashed gray curve, dotted black curve, and dashed black curve, respectively. Approximation $(0, 0)$ using cumulants is identical to approximation $(0, 1)$ using cumulants and is represented by the curve depicted by crosses. Approximation $(1, 0)$ using cumulants is identical to approximation $(1, 1)$ using cumulants and is represented by the curve depicted by circles.

In the next subsection we compare the approximations to the true boundary of stability when the kernel is a gamma distribution.

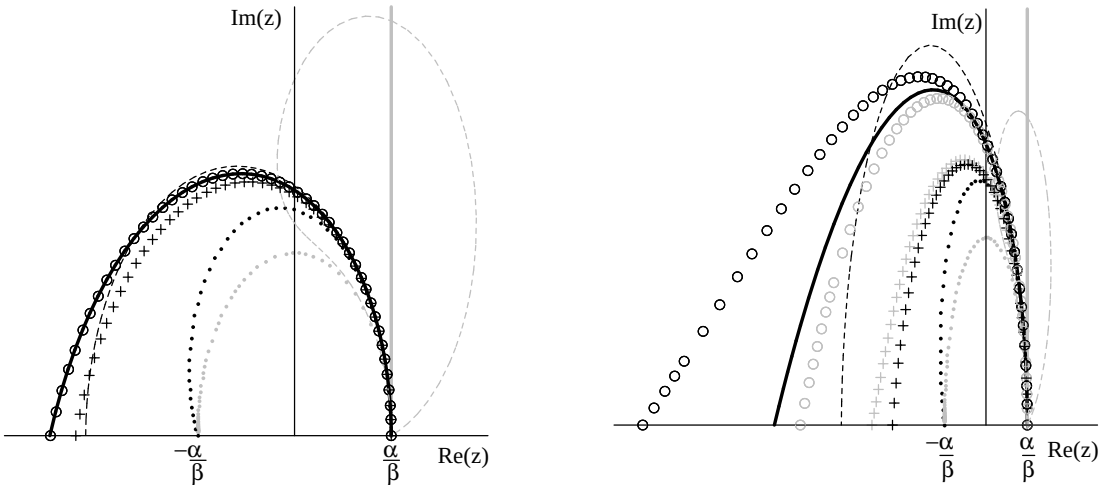

(a) Uniform, $\rho = 4/5$

(b) Gamma, $p = 3$

Figure 4.13: Stability region for the uniform distribution with $\rho = 4/5$ and for the gamma distribution with $p = 3$ when $\tau = 1/2$. The true region of stability lies between the solid black curve and the real-axis. Without delay, the stability region lies to the left of the solid gray line. Approximations $(0,0)$, $(0,1)$, $(1,0)$ and $(1,1)$ using moments are represented by the dotted gray curve, dashed gray curve, dotted black curve, and dashed black curve, respectively. Approximations $(0,0)$, $(0,1)$, $(1,0)$ and $(1,1)$ using cumulants are represented by the curves depicted by black crosses, gray crosses, black circles, and gray circles, respectively. In the case of the uniform distribution, approximation $(0,0)$ using cumulants is identical to approximation $(0,1)$ using cumulants, and approximation $(1,0)$ using cumulants is identical to approximation $(1,1)$ using cumulants.

4.2.3 Verifying the Approximations for the Gamma Distribution

In this subsection we plot the true region of stability for the gamma distribution (i.e. $\hat{g}(v)$ represents the normalized gamma distribution in (2.39)) in order to compare it to the approximations using the moments and the cumulants. We again look at the three cases: $p = 3$, $p = 4$ and $p = 5$.

We substitute the values for the moments from Table 2.2 into the expressions for $C(\omega)$ and $S(\omega)$ from Table 4.1, and then we use these into (4.25) to obtain approximations to $R(\omega)$ and $I(\omega)$, thus determining the approximate stability boundary using moments. The first four approximations using moments are illustrated in Figures 4.13(b) and 4.14: approximations $(0,0)$, $(0,1)$, $(1,0)$ and $(1,1)$ using moments are represented by the dotted

gray curve, dashed gray curve, dotted black curve, and dashed black curve, respectively.

We substitute the values for the cumulants from Table 2.2 into the expressions for $C(\omega)$ and $S(\omega)$ from Table 4.2, and then we use these into (4.25) to obtain approximations to $R(\omega)$ and $I(\omega)$, thus determining the approximate stability boundary using cumulants. The first four approximations using cumulants are illustrated in Figures 4.13(b) and 4.14: approximations $(0,0)$, $(0,1)$, $(1,0)$ and $(1,1)$ using cumulants are represented by the curves depicted by black crosses, gray crosses, black circles, and gray circles, respectively.

We next determine the true boundary of stability. From (3.43) and (3.44), we have

$$\begin{aligned} C(\omega)^2 + S^2(\omega) &= \left(\frac{p}{p^2+\omega^2}\right)^{2p} \left[\left(\mathrm{Re}\,(p-i\omega)^p\right)^2 + \left(\mathrm{Im}\,(p-i\omega)^p\right)^2\right] \\ &= \left(\frac{p}{p^2+\omega^2}\right)^{2p} |p-i\omega|^{2p} \\ &= \left(\frac{p}{p^2+\omega^2}\right)^{2p} (p^2+\omega^2)^p \\ &= \left(\frac{p^2}{\omega^2+p^2}\right)^{p}. \end{aligned}$$

Substituting this, (3.43) and (3.44) into (4.25) we obtain

$$\begin{aligned} a_k &= \frac{\alpha}{\beta} p^{-p} \mathrm{Re}\,(p-i\omega)^p + \frac{\omega}{\beta\tau} p^{-p} \mathrm{Im}\,(p-i\omega)^p = R(\omega), \\ b_k &= -\frac{\alpha}{\beta} p^{-p} \mathrm{Im}\,(p-i\omega)^p + \frac{\omega}{\beta\tau} p^{-p} \mathrm{Re}\,(p-i\omega)^p = I(\omega). \end{aligned} \tag{4.30}$$

The above curve is represented by the solid black line in Figures 4.13(b) and 4.14. From the figures we can see that the magnitude of points on the this curve is an increasing function of ω, for $\omega \in [0, \bar{\omega}]$. Next we show that this is the case analytically. For $p = 3$, we differentiate (3.45) to obtain

$$\begin{aligned} C'(\omega) &= \frac{972\omega(\omega^2-9)}{(\omega^2+9)^4}, \\ S'(\omega) &= \frac{81(\omega^4-54\omega^2+81)}{(\omega^2+9)^4}. \end{aligned}$$

Substituting this and (3.45) into the expression for $N(\omega)$ in (4.29) we get

$$N(\omega) = -\frac{2187\omega}{(\omega^2+9)^4}.$$

For $p = 4$, differentiating (3.49) we have

$$C'(\omega) = -\frac{1024\omega(\omega^4 - 160\omega^2 + 1280)}{(\omega^2 + 16)^5},$$
$$S'(\omega) = \frac{4096(5\omega^4 - 160\omega^2 + 256)}{(\omega^2 + 16)^5}.$$

Thus $N(\omega)$ becomes

$$N(\omega) = -\frac{262144\omega}{(\omega^2 + 16)^5}.$$

For $p = 5$, from (3.53) we obtain

$$C'(\omega) = -\frac{156250\omega(3\omega^4 - 250\omega^2 + 1875)}{(\omega^2 + 25)^5},$$
$$S'(\omega) = -\frac{15625(\omega^6 - 375\omega^4 + 9375\omega^2 - 15625)}{(\omega^2 + 25)^5},$$

and hence $N(\omega)$ is given by

$$N(\omega) = -\frac{48828125\omega}{(\omega^2 + 25)^5}.$$

In all three cases we obtain that $N(\omega) < 0$. We can then apply Theorem 13 to conclude that the curve in (4.30) represents the true boundary of stability in the case of the gamma distribution, i.e. if all $z_k, k = 1, \ldots, n$, lie inside this curve, then the equilibrium point $\boldsymbol{v}^*$ of (4.4) is locally asymptotically stable.

In conclusion, for both the uniform and gamma cases, we notice that the approximations seem to improve as more moments or cumulants are added, except for approximation $(0, 1)$ using moments, which gives a worse estimate than approximation $(0, 0)$ using moments. Approximation $(0, 1)$ using moments is very different than all other approximations, since it is the only one that enters the region $\mathrm{Re}(z) > \alpha/\beta$. We note that approximation $(1, 1)$ using cumulants lies very close to the true boundary of stability. We again observe that the approximations using cumulants give better results than the ones using moments.

In Figures 4.15 and 4.16 we plot the true boundary of stability for the uniform distribution (with $\rho = 1$) for different values of τ. In contrast with Figure 4.7 which plots the stability region for the gamma distribution (with $p = 3$) for different values of τ, we can see that for the uniform distribution, the true stability region and the approximations of the stability region decrease as the mean delay τ increases. In Figure 4.15(a) we show a comparison between the true region of stability and the approximation $(0, 0)$ using moments and how they behave as τ increases. In Figure 4.15(b) we compare the true region of stability and the approximation $(0, 0)$ using cumulants for different values of τ. We note

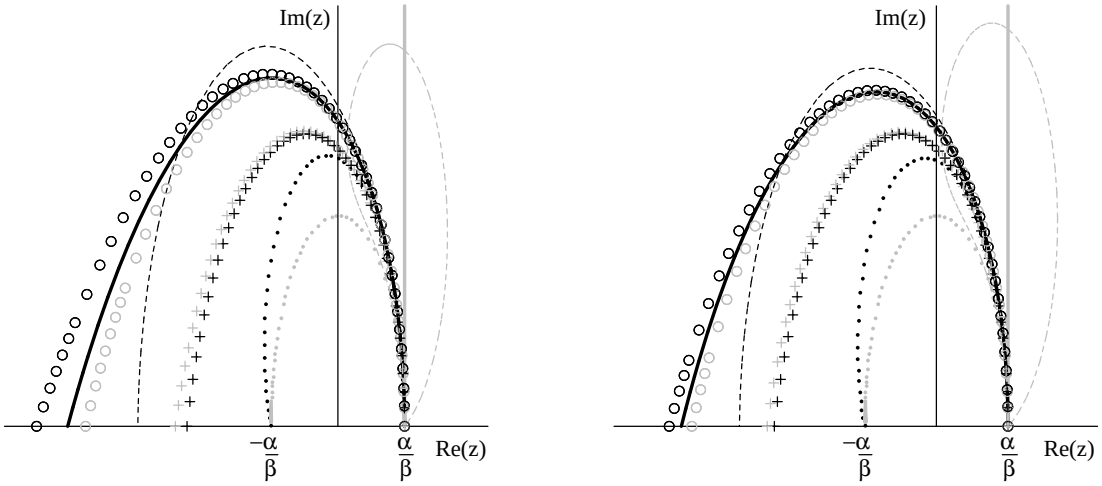

(a) Gamma, $p = 4$

(b) Gamma, $p = 5$

Figure 4.14: Stability region for the gamma distribution with $p = 4$ and $p = 5$ when $\tau = 1/2$. The true region of stability lies between the solid black curve and the real-axis. Without delay, the stability region lies to the left of the solid gray line. Approximations $(0, 0)$, $(0, 1)$, $(1, 0)$ and $(1, 1)$ using moments are represented by the dotted gray curve, dashed gray curve, dotted black curve, and dashed black curve, respectively. Approximations $(0, 0)$, $(0, 1)$, $(1, 0)$ and $(1, 1)$ using cumulants are represented by the curves depicted by black crosses, gray crosses, black circles, and gray circles, respectively.

again that the approximation $(0, 0)$ using cumulants recovers the stability results of the corresponding model with fixed delay τ. Hence in Figure 4.15(b) also shows a comparison between the stability regions of the distributed and fixed delay models for different values of τ. In Figure 4.16(a) we show a comparison between the true region of stability and the approximation $(1, 0)$ using moments and how they behave as τ increases. In Figure 4.16(b) we compare the true region of stability and the approximation $(1, 0)$ using cumulants for different values of τ. In both Figures 4.15 and 4.16, it is again confirmed that the approximations using cumulants give better results.

In the next chapter we investigate the stability of nonhyperbolic equilibrium points of the scalar Hopfield model using the centre manifold technique.

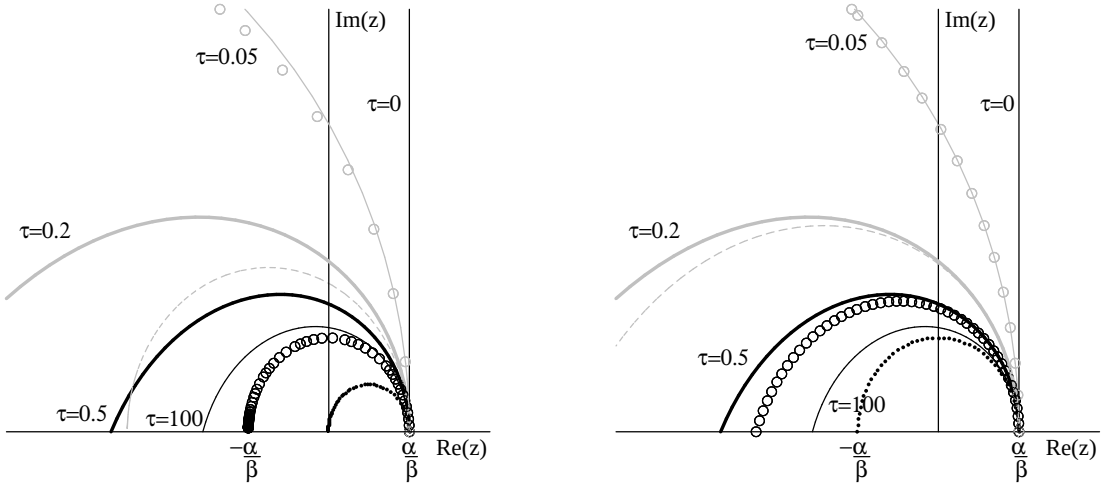

(a) Moments

(b) Cumulants

Figure 4.15: The stability region for the uniform distribution with $\rho = 1$ for different values of τ is compared to the approximation $(0, 0)$ using moments in (a) and to approximation $(0, 0)$ using cumulants in (b). Without delay, the stability region lies to the left of the black line $z_k = \alpha/\beta$. The true boundary of stability is depicted as the thin gray line, the thick gray line, the thick black line, and the thin black line for $\tau = 0.05, \tau = 0.2, \tau = 0.5$, and $\tau = 100$, respectively. Approximation $(0, 0)$ using (a) moments or (b) cumulants is shown as gray circles, gray dash line, black circles, and black dotted line for $\tau = 0.05, \tau = 0.2, \tau = 0.5$, and $\tau = 100$, respectively.

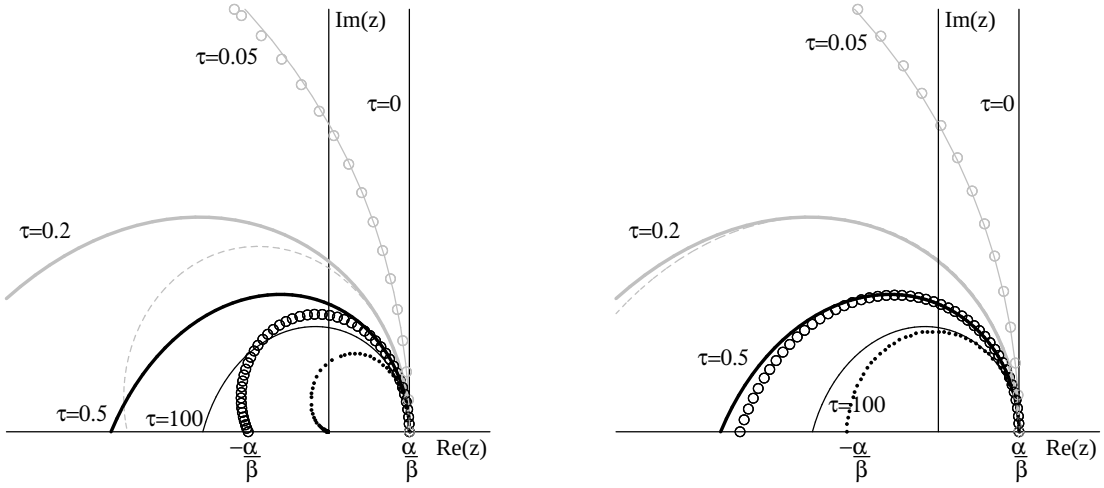

(a) Moments

(b) Cumulants

Figure 4.16: The stability region for the uniform distribution with $\rho = 1$ for different values of τ is compared to the approximation $(1, 0)$ using moments in (a) and to approximation $(1, 0)$ using cumulants in (b). Without delay, the stability region lies to the left of the black line $z_k = \alpha/\beta$. The true boundary of stability is depicted as the thin gray line, the thick gray line, the thick black line, and the thin black line for $\tau = 0.05, \tau = 0.2, \tau = 0.5$, and $\tau = 100$, respectively. The approximation $(1, 0)$ using (a) moments or (b) cumulants is shown as gray circles, gray dash line, black circles, and black dotted line for $\tau = 0.05, \tau = 0.2, \tau = 0.5$, and $\tau = 100$, respectively.

Chapter 5

Calculating the Centre Manifold for the Scalar Model

In this chapter we will study the stability of nonhyperbolic equilibrium points of the scalar Hopfield model with a general distribution of delays. A nonhyperbolic equilibrium point is an equilibrium point for which at least one root of the associated characteristic equation has a zero real part. In the case of hyperbolic equilibrium points, as discussed in Section 2.3, the stability of the equilibrium point of the nonlinear system is guaranteed by the stability of the equilibrium point of the corresponding linear system. For nonhyperbolic equilibrium points, the linear system does not provide enough information regarding the stability of the equilibrium point of the nonlinear system. In this case we construct a centre manifold, which is a nonlinear manifold tangent to the centre eigenspace. If the rest of the eigenvalues of the characteristic equation have negative real parts, then the centre manifold is attracting and thus the behaviour of solutions near the nonhyperbolic equilibrium point is well approximated by the flow on this manifold [26]. Nonhyperbolic equilibrium points often occur at bifurcation points of a DE and thus the centre manifold analysis also gives insights into the nature of the bifurcation. For our model, we show under what conditions a Hopf bifurcation can occur and we use the centre manifold technique to determine the criticality of the Hopf bifurcation.

We start by laying the theoretical basis to the computation of the centre manifold, then we apply the theory to the scalar Hopfield model with a general distribution of delays. We then verify our results when the kernel is a gamma distribution. In this case the scalar DDE can be transformed into a system of ODEs, where we can apply the theory of ODEs to compute the centre manifold and determine the criticality of the Hopf bifurcation. And finally, we apply the approximations we developed in Chapter 3 to predict the criticality of the Hopf bifurcation when the distribution of delays is not known, but the first moments or cumulants of the distribution are.

We consider the scalar Hopfield model,

$$\dot{x}(t) = -\alpha x(t) + w \int_0^\infty f(x(t-u))g(u)\,du + c,$$

where $\alpha > 0, w, c \in \mathbb{R}$, $g(u)$ is a p.d.f. and $f \in C^r$ with r large enough for our subsequent calculations. After we perform the change of variables presented in Section 2.2 and renaming s back to t, the above DDE becomes

$$x'(t) = -\alpha\tau x(t) + w\tau \int_0^\infty f(x(t-v))\hat{g}(v)\,dv + c\tau.$$

For reasons that will become clear later in the section, we rewrite the above DDE as

$$x'(t) = -\alpha\tau x(t) + w\tau \int_{-\infty}^0 f(x(t+\theta))\hat{g}(-\theta)\,d\theta + c\tau. \tag{5.1}$$

where we let $v = -\theta$. Let $\phi_0 \in \mathcal{C} = C((-\infty, 0], \mathbb{R})$ be a given function, then the corresponding initial condition is

$$x(t_0 + \theta) = \phi_0(\theta), \qquad \theta \le 0. \tag{5.2}$$

If ϕ_0 and f satisfy the conditions of Theorem 3, then there exists a unique solution to the IVP (5.1)–(5.2) on any interval $[0, t] \subset [0, t_{\phi_0})$, where $t_{\phi_0} \in [0, \infty]$.

We assume the above equation admits an equilibrium solution x^* satisfying

$$0 = -\alpha\tau x^* + w\tau f\,(x^*) + c\tau. \tag{5.3}$$

We next shift the equilibrium to zero and separate the linear and nonlinear terms. Let $y(t) = x(t) - x^*$, $\bar{\beta} = f'(x^*), \bar{\gamma} = f''(x^*)$, and $\bar{\delta} = f'''(x^*)$. Then the Taylor series expansion of f about x^* is

$$f(x(t+\theta)) = f(x^*) + \bar{\beta}y(t+\theta) + \frac{\bar{\gamma}}{2}(y(t+\theta))^2 + \frac{\bar{\delta}}{6}(y(t+\theta))^3 + \text{h.o.t.}$$

Using this along with (5.3), we obtain

$$\begin{aligned} y'(t) = &-\alpha\tau y(t) - w\tau f(x^*) - c\tau + w\tau f(x^*) + w\bar{\beta}\tau \int_{-\infty}^0 y(t+\theta)\hat{g}(-\theta)\,d\theta \\ &+ \frac{w\bar{\gamma}\tau}{2} \int_{-\infty}^0 (y(t+\theta))^2\hat{g}(-\theta)\,d\theta + \frac{w\bar{\delta}\tau}{6} \int_{-\infty}^0 (y(t+\theta))^3\hat{g}(-\theta)\,d\theta + c\tau + \text{h.o.t.} \end{aligned}$$

Simplifying and renaming back to x, we have

$$x'(t) = -\alpha\tau x(t) + \beta\tau \int_{-\infty}^{0} x(t+\theta)\hat{g}(-\theta)\,d\theta + \gamma\tau \int_{-\infty}^{0} (x(t+\theta))^2\hat{g}(-\theta)\,d\theta + \delta\tau \int_{-\infty}^{0} (x(t+\theta))^3\hat{g}(-\theta)\,d\theta + \text{h.o.t.}\,,$$

where we let $\beta = w\bar{\beta}, \gamma = w\bar{\gamma}/2$, and $\delta = w\bar{\delta}/6$.

In the following section we present the theoretical background for calculating the centre manifold for a scalar DDE with one distributed delay. The theoretical basis for analyzing Hopf bifurcations and calculating the centre manifold has been rigourously developed for DDEs with finite delay [26]. In Section 2.1, we saw that under the right constraints imposed on the function space, the existence and uniqueness results carry over from DDEs with finite distributed delay to the ones with infinite distributed delay (see Theorem 3). Under similar constraints on the function space, Hino et al. [29] obtain results on the decomposition of the function space in terms of the eigenvalues of the infinitesimal generator of the solution operator for the linearized equation corresponding to DDEs with infinite delay (Theorem 3.1 on page 144 in [29]).

In this chapter we assume that within the appropriate restricted function space, the Hopf bifurcation and centre manifold theory holds for DDEs with infinite delay. In Sections 5.3 and 5.4, we test this assumption by transforming our DDE model with a gamma distributed delay into an ODE system, for which the Hopf bifurcation and centre manifold theory is well established. We then compare the centre manifold computation for the DDE case to the one we obtain in the ODE case. In the literature, the Hopf bifurcation and centre manifold theory has been applied to DDEs with infinite delay, and hence it is assumed that it holds [43, 44, 54, 55]. In these papers, the authors only take into considerations gamma distributed delays, and therefore their models are equivalent to ODE systems. We note that in [56, 64], the analysis of the Hopf bifurcation problem for DDEs with infinite delay is based on the method of Liapunov-Schmidt, which avoids all reference to the infinite dimensional nature of the problem.

5.1 Theoretical Background

In this section we present the theoretical background for calculating the centre manifold for the scalar DDE (5.1). We start by defining the flow for the above DDE as a mapping from $\mathcal{C}$ which takes the initial function $\phi_0(\theta)$ into the function $x_t(\theta) = x(t+\theta), \theta \leq 0$. Hence we can rewrite the DDE as

$$x'(t) = L(x_t) + F(x_t), \tag{5.4}$$

where $L : \mathcal{C} \to \mathbb{R}$ is a linear mapping defined by

$$L(\phi) = -\alpha\tau\phi(0) + \beta\tau \int_{-\infty}^{0} \phi(\theta)\hat{g}(-\theta)\, d\theta, \tag{5.5}$$

and $F : \mathcal{C} \to \mathbb{R}$ is a nonlinear functional defined by

$$F(\phi) = \gamma\tau \int_{-\infty}^{0} (\phi(\theta))^2 \hat{g}(-\theta)\, d\theta + \delta\tau \int_{-\infty}^{0} (\phi(\theta))^3 \hat{g}(-\theta)\, d\theta + \text{h.o.t.} \tag{5.6}$$

We can extend (5.4) to a differential equation for $x_t(\theta)$ as follows [18, 19, 59]

$$\frac{d}{dt}x_t(\theta) = \begin{cases} \dfrac{d}{d\theta}x_t(\theta), & \theta < 0, \\ \\ L(x_t) + F(x_t), & \theta = 0. \end{cases} \tag{5.7}$$

In the following subsection we examine the linearized equation corresponding to (5.1) in more detail.

5.1.1 Linear Equation

Since in this chapter we investigate nonhyperbolic equilibrium points, the linearized equation

$$x'(t) = -\alpha\tau x(t) + \beta\tau \int_{-\infty}^{0} x(t+\theta)\hat{g}(-\theta)\, d\theta \tag{5.8}$$

cannot give enough information about the stability of the equilibrium point of (5.1). In this section we present what information we can draw from the linearization. We first compute the characteristic equation by substituting $x(t) = ce^{\lambda t}$ into the above equation,

$$\Delta(\lambda) = \lambda + \alpha\tau - \beta\tau \int_{-\infty}^{0} e^{\lambda\theta}\hat{g}(-\theta)\, d\theta = 0. \tag{5.9}$$

We assume that the characteristic equation has m roots with zero real part and the rest of the roots have negative real parts. In this case there exists a decomposition of the solution space for the linear DDE

$$x'(t) = L(x_t) \tag{5.10}$$

as $\mathcal{C} = N \oplus S$, where N is an m-dimensional subspace spanned by the solutions to (5.10) corresponding to the eigenvalues with zero real part, S is infinite dimensional, and N and S are invariant under the flow associated with (5.10) [29]. We further assume, for simplicity, that all the eigenvalues with zero real part have multiplicity one.

The following results can be found in [29]. The centre eigenspace N is the null space of $(\lambda I - A)^k$, where A is the infinitesimal generator associated with the solution operator of (5.10), $T(t) : \mathcal{C} \to \mathcal{C}, x_t(;, \phi) = T(t)\phi$ and satisfies

$$\begin{aligned} \mathcal{D}(A) &= \left\{ \phi \in \mathcal{C} : \frac{d\phi}{d\theta} \in \mathcal{C}, \frac{d\phi}{d\theta}(0) = L\phi \right\} \\ A\phi &= \frac{d\phi}{d\theta}. \end{aligned} \tag{5.11}$$

Let $\{\phi_1(t), \phi_2(t), \ldots, \phi_m(t)\}$ be a basis for N and $\{\lambda_1, \lambda_2, \ldots, \lambda_m\}$ the corresponding eigenvalues. If $\lambda_k = 0$ then $\phi_k(t) = c_k$, where c_k is a solution of $\Delta(0)c_k = 0$. If $\lambda_k = i\omega$ then $-i\omega$ is also a root of the characteristic equation, and we let $\lambda_{k+1} = -i\omega$. In this case $\phi_k(t) = \mathrm{Re}(e^{i\omega t}c_k)$ and $\phi_{k+1}(t) = \mathrm{Im}(e^{i\omega t}c_k)$, where c_k is a solution of $\Delta(i\omega)c_k = 0$. Since we are working with a scalar model, c_k is just a scalar constant, and thus we can choose $c_k = 1$ in all cases. Therefore for $\lambda_k = 0$ we have $\phi_k(t) = 1$, and for $\lambda_k = i\omega, \lambda_{k+1} = -i\omega$ we have $\phi_k(t) = \mathrm{Re}(e^{i\omega t}) = \cos(\omega t)$ and $\phi_{k+1}(t) = \mathrm{Im}(e^{i\omega t}) = \sin(\omega t)$.

We can also write the basis for N as an $1 \times m$ matrix, with the k^{th} column given by ϕ_k,

$$\boldsymbol{\Phi}(t) = [\phi_1(t) \mid \phi_2(t) \mid \cdots \mid \phi_m(t)]. \tag{5.12}$$

Since, the eigenspace N satisfies $AN \subseteq N$ [29], for $b_{kj} \in \mathbb{R}$, we have that

$$A\phi_k = b_{k1}\phi_1 + b_{k2}\phi_2 + \cdots + b_{km}\phi_m, \qquad k = 1, \ldots, m, \tag{5.13}$$

i.e. $A\phi_k$ is a linear combination of the basis functions. We note that the basis functions may also be treated as functions on $\mathcal{C}$ by changing their argument to $\theta \in (-\infty, 0]$. From (5.11) and (5.13) we have that

$$\begin{aligned} \boldsymbol{\Phi}' &= [\phi_1' \mid \phi_2' \mid \cdots \mid \phi_m'] \\ &= [A\phi_1 \mid A\phi_2 \mid \cdots \mid A\phi_m] \\ &= [b_{11}\phi_1 + \cdots + b_{1m}\phi_m \mid b_{21}\phi_1 + \cdots + b_{2m}\phi_m \mid \cdots \mid b_{m1}\phi_1 + \cdots + b_{mm}\phi_m] \\ &= [\phi_1 \mid \phi_2 \mid \cdots | \phi_m] \begin{bmatrix} b_{11} & \cdots & b_{1m} \\ \vdots & \ddots & \vdots \\ b_{m1} & \cdots & b_{mm} \end{bmatrix} \\ &= \boldsymbol{\Phi}\boldsymbol{B}. \end{aligned} \tag{5.14}$$

Thus we showed that $\boldsymbol{\Phi}$ satisfies the matrix ODE, $\boldsymbol{\Phi}' = \boldsymbol{\Phi}\boldsymbol{B}$. Since the only eigenvalue of $\boldsymbol{B}$ is λ [29], we can conclude that $\boldsymbol{B}$ is a block diagonal matrix with block [0] for the zero eigenvalue and block

$$\begin{bmatrix} 0 & \omega \\ -\omega & 0 \end{bmatrix} \tag{5.15}$$

for the pair of complex conjugate eigenvalues $\pm i\omega$. From (5.5) and (5.9) we have

$$L\left(e^{\lambda_k\theta}\right) = -\alpha\tau + \beta\tau\int_{-\infty}^{0} e^{\lambda_k\theta}\hat{g}(-\theta)\,d\theta = \lambda_k.$$

Thus for $\lambda_k = 0$ we have $L(\phi_k) = 0$, and for $\lambda_k = i\omega$ we have

$$L\left(e^{\lambda_k\theta}\right) = L\left(\mathrm{Re}\left(e^{\lambda_k\theta}\right)\right) + iL\left(\mathrm{Im}\left(e^{\lambda_k\theta}\right)\right) = L(\phi_k) + iL(\phi_{k+1}) = i\omega.$$

Therefore

$$L(\phi_k) = 0 \qquad \text{and} \qquad L(\phi_{k+1}) = \omega.$$

But $\phi_k(0) = 1$ and $\phi_{k+1}(0) = 0$, hence we have that

$$L(\phi_k) = -\omega\phi_{k+1}(0) \qquad \text{and} \qquad L(\phi_{k+1}) = \omega\phi_k(0).$$

For example if ϕ_1, ϕ_2, and ϕ_3 are the basis functions corresponding to $\lambda_1 = 0, \lambda_2 = i\omega$ and $\lambda_3 = -i\omega$, respectively, then we have

$$\begin{aligned}\boldsymbol{\Phi}(0)\boldsymbol{B} &= [\phi_1(0) \mid \phi_2(0) \mid \phi_3(0)]\begin{bmatrix} 0 & 0 & 0 \\ 0 & 0 & \omega \\ 0 & -\omega & 0 \end{bmatrix} \\ &= [0 \mid -\omega\phi_3(0) \mid \omega\phi_2(0)] \\ &= [L(\phi_1) \mid L(\phi_2) \mid L(\phi_3)]\end{aligned}$$

And thus we can conclude that

$$L\left(\boldsymbol{\Phi}\right) = \boldsymbol{\Phi}(0)\boldsymbol{B}. \tag{5.16}$$

The solution space will be decomposed by defining an equation dual to (5.10). Let $\mathcal{C}^* = C([0, +\infty), \mathbb{R})$. For $\psi \in \mathcal{C}^*$ and $\phi \in \mathcal{C}$, we define the bilinear form [27],

$$\langle \psi, \phi \rangle = \psi(0)\phi(0) - \beta\tau\int_{\theta=-\infty}^{\theta=0}\int_{\xi=0}^{\xi=\theta} \psi(\xi - \theta)\hat{g}(-\theta)\phi(\xi)\,d\xi\,d\theta. \tag{5.17}$$

This is used to define the dual equation [29]

$$y'(s) = L^T(y^s), \qquad s \le 0, \tag{5.18}$$

where $y^s = y(s + \xi), \xi \ge 0$ and L^T is a linear mapping on $\mathcal{C}^*$ given by

$$L^T(\psi) = \alpha\tau\psi(0) - \beta\tau\int_0^{\infty} \psi(\xi)\hat{g}(\xi)\,d\xi.$$

The corresponding DE is

$$y'(s) = \alpha\tau y(s) - \beta\tau \int_0^\infty y(s+w)\hat{g}(w)\,dw, \qquad s \le 0.$$

Substituting $y(s) = ce^{-\lambda s}$ into the above equation, we obtain the characteristic equation corresponding to the above DE, which is exactly (5.9). Thus the trivial solutions of (5.9) and the above DE have the same eigenvalues.

Let

$$\boldsymbol{\Psi}(s) = \begin{bmatrix} \psi_1(s) \\ \vdots \\ \psi_m(s) \end{bmatrix}$$

be a basis for the solutions of (5.18) corresponding to the m eigenvalues with zero real part. We note that $\psi_j, j = 1, \ldots, m$, can be considered as functions on $\mathcal{C}^*$ if we change their argument to $\xi \in [0, +\infty)$. Similar to the proofs for $\boldsymbol{\Phi}$, one can show that

$$\boldsymbol{\Psi}' = -\boldsymbol{B}\boldsymbol{\Psi} \qquad \text{and} \qquad L^T(\boldsymbol{\Psi}) = -\boldsymbol{B}\boldsymbol{\Psi}(0), \tag{5.19}$$

where $\boldsymbol{B}$ is the same block diagonal matrix as in (5.15). For any $\zeta \in S$, we have [26]

$$\langle \psi_j, \zeta \rangle = 0, \qquad j = 1, \ldots, m. \tag{5.20}$$

Further we can choose a basis $\boldsymbol{\Psi}$ so that

$$\langle \boldsymbol{\Psi}, \boldsymbol{\Phi} \rangle = \boldsymbol{I}, \tag{5.21}$$

where $\langle \boldsymbol{\Psi}, \boldsymbol{\Phi} \rangle$ is an $m \times m$ matrix with the $(jk)^{\text{th}}$ entry given by $\langle \psi_j, \phi_k \rangle$, and $\boldsymbol{I}$ is the $m \times m$ identity matrix. For any $\zeta \in N$ we have [26]

$$\zeta = \boldsymbol{\Phi}\boldsymbol{u} \qquad \text{where} \qquad \boldsymbol{u} = \langle \boldsymbol{\Psi}, \zeta \rangle \in \mathbb{R}^m.$$

In the next subsection we take a closer look at the nonlinear equation.

5.1.2 Nonlinear Equation

In this subsection we analyze the nonlinear equation (5.4). Since the characteristic equation (5.9) has m eigenvalues with zero real part and the rest have negative real part, there exists an m dimensional centre manifold which is attracting and the behaviour of solutions to the nonlinear equation is well approximated by the flow on this manifold [26]. The points

on the local centre manifold of $x = 0$ can be expressed as a sum of the linear part in N and the nonlinear part in S,

$$W^c_{\text{loc}}(0) = \{\phi \in \mathcal{C} : \phi = \mathbf{\Phi}\boldsymbol{u} + h(\boldsymbol{u})\}, \tag{5.22}$$

where $\mathbf{\Phi}(\theta), \theta \in (-\infty, 0]$ is given in (5.12) as the basis of N, $\boldsymbol{u} \in \mathbb{R}^m$, $h(\boldsymbol{u}) \in S$ and $||\boldsymbol{u}||$ is sufficiently small. The solution to (5.4) on this centre manifold is then given by $x(t) = x_t(0)$, where $x_t(\theta)$ is a solution of (5.7) satisfying

$$x_t(\theta) = \mathbf{\Phi}(\theta)\boldsymbol{u}(t) + h(\theta, \boldsymbol{u}(t)). \tag{5.23}$$

Substituting this into (5.7), we obtain

$$\left[\mathbf{\Phi}(\theta) + \frac{\partial h}{\partial \boldsymbol{u}}\right]\boldsymbol{u}'(t) = \begin{cases} \mathbf{\Phi}'(\theta)\boldsymbol{u}(t) + \dfrac{\partial h}{\partial \theta}, & \theta < 0, \\ L\left(\mathbf{\Phi}(\theta)\right)\boldsymbol{u}(t) + L\left(h(\theta, \boldsymbol{u}(t))\right) & \\ +F\left(\mathbf{\Phi}(\theta)\boldsymbol{u}(t) + h(\theta, \boldsymbol{u}(t))\right), & \theta = 0. \end{cases}$$

Using (5.14) and (5.16), the above ODE becomes

$$\left[\mathbf{\Phi}(\theta) + \frac{\partial h}{\partial \boldsymbol{u}}\right]\boldsymbol{u}'(t) = \begin{cases} \mathbf{\Phi}(\theta)\boldsymbol{B}\boldsymbol{u}(t) + \dfrac{\partial h}{\partial \theta}, & \theta < 0, \\ \mathbf{\Phi}(0)\boldsymbol{B}\boldsymbol{u}(t) + L\left(h(\theta, \boldsymbol{u}(t))\right) & \\ +F\left(\mathbf{\Phi}(\theta)\boldsymbol{u}(t) + h(\theta, \boldsymbol{u}(t))\right), & \theta = 0. \end{cases} \tag{5.24}$$

We next obtain an ODE for $\boldsymbol{u}(t)$ and a PDE for $h(\theta, \boldsymbol{u}(t))$. To obtain the equation for $\boldsymbol{u}(t)$ we use the bilinear form in (5.17). First we note that for any $\boldsymbol{u}$, since $h(\theta, \boldsymbol{u}(t)) \in S$, by (5.20) we have that

$$\langle \mathbf{\Psi}(\xi), h(\theta, \boldsymbol{u}(t))\rangle = 0. \tag{5.25}$$

And therefore

$$\left\langle \mathbf{\Psi}(\xi), \frac{\partial h}{\partial \boldsymbol{u}}(\theta, \boldsymbol{u}(t)) \right\rangle = 0. \tag{5.26}$$

We next apply the bilinear form in (5.17) to $\mathbf{\Psi}$ and (5.24). For the left-hand side of (5.24) we have

$$\begin{aligned} \left\langle \mathbf{\Psi}, \left[\mathbf{\Phi}(\theta) + \frac{\partial h}{\partial \boldsymbol{u}}\right]\boldsymbol{u}'(t) \right\rangle &= \langle \mathbf{\Psi}, \mathbf{\Phi}(\theta)\boldsymbol{u}'(t)\rangle + \left\langle \mathbf{\Psi}, \frac{\partial h}{\partial \boldsymbol{u}}\boldsymbol{u}'(t) \right\rangle \\ &= \langle \mathbf{\Psi}, \mathbf{\Phi}(\theta)\rangle\,\boldsymbol{u}'(t) + \left\langle \mathbf{\Psi}, \frac{\partial h}{\partial \boldsymbol{u}} \right\rangle \boldsymbol{u}'(t) \\ &= \boldsymbol{u}'(t) \end{aligned} \tag{5.27}$$

where we used (5.21) and (5.26). Since the right-hand side of (5.24) is defined as piece-wise, when we apply the bilinear form we get

$$\begin{aligned}&\langle \boldsymbol{\Psi}, \boldsymbol{\Phi}(\theta) B\boldsymbol{u}(t)\rangle + \boldsymbol{\Psi}(0) L\left(h(\theta, \boldsymbol{u}(t))\right) + \boldsymbol{\Psi}(0) F\left(\boldsymbol{\Phi}(\theta)\boldsymbol{u}(t) + h(\theta, \boldsymbol{u}(t))\right)\\ &- \beta\tau \int_{\theta=-\infty}^{\theta=0} \int_{\xi=0}^{\xi=\theta} \boldsymbol{\Psi}(\xi-\theta)\hat{g}(-\theta)\frac{\partial h}{\partial \xi}(\xi, \boldsymbol{u}(t))\, d\xi\, d\theta.\end{aligned} \tag{5.28}$$

Using integration by parts, (5.5), (5.17), (5.19) and (5.25), we obtain

$$\begin{aligned}&\boldsymbol{\Psi}(0) L\left(h(\theta, \boldsymbol{u}(t))\right) - \beta\tau \int_{\theta=-\infty}^{\theta=0} \int_{\xi=0}^{\xi=\theta} \boldsymbol{\Psi}(\xi-\theta)\hat{g}(-\theta)\frac{\partial h}{\partial \xi}(\xi, \boldsymbol{u}(t))\, d\xi\, d\theta\\ &\quad= \boldsymbol{\Psi}(0)\left(-\alpha\tau h(0, \boldsymbol{u}(t)) + \beta\tau \int_{-\infty}^{0} h(\theta, \boldsymbol{u}(t))\hat{g}(-\theta)\, d\theta\right)\\ &\quad- \beta\tau \int_{\theta=-\infty}^{\theta=0} \int_{\xi=0}^{\xi=\theta} \boldsymbol{\Psi}(\xi-\theta)\frac{\partial h}{\partial \xi}(\xi, \boldsymbol{u}(t))\, d\xi\, \hat{g}(-\theta)\, d\theta\\ &\quad= -\alpha\tau \boldsymbol{\Psi}(0) h(0, \boldsymbol{u}(t)) + \beta\tau \int_{-\infty}^{0} \boldsymbol{\Psi}(0) h(\theta, \boldsymbol{u}(t))\hat{g}(-\theta)\, d\theta\\ &\quad- \beta\tau \int_{\theta=-\infty}^{\theta=0} \left[\boldsymbol{\Psi}(0) h(\theta, \boldsymbol{u}(t)) - \boldsymbol{\Psi}(-\theta) h(0, \boldsymbol{u}(t))\right] \hat{g}(-\theta)\, d\theta\\ &\quad+ \beta\tau \int_{\theta=-\infty}^{\theta=0} \int_{\xi=0}^{\xi=\theta} \boldsymbol{\Psi}'(\xi-\theta) h(\xi, \boldsymbol{u}(t))\hat{g}(-\theta)\, d\xi\, d\theta\\ &\quad= -\left(\alpha\tau \boldsymbol{\Psi}(0) - \beta\tau \int_{\theta=-\infty}^{\theta=0} \boldsymbol{\Psi}(-\theta)\hat{g}(-\theta)\, d\theta\right) h(0, \boldsymbol{u}(t))\\ &\quad- \beta\tau \int_{\theta=-\infty}^{\theta=0} \int_{\xi=0}^{\xi=\theta} \boldsymbol{B}\boldsymbol{\Psi}(\xi-\theta) h(\xi, \boldsymbol{u}(t))\hat{g}(-\theta)\, d\xi\, d\theta\\ &\quad= -L^T(\boldsymbol{\Psi}(\xi)) h(0, \boldsymbol{u}(t)) - \beta\tau \int_{\theta=-\infty}^{\theta=0} \int_{\xi=0}^{\xi=\theta} \boldsymbol{B}\boldsymbol{\Psi}(\xi-\theta) h(\xi, \boldsymbol{u}(t))\hat{g}(-\theta)\, d\xi\, d\theta\\ &\quad= \boldsymbol{B}\boldsymbol{\Psi}(0)) h(0, \boldsymbol{u}(t)) - \beta\tau \int_{\theta=-\infty}^{\theta=0} \int_{\xi=0}^{\xi=\theta} \boldsymbol{B}\boldsymbol{\Psi}(\xi-\theta) h(\xi, \boldsymbol{u}(t))\hat{g}(-\theta)\, d\xi\, d\theta\\ &\quad= \boldsymbol{B}\left\langle \boldsymbol{\Psi}(\xi), h(\theta, \boldsymbol{u}(t))\right\rangle\\ &\quad= 0.\end{aligned}$$

Therefore from the above result, (5.27) and (5.28), we obtain the following system of ODEs for $\boldsymbol{u}(t)$,

$$\boldsymbol{u'}(t) = \boldsymbol{B}\boldsymbol{u}(t) + \boldsymbol{\Psi}(0) F\left(\boldsymbol{\Phi}(\theta)\boldsymbol{u}(t) + h(\theta, \boldsymbol{u}(t))\right). \tag{5.29}$$

Using this in (5.24) we obtain a partial differential equation (PDE) for $h(\theta, \boldsymbol{u}(t))$,

$$\frac{\partial h}{\partial \boldsymbol{u}}[\boldsymbol{B}\boldsymbol{u}(t) + \boldsymbol{\Psi}(0)F(\boldsymbol{\Phi}(\theta)\boldsymbol{u}(t) + h(\theta, \boldsymbol{u}(t)))] + \boldsymbol{\Phi}(\theta)\boldsymbol{\Psi}(0)F(\boldsymbol{\Phi}(\theta)\boldsymbol{u}(t) + h(\theta, \boldsymbol{u}(t))) = \begin{cases} \dfrac{\partial h}{\partial \theta}, & \theta < 0, \\ \\ L(h(\theta, \boldsymbol{u}(t))) + F(\boldsymbol{\Phi}(\theta)\boldsymbol{u}(t) + h(\theta, \boldsymbol{u}(t))), & \theta = 0. \end{cases} \tag{5.30}$$

We need to solve the above PDE for $h(\theta, \boldsymbol{u}(t))$ and then substitute it into (5.29) in order to determine the behaviour of solutions on the centre manifold. In order to solve (5.30), we assume that $h(\theta, \boldsymbol{u}(t))$ may be expanded in a power series in $\boldsymbol{u}$,

$$h(\theta, \boldsymbol{u}(t)) = h_2(\theta, \boldsymbol{u}(t)) + h_3(\theta, \boldsymbol{u}(t)) + \cdots,$$

where

$$h_2(\theta, \boldsymbol{u}(t)) = h_{11}(\theta)u_1^2(t) + \cdots + h_{1m}(\theta)u_1(t)u_m(t) + h_{22}(\theta)u_2^2(t) + \cdots + h_{mm}(\theta)u_m^2(t),$$

and similarly for h_3 and higher order terms. We next write F in series form and expand each F_j about $\boldsymbol{\Phi}(\theta)\boldsymbol{u}(t)$,

$$\begin{aligned} F &= F_2(\boldsymbol{\Phi}(\theta)\boldsymbol{u}(t) + h(\theta, \boldsymbol{u}(t))) + F_3(\boldsymbol{\Phi}(\theta)\boldsymbol{u}(t) + h(\theta, \boldsymbol{u}(t))) + O(||u||^4||) \\ &= F_2(\boldsymbol{\Phi}(\theta)\boldsymbol{u}(t)) + DF_2(\boldsymbol{\Phi}(\theta)\boldsymbol{u}(t))h_2(\theta, \boldsymbol{u}(t)) + F_3(\boldsymbol{\Phi}(\theta)\boldsymbol{u}(t)) + O(||u||^4). \end{aligned}$$

From here we can see that only h_2 is needed to calculate up to the third order terms in (5.29). Substituting the expansions of F and h into the first part of (5.30) we obtain the following equation containing second order terms

$$\frac{\partial h_2}{\partial \theta} + O(||u||^3) = \frac{\partial h_2}{\partial \boldsymbol{u}}\boldsymbol{B}\boldsymbol{u}(t) + \boldsymbol{\Phi}(\theta)\boldsymbol{\Psi}(0)F_2(\boldsymbol{\Phi}(\theta)\boldsymbol{u}(t)) + O(||u||^3). \tag{5.31}$$

Equating terms with like powers of $u_1, \ldots, u_m$ in the above equation yields a system of ODEs for $h_{jk}(\theta), j, k = 1, \ldots, m$. This system is linear and it is solved to find the general solutions for the $h_{jk}(\theta)$ in terms of arbitrary constants. To determine these arbitrary constants, we use the second part of (5.30),

$$\begin{aligned} \frac{\partial h_2}{\partial \boldsymbol{u}}\bigg|_{\theta=0} &\boldsymbol{B}\boldsymbol{u}(t) + \boldsymbol{\Phi}(0)\boldsymbol{\Psi}(0)F_2(\boldsymbol{\Phi}(\theta)\boldsymbol{u}(t)) + O(||u||^3) \\ &= L(h_2(\theta, \boldsymbol{u}(t))) + F_2(\Phi(\theta)\boldsymbol{u}(t)) + O(||u||^3). \end{aligned} \tag{5.32}$$

Equating terms with like powers of $u_1, \ldots, u_m$ in the above equation yields a system of equations for the arbitrary constants. Once h_2 has been calculated, we can proceed to the next order of approximation and calculate h_3. We can then use these into (5.29) to analyze the flow of solutions on the centre manifold. Since (5.29) is an ODE, whether the equilibrium is attracting or not on the centre manifold will be determined using the well established theory of ODEs.

In the next section we apply the theory we have just developed to our DDE (5.1).

5.2 Computation of the Centre Manifold for our Model

In this section we compute the centre manifold for DDE (5.1). The computations can be quite cumbersome and thus will be implemented in the symbolic algebra package Maple$^{\text{TM}}$. The Maple$^{\text{TM}}$ code can be seen in Appendix A and adapts the Maple$^{\text{TM}}$ implementation of the centre manifold calculation for DDEs with discrete delays presented in [9] to DDEs with distributed delay.

The linearized system (5.8) is identical to the linear system we studied in Chapter 3. The characteristic equation (5.9) has a zero root when $\beta = \alpha$ and a pair of pure imaginary roots when

$$\begin{aligned} \alpha\tau &= \beta\tau \textstyle\int_{-\infty}^{0} \cos(\omega\theta)\, \hat{g}(-\theta)\, d\theta = \beta\tau C(\omega), \\ \omega &= \beta\tau \textstyle\int_{-\infty}^{0} \sin(\omega\theta)\, \hat{g}(-\theta)\, d\theta = -\beta\tau S(\omega), \end{aligned} \tag{5.33}$$

where

$$C(\omega) = \int_{-\infty}^{0} \cos(\omega\theta)\, \hat{g}(-\theta)\, d\theta \qquad \text{and} \qquad S(\omega) = -\int_{-\infty}^{0} \sin(\omega\theta)\, \hat{g}(-\theta)\, d\theta. \tag{5.34}$$

We note that the minus sign in front of the integral in the expression for $S(\omega)$ makes $S(\omega)$ consistent with the definition we used for $S(\omega)$ in Chapters 3 and 4.

The curves in the $\beta\tau$-plane along which equations (5.33) are satisfied are given by

$$\beta = \frac{\alpha}{C(\omega)}, \qquad \tau = -\frac{\omega C(\omega)}{\alpha S(\omega)}, \tag{5.35}$$

for all $\omega > 0$ such that $C(\omega)$ and $S(\omega)$ are nonzero. From Theorems 5 and 6, we know that the curves defined by (5.35) can only exist in the region $\beta < -\alpha$ and thus they can never intersect the line $\beta = \alpha$. Therefore the characteristic equation cannot have a pair of pure imaginary roots and a zero root simultaneously. For the rest of the chapter, we assume that we are at a critical point in the parameter space such that equations (5.35) are satisfied, i.e. the characteristic equation has a pair of pure imaginary roots. We also assume that at such a critical point all the other roots of the characteristic equation have negative real parts. From Section 3.1 we have that

$$\left.\frac{d\mathrm{Re}(\lambda)}{d\beta}\right|_{\lambda=i\omega} = \frac{\alpha}{\beta}\frac{\omega}{H^2(\omega)}\frac{d\tau}{d\omega}, \tag{5.36}$$

and thus

$$\left.\frac{d\mathrm{Re}(\lambda)}{d\beta}\right|_{\lambda=i\omega} \neq 0 \qquad \text{if} \qquad \frac{d\tau}{d\omega} \neq 0.$$

If the above condition is met, since the characteristic equation (5.9) has one pair of pure imaginary roots, the DDE (5.1) satisfies the conditions for a Hopf bifurcation to occur as

the bifurcation parameter passes through a point on the curves in (5.35) (Theorem 1.1, Section 11.1 in [26]). To determine the criticality of this Hopf bifurcation, we compute the centre manifold of the equilibrium point at the Hopf bifurcation.

From Subsection (5.1.1) we have that the basis for centre eigenspace N is given by

$$\boldsymbol{\Phi}(\theta) = \left[\begin{array}{c|c} \cos(\omega\theta) & \sin(\omega\theta) \end{array} \right]. \tag{5.37}$$

Since $m = 2$, the vector $\boldsymbol{u}(t)$ is given by

$$\boldsymbol{u}(t) = \begin{bmatrix} u_1(t) \\ u_2(t) \end{bmatrix},$$

and matrix $\boldsymbol{B}$ is

$$\boldsymbol{B} = \begin{bmatrix} 0 & \omega \\ -\omega & 0 \end{bmatrix}.$$

To determine the criticality of the Hopf bifurcation, we only need to find the terms up to and including those which are $O(||\boldsymbol{u}(t)||^3)$ in (5.29). Thus we only need the quadratic terms in the series for h,

$$h_2(\theta, \boldsymbol{u}(t)) = h_{11}(\theta)u_1^2 + h_{12}(\theta)u_1u_2 + h_{22}(\theta)u_2^2.$$

We next find the basis $\boldsymbol{\Psi}(\xi), \xi \geq 0$, for the centre eigenspace of the dual equation. We first determine a general basis $\boldsymbol{\Psi}^g(\xi)$ in the same way we found $\boldsymbol{\Phi}(\theta)$,

$$\psi_1^g(\xi) = \mathrm{Re}(e^{-i\omega\xi}) = \cos(\omega\xi)$$

and

$$\psi_2^g(\xi) = \mathrm{Im}(e^{-i\omega\xi}) = -\sin(\omega\xi).$$

Thus the general basis corresponding to centre eigenspace of the dual equation is given by the matrix

$$\boldsymbol{\Psi}^g = \begin{bmatrix} \cos(\omega\xi) \\ -\sin(\omega\xi) \end{bmatrix}. \tag{5.38}$$

We next want to find a basis $\boldsymbol{\Psi}$ such that $\langle \boldsymbol{\Psi}, \boldsymbol{\Phi} \rangle = \boldsymbol{I}$. The elements of the new basis $\boldsymbol{\Psi}$ will be a linear combinations of those of $\boldsymbol{\Psi}^g$, i.e. $\boldsymbol{\Psi} = \boldsymbol{K}\boldsymbol{\Psi}^g$, where $\boldsymbol{K}$ is a 2×2 matrix of constants. We thus impose

$$\boldsymbol{I} = \langle \boldsymbol{\Psi}, \boldsymbol{\Phi} \rangle = \langle \boldsymbol{K}\boldsymbol{\Psi}^g, \boldsymbol{\Phi} \rangle = \boldsymbol{K}\langle \boldsymbol{\Psi}^g, \boldsymbol{\Phi} \rangle.$$

From here we have that $\boldsymbol{K} = \langle \boldsymbol{\Psi}^g, \boldsymbol{\Phi} \rangle^{-1}$, where

$$\langle \boldsymbol{\Psi}^g, \boldsymbol{\Phi} \rangle = \begin{bmatrix} \langle \psi_1^g, \phi_1 \rangle & \langle \psi_1^g, \phi_2 \rangle \\ \langle \psi_2^g, \phi_1 \rangle & \langle \psi_2^g, \phi_2 \rangle \end{bmatrix}, \tag{5.39}$$

and the bilinear form $\langle \psi, \phi \rangle$ is defined in (5.17). We calculate the elements in (5.39) by substituting (5.37) and (5.38) into (5.17). We first compute

$$C'(\omega) = -\int_{-\infty}^{0} \theta \sin(\omega\theta)\, \hat{g}(-\theta)\, d\theta \qquad \text{and} \qquad S'(\omega) = -\int_{-\infty}^{0} \theta \cos(\omega\theta)\, \hat{g}(-\theta)\, d\theta.$$

Since from (5.33), $\beta\tau = -\omega/S(\omega)$, we then have

$$\begin{aligned}
\langle \psi_1^g, \phi_1 \rangle &= \cos(0)\cos(0) - \beta\tau \int_{\theta=-\infty}^{\theta=0} \int_{\xi=0}^{\xi=\theta} \cos(\omega(\xi-\theta))\hat{g}(-\theta)\cos(\omega\xi)\, d\xi\, d\theta \\
&= 1 + \frac{\omega}{S(\omega)} \int_{\theta=-\infty}^{\theta=0} \left(\int_{\xi=0}^{\xi=\theta} \cos(\omega(\xi-\theta))\cos(\omega\xi)\, d\xi \right) \hat{g}(-\theta)\, d\theta \\
&= 1 + \frac{\omega}{S(\omega)} \int_{\theta=-\infty}^{\theta=0} \left(\frac{\sin(\omega\theta) + \omega\theta\cos(\omega\theta)}{2\omega} \right) \hat{g}(-\theta)\, d\theta \\
&= 1 + \frac{1}{2S(\omega)} \int_{\theta=-\infty}^{\theta=0} \sin(\omega\theta)\hat{g}(-\theta)\, d\theta + \frac{\omega}{2S(\omega)} \int_{\theta=-\infty}^{\theta=0} \theta\cos(\omega\theta)\hat{g}(-\theta)\, d\theta \\
&= \frac{1}{2} - \frac{\omega}{2}\frac{S'(\omega)}{S(\omega)},
\end{aligned}$$

$$\begin{aligned}
\langle \psi_1^g, \phi_2 \rangle &= \cos(0)\sin(0) - \beta\tau \int_{\theta=-\infty}^{\theta=0} \int_{\xi=0}^{\xi=\theta} \cos(\omega(\xi-\theta))\hat{g}(-\theta)\sin(\omega\xi)\, d\xi\, d\theta \\
&= \frac{\omega}{S(\omega)} \int_{\theta=-\infty}^{\theta=0} \left(\int_{\xi=0}^{\xi=\theta} \cos(\omega(\xi-\theta))\sin(\omega\xi)\, d\xi \right) \hat{g}(-\theta)\, d\theta \\
&= \frac{\omega}{S(\omega)} \int_{\theta=-\infty}^{\theta=0} \frac{\theta\sin(\omega\theta)}{2} \hat{g}(-\theta)\, d\theta \\
&= -\frac{\omega}{2}\frac{C'(\omega)}{S(\omega)},
\end{aligned}$$

$$\begin{aligned}
\langle \psi_2^g, \phi_1 \rangle &= -\sin(0)\cos(0) + \beta\tau \int_{\theta=-\infty}^{\theta=0} \int_{\xi=0}^{\xi=\theta} \sin(\omega(\xi-\theta))\hat{g}(-\theta)\cos(\omega\xi)\, d\xi\, d\theta \\
&= -\frac{\omega}{S(\omega)} \int_{\theta=-\infty}^{\theta=0} \left(\int_{\xi=0}^{\xi=\theta} \sin(\omega(\xi-\theta))\cos(\omega\xi)\, d\xi \right) \hat{g}(-\theta)\, d\theta \\
&= \frac{\omega}{S(\omega)} \int_{\theta=-\infty}^{\theta=0} \frac{\theta\sin(\omega\theta)}{2} \hat{g}(-\theta)\, d\theta \\
&= -\frac{\omega}{2}\frac{C'(\omega)}{S(\omega)},
\end{aligned}$$

$$
\begin{aligned}
\langle \psi_2^g, \phi_2 \rangle &= -\sin(0)\sin(0) + \beta\tau \int_{\theta=-\infty}^{\theta=0} \int_{\xi=0}^{\xi=\theta} \sin(\omega(\xi-\theta))\hat{g}(-\theta)\sin(\omega\xi)\, d\xi\, d\theta \\
&= -\frac{\omega}{S(\omega)} \int_{\theta=-\infty}^{\theta=0} \left(\int_{\xi=0}^{\xi=\theta} \sin(\omega(\xi-\theta))\sin(\omega\xi)\, d\xi \right) \hat{g}(-\theta)\, d\theta \\
&= -\frac{\omega}{S(\omega)} \int_{\theta=-\infty}^{\theta=0} \left(\frac{-\sin(\omega\theta) + \omega\theta\cos(\omega\theta)}{2\omega} \right) \hat{g}(-\theta)\, d\theta \\
&= \frac{1}{2S(\omega)} \int_{\theta=-\infty}^{\theta=0} \sin(\omega\theta)\hat{g}(-\theta)\, d\theta - \frac{\omega}{2S(\omega)} \int_{\theta=-\infty}^{\theta=0} \theta\cos(\omega\theta)\hat{g}(-\theta)\, d\theta \\
&= -\frac{1}{2} + \frac{\omega}{2}\frac{S'(\omega)}{S(\omega)}.
\end{aligned}
$$

Thus (5.39) becomes

$$
\langle \boldsymbol{\Psi}^g, \boldsymbol{\Phi} \rangle = \frac{1}{2S(\omega)} \begin{bmatrix} S(\omega) - \omega S'(\omega) & -\omega C'(\omega) \\ -\omega C'(\omega) & -S(\omega) + \omega S'(\omega) \end{bmatrix}.
$$

Taking its inverse and letting $D(\omega) = S^2(\omega) - 2\omega S(\omega)S'(\omega) + \omega^2\left[(C'(\omega))^2 + (S'(\omega))^2\right]$, we obtain

$$
\boldsymbol{K} = \frac{2S(\omega)}{D(\omega)} \begin{bmatrix} S(\omega) - \omega S'(\omega) & -\omega C'(\omega) \\ -\omega C'(\omega) & -S(\omega) + \omega S'(\omega) \end{bmatrix}.
$$

Now we can compute our new basis $\boldsymbol{\Psi}(\xi) = \boldsymbol{K}\boldsymbol{\Psi}^g(\xi)$, but since later we only need this basis evaluated at $\xi = 0$, we only display $\boldsymbol{\Psi}(0)$,

$$
\boldsymbol{\Psi}(0) = \begin{bmatrix} \psi_{10} \\ \psi_{20} \end{bmatrix} = \frac{2S(\omega)}{D(\omega)} \begin{bmatrix} S(\omega) - \omega S'(\omega) \\ -\omega C'(\omega) \end{bmatrix}. \tag{5.40}
$$

We can now define the ODEs for $h_{11}(\theta), h_{12}(\theta)$ and $h_{22}(\theta)$. The left-hand side of (5.31) becomes

$$
\frac{\partial h_2}{\partial \theta} = \frac{dh_{11}(\theta)}{d\theta}u_1^2 + \frac{dh_{12}(\theta)}{d\theta}u_1u_2 + \frac{dh_{22}(\theta)}{d\theta}u_2^2. \tag{5.41}
$$

The first term in the right-hand side of (5.31) is given by

$$
\begin{aligned}
\frac{\partial h_2}{\partial \boldsymbol{u}}\boldsymbol{B}\boldsymbol{u} &= \begin{bmatrix} 2h_{11}(\theta)u_1 + h_{12}(\theta)u_2 & h_{12}(\theta)u_1 + 2h_{22}(\theta)u_2 \end{bmatrix} \begin{bmatrix} \omega u_2 \\ -\omega u_1 \end{bmatrix} \\
&= -\omega h_{12}(\theta)u_1^2 + 2\omega[h_{11}(\theta) - h_{22}(\theta)]u_1u_2 + \omega h_{12}(\theta)u_2^2.
\end{aligned} \tag{5.42}
$$

For the second term in the right-hand side of (5.31), we first need to compute $F_2(\boldsymbol{\Phi}(\theta)\boldsymbol{u})$.

Since $\mathbf{\Phi}(\theta)\boldsymbol{u} = \cos(\omega\theta)u_1 + \sin(\omega\theta)u_2$, from (5.6) and (5.34) we then have

$$\begin{aligned}
F_2(\mathbf{\Phi}(\theta)\boldsymbol{u}) &= \gamma\tau \int_{-\infty}^{0} [\cos(\omega\theta)u_1 + \sin(\omega\theta)u_2]^2 \hat{g}(-\theta)\, d\theta \\
&= \gamma\tau \int_{-\infty}^{0} \left[\cos^2(\omega\theta)u_1^2 + 2\cos(\omega\theta)\sin(\omega\theta)u_1u_2 + \sin^2(\omega\theta)u_2^2\right] \hat{g}(-\theta)\, d\theta \\
&= \gamma\tau \int_{-\infty}^{0} \left[\frac{1+\cos(2\omega\theta)}{2}u_1^2 + \sin(2\omega\theta)u_1u_2 + \frac{1-\cos(2\omega\theta)}{2}u_2^2\right] \hat{g}(-\theta)\, d\theta \\
&= \gamma\tau \left(\frac{1+C(2\omega)}{2}u_1^2 - S(2\omega)u_1u_2 + \frac{1-C(2\omega)}{2}u_2^2\right).
\end{aligned}$$

Now $\mathbf{\Phi}(\theta)\mathbf{\Psi}(0) = \cos(\omega\theta)\psi_{10} + \sin(\omega\theta)\psi_{20}$, and thus the second term in the right-hand side of (5.31) becomes

$$\begin{aligned}
\mathbf{\Phi}(\theta)\mathbf{\Psi}(0)F_2(\mathbf{\Phi}(\theta)\boldsymbol{u}) &= \gamma\tau[\cos(\omega\theta)\psi_{10} + \sin(\omega\theta)\psi_{20}]\frac{1+C(2\omega)}{2}u_1^2 \\
&\quad - \gamma\tau[\cos(\omega\theta)\psi_{10} + \sin(\omega\theta)\psi_{20}]S(2\omega)u_1u_2 \\
&\quad + \gamma\tau[\cos(\omega\theta)\psi_{10} + \sin(\omega\theta)\psi_{20}]\frac{1-C(2\omega)}{2}u_2^2,
\end{aligned} \tag{5.43}$$

where the expression for ψ_{10} and ψ_{20} are given in (5.40). Equating the coefficients of u_1^2, u_1u_2 and u_2^2 in (5.41), (5.42) and (5.43) we obtain the following system of ODEs,

$$\begin{aligned}
\frac{dh_{11}(\theta)}{d\theta} &= -\omega h_{12}(\theta) + \gamma\tau[\cos(\omega\theta)\psi_{10} + \sin(\omega\theta)\psi_{20}]\frac{1+C(2\omega)}{2} \\
\frac{dh_{12}(\theta)}{d\theta} &= 2\omega h_{11}(\theta) - 2\omega h_{22}(\theta) - \gamma\tau[\cos(\omega\theta)\psi_{10} + \sin(\omega\theta)\psi_{20}]S(2\omega) \\
\frac{dh_{22}(\theta)}{d\theta} &= \omega h_{12}(\theta) + \gamma\tau[\cos(\omega\theta)\psi_{10} + \sin(\omega\theta)\psi_{20}]\frac{1-C(2\omega)}{2}.
\end{aligned}$$

This is a system of linear ODEs which can be solved in Maple$^{\text{TM}}$ for $h_{11}(\theta), h_{12}(\theta)$ and

$h_{22}(\theta)$ in terms of the three arbitrary constants c_1, c_2, and c_3,

$$\begin{aligned}
h_{11}(\theta) &= -\frac{1}{6\omega}\left[-6\omega c_3\cos^2(\omega\theta) + 6\omega c_2\sin(\omega\theta)\cos(\omega\theta) + 3\gamma\tau\psi_{20}\cos(\omega\theta)\right.\\
&\quad - 3\gamma\tau\psi_{10}\sin(\omega\theta) + \gamma\tau\psi_{10}\sin(\omega\theta)C(2\omega) - 2\gamma\tau\psi_{10}\cos(\omega\theta)S(2\omega)\\
&\quad \left.-2\gamma\tau\psi_{20}\sin(\omega\theta)S(2\omega) - \gamma\tau\psi_{20}\cos(\omega\theta)C(2\omega) - 6\omega c_1 + 3\omega c_3\right],\\
h_{12}(\theta) &= \frac{1}{3\omega}\left[6\omega c_2\cos^2(\omega\theta) + 6\omega c_3\sin(\omega\theta)\cos(\omega\theta) + 2\gamma\tau\psi_{10}\cos(\omega\theta)C(2\omega)\right.\\
&\quad + 2\gamma\tau\psi_{20}\sin(\omega\theta)C(2\omega) + \gamma\tau\psi_{10}\sin(\omega\theta)S(2\omega)\\
&\quad \left.-\gamma\tau\psi_{20}\cos(\omega\theta)S(2\omega) - 3\omega c_2\right],\\
h_{22}(\theta) &= \frac{1}{6\omega}\left[-6\omega c_3\cos^2(\omega\theta) + 6\omega c_2\sin(\omega\theta)\cos(\omega\theta) - 3\gamma\tau\psi_{20}\cos(\omega\theta)\right.\\
&\quad + 3\gamma\tau\psi_{10}\sin(\omega\theta) + \gamma\tau\psi_{10}\sin(\omega\theta)C(2\omega) - 2\gamma\tau\psi_{10}\cos(\omega\theta)S(2\omega)\\
&\quad \left.-2\gamma\tau\psi_{20}\sin(\omega\theta)S(2\omega) - \gamma\tau\psi_{20}\cos(\omega\theta)C(2\omega) + 6\omega c_1 + 3\omega c_3\right].
\end{aligned} \tag{5.44}$$

We next determine the three constants of integration using (5.32). To compute $L(h_2(\theta, \boldsymbol{u}(t)))$ we need $h_2(0, \boldsymbol{u}(t))$ and thus substituting $\theta = 0$ into the above expressions we have

$$\begin{aligned}
h_{11}(0) &= \frac{1}{6\omega}\left[\gamma\tau\psi_{20}C(2\omega) + 2\gamma\tau\psi_{10}S(2\omega) - 3\gamma\tau\psi_{20} + 6\omega c_1 + 3\omega c_3\right],\\
h_{12}(0) &= \frac{1}{3\omega}\left[2\gamma\tau\psi_{10}C(2\omega) - \gamma\tau\psi_{20}S(2\omega) + 3\omega c_2\right],\\
h_{22}(0) &= -\frac{1}{6\omega}\left[\gamma\tau\psi_{20}C(2\omega) + 2\gamma\tau\psi_{10}S(2\omega) + 3\gamma\tau\psi_{20} - 6\omega c_1 + 3\omega c_3\right].
\end{aligned} \tag{5.45}$$

In the calculation of $L(h_2(\theta, \boldsymbol{u}(t)))$ we also need $\int_{-\infty}^{0} h_2(\theta, \boldsymbol{u}(t))\hat{g}(-\theta)\,d\theta$, and thus we next compute

$$\begin{aligned}
\int_{-\infty}^{0} h_{11}(\theta)\hat{g}(-\theta)\,d\theta &= \frac{1}{6\omega}\left[\gamma\tau\psi_{20}C(\omega)C(2\omega) + \gamma\tau\psi_{10}S(\omega)C(2\omega) + 3\omega c_3C(2\omega)\right.\\
&\quad + 2\gamma\tau\psi_{10}C(\omega)S(2\omega) - 2\gamma\tau\psi_{20}S(\omega)S(2\omega) + 3\omega c_2S(2\omega)\\
&\quad \left.- 3\gamma\tau\psi_{20}C(\omega) - 3\gamma\tau\psi_{10}S(\omega) + 6\omega c_1\right],\\
\int_{-\infty}^{0} h_{12}(\theta)\hat{g}(-\theta)\,d\theta &= -\frac{1}{3\omega}\left[-2\gamma\tau\psi_{10}C(\omega)C(2\omega) + 2\gamma\tau\psi_{20}S(\omega)C(2\omega)\right.\\
&\quad + \gamma\tau\psi_{20}C(\omega)S(2\omega) + \gamma\tau\psi_{10}S(\omega)S(2\omega)\\
&\quad \left.- 3\omega c_2C(2\omega) + 3\omega c_3S(2\omega)\right],\\
\int_{-\infty}^{0} h_{22}(\theta)\hat{g}(-\theta)\,d\theta &= -\frac{1}{6\omega}\left[\gamma\tau\psi_{20}C(\omega)C(2\omega) + \gamma\tau\psi_{10}S(\omega)C(2\omega) + 3\omega c_3C(2\omega)\right.\\
&\quad + 2\gamma\tau\psi_{10}C(\omega)S(2\omega) - 2\gamma\tau\psi_{20}S(\omega)S(2\omega) + 3\omega c_2S(2\omega)\\
&\quad \left.+ 3\gamma\tau\psi_{20}C(\omega) + 3\gamma\tau\psi_{10}S(\omega) - 6\omega c_1\right].
\end{aligned} \tag{5.46}$$

Therefore equation (5.32) becomes

$$\begin{aligned}
&-\omega h_{12}(0)u_1^2 + 2\omega[h_{11}(0) - h_{22}(0)]u_1u_2 + \omega h_{12}(0)u_2^2 \\
&\qquad + \gamma\tau\psi_{10}\left(\frac{1+C(2\omega)}{2}u_1^2 - S(2\omega)u_1u_2 + \frac{1-C(2\omega)}{2}u_2^2\right) \\
&\qquad = -\alpha\tau\left[h_{11}(0)u_1^2 + h_{12}(0)u_1u_2 + h_{22}(0)u_2^2\right] \\
&\qquad + \beta\tau\left[u_1^2\int_{-\infty}^{0} h_{11}(\theta)\hat{g}(-\theta)\,d\theta + u_1u_2\int_{-\infty}^{0} h_{12}(\theta)\hat{g}(-\theta)\,d\theta + u_2^2\int_{-\infty}^{0} h_{22}(\theta)\hat{g}(-\theta)\,d\theta\right] \\
&\qquad + \gamma\tau\left(\frac{1+C(2\omega)}{2}u_1^2 - S(2\omega)u_1u_2 + \frac{1-C(2\omega)}{2}u_2^2\right).
\end{aligned}$$

Substituting (5.45) and (5.46) into the above equation and equating the coefficients of u_1^2, u_1u_2 and u_2^2 yields a system of three equations for c_1, c_2, and c_3, which is solved in Maple$^{\text{TM}}$. Let $E(\omega) = C^2(2\omega) + S^2(2\omega) + C^2(\omega) + 4S^2(\omega) - 2C(\omega)C(2\omega) - 4S(\omega)S(2\omega)$, then the three constants of integration are given by

$$\begin{aligned}
c_1 &= \frac{\gamma\tau S(\omega)}{2\omega(1-C(\omega))}, \\
c_2 &= \frac{\gamma\tau S(\omega)[C(\omega)S(2\omega) - 2S(\omega)C(2\omega)]}{\omega E(\omega)}, \\
c_3 &= \frac{\gamma\tau S(\omega)[C^2(\omega) + S^2(\omega) - C(\omega)C(2\omega) - 2S(\omega)S(2\omega)]}{\omega E(\omega)}.
\end{aligned} \tag{5.47}$$

Plugging in the above values into (5.44), we obtain the expressions for $h_{11}(\theta), h_{12}(\theta)$ and $h_{22}(\theta)$ which will be substituted into equation (5.29). Since (5.29) is an ODE of the form

$$\begin{bmatrix} u_1'(t) \\ u_2'(t) \end{bmatrix} = \begin{bmatrix} 0 & \omega \\ -\omega & 0 \end{bmatrix}\begin{bmatrix} u_1(t) \\ u_2(t) \end{bmatrix} + \begin{bmatrix} M(u_1,u_2) \\ N(u_1,u_2) \end{bmatrix},$$

where M and N represent nonlinear functions, the stability of the equilibrium point and the criticality of the Hopf bifurcation is determined by the sign of the cubic coefficient [25]

$$\begin{aligned}
a = \frac{1}{16}\left[M_{u_1u_1u_1} + M_{u_1u_2u_2} + N_{u_1u_1u_2} + N_{u_2u_2u_2}\right] - \frac{1}{16\omega}\left[M_{u_1u_2}(M_{u_1u_1} + M_{u_2u_2})\right. \\
\left. -N_{u_1u_2}(N_{u_1u_1} + N_{u_2u_2}) - M_{u_1u_1}N_{u_1u_1} + M_{u_2u_2}N_{u_2u_2}\right],
\end{aligned} \tag{5.48}$$

where $M_{u_1u_2}$ denotes $\partial^2 M/\partial u_1\partial u_2(0,0)$, and so on. If $a < 0$ the periodic solutions are stable limit cycles, while if $a > 0$ the periodic solutions are repelling.

In our case we have

$$\begin{aligned}
M(u_1,u_2) &= \psi_{10}F\left(\mathbf{\Phi}(\theta)\boldsymbol{u}(t) + h(\theta,\boldsymbol{u}(t))\right) \\
N(u_1,u_2) &= \psi_{20}F\left(\mathbf{\Phi}(\theta)\boldsymbol{u}(t) + h(\theta,\boldsymbol{u}(t))\right),
\end{aligned}$$

where

$$
\begin{aligned}
&F\left(\boldsymbol{\Phi}(\theta)\,\boldsymbol{u}(t)+h(\theta,\boldsymbol{u}(t))\right)\\
&\qquad=\gamma\tau\int_{-\infty}^{0}[\cos(\omega\theta)u_1+\sin(\omega\theta)u_2+h_{11}(\theta)u_1^2+h_{12}(\theta)u_1u_2+h_{22}(\theta)u_2^2]^2\hat{g}(-\theta)\,d\theta\\
&\qquad+\delta\tau\int_{-\infty}^{0}[\cos(\omega\theta)u_1+\sin(\omega\theta)u_2+h_{11}(\theta)u_1^2+h_{12}(\theta)u_1u_2+h_{22}(\theta)u_2^2]^3\hat{g}(-\theta)\,d\theta.
\end{aligned}
$$

After performing the calculations and simplifications in Maple$^{\text{TM}}$ (see Appendix A), we obtain the cubic coefficient to be

$$
\begin{aligned}
a_{\text{DDE}}=&\frac{\tau\psi_{10}}{8}\left(2\gamma c_3C(\omega)+8\gamma c_1C(\omega)+3\delta C(\omega)+2\gamma c_2S(\omega)\right)\\
&-\frac{\tau\psi_{20}}{8}\left(-2\gamma c_2C(\omega)+8\gamma c_1S(\omega)+2\gamma c_3S(\omega)+3\delta S(\omega)\right),
\end{aligned}
\tag{5.49}
$$

where ψ_{10} and ψ_{20} are given in (5.40), and c_1, c_2 and c_3 are given in (5.47).

Since the curves in (5.35) that form part of the stability boundary must lie in the region $\beta \leq -\alpha$ where $\alpha > 0$, from (5.36) and (3.15), we have that

$$
\left.\frac{d\text{Re}(\lambda)}{d\beta}\right|_{\lambda=i\omega}\lessgtr 0 \qquad \text{if} \qquad \mu=\frac{d\tau}{d\omega}\gtrless 0,
$$

where

$$
\mu=-\frac{1}{\alpha S(\omega)}\left(C(\omega)+\omega\frac{C'(\omega)S(\omega)-S'(\omega)C(\omega)}{S(\omega)}\right). \tag{5.50}
$$

Since our calculations are formal, i.e. they assume that the centre manifold theory holds for DDEs with infinite distributed delay although it has not been rigorously proven, we summarize the results of this section in the following conjecture.

Conjecture 1 *If $\mu \neq 0$, as β passes through a critical value β_c on the curves in* (5.35)*, there is a Hopf bifurcation at the equilibrium point x^* of* (5.1)*. If $\mu > 0$ then x^* is locally asymptotically stable (unstable) for $\beta > \beta_c$ ($\beta < \beta_c$). If $\mu < 0$ then x^* is locally asymptotically stable (unstable) for $\beta < \beta_c$ ($\beta > \beta_c$). The periodic solutions are stable (unstable) if $a_{DDE} < 0$ ($a_{DDE} > 0$).*

In the next two subsections, we compute the cubic coefficient a_{DDE} in the specific cases of the weak and strong kernels, i.e. the gamma distribution with $p = 1$ and $p = 2$, respectively.

5.2.1 The Cubic Coefficient in the Case of the Weak Kernel

When $\hat{g}(-\theta)$ is the weak kernel, i.e. $\hat{g}(-\theta) = e^{\theta}$, we have

$$\begin{aligned} C(\omega) &= \frac{1}{1+\omega^2}, & S(\omega) &= \frac{\omega}{1+\omega^2}, \\ C(2\omega) &= \frac{1}{1+4\omega^2}, & S(2\omega) &= \frac{2\omega}{1+4\omega^2}, \\ C'(\omega) &= -\frac{2\omega}{(1+\omega^2)^2}, & S'(\omega) &= \frac{1-\omega^2}{(1+\omega^2)^2}. \end{aligned} \tag{5.51}$$

Plugging the expressions for $C(\omega)$ and $S(\omega)$ obtained above into (5.33) we get that $\alpha\tau = -1$ and $\omega^2 = -1 - \beta\tau$. Therefore α must be negative in order for the characteristic equation to have a pair of pure imaginary roots. We note that in this case equation (5.1) does not represent a scalar Hopfield model (for which α is positive), but we still compute the cubic coefficient in this case in order to observe how it compares to the cubic coefficient of the corresponding ODE model.

From (5.51) we obtain

$$\psi_{10} = 1, \qquad \psi_{20} = \frac{1}{\omega},$$

and

$$c_1 = \frac{\gamma\tau}{2\omega^2}, \qquad c_2 = 0, \qquad c_3 = -\frac{\gamma\tau}{3\omega^2}.$$

Substituting the above expressions into (5.49), we obtain $a_{\mathrm{DDE}} = 0$. Hence, in the case of the weak kernel, we cannot conclude anything about the stability of the periodic solutions or even if they exist. In fact, plugging in (5.51) into (5.50), we get

$$\mu = 0 \qquad \Rightarrow \qquad \left.\frac{d\mathrm{Re}(\lambda)}{d\beta}\right|_{\lambda=i\omega} = 0,$$

and therefore Conjecture 1 cannot predict whether a Hopf bifurcation can occur at the equilibrium point x^* of (5.1) in the weak kernel case.

5.2.2 The Cubic Coefficient in the Case of the Strong Kernel

When $\hat{g}(-\theta)$ represents the strong kernel, i.e. $\hat{g}(-\theta) = -4\theta e^{2\theta}$, we have

$$\begin{aligned} C(\omega) &= \frac{4(4-\omega^2)}{(4+\omega^2)^2}, & S(\omega) &= \frac{16\omega}{(4+\omega^2)^2}, \\ C(2\omega) &= \frac{4(4-4\omega^2)}{(4+4\omega^2)^2}, & S(2\omega) &= \frac{32\omega}{(4+4\omega^2)^2}, \\ C'(\omega) &= \frac{8\omega(\omega^2-12)}{(4+\omega^2)^3}, & S'(\omega) &= -\frac{16(3\omega^2-4)}{(4+\omega^2)^3}. \end{aligned} \tag{5.52}$$

Therefore from (5.40) and (5.47) we get

$$\psi_{10} = \frac{32}{\omega^2+36}, \qquad \psi_{20} = \frac{4(12-\omega^2)}{\omega(\omega^2+36)}, \tag{5.53}$$

and

$$c_1 = \frac{8\gamma\tau}{\omega^2(\omega^2+12)}, \quad c_2 = \frac{128\gamma\tau}{3\omega(\omega^4+88\omega^2+144)}, \quad c_3 = -\frac{16\gamma\tau(\omega^2+12)}{3\omega^2(\omega^4+88\omega^2+144)}. \tag{5.54}$$

Substituting (5.52) into (5.50), we get

$$\mu = \frac{\omega(\omega^2+4)^2}{8\beta(4-\omega^2)} \neq 0 \qquad \Rightarrow \qquad \left.\frac{d\mathrm{Re}(\lambda)}{d\beta}\right|_{\lambda=i\omega} \neq 0. \tag{5.55}$$

Hence Conjecture 1 predicts that a Hopf bifurcation does occur in this case. Plugging in (5.52), (5.53) and (5.54) into (5.49), we obtain that, for the strong kernel, the cubic coefficient is given by

$$\begin{aligned} a_{\mathrm{DDE}} = &\frac{\omega^2+4}{2\beta^2\omega^2(\omega^2+36)(\omega^2+12)(\omega^4+88\omega^2+144)} \\ &\times \left[(3\beta\delta-2\gamma^2)\omega^8 + (300\beta\delta-320\gamma^2)\omega^6 + (3600\beta\delta-2752\gamma^2)\omega^4\right. \\ &\left.+(5184\beta\delta-7168\gamma^2)\omega^2 - 4608\gamma^2\right]. \end{aligned} \tag{5.56}$$

In this case, the sign of a_{DDE} is given by the expression inside the square brackets.

We next exemplify the predictions of Conjecture 1 by looking at a particular example. Let $\alpha = 2$, then substituting the expressions for $C(\omega)$ and $S(\omega)$ from (5.52) into (5.35), we obtain

$$\beta = \frac{(\omega^2+4)^2}{2(4-\omega^2)}, \qquad \tau = -\frac{\omega^4+4}{8}, \tag{5.57}$$

where the interval for ω is chosen such that we obtain the closest curve to the τ-axis, i.e. the curve which forms part of the stability boundary. From Section 3.1, the region of stability of the equilibrium point x^* of (5.1) is the region to the right of the curve in (5.57) and to the left of the vertical line $\beta = \alpha$. This region of stability can be seen in Figure 5.1(a), as the region between the solid black curve and the solid gray line. For a particular value of the mean delay, say $\tau_c = 0.6$, we obtain the critical values of β and ω, by solving system (5.57). In this case we get $\beta_c = -17.07$ and $\omega_c = 2.97$, as seen in Figure 5.1(a). Thus we have that the equilibrium point is stable for $-17.07 = \beta_c < \beta < \alpha$ and unstable for $\beta < \beta_c = -17.07$.

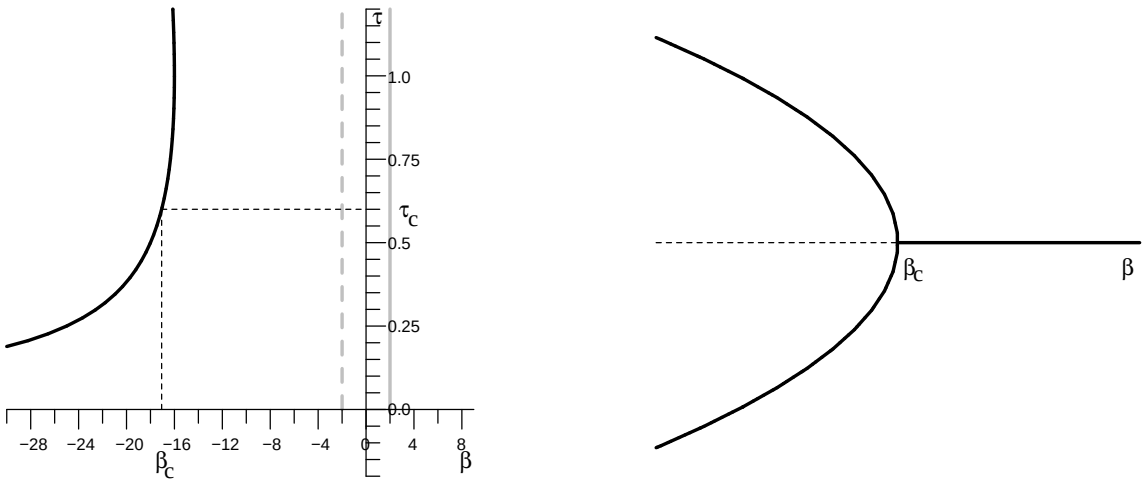

(a) Stability diagram, strong kernel

(b) Predicted bifurcation diagram

Figure 5.1: (a) Stability region for the gamma distribution with $p = 2$ when $\alpha = 2$. The region of stability of the equilibrium point x^* of (5.1) lies between the solid black curve defined by equations (5.57) and the solid gray line. For $\tau_c = 0.6$, we obtain $\beta_c = -17.07$ and $\omega_c = 2.97$; (b) When $f = \tanh(0.176x), w = -100, c = 19.421$, Conjecture 1 predicts that as β passes through the critical value $\beta_c = -17.07$, there is a Hopf bifurcation at the equilibrium point $x^* = 1$ of (5.1) giving rise to stable periodic solutions in the region $\beta < \beta_c = -17.07$.

Let $f = \tanh(Ax), x^* = 1$ and $w = -100$. Then A solves the equation $\beta/w = A\,\mathrm{sech}^2(A)$ since $\beta = f'(x^*)$ and $c = \alpha - w\tanh(A)$ by (5.3). In this case we obtain $A = 0.176, c = 19.421, \gamma = 0.523$ and $\delta = 0.160$. From (5.55), we have $\mu > 0$ if $\omega > 2$.

Calculating a_{DDE} in (5.56) at the critical parameter values, we obtain $a_{\text{DDE}} < 0$. Using Conjecture 1 we predict that as β passes through the critical value $\beta_c = -17.07$, there is a Hopf bifurcation at the equilibrium point $x^* = 1$ of (5.1) giving rise to stable periodic solutions in the region $\beta < \beta_c = -17.07$. Hence Conjecture 1 predicts a bifurcation diagram as seen in Figure 5.1(b). We check this prediction numerically in Section 5.4.

In the next two sections we verify the predictions of Conjecture 1 by transforming the DDE (5.1) with $\hat{g}(-\theta)$ representing the weak and strong kernels into equivalent systems of ODEs, computing the cubic coefficient for the ODE cases, and performing numerical simulations.

5.3 The Equivalent Two Dimensional ODE System

In this section we verify the results we obtained in Subsection 5.2.1 by transforming the scalar DDE (5.1) where $\hat{g}(-\theta)$ represents the weak kernel (i.e. the gamma distribution with $p = 1$) into a two dimensional ODE system.

Applying the linear chain trick presented in Section 2.5, equation (5.1) becomes

$$\begin{cases} x_0'(t) = -\alpha\tau x_0(t) + w\tau x_1(t) + c\tau \\ x_1'(t) = f(x_0(t)) - x_1(t) \end{cases} \tag{5.58}$$

We assume the above system admits an equilibrium solution (x_0^*, x_1^*) satisfying

$$\begin{cases} 0 = -\alpha\tau x_0^* + w\tau x_1^* + c\tau \\ 0 = f(x_0^*) - x_1^*. \end{cases} \tag{5.59}$$

We next shift the equilibrium to zero and separate the linear and nonlinear terms. Let $y_0(t) = x_0(t) - x_0^*$ and $y_1(t) = x_1(t) - x_1^*$. Then the Taylor series expansion of f about x_0^* is

$$f(x_0) = f(x_0^*) + \bar{\beta} y_0 + \frac{\bar{\gamma}}{2} y_0^2 + \frac{\bar{\delta}}{6} y_0^3 + \text{h.o.t.}\ , \tag{5.60}$$

where $\bar{\beta} = f'(x_0^*), \bar{\gamma} = f''(x_0^*)$, and $\bar{\delta} = f'''(x_0^*)$. Using this along with (5.59) and renaming back to x_0 and x_1, we have

$$\begin{cases} x_0'(t) = -\alpha\tau x_0(t) + w\tau x_1(t) \\ x_1'(t) = \bar{\beta} x_0(t) - x_1(t) + \dfrac{\bar{\gamma}}{2}(x_0(t))^2 + \dfrac{\bar{\delta}}{6}(x_0(t))^3 + \text{h.o.t.} \end{cases}$$

This can be written in vector form as $\boldsymbol{x}' = \boldsymbol{A}\boldsymbol{x} + \boldsymbol{F}(\boldsymbol{x})$, where $\boldsymbol{x} = [x_0, x_1]^T$, i.e.

$$\begin{bmatrix} x_0' \\ x_1' \end{bmatrix} = \begin{bmatrix} -\alpha\tau & w\tau \\ \bar{\beta} & -1 \end{bmatrix} \begin{bmatrix} x_0 \\ x_1 \end{bmatrix} + \begin{bmatrix} 0 \\ \bar{\gamma} x_0^2/2 + \bar{\delta} x_0^3/6 + \cdots \end{bmatrix}. \tag{5.61}$$

For a Hopf bifurcation to occur, the characteristic equation must have a pair of pure imaginary roots. The two eigenvalues are given by

$$\begin{aligned}\lambda_{1,2} &= \frac{\mathrm{tr}(\boldsymbol{A})}{2} \pm \frac{\sqrt{[\mathrm{tr}(\boldsymbol{A})]^2 - 4\det(\boldsymbol{A})}}{2} \\ &= -\frac{\alpha\tau + 1}{2} \pm \frac{\sqrt{(\alpha\tau+1)^2 - 4\tau(\alpha-\beta)}}{2},\end{aligned} \tag{5.62}$$

where $\beta = \bar{\beta}w$. Hence $\boldsymbol{A}$ has a pair of pure imaginary roots, $\lambda_{1,2} = \pm i\sqrt{-1-\beta\tau}$, if $\alpha\tau = -1$ and $\beta < \alpha$. From (5.62) we also have that

$$\left.\frac{d\mathrm{Re}(\lambda)}{d\beta}\right|_{\lambda=i\omega} = 0,$$

and thus the Hopf Bifurcation Theorem ([25], Theorem 3.4.2) cannot guarantee the existence of a Hopf bifurcation.

We next perform a change of variables so that the linear part in (5.61) is in standard block diagonal form. When $\lambda_{1,2} = \pm i\omega$, the matrix $\boldsymbol{A}$ becomes

$$\boldsymbol{A}|_{\lambda=\pm i\omega} = \begin{bmatrix} 1 & -\dfrac{w(\omega^2+1)}{\beta} \\ \beta/w & -1 \end{bmatrix}.$$

The corresponding eigenvectors are given by

$$\boldsymbol{u}_1 = \begin{bmatrix} 1 \\ \beta/w \end{bmatrix}, \boldsymbol{u}_2 = \begin{bmatrix} \omega \\ 0 \end{bmatrix}.$$

We let $\boldsymbol{P} = [\boldsymbol{u}_1 \mid \boldsymbol{u}_2\ ]$ and with the change of variables $\boldsymbol{x} = P\boldsymbol{y}$, where $\boldsymbol{y} = [y_0, y_1]^T$, system (5.61) becomes

$$\begin{bmatrix} y_0' \\ y_1' \end{bmatrix} = \begin{bmatrix} 0 & \omega \\ -\omega & 0 \end{bmatrix} \begin{bmatrix} y_0 \\ y_1 \end{bmatrix} + \boldsymbol{P}^{-1} \begin{bmatrix} 0 \\ F(x_0) \end{bmatrix}, \tag{5.63}$$

where $F(x_0) = \bar{\gamma}x_0^2/2 + \bar{\delta}x_0^3/6 + \text{h.o.t.}\ , x_0 = y_0 + \omega y_1$, and

$$\boldsymbol{P}^{-1} = \frac{1}{\omega\beta} \begin{bmatrix} 0 & \omega w \\ \beta & -w \end{bmatrix}.$$

System (5.63) is now in standard form,

$$\begin{bmatrix} y_0' \\ y_1' \end{bmatrix} = \boldsymbol{B} \begin{bmatrix} y_0 \\ y_1 \end{bmatrix} + \begin{bmatrix} M(y_0, y_1) \\ N(y_0, y_1) \end{bmatrix}, \qquad \boldsymbol{B} = \begin{bmatrix} 0 & \omega \\ -\omega & 0 \end{bmatrix}, \tag{5.64}$$

where M and N represent nonlinear functions of second order or higher given by

$$M(y_0, y_1) = \frac{w}{\beta} F(y_0 + \omega y_1),$$
$$N(y_0, y_1) = -\frac{w}{\omega\beta} F(y_0 + \omega y_1).$$

Computing the partial derivatives of M and N and plugging them into (5.48), we obtain the cubic coefficient associated with system (5.58) to be $a_{\text{ODE}} = 0$, which is exactly what we arrived at in Subsection 5.2.1. As in the DDE case, we cannot determine whether periodic solutions exist or whether they are attracting or repelling.

In fact, we notice that when $\alpha\tau = -1$, system (5.58) is a Hamiltonian system,

$$\begin{cases} x_0' = \dfrac{\partial \mathcal{H}}{\partial x_1}(x_0, x_1) \\ x_1' = -\dfrac{\partial \mathcal{H}}{\partial x_0}(x_0, x_1), \end{cases}$$

where the Hamiltonian function is given by

$$\mathcal{H}(x_0, x_1) = x_0 x_1 + \frac{w\tau}{2} x_1^2 + c\tau x_1 - \int f(x_0) dx_0. \tag{5.65}$$

The solutions of system (5.58) lie on the level curves $\mathcal{H}(x_0, x_1) = \text{constant}$. In Figure 5.2 we plot the level curves of $\mathcal{H}(x_0, x_1) = \text{constant}$ for $f(x_0) = \tanh(x_0), \alpha = -2, \tau = 0.5, w = -10$ and $c = 5.616$. We notice that the equilibrium point $(x_0^*, x_1^*) = (1, \tanh 1)$ of (5.58) is a centre and thus a Hopf bifurcation does not occur for this system.

5.4 The Equivalent Three Dimensional ODE System

In this section we verify the results we obtained in Subsection 5.2.2 by transforming the scalar DDE (5.1) where $\hat{g}(-\theta)$ represents a gamma distribution with $p = 2$ (called the strong kernel) into a three dimensional ODE system. We perform the centre manifold calculation for the ODE system and compare the sign of the cubic coefficient with the sign of the expression we obtained in Subsection 5.2.2.

Applying the linear chain trick presented in Section 2.5, equation (5.1) becomes

$$\begin{cases} x_0'(t) = -\alpha\tau x_0(t) + w\tau x_2(t) + c\tau \\ x_1'(t) = 2[f(x_0(t)) - x_1(t)] \\ x_2'(t) = 2[x_1(t) - x_2(t)]. \end{cases} \tag{5.66}$$

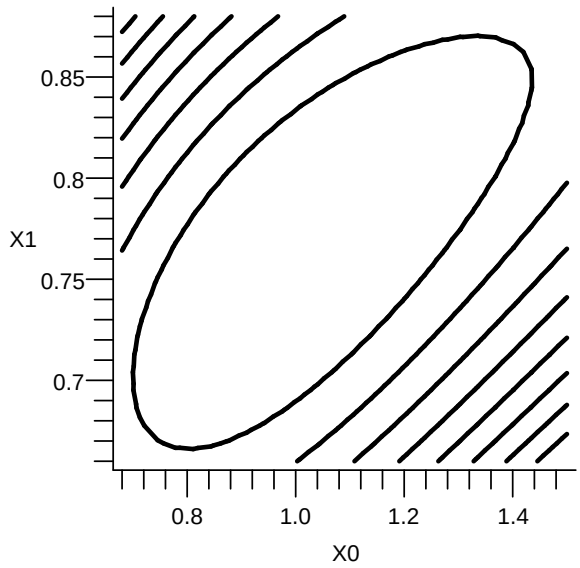

Figure 5.2: The solutions of the Hamiltonian system (5.58) (when $f(x_0) = \tanh(x_0), \alpha = -2, \tau = 0.5, w = -10, c = 5.616$) lie on the level curves $\mathcal{H}(x_0, x_1) =$ constant, with $\mathcal{H}(x_0, x_1)$ given in (5.65). The equilibrium point $(x_0^*, x_1^*) = (1, \tanh 1)$ of (5.58) is a centre and thus a Hopf bifurcation does not occur for this system.

We assume the above equation admits an equilibrium solution (x_0^*, x_1^*, x_2^*) satisfying

$$\begin{cases} 0 = -\alpha\tau x_0^* + w\tau x_2^* + c\tau \\ 0 = f(x_0^*) - x_1^* \\ 0 = x_1^* - x_2^*. \end{cases} \tag{5.67}$$

Using(5.60) and (5.67), we obtain

$$\begin{cases} x_0'(t) = -\alpha\tau x_0(t) + w\tau x_2(t) \\ x_1'(t) = 2[\bar{\beta} x_0(t) - x_1(t) + \dfrac{\bar{\gamma}}{2}(x_0(t))^2 + \dfrac{\bar{\delta}}{6}(x_0(t))^3 + \text{h.o.t. }] \\ x_2'(t) = 2[x_1(t) - x_2(t)]. \end{cases}$$

This can be written in vector form as $\boldsymbol{x}' = \boldsymbol{A}\boldsymbol{x} + \boldsymbol{F}(\boldsymbol{x})$, where $\boldsymbol{x} = [x_0, x_1, x_2]^T$, i.e.

$$\begin{bmatrix} x_0' \\ x_1' \\ x_2' \end{bmatrix} = \begin{bmatrix} -\alpha\tau & 0 & w\tau \\ 2\bar{\beta} & -2 & 0 \\ 0 & 2 & -2 \end{bmatrix} \begin{bmatrix} x_0 \\ x_1 \\ x_2 \end{bmatrix} + \begin{bmatrix} 0 \\ \bar{\gamma} x_0^2 + \bar{\delta} x_0^3/3 + \text{h.o.t.} \\ 0 \end{bmatrix}. \tag{5.68}$$

The characteristic equation corresponding to the linear system $\boldsymbol{x}' = \boldsymbol{A}\boldsymbol{x}$ is given by

$$0 = \det(\lambda \boldsymbol{I} - \boldsymbol{A}) = \lambda^3 + (\alpha\tau + 4)\lambda^2 + 4\alpha\tau - 4\beta\tau, \tag{5.69}$$

where $\beta = \bar{\beta}w$. A Hopf bifurcation occurs when the characteristic equation has a simple pair of pure imaginary roots, no other root with zero real part and $d\mathrm{Re}(\lambda)/d\beta|_{\lambda=i\omega} \neq 0$ ([25], Theorem 3.4.2). Substituting $\lambda = i\omega$ into (5.69) and separating into real and imaginary parts we obtain

$$\begin{aligned} 4\alpha\tau - 4\beta\tau &= 4\omega^2 + \omega^2\alpha\tau, \\ 4\alpha\tau + 4 &= \omega^2. \end{aligned} \tag{5.70}$$

From (5.69) we get

$$\frac{\partial \Delta}{\partial \beta} = -4\tau \qquad \text{and} \qquad \frac{\partial \Delta}{\partial \lambda} = 3\lambda^2 + 2(\alpha\tau + 4)\lambda.$$

Therefore

$$\left.\frac{d\mathrm{Re}(\lambda)}{d\beta}\right|_{\lambda=i\omega} = -\mathrm{Re}\left(\frac{\partial \Delta}{\partial \beta} \Big/ \left.\frac{\partial \Delta}{\partial \lambda}\right|_{\lambda=i\omega}\right) = -\frac{12\tau\omega^2}{9\omega^4 + (2\alpha\tau\omega + 8\omega)^2} \neq 0.$$

Thus by Theorem 3.4.2 from [25] we conclude that system (5.66) does undergo a Hopf bifurcation .

We next perform a change of variables so that the linear part of (5.68) is in standard block diagonal form. From (5.70) we get that $\alpha\tau = (\omega^2 - 4)/4$ and $\tau = -(\omega^2 + 4)^2/(16\beta)$ and thus matrix $\boldsymbol{A}$ becomes

$$\boldsymbol{A}|_{\lambda=\pm i\omega} = \begin{bmatrix} \dfrac{4-\omega^2}{4} & 0 & -\dfrac{w(\omega^2+4)^2}{16\beta} \\ 2\beta/w & -2 & 0 \\ 0 & 2 & -2 \end{bmatrix}.$$

with eigenvalues $\lambda_1 = i\omega$, $\lambda_2 = -i\omega$ and $\lambda_3 = -3 - \omega^2/4$. We note that since λ_3 is always negative, the stability of the equilibrium point is dictated by the flow on the centre manifold [25]. The corresponding eigenvectors are

$$\boldsymbol{u}_1 = \begin{bmatrix} 4-\omega^2 \\ 4\beta/w \\ 4\beta/w \end{bmatrix}, \boldsymbol{u}_2 = \begin{bmatrix} 4\omega \\ 2\beta\omega/w \\ 0 \end{bmatrix}, \boldsymbol{u}_3 = \begin{bmatrix} (\omega^2+4)^2 \\ -8\beta(\omega^2+4)/w \\ 64\beta/w \end{bmatrix}.$$

We let $\boldsymbol{P} = [\boldsymbol{u}_1 \mid \boldsymbol{u}_2 \mid \boldsymbol{u}_3]$ and with the change of variables $\boldsymbol{x} = P\boldsymbol{y}$, where $\boldsymbol{y} = [y_0, y_1, y_2]^T$, the system becomes

$$\begin{bmatrix} y_0' \\ y_1' \\ y_2' \end{bmatrix} = \begin{bmatrix} 0 & \omega & 0 \\ -\omega & 0 & 0 \\ 0 & 0 & -3-\omega^2/4 \end{bmatrix} \begin{bmatrix} y_0 \\ y_1 \\ y_2 \end{bmatrix} + \boldsymbol{P}^{-1} \begin{bmatrix} 0 \\ F(x_0) \\ 0 \end{bmatrix}, \tag{5.71}$$

where $F(x_0) = \bar{\gamma}x_0^2 + \bar{\delta}x_0^3/3 + \text{h.o.t.}$, $x_0 = (4-\omega^2)y_0 + 4\omega y_1 + (\omega^2+4)^2 y_2$, and

$$\boldsymbol{P}^{-1} = \begin{bmatrix} -\dfrac{16}{\omega^4+40\omega^2+144} & \dfrac{32w}{\beta(\omega^4+40\omega^2+144)} & \dfrac{w(\omega^2+20)}{4\beta(\omega^2+36)} \\ \dfrac{4(\omega^2+12)}{\omega(\omega^4+40\omega^2+144)} & \dfrac{w(\omega^4+24\omega^2-48)}{2\beta\omega(\omega^4+40\omega^2+144)} & \dfrac{w(\omega^2-12)}{2\beta\omega(\omega^2+36)} \\ \dfrac{1}{\omega^4+40\omega^2+144} & -\dfrac{2w}{\beta(\omega^4+40\omega^2+144)} & \dfrac{w}{4\beta(\omega^2+36)} \end{bmatrix}.$$

System (5.71) is now in standard form,

$$\begin{aligned} \begin{bmatrix} y_0' \\ y_1' \end{bmatrix} &= \boldsymbol{B}\begin{bmatrix} y_0 \\ y_1 \end{bmatrix} + \boldsymbol{G}(y_0, y_1, y_2) \\ y_2' &= Cy_2 + H(y_0, y_1, y_2), \end{aligned} \tag{5.72}$$

where

$$\boldsymbol{B} = \begin{bmatrix} 0 & \omega \\ -\omega & 0 \end{bmatrix} \qquad \text{and} \qquad C = -3 - \omega^2/4.$$

Since the centre manifold is tangent to the centre eigenspace, we can represent it as a local graph

$$W^c = \{(y_0, y_1, y_2) : y_2 = h(y_0, y_1), h(0) = Dh(0) = 0\},$$

where $h : U \to \mathbb{R}$ is defined on some neighborhood $U \subset \mathbb{R}^2$ of the origin [25]. We consider the projection of the vector field on $y_2 = h(y_0, y_1)$ onto the centre eigenspace,

$$\begin{bmatrix} y_0' \\ y_1' \end{bmatrix} = \boldsymbol{B}\begin{bmatrix} y_0 \\ y_1 \end{bmatrix} + \boldsymbol{G}(y_0, y_1, h(y_0, y_1)). \tag{5.73}$$

If the origin of the above reduced system is locally asymptotically stable then the origin of (5.72) is also locally asymptotically stable [25]. We approximate $h(y_0, y_1)$ as

$$h(y_0, y_1) = ay_0^2 + by_0y_1 + cy_1^2 \tag{5.74}$$

and we calculate its coefficients by substituting it into

$$Dh(y_0, y_1)[\boldsymbol{B}h(y_0, y_1) + \boldsymbol{G}(y_0, y_1, h(y_0, y_1))] - Ch(y_0, y_1) - H(y_0, y_1, h(y_0, y_1)) = 0.$$

Equating the coefficients of y_0^2, y_0y_1 and y_1^2 in the above expression we obtain a system of three equations which is solved in Maple$^{\text{TM}}$ for a, b and c,

$$\begin{aligned} a &= -\frac{8w\bar{\gamma}(\omega^8 + 16\omega^6 - 32\omega^4 + 1280\omega^2 + 2304)}{\beta(\omega^{10} + 140\omega^8 + 5344\omega^6 + 64128\omega^4 + 241920\omega^2 + 248832)}, \\ b &= \frac{128w\omega\bar{\gamma}(\omega^4 - 8\omega^2 - 16)}{\beta(\omega^8 + 128\omega^6 + 3808\omega^4 + 18432\omega^2 + 20736)}, \\ c &= -\frac{128w\omega^2\bar{\gamma}(5\omega^4 + 56\omega^2 + 80)}{\beta(\omega^{10} + 140\omega^8 + 5344\omega^6 + 64128\omega^4 + 241920\omega^2 + 248832)}. \end{aligned}$$

Plugging these into (5.74) we obtain the approximation for $h(y_0, y_1)$, which will be substituted into the reduced system (5.73). This system is of the form (5.64) with M and N given by

$$M(y_0, y_1) = \frac{32w}{\beta(\omega^4 + 40\omega^2 + 144)} F((4-\omega^2)y_0 + 4\omega y_1 + (\omega^2+4)^2 h(y_0, y_1)),$$
$$N(y_0, y_1) = \frac{w(\omega^4 + 24\omega^2 - 48)}{2\beta\omega(\omega^4 + 40\omega^2 + 144)} F((4-\omega^2)y_0 + 4\omega y_1 + (\omega^2+4)^2 h(y_0, y_1)).$$

Letting $\bar{\gamma} = 2\gamma/w$ and $\bar{\delta} = 6\delta/w$ and computing the partial derivatives of M and N in Maple$^{\text{TM}}$ and plugging them into (5.48), we obtain the cubic coefficient associated with system (5.66),

$$\begin{aligned} a_{\text{ODE}} = & \frac{(\omega^2+4)^3}{2\beta^2\omega^2(\omega^2+36)(\omega^2+12)(\omega^4+88\omega^2+144)} \\ & \times \left[(3\beta\delta - 2\gamma^2)\omega^8 + (300\beta\delta - 320\gamma^2)\omega^6 + (3600\beta\delta - 2752\gamma^2)\omega^4 \right. \\ & \left. + (5184\beta\delta - 7168\gamma^2)\omega^2 - 4608\gamma^2\right]. \end{aligned}$$

The sign of a_{ODE} is determined by the sign of expression in the square brackets, which is identical to the expression in the square brackets that we obtained in (5.56). Thus the sign of a_{ODE} is the same as the sign of a_{DDE} and therefore we obtained the same result about the criticality of the Hopf bifurcation as in Subsection 5.2.2.

We next perform numerical simulations using the XPPAUT package [17] to verify our results. Using the same nonlinear function f and parameter values as in the example at the end of Subsection 5.2.2, i.e. $f(x) = \tanh(0.176x), \alpha = 2, \tau = 0.6, w = -100$ and $c = 19.421$, we generate a bifurcation diagram for system (5.66) as seen in Figure 5.3, which shows that as β passes through the critical value $\beta_c = -17.07$, there is a Hopf bifurcation at the equilibrium point $(x_0^*, x_1^*, x_2^*) = (1, \tanh 0.176, \tanh 0.176)$ giving rise to stable periodic solutions in the region $\beta < \beta_c = -17.07$. This bifurcation diagram verifies the predictions of Conjecture 1, which indicated the same bifurcation diagram in Figure 5.1(b). For $\beta = -15 > \beta_c$, the numerical simulation in Figure 5.4(a) shows that $x_0(t)$ approaches $x_0^* = 1$ for large t, i.e. the equilibrium point $(x_0^*, x_1^*, x_2^*) = (1, \tanh 0.176, \tanh 0.176)$ of (5.66) is stable. For $\beta = -18 < \beta_c$, $x_0(t)$ approaches a stable periodic solution as seen in Figure 5.4(b), i.e. the equilibrium point $(x_0^*, x_1^*, x_2^*) = (1, \tanh 0.176, \tanh 0.176)$ of (5.66) is unstable.

In the following section we show how the approximations we developed in Chapter 3 can be applied to the centre manifold calculations in Section 5.2.

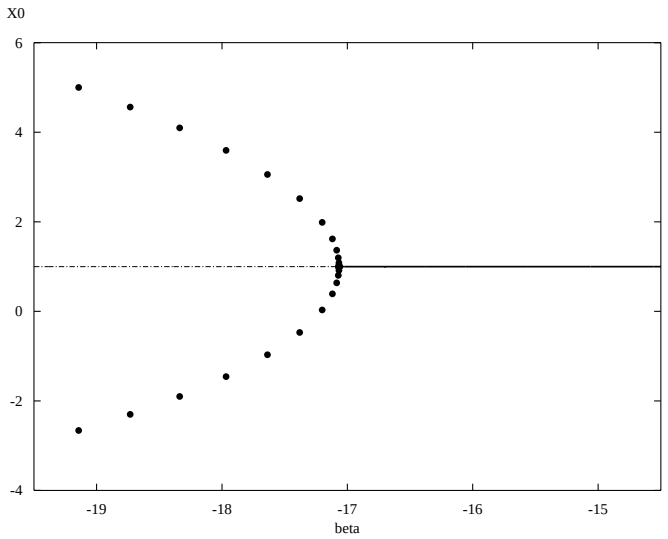

Figure 5.3: Bifurcation diagram for system (5.66) generated using the XPPAUT package (where stable periodic solutions are depicted by solid points). When $f(x) = \tanh(0.176x), \alpha = 2, \tau = 0.6, w = -100$ and $c = 19.421$, as β passes through the critical value $\beta_c = -17.07$, there is a Hopf bifurcation at the equilibrium point $(x_0^*, x_1^*, x_2^*) = (1, \tanh 0.176, \tanh 0.176)$ of (5.66) giving rise to stable periodic solutions in the region $\beta < \beta_c = -17.07$, which is exactly what Conjecture 1 predicted.

5.5 Approximations

In this section we apply the approximations in terms of the first few moments or cumulants of a distribution along with Conjecture 1 to predict whether model (5.1) can undergo a Hopf bifurcation at the equilibrium point and to determine the direction and criticality of the bifurcation. To do so, we must determine the sign of μ in (5.50) and a_{DDE} in (5.49) using the approximations for $C(\omega)$ and $S(\omega)$ that we developed in Chapter 3. The expressions for μ and a_{DDE} are evaluated at the critical value of the parameters. We fix α and for a particular value of the mean delay, τ_c, we solve system (5.33) for β_c and ω_c. Figure 5.5 shows the true and an approximate boundary of stability for a given distribution. The true stability region is between the solid black curve and the vertical solid gray line. The approximate stability boundary is depicted as the dotted curve. It can be seen that the point (β_c, τ_c) is on the true boundary of stability, while the point (β_c^*, τ_c) is on the approximate boundary of stability. The value for β_c is obtained by solving system (5.33), where we substitute the exact expressions for $C(\omega)$ and $S(\omega)$ from (5.34). The value for

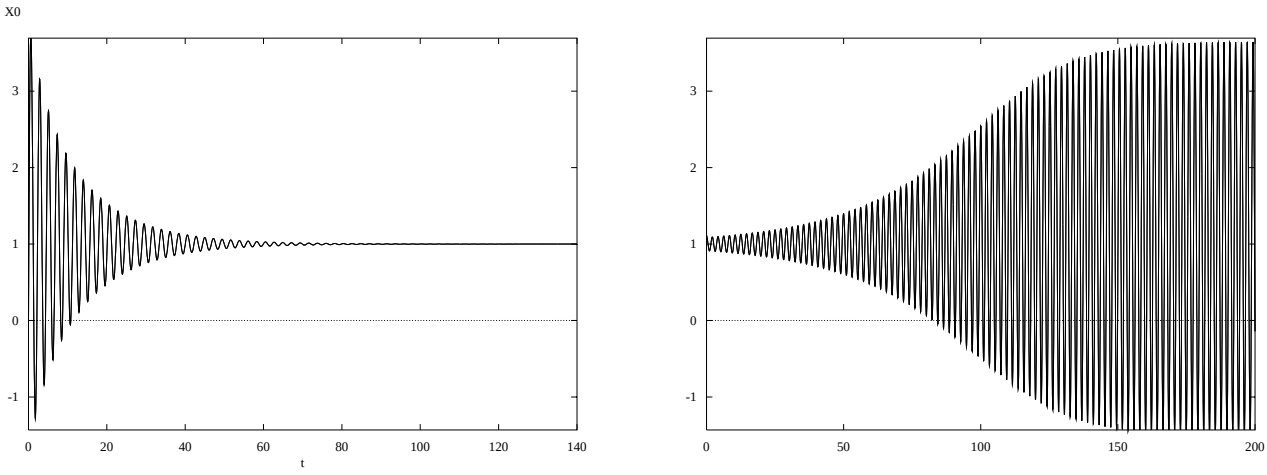

(a) $\beta = -15 > \beta_c$ (b) $\beta = -18 < \beta_c$

Figure 5.4: Numerical simulations for system (5.66) when $f(x) = \tanh(0.176x), \alpha = 2, \tau = 0.6, w = -100$ and $c = 19.421$. (a) For $\beta = -15 > \beta_c$, $x_0(t)$ approaches $x_0^* = 1$ for large t, i.e. the equilibrium point $(x_0^*, x_1^*, x_2^*) = (1, \tanh 0.176, \tanh 0.176)$ of (5.66) is stable. (b) For $\beta = -18 < \beta_c$, $x_0(t)$ approaches a stable periodic solution, i.e. the equilibrium point $(x_0^*, x_1^*, x_2^*) = (1, \tanh 0.176, \tanh 0.176)$ of (5.66) is unstable.

β_c^* is obtained by solving system (5.33), where we use the approximations for $C(\omega)$ and $S(\omega)$ from Tables 3.1 and 3.2.

When $\mu > 0$, if a_{DDE} is negative, Conjecture 1 predicts a supercritical Hopf bifurcation as seen in Figure 5.6(a), while if $a_{\text{DDE}} > 0$, the Hopf bifurcation is predicted as subcritical as seen in Figure 5.6(b).

We now draw a few conclusions about the approximations using moments for any distribution. From Table 3.1, the approximations $(0, 0)$ and $(0, 1)$ using moments give $C(\omega) = 1$. In this case the denominator of c_1 in (5.47) is zero and hence c_1 is undefined. Since the expression for a_{DDE} in (5.49) is in terms of c_1, this makes a_{DDE} undefined. Therefore we cannot use the approximations $(0, 0)$ and $(0, 1)$ using moments to predict the criticality of the bifurcation. From Table 3.1, for the approximations $(0, 0)$ and $(0, 1)$ using moments we have $S(\omega) = \omega$ and $S(\omega) = \omega - m_3\omega^3/6$, respectively. Therefore we can conclude that we must have knowledge of the second moment of a particular distribution in order to make predictions about the criticality of the Hopf bifurcation.

For the approximation $(0, 0)$ using moments, substituting $C(\omega) = 1$ and $S(\omega) = \omega$ into (5.50) we obtain $\mu = 0$. Thus for this approximation we cannot use Conjecture 1 to predict whether (5.1) can undergo a Hopf bifurcation at the equilibrium point.

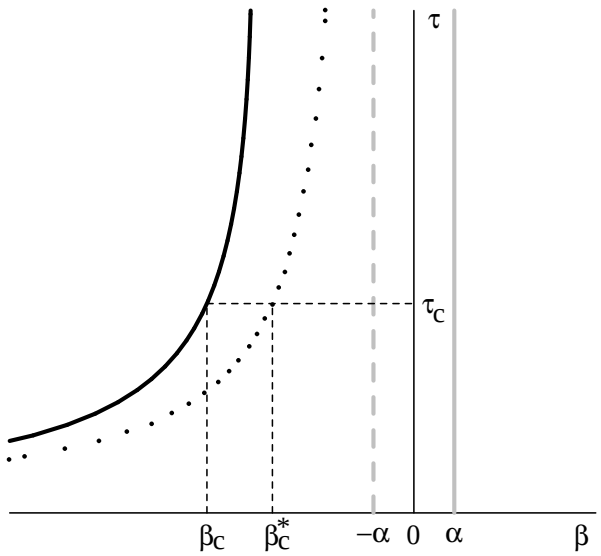

Figure 5.5: Stability diagram showing the true and approximate boundaries of stability for a given distribution. The true stability region is between the solid black curve and the vertical solid gray line. The approximate stability boundary is depicted as the dotted curve. The critical point (β_c, τ_c) belongs to the true boundary of stability, while the approximate critical point (β_c^*, τ_c) belongs on the approximate boundary of stability.

For the approximation $(0, 1)$ using moments, substituting $C(\omega) = 1$ and $S(\omega) = \omega - m_3\omega^3/6$ into (5.50) we obtain

$$\mu = -\frac{12\omega m_3}{\beta(\omega^2 m_3 - 6)^2} > 0,$$

since $m_3 > 0$ for any distribution. Therefore for this approximation Conjecture 1 predicts that a Hopf bifurcation occurs at the equilibrium point x^* of (5.1) and that x^* is locally asymptotically stable for $\beta > \beta_c^*$.

From Table 3.1, for the approximation $(1, 0)$ using moments, we have $C(\omega) = 1 - m_2\omega^2/2$ and $S(\omega) = \omega$. Then (5.50) becomes

$$\mu = \frac{\omega m_2}{\alpha} > 0,$$

since $m_2 > 0$ for any distribution. Therefore for this approximation Conjecture 1 predicts that a Hopf bifurcation occurs at the equilibrium point x^* of (5.1) and that x^* is locally asymptotically stable for $\beta > \beta_c^*$.

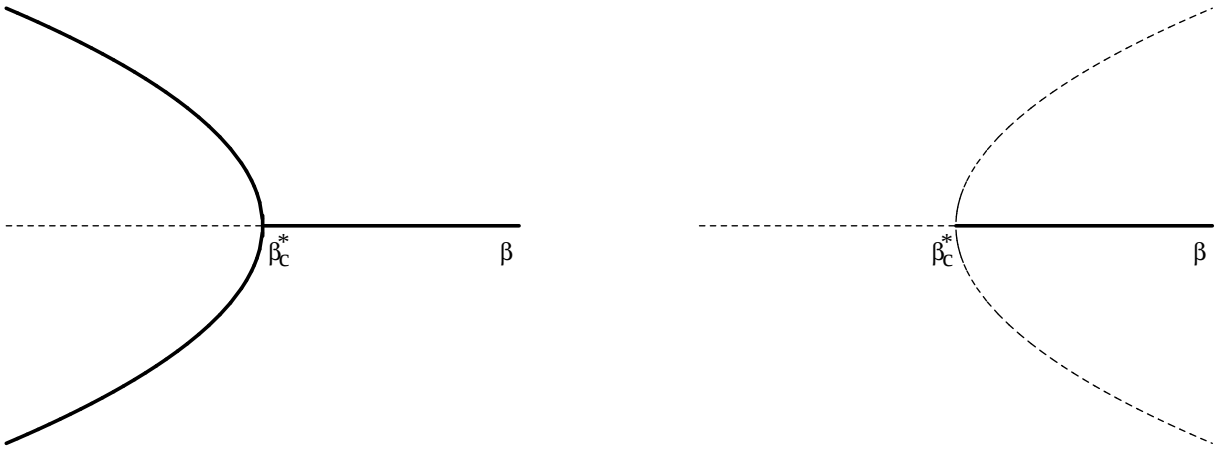

(a) Supercritical bifurcation at β_c^* (b) Subcritical bifurcation at β_c^*

Figure 5.6: Approximate bifurcation diagrams as predicted by Conjecture 1: (a) a supercritical Hopf bifurcation occurs if $\mu > 0$ and $a_{\text{DDE}} < 0$. (b) a subcritical Hopf bifurcation occurs if $\mu > 0$ and $a_{\text{DDE}} > 0$.

For the approximation $(1, 1)$ using moments, we have $C(\omega) = 1 - m_2\omega^2/2$ and $S(\omega) = \omega - m_3\omega^3/6$. Then (5.50) becomes

$$\mu = \frac{12\omega(3m_2 - m_3)}{\alpha(\omega^2 m_3 - 6)^2}.$$

Thus $\mu > 0$ ($\mu < 0$) if $3m_2 > m_3$ ($3m_2 < m_3$) and by Conjecture 1 we predict that a Hopf bifurcation occurs at the equilibrium point x^* of (5.1) and that x^* is locally asymptotically stable (unstable) for $\beta > \beta_c^*$.

We cannot make any general statements about the criticality of the Hopf bifurcations for the approximations $(1, 0)$ and $(1, 1)$ using moments or for any of the approximations using cumulants. Neither can we make any predictions about whether for the approximations using cumulants a Hopf bifurcation occurs at the equilibrium point. For these cases we use Conjecture 1 for the particular values of the moments or cumulants, as we do in the next two subsections where we apply the approximations in the specific cases of the uniform distribution with $\rho = 2$ and of the gamma distribution with $p = 3$. We continue to use the same f and parameter values as in the previous examples in this chapter, $f = \tanh(Ax), x^* = 1, w = -100$, where A solves the equation $\beta/w = A\,\text{sech}^2(A)$ and $c = \alpha - w\tanh(A)$. We note that in each case the values of A, c, γ and δ depend on $\beta = \beta_c$.

Table 5.1: The critical values for β and ω in the case of the uniform distribution with $\rho = 2$ and of the corresponding approximations using moments and cumulants. Approximation $(0, 1)$ using cumulants is identical to approximation $(0, 0)$, and approximation $(1, 1)$ using cumulants is identical to approximation $(1, 0)$. "M" stands for approximation using moments and "C" stands for approximation using cumulants.

	$\tau = 0.45$		$\tau = 0.6$		$\tau = 0.8$	
Exact	$\beta_c = -11.19$	$\omega_c = 1.96$	$\beta_c = -9.69$	$\omega_c = 2.09$	$\beta_c = -9.25$	$\omega_c = 2.20$
M $(1, 0)$	$\beta_c^* = -2.50$	$\omega_c^* = 1.64$	-	-	-	-
M $(1, 1)$	$\beta_c^* = -7.00$	$\omega_c^* = 1.39$	$\beta_c^* = -5.33$	$\omega_c^* = 1.43$	$\beta_c^* = -4.50$	$\omega_c^* = 1.47$
C $(0, 0)$	$\beta_c^* = -5.29$	$\omega_c^* = 1.96$	$\beta_c^* = -4.02$	$\omega_c^* = 2.09$	$\beta_c^* = -3.40$	$\omega_c^* = 2.20$
C $(1, 0)$	$\beta_c^* = -10.02$	$\omega_c^* = 1.96$	$\beta_c^* = -8.33$	$\omega_c^* = 2.09$	$\beta_c^* = -7.62$	$\omega_c^* = 2.20$

5.5.1 Applying the Approximations in the Case of the Uniform Distribution with $\rho = 2$

In this subsection we apply the approximations for $C(\omega)$ and $S(\omega)$ in the case of the uniform distribution with $\rho = 2$ to predict whether (5.1) can undergo a Hopf bifurcation and if so to determine the direction and criticality of the bifurcation.

Following the procedure presented in Section 3.3, we generate a stability diagram for the uniform distribution with $\rho = 2$ when $\alpha = 2$ as seen in Figure 5.7. The true boundary of stability is depicted as the solid black curve. Approximations $(1, 0)$ and $(1, 1)$ using moments correspond to the dotted and dashed black curves, respectively. Approximations $(0, 0)$ and $(1, 0)$ using cumulants correspond to the curves depicted by the black crosses and black circles, respectively. Approximation $(0, 1)$ using cumulants is identical to approximation $(0, 0)$, and approximation $(1, 1)$ using cumulants is identical to approximation $(1, 0)$, since by (2.34), the third cumulant is always zero for the uniform distribution.

In Table 5.1 we present the values for β_c, ω_c, β_c^* and ω_c^*, which we obtain numerically in Maple$^{\text{TM}}$, for the three different critical values of the mean delay, $\tau_c = 0.4, 0.6$ and 0.8 in the case of the exact distribution, of the approximations $(1, 0)$ and $(1, 1)$ using moments and of the approximations $(0, 0)$ and $(1, 0)$ using cumulants. The value for β_c is obtained by solving system (5.33), where we substitute the exact expressions for $C(\omega)$ and $S(\omega)$ from (3.38). The value for β_c^* is obtained by solving system (5.33), where we use the approximations for $C(\omega)$ and $S(\omega)$ from Tables 3.1 and 3.2, and the values for the moments and cumulants from Table 2.1. We can see that the points (β_c, τ_c) in Table 5.1 belong to the true boundary of stability, while the points (β_c^*, τ_c^*) belong to the approximate stability curves, as seen in Figure 5.7. For the approximation $(1, 0)$ using moments, when $\tau_c = 0.6$ and 0.8, we have $\beta_c > -2 = -\alpha$, i.e. the approximate curve enters the distribution independent region of

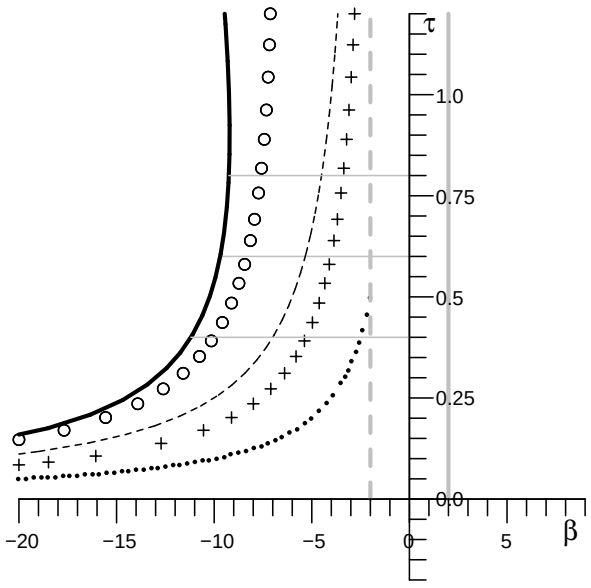

Figure 5.7: Stability diagram showing the true and approximate boundaries of stability for the uniform distribution with $\rho = 2$ when $\alpha = 2$. The true region of stability is between the solid black curve and the vertical solid gray line. Approximations $(1, 0)$ and $(1, 1)$ using moments correspond to the dotted and dashed black curve, respectively. Approximations $(0, 0)$ and $(1, 0)$ using cumulants correspond to the curves depicted by the black crosses and black circles, respectively. Approximation $(0, 1)$ using cumulants is identical to approximation $(0, 0)$, and approximation $(1, 1)$ using cumulants is identical to approximation $(1, 0)$. The horizontal gray lines indicate the three critical values of τ: $0.4, 0.6$ and 0.8.

stability predicted by Theorem 7 and thus we do not use this approximation in these two cases.

Evaluating the expressions for μ and a_{DDE} in (5.50) and (5.49), respectively, at the critical value of the parameters from Table 5.1 we obtain, in all cases,

$$\begin{aligned} \mu|_{\beta=\beta_c} &> 0, \quad a_{\text{DDE}}|_{\beta=\beta_c} < 0, \\ \mu|_{\beta=\beta_c^*} &> 0, \quad a_{\text{DDE}}|_{\beta=\beta_c^*} < 0. \end{aligned}$$

Thus, for DDE (5.1) when the kernel is a uniform distribution with $\rho = 2$, Conjecture 1 predicts a supercritical Hopf bifurcation as seen in Figure 5.1(b). Approximations $(1, 0)$ using moments when $\tau_c = 0.4$, approximation $(1, 1)$ using moments and all of the approximations using cumulants for all three critical values of τ also predict that there is a supercritical Hopf bifurcation at the equilibrium point x^* of (5.1) as seen in Figure 5.6(a),

only that this Hopf bifurcation occurs as β passes through the critical value β_c^*, instead of β_c.

In the next subsection, we apply the approximations in the case of the gamma distribution with $p = 3$.

5.5.2 Applying the Approximations in the Case of the Gamma Distribution with $p = 3$

In this subsection we apply the approximations for $C(\omega)$ and $S(\omega)$ in the case of the gamma distribution with $p = 3$ to predict whether (5.1) can undergo a Hopf bifurcation and if so to determine the direction and criticality of the bifurcation.

Following the procedure presented in Section 3.4, we generate a stability diagram for the gamma distribution with $p = 3$ when $\alpha = 2$ as seen in Figure 5.8. The true boundary of stability is depicted as the solid black curve. Approximations $(1, 0)$ and $(1, 1)$ using moments correspond to the dotted and dashed black curves, respectively. Approximations $(0, 0)$, $(0, 1)$, $(1, 0)$ and $(1, 1)$ using cumulants correspond to the curves depicted by the black crosses, gray crosses, black circles and gray circles, respectively.

In Table 5.2 we present the values for β_c, ω_c, β_c^* and ω_c^*, which we obtain numerically in Maple$^{\text{TM}}$, for the three different critical values of the mean delay, $\tau_c = 0.4, 0.6$ and 0.8 in the case of the exact distribution, of the approximations $(1, 0)$ and $(1, 1)$ using moments and of the approximations $(0, 0)$, $(0, 1)$, $(1, 0)$ and $(1, 1)$ using cumulants. The value for β_c is obtained by solving system (5.33), where we substitute the exact expressions for $C(\omega)$ and $S(\omega)$ from (3.45). The value for β_c^* is obtained by solving system (5.33), where we use the approximations for $C(\omega)$ and $S(\omega)$ from Tables 3.1 and 3.2, and the values for the moments and cumulants from Table 2.2. We can see that the points (β_c, τ_c) in Table 5.2 belong to the true boundary of stability, while the points (β_c^*, τ_c^*) belong to the approximate stability curves, as seen in Figure 5.8. For the approximation $(1, 0)$ using moments, when $\tau_c = 0.6$ and 0.8, we have $\beta_c > -2 = -\alpha$, i.e. the approximate curve enters the distribution independent region of stability predicted by Theorem 7 and thus we do not use this approximation in these cases. Approximations $(0, 1)$ and $(1, 1)$ using cumulants are not defined for $\tau = 0.8$ and thus no critical value for β can be found in these two cases. This can be seen in Figure 5.8, where approximations $(0, 1)$ and $(1, 1)$ using cumulants are below the horizontal line $\tau = 0.8$.

Evaluating the expressions for μ and a_{DDE} in (5.50) and (5.49), respectively, at the critical value of the parameters from Table 5.2 we obtain, in all cases,

$$\begin{aligned} \mu|_{\beta=\beta_c} &> 0, \quad a_{\text{DDE}}|_{\beta=\beta_c} < 0, \\ \mu|_{\beta=\beta_c^*} &> 0, \quad a_{\text{DDE}}|_{\beta=\beta_c^*} < 0. \end{aligned}$$

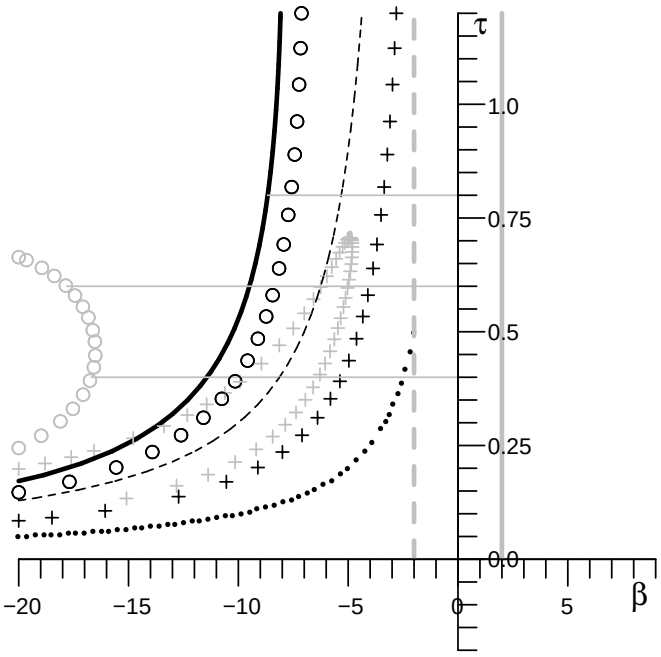

Figure 5.8: Stability diagram showing the true and approximate boundaries of stability for the gamma distribution with $p = 3$. The true region of stability is between the solid black curve and the vertical solid gray line. Approximations $(1, 0)$ and $(1, 1)$ using moments correspond to the dotted and dashed black curve, respectively. Approximations $(0, 0)$, $(0, 1)$, $(1, 0)$ and $(1, 1)$ using cumulants correspond to the curves depicted by the black crosses, gray crosses, black circles and gray circles, respectively. The horizontal gray lines indicate the three critical values of τ: $0.4, 0.6$ and 0.8.

Hence, applying Conjecture 1, we get that the equilibrium point x^* of (5.1) when the kernel is a gamma distribution with $p = 3$ undergoes a supercritical Hopf bifurcation as seen in Figure 5.1(b). Approximations $(1, 0)$ using moments when $\tau_c = 0.4$, approximation $(1, 1)$ using moments and all of the approximations using cumulants (if defined) for all three critical values of τ also predict that there is a supercritical Hopf bifurcation at the equilibrium point x^* of (5.1) as seen in Figure 5.6(a), only that this Hopf bifurcation occurs as β passes through the critical value β_c^*, instead of β_c.

In conclusion, when defined, all of the approximations in the case of the uniform distribution with $\rho = 2$ and of the gamma distribution with $p = 3$ predict the correct criticality and direction of the Hopf bifurcation, except that the bifurcation occurs at a shifted critical value of β.

Table 5.2: The critical values for β and ω in the case of the gamma distribution with $p = 3$ and of the corresponding approximations using moments and cumulants. "M" stands for approximation using moments and "C" stands for approximation using cumulants.

	$\tau = 0.4$		$\tau = 0.6$		$\tau = 0.8$	
Exact	$\beta_c = -11.43$	$\omega_c = 2.23$	$\beta_c = -9.49$	$\omega_c = 2.41$	$\beta_c = -8.66$	$\omega_c = 2.57$
M $(1,0)$	$\beta_c^* = -2.50$	$\omega_c^* = 1.64$	-	-	-	-
M $(1,1)$	$\beta_c^* = -8.13$	$\omega_c^* = 1.37$	$\beta_c^* = -6.25$	$\omega_c^* = 1.41$	$\beta_c^* = -5.31$	$\omega_c^* = 1.44$
C $(0,0)$	$\beta_c^* = -5.29$	$\omega_c^* = 1.96$	$\beta_c^* = -4.02$	$\omega_c^* = 2.09$	$\beta_c^* = -3.40$	$\omega_c^* = 2.20$
C $(0,1)$	$\beta_c^* = -6.35$	$\omega_c^* = 2.41$	$\beta_c^* = -5.01$	$\omega_c^* = 2.76$	-	-
C $(1,0)$	$\beta_c^* = -10.02$	$\omega_c^* = 1.96$	$\beta_c^* = -8.33$	$\omega_c^* = 2.09$	$\beta_c^* = -7.62$	$\omega_c^* = 2.20$
C $(1,1)$	$\beta_c^* = -16.70$	$\omega_c^* = 2.41$	$\beta_c^* = -17.82$	$\omega_c^* = 2.75$	-	-

In the next and final chapter we present the conclusions of this thesis and possible directions for future work.

Chapter 6

Discussion and Conclusions

In this thesis we have studied the linear stability and Hopf bifurcation of Hopfield neural networks with a general distribution of delays, where the neurons are identical. In the first chapter, we presented biological neuronal networks as the underlying motivating factor of artificial neural networks and gave the physical interpretation behind the development of the Hopfield model. We discussed how time delays arise in biological and physical models and reviewed the literature on such models. We indicated why it is important to keep the delay distributions in a model as general as possible. In the second chapter, we gave an overview of DDEs with emphasis on DDEs with infinite distributed delay.

In the third chapter, we investigated the linear stability of a generic scalar DDE with one distributed delay, whose linearization represents the linearization of the scalar Hopfield model. We showed how to obtain the distribution independent region of stability of an equilibrium point when the kernel is arbitrary. This region is similar to the delay independent region of stability for equations with discrete delays. For the equation we studied, the distribution independent region of stability is the same as the delay independent region if the distributed delay is replaced by a discrete delay equal to the mean of the distribution. We showed how to reformulate the distribution so that the mean delay occurs as a natural parameter in the distribution. This allowed us to determine a region of stability which depends on the mean delay, but is independent of other properties of the distribution. Both the distribution independent region of stability and the mean delay dependent region (described by Theorem 7) are conservative estimates of the true region of stability of the equilibrium point. We then formulated an approach to approximate the boundary of the true region of stability using the first few moments or cumulants of the distribution. We showed that approximation $(1, 0)$ using moments is always conservative, i.e. it underestimates the region of stability, since this approximation recovers the results of Theorem 7. We also showed approximation $(0, 0)$ using cumulants always recovers the results of the corresponding model with one fixed delay, and for distributions symmetric

around their mean this approximation represents a conservative boundary of stability by Theorem 4.0.5 from [7]. By comparing our approximations to the true stability region boundary in the specific cases of the uniform and gamma distributions, we found, in general, that the approximations improved as more moments or cumulants are included. The approximations using cumulants gave better results than those using moments. No approximation using cumulants entered the distribution independent region of stability or the mean delay dependent region and in almost all cases, the approximate stability regions were always conservative.

We now compare our conservative stability result from Theorem 7 and the approximate stability regions we obtained in Section 3.2 with another conservative stability result from the literature. As noted in the introductory chapter of this thesis, Bernard et al. [7] obtain sufficient conditions on the mean delay such that the equilibrium point of (3.1) is locally asymptotically stable. For our parameters, when $\tau_{\min} = 0$, condition (1.23) from [7] translates into

$$\tau < \frac{\pi(1-\alpha/\beta)}{c\sqrt{\beta^2-\alpha^2}}, \qquad \beta < -|\alpha|, \tag{6.1}$$

where $c \approx 2.2764$. For the symmetric distribution case, their stronger stability result (1.24) translates into

$$\tau < \frac{\arccos(\alpha/\beta)}{\sqrt{\beta^2-\alpha^2}}, \qquad \beta < -|\alpha|. \tag{6.2}$$

When $\alpha > 0$ their sufficient condition in (6.1) gives a larger conservative stability region than the stability region described by Theorem 7 since we can show that

$$-\frac{1}{\beta} < \frac{\pi(1-\alpha/\beta)}{c\sqrt{\beta^2-\alpha^2}} \qquad \text{for all } \beta < -\alpha.$$

When $\alpha < 0$, the above inequality is satisfied only for small enough β and hence their conservative stability region gives a worse estimate than our result in Theorem 7 for β close enough to $-|\alpha|$. We note that the stronger condition in (6.2) represents the true boundary of stability of the equilibrium point of the corresponding discrete delay model. Hence, for distributions symmetric around their mean, the curve described by (6.2) represents approximation $(0, 0)$ using cumulants.

Conditions (6.1) and (6.2) differ only when α is small or negative [7]. Thus for α positive and large enough, condition (6.1) is equivalent to condition (6.2), which represents approximation $(0, 0)$ using cumulants. For the uniform and gamma distributions, we found, in general, that the approximations improved as more cumulants were added and thus the higher approximations using cumulants should give a better estimate of the true boundary of stability than the sufficient condition in (6.1). For example, in Figure 3.6(a) for the gamma distribution with $p = 4$ and $\alpha = 2$, condition (6.1) corresponds to the curve depicted

by black crosses, since it is equivalent to approximation $(0,0)$ using cumulants. We can see that condition (6.1) gives a better result than approximation $(1,0)$ using moments (which also represents the result in Theorem 7), but gives a worse estimate of the true boundary of stability than approximation $(1,1)$ using moments and all the other three approximations using cumulants.

For small positive α, for example $\alpha = 0.01$, we compare condition (6.1) represented by the gray solid curve to our approximations in Figure 6.1(a). We see that the result in (6.1) gives a worse estimate for the region of stability than all the approximations, except approximation $(1,0)$ using moments.

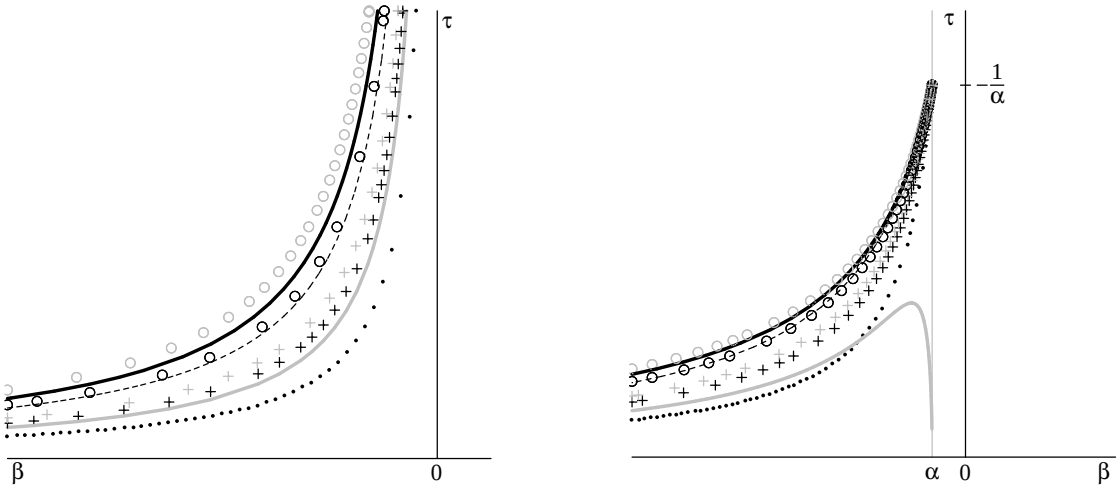

(a) $\alpha = 0.01$ (b) $\alpha = -2$

Figure 6.1: Stability region for the gamma distribution with $p = 4$ for (a) $\alpha = 0.01$; (b) $\alpha = -2$. The true region of stability lies between the solid black curve and the vertical line $\beta = \alpha$. Approximation $(1,0)$ using moments corresponds to the dotted curve, and approximation $(1,1)$ using moments corresponds to the dashed black curve. Approximations $(0,0)$, $(0,1)$, $(1,0)$ and $(1,1)$ using cumulants correspond to the curves depicted by the black crosses, gray crosses, black circles and gray circles, respectively. Condition (6.1) is represented by the gray solid curve .

For negative α, for example $\alpha = -2$, condition (6.1) is represented by the gray solid

curve in Figure 6.1(b). We can see that for β large enough, the result in (6.1) gives a worse estimate of the boundary of stability than all the approximations, whereas for β small enough, it gives a better result than approximation $(1, 0)$ using moments. We note that for general distributions, our approximations cannot guarantee conservative regions of stability, whereas the condition in (6.1) is a conservative stability result for any arbitrary kernel and the condition in (6.2) is a conservative stability result for any symmetric kernel.

In the fourth chapter, we extended the results for the scalar DDE to the Hopfield neural network consisting of n identical neurons by examining the linear stability of a symmetric equilibrium point both when the connection matrix is symmetric and when it is not. We again obtained several distribution independent results. For the case of a symmetric connection matrix, we obtained a conservative region of stability which is independent of the properties of the distribution save the mean delay. For the case of a general connection matrix, we determined the region of stability as the mean delay τ approaches zero for any distribution. We also showed that as in the limit τ approaches infinity, the region of stability of the distributed delay model is always greater or equal to the region of stability of the corresponding discrete delay model. Hence we were able to partially prove the conjecture that a system with a distribution of delays is more stable than the corresponding one with a discrete delay. We also obtained a conservative region of stability for any value of the mean delay and for any distribution, which coincides with the delay independent region of stability for the discrete delay model.

Our distribution independent results for the n dimensional Hopfield model compare favorably with others found in the literature. To see this, we compare our distribution independent stability result described by Theorem 12 with an equivalent result obtained in [22] using Liapunov functionals. In their paper, without assuming that the connection matrix is symmetric or that neurons are identical, Gopalsamy and He find sufficient conditions that guarantee the existence and stability of a global attractor for systems of the form (1.16). For our model, the sufficient condition (1.19) translates into

$$||\boldsymbol{W}||_\infty = \max_{1\le k\le n} \sum_{j=1}^{n} |w_{kj}| < \frac{\alpha}{\beta}, \tag{6.3}$$

where $||\boldsymbol{W}||_\infty$ represents the maximum row sum matrix norm of $\boldsymbol{W}$. Whereas, our conservative mean delay and distribution independent stability region given by Theorem 12 is

$$\rho(\boldsymbol{W}) = \max_{1\le k\le n} |z_k| < \frac{\alpha}{\beta}, \tag{6.4}$$

where $\rho(\boldsymbol{W})$ is called the spectral radius of $\boldsymbol{W}$. But by Theorem 5.6.9 from [34] we have that $||\boldsymbol{W}||_\infty \le \rho(\boldsymbol{W})$ for any matrix $\boldsymbol{W}$. Therefore the stability result using Liapunov functionals from [22] always gives a stronger, but more conservative result than our result in Theorem 12. We illustrate this through our example presented in Section 4.2. In this case,

$||\boldsymbol{W}||_\infty \approx 2$ and $\rho(\boldsymbol{W}) \approx 1$. Using (6.3) we cannot conclude anything about the stability of the equilibrium point for values of β greater than 0.5. Whereas our most conservative result in (6.4) guarantees stability for $\beta < 1$.

Our distribution independent results are all conservative estimates of the true stability region, thus we gave a general formulation for the boundary of this region. See equation (4.12) for the symmetric connection matrix case and Theorem 13 for the general connection matrix case. Using examples, we showed that the variation of the boundary of the stability region as the mean delay varies can be quite different for different distributions. There exists a particular value of the mean delay $\tau = \tau_c$, such that if all eigenvalues of the connection matrix are inside the boundary of stability with $\tau = \tau_c$, then the equilibrium point is stable, but unlike the discrete delay model, the value of τ_c is not necessarily infinity for other distributions.

We next showed how the boundary of the region of stability can be approximated using the first few moments or cumulants of the distribution. The approximations gave good results when compared to the true region of stability of the equilibrium point of the uniform and gamma distributed models. We again found that the approximations using cumulants always gave better results than the approximations using moments, and that in most cases the approximations improved as more cumulants or moments were added. In conclusion, the distribution independent and approximation approaches may be valuable for studying models of real applications. In such situations, the exact distribution is generally unknown, but it may be reasonable to obtain the mean, variance and possibly other moments of the distribution.

Finally, in the fifth chapter, we performed the Hopf bifurcation analysis of the scalar Hopfield model using the centre manifold technique. The theoretical basis for analyzing Hopf bifurcations and calculating the centre manifold has been rigourously developed for DDEs with finite delay. Assuming the theory still holds for DDEs with infinite delay within the appropriate restricted function space, we performed the centre manifold reduction for the scalar Hopfield model with a general distribution of delays. We showed under what conditions a Hopf bifurcation occurs and computed the cubic coefficient, which determines the criticality of the Hopf bifurcation. We verified our results by transforming the scalar Hopfield model with weak and strong kernels into the corresponding ODE systems. In both ODE cases, we arrived at the same results as for the DDE case. This seems to imply that the centre manifold technique does indeed work for DDEs with infinite delay and represents a motivation for such a theory to be developed. Further, we showed how to apply the approximations in order to predict the direction and criticality of the Hopf bifurcation. For the case of the uniform distribution with $\rho = 2$ and the gamma distribution with $p = 3$, all the approximations predicted the correct direction and criticality of the bifurcation, except that the Hopf bifurcation occurred at a shifted critical value of the bifurcation parameter.

Possible directions for future work include:

- extending all our results to Hopfield models with delay distributions with a gap (where the minimum delay is not zero),
- applying our linear stability analysis and centre manifold computation to different models other than Hopfield neural networks,
- extending the centre manifold calculation to higher dimensions,
- showing that the stability region for the distributed delay model is always greater than the corresponding model with discrete delay for any general kernel,
- finding a relationship among the approximations as more moments or cumulants are added,
- predicting whether a certain approximate stability region is conservative or not.

Appendix A

Maple^{TM} Implementation of the Centre Manifold Computation for the scalar DDE with Distributed Delay

This appendix presents the implementation of the centre manifold computations presented in Section 5.2 in the symbolic algebra package Maple^{TM}10. The commands will be preceded by a >. Since no output is printed, each command will be followed by a colon. The comments are introduced by a number sign. This code adapts the Maple^{TM} implementation of the centre manifold calculation for DDEs with discrete delays presented in [9] to DDEs with distributed delay.

```
> restart: with(linalg):
> # Define the linear system, where x is x(t) and
  # xt is \int_0^{-infinity}x(t+theta)\hat g(-theta) d theta
  lin:=-alpha*tau*x+beta*tau*xt;
> # The characteristic equation
  char_eq:=lambda+alpha*tau-beta*tau*int(exp(lambda*theta)*g(-theta),
           theta=-infinity..0):
> # Define simplifying relations at bifurcation point
  char_eq_iomega:=I*omega+alpha*tau-beta*tau*(C(omega)+I*(-S(omega))):
  eq_Re:=coeff(char_eq_iomega,I,0):
  eq_Im:=coeff(char_eq_iomega,I,1):
  simpres:=[tau=omega/beta/(-S(omega)), alpha=beta*C(omega)]:
> # Basis Phi for centre eigenspace (CE)
  Phi:=array(1..2,[cos(omega*theta), sin(omega*theta)]):
> # A basis, Psi_gen, for the CE of the dual problem
```

```
> Psi_g:=array([[cos(omega*xi)],[-sin(omega*xi)]]):

> # Find basis, PPsi, for CE of dual problem which satisfies
  # <PPsi,Phi>=I; bilinear_form is the bilinear form < , >
  # PPsi is the basis for the CE of the dual problem;
  # C_p(omega)=C'(omega) and S_p(omega)=S'(omega)
  bilin_psig1_phi1:=1/2-omega/S(omega)/2*S_p(omega):
  bilin_psig1_phi2:=-omega/S(omega)/2*C_p(omega):
  bilin_psig2_phi1:=-omega/S(omega)/2*C_p(omega):
  bilin_psig2_phi2:=-1/2+omega/S(omega)/2*S_p(omega):
  bilinear_form:=array(1..2,1..2,[[bilin_psig1_phi1,bilin_psig1_phi2],
                 [bilin_psig2_phi1,bilin_psig2_phi2]]):
  K:=inverse(bilinear_form):
  PPsi:=map(simplify,multiply(K,Psi_g)):
> # The matrix Psi(0) will be a place holder for now
  # Save values of Psi(0) for later use
  Psi0:=matrix(2,1):
  Psi0_res:=map(simplify,map(eval,subs(xi=0,evalm(PPsi)))):
  Psi0_vals:=[Psi0[1,1]=Psi0_res[1,1],Psi0[2,1]=Psi0_res[2,1]]:
> # B is the matrix of the eigenvalues
  B:=matrix([[0,omega],[-omega,0]]):
> # u1 and u2 are the coordinates on the centre manifold (CM)
  u:=matrix([[u1],[u2]]):
> # h is the Taylor expansion of the nonlinear terms of the CM
  h:=h_11(theta)*u1^2+h_12(theta)*u1*u2+h_22(theta)*u2^2:
> # Setup the differential equations to solve for the h_ij
  delhs:=matrix(1,1,[map(diff,h,theta)]):
  dhdu:=matrix([[diff(h,u1),diff(h,u2)]]):
  F2_inside_int:=combine(expand(gamma0*tau*(u1*cos(omega*theta)
                +u2*sin(omega*theta))^2)):
  F2_x_ce:=matrix([[subs(cos(2*omega*theta)=C_2om(omega),sin(2*omega*theta)
          =-S_2om(omega),F2_inside_int)]]):
  derhs:=map(collect,map(expand,evalm(multiply(dhdu,multiply(B,u))+
         multiply(Phi,multiply(Psi0,F2_x_ce)))),[u1,u2],distributed,factor):
  hdes:=evalm(delhs-derhs):
  de1:=coeff(coeff(hdes[1,1],u1^2),u2,0):
  de2:=coeff(coeff(hdes[1,1],u1),u2):
  de3:=coeff(coeff(hdes[1,1],u2^2),u1,0):
  des:={de1,de2,de3}:
  fns:={coeff(h,u1^2),coeff(coeff(h,u1),u2),coeff(h,u2^2)}:
```

```
  temp:=dsolve(des,fns):
  changeC:=[_C1=C1,_C2=C2,_C3=C3]:
  hsoln:=simplify(expand(evalc(subs(changeC,value(temp))))):
> # Evaluate h_ij at theta=0
  hsoln0:=simplify(eval(subs(theta=0,hsoln))):
> # Evaluate \int_0^{-infinity} h(theta,u) \hat g(-theta) d theta
  hsoln1:=combine(hsoln):
  g_hsoln:=simplify(subs(cos(omega*theta)=C(omega),sin(omega*theta)
          =-S(omega), cos(2*omega*theta)=C_2om(omega),
          sin(2*omega*theta)=-S_2om(omega),hsoln1)):
  int_gh:=u1^2*h_11(theta)+u1*u2*h_12(theta)+u2^2*h_22(theta):
> # Evaluate x on the CE and CM
  x_cm_ce:=[x=subs(theta=0,hsoln0,h), xt=subs(g_hsoln,int_gh)]:
> # Solving the boundary conditions for C1, C2,C3
  bclhs:=map(eval,subs(hsoln0,theta=0,evalm(derhs))):
  bcrhs:=matrix(1,1,[map(collect,simplify(evalm(subs(simpres,x_cm_ce,
         evalm(lin)))+F2_x_ce[1,1]),[u1,u2])]):
  consts:=[C1,C2,C3]:
  bceq:=subs(hsoln0,evalm(bclhs-bcrhs)):
  bc1:=collect(coeff(coeff(bceq[1,1],u1,2),u2,0),consts):
  bc2:=collect(coeff(coeff(bceq[1,1],u1,1),u2,1),consts):
  bc3:=collect(coeff(coeff(bceq[1,1],u1,0),u2,2),consts):
  bcs:={bc1,bc2,bc3}:
  consts:=convert(consts,set):
  Csoln:=solve(bcs,consts):
> # Determine the nonlinear terms of ODE for u(t) on the CM
  # ODE_nonlin = Psi(0) F(Phi(theta) u + h(theta,u)), F=F2+F3
  F2a:=gamma0*tau*(u1*cos(omega*theta)+u2*sin(omega*theta)+h)^2:
  F2b:=subs(hsoln,F2a):
  F2c:=combine(F2b):
  F2:=simplify(subs(cos(omega*theta)=C(omega),sin(omega*theta)=-S(omega),
      cos(2*omega*theta)=C_2om(omega),sin(2*omega*theta)=-S_2om(omega),
      cos(3*omega*theta)=C_3om(omega),sin(3*omega*theta)=-S_3om(omega),F2c)):
  F3a:=delta*tau*(u1*cos(omega*theta)+u2*sin(omega*theta)+h)^3:
  F3b:=subs(hsoln,F3a):
  F3c:=combine(F3b):
  F3:=simplify(subs(cos(omega*theta)=C(omega),sin(omega*theta)=-S(omega),
     cos(2*omega*theta)=C_2om(omega),sin(2*omega*theta)=-S_2om(omega),
     cos(3*omega*theta)=C_3om(omega),sin(3*omega*theta)=-S_3om(omega),
     cos(4*omega*theta)=C_4om(omega),sin(4*omega*theta)=-S_4om(omega),
```

```
     cos(5*omega*theta)=C_5om(omega),sin(5*omega*theta)=-S_5om(omega),
     F3c)):
> # Define the nonlinear part of the ODE
  nonlin:=matrix([[F2+F3]]):
  ODE_nonlin:=multiply(Psi0,nonlin):
> # Get quadratic and cubic terms for evaluation of normal form
  # quad contains the coefficients of the quadratic terms of ODE_nonlin
  quad:=array(1..2,1..3):
  quad[1,1]:=coeff(coeff(ODE_nonlin[1,1],u1,2),u2,0):
  quad[1,2]:=coeff(coeff(ODE_nonlin[1,1],u1,1),u2,1):
  quad[1,3]:=coeff(coeff(ODE_nonlin[1,1],u1,0),u2,2):
  quad[2,1]:=coeff(coeff(ODE_nonlin[2,1],u1,2),u2,0):
  quad[2,2]:=coeff(coeff(ODE_nonlin[2,1],u1,1),u2,1):
  quad[2,3]:=coeff(coeff(ODE_nonlin[2,1],u1,0),u2,2):
> # cub contains the coefficients of the necessary cubic terms
  # of ODE_nonlin; we only get those terms we need to evaluate
  # the criticality of the Hopf bifurcation
  cub:=array(1..2,1..4):
  cub[1,1]:=coeff(coeff(ODE_nonlin[1,1],u1,3),u2,0):
  cub[1,3]:=coeff(coeff(ODE_nonlin[1,1],u1,1),u2,2):
  cub[2,2]:=coeff(coeff(ODE_nonlin[2,1],u1,2),u2,1):
  cub[2,4]:=coeff(coeff(ODE_nonlin[2,1],u1,0),u2,3):
> # Find the cubic coefficient that determines the criticality
  # of the Hopf bifurcation (Guckenheimer and Holmes p. 152)
  a:=collect(simplify(1/8*(3*cub[1,1]+cub[1,3]+cub[2,2]+3*cub[2,4]
    -1/omega*(quad[1,2]*(quad[1,1]+quad[1,3])-quad[2,2]*(quad[2,1]
    +quad[2,3])-2*quad[1,1]*quad[2,1]+2*quad[1,3]*quad[2,3]))),
    [Psi0[1,1],Psi0[2,1]],distributed,factor):
  a_final:=subs(simpres,Csoln,Psi0_vals,a):
```

Bibliography

[1] M. Adimy, F. Crauste, and S. Ruan. A mathematical study of the hematopoiesis process with applications to chronic myelogenous leukemia. *SIAM J. Appl. Math.*, 65(4):1328–1352, 2005. 16, 49

[2] M. Adimy, F. Crauste, and S. Ruan. Stability and Hopf bifurcation in a mathematical model of pluripotent stem cell dynamics. *Nonlin. Anal.: Real World Appl.*, 6:651–670, 2005. 66

[3] J. Arino and P. van den Driessche. Time delays in epidemic models: Modeling and numerical considerations. In M.L. Hbid O.Arino and E. Ait Dads, editors, *Delay Differential Equations and Applications*, chapter 13, pages 539–558. Springer, Dordrecht, The Netherlands, 2006. 12

[4] F.M. Atay. Delayed feedback control near Hopf bifurcation. *DCDS*, 1:197–205, 2008. 14, 15, 108

[5] J. Bélair, S.A. Campbell, and P. van den Driessche. Frustration, stability, and delay-induced oscillations in a neural network model. *SIAM J. Appl. Math.*, 56(1). 12

[6] J. Bélair and M.C. Mackey. Consumer memory and price fluctuations in commodity markets: An integrodifferential model. *J. Dyn. Diff. Eqs.*, 1(3):299–325, 1989. 16

[7] S. Bernard, J. Bélair, and M.C. Mackey. Sufficient conditions for stability of linear differential equations with distributed delay. *DCDS*, 1B:233–256, 2001. 14, 15, 63, 108, 163

[8] F. Brauer and C. Castillo-Chávez. *Mathematical Models in Population Biology and Epidemiology*. Springer, New York, 2001. 12

[9] S.A. Campbell. Calculating centre manifolds for delay differential equations using Maple. In B. Balachandran, T. Kalmár-Nagy, and D.E. Gilsinn, editors, *Delay Differential Equations: Recent Advances and New Directions*. Springer-Verlag, New York, 2009. 135, 168

[10] S.A. Campbell and R. Jessop. Approximating the stability region for a differential equation with a distributed delay. *Math. Model. Nat. Phenom.*, 4(2):1–27, 2009, Copyright EDP Sciences, reproduced with permission. 46

[11] S.A. Campbell, Y. Yuan, and S.D. Bungay. Equivariant Hopf bifurcation in a ring of identical cells with delayed coupling. *Nonlin.*, 18:2827–2846, 2005. 12

[12] Y. Chen. Global stability of neural networks with distributed delays. *Neur. Net.*, 15:867–871, 2002. 18

[13] R.V. Churchill and J.W. Brown. *Complex Variables and Applications*. McGraw-Hill, New York, 1984. 47

[14] M. Cohen and S. Grossberg. Absolute stability of global pattern formation and parallel memory storage by competitive neural networks. *IEEE Trans. Syst. Man and Cyber.*, 13(5):815–826, 1983. 6

[15] J.M. Cushing. *Integrodifferential Equations and Delay Models in Population Dynamics*, volume 20 of *Lecture Notes in Biomathematics*. Springer-Verlag, Berlin; New York, 1977. 12, 26

[16] Leah Edelstein-Keshet. *Mathematical Models in Biology*. McGraw Hill Ryerson, United States, 1988. 4

[17] B. Ermentrout. *Simulating, Analyzing, and Animating Dynamical Systems: A Guide to XPPAUT for Researchers and Students*. SIAM, Philadelphia, 2002. 110, 152

[18] T. Faria and L. Magalhães. Normal forms for retarded functiona differential equations with parameters and applications to Bogdanov-Takens singularity. *J. Diff. Eqs.*, 122:201–224, 1995. 128

[19] T. Faria and L. Magalhães. Normal forms for retarded functiona differential equations with parameters and applications to Hopf bifurcation. *J. Diff. Eqs.*, 122:181–200, 1995. 128

[20] T. Faria and J.J. Oliveira. Local and global stability for Lotka-Volterra systems with distributed delays and instantaneous negative feedbacks. *J. Diff. Eqs.*, 244:1049–1079, 2008. 14, 17

[21] K. Gopalsamy. *Stability and oscillations in delay differential equations of population dynamics*. Kluwer, Dordrecht, 1992. 12

[22] K. Gopalsamy and X.-Z. He. Stability in asymmetric Hopfield nets with transmission delays. *Physica D*, 76:344–358, 1994. 1, 6, 11, 17, 19, 165

[23] K. Gopalsamy and I. Leung. Delay induced periodicity in a neural netlet of excitation and inhibition. *Physica D*, 89:394–426, 1996. 12

[24] F. Grégorie-Lacoste. *Stabilité d'un réseau de neurones à délai distribué modélisant la mémoire spatiale*. Master's Thesis, Université de Montréal, 2006. 14, 18, 108

[25] J. Guckenheimer and P.J. Holmes. *Nonlinear Oscillations, Dynamical Systems and Bifurcations of Vector Fields*. Springer-Verlag, New York, 1983. 141, 147, 150, 151

[26] J.K. Hale and S.M. Lunel. *Introduction to Functional Differential Equations*. Springer-Verlag, New York, 1993. 10, 22, 29, 125, 127, 131, 136

[27] B.D. Hassard. *Theory and Applications of Hopf Bifurcation*, volume 41 of *London Mathematical Society Lecture Note Series*. Cambridge University Press, Cambridge, 1981. 130

[28] S. Haykin. *Neural Networks: A Comprehensive Fundation*. Macmillan College Publishing Company, New York, 1994. 1, 6

[29] Y. Hino, S. Murakami, and T. Naito. *Functional differential equations with infinite delay*. Springer-Verlag, Berlin, 1991. 29, 127, 128, 129, 130

[30] A.L. Hodgkin and A.F. Huxley. A quantitative description of membrane current and its application to conduction and excitation in nerve. *J. Physiol.*, 117:500–544, 1952. 2, 4

[31] R.V. Hogg and A.T. Craig. *Introduction to mathematical statistics*. Prentice Hall, United States, 1995. 24, 30

[32] J.J. Hopfield. Neural networks and physical systems with emergent collective computational abilities. *Proc. Natl. Acad. Sci. Biophys.*, 79:2554–2558, 1982. 1

[33] J.J. Hopfield. Neurons with graded response have collective computational properties like those of two-state neurons. *Proc. Natl. Acad. Sci. Biophys.*, 81:3088–3092, 1984. 1, 6, 9

[34] R.A. Horn and C. R. Johnson. *Matrix Analysis*. Cambridge University Press, Cambridge, 1985. 88, 89, 165

[35] R. Jessop and S.A. Campbell. Approximating the stability region of a neural network with a general distribution of delays. *Neur. Net.*, 23:1187–1201, 2010. 86

[36] V.K. Jirsa and M. Ding. Will a large complex system with delays be stable? *Phys. Rev. Lett.*, 93:070602, 2004. 14, 15, 108

[37] C. Jordan. *Calculus of Finite Differences*. AMS Chelsea Publishing, New Jersey, 1965. 32

[38] C. Koch. *Biophysics of Computation: Information Processing in Single Neurons*. Oxford University Press, New York, 1999. 5, 9

[39] C. Koch and I. Segev, editors. *Methods in Neuronal Modeling: From Ions to Networks*. MIT Press, Cambridge, MA, second edition, 1998. 5

[40] V.B. Kolmanovskii and A.D. Myshkis. *Introduction to the Theory and Applications of Functional Differential Equations*. Kluwer Academic Publishers, Dordrecht, The Netherlands, 1999. 23

[41] V.B. Kolmanovskii and V.R. Nosov. *Stability of functional differential equations*, volume 180 of *Mathematics in Science and Engineering*. Academic Press, London, England, 1986. 102

[42] Y. Kuang. *Delay differential equations: with applications in population dynamics*, volume 191 of *Mathematics in Science and Engineering*. Academic Press, New York, 1993. 12

[43] X. Liao, K.-W. Wong, and Z. Wu. Bifurcation analysis on a two-neuron system with distributed delays. *Physica D*, 149:123–141, 2001. 17, 127

[44] X. Liao, K.-W. Wong, and Z. Wu. Hopf bifurcation and stability of periodic solutions for van der Pol equation with distributed delay. *Nonlin. Dynam.*, 149:23–44, 2001. 127

[45] N. MacDonald. *Time lags in biological models*, volume 27 of *Lecture notes in biomathematics*. Springer-Verlag, Berlin; New York, 1978. 29, 42

[46] N. MacDonald. *Biological Delay Systems: Linear Stability Theory*. Cambridge University Press, Cambridge, 1989. 13, 16, 42, 108

[47] C.M. Marcus and R.M. Westervelt. Stability of analog neural networks with delay. *Phys. Rev. A*, 39(1):347–359, 1989. 1, 6, 10, 107, 108

[48] J.E. Marsden and M.J. Hoffman. *Basic Complex Analysis*. W.H. Freeman and Company, New York, NY, 1999. 55

[49] R.K. Miller and A.N. Michel, editors. *Ordinary Differential Equations*. Academic Press, New York, 1982. 8

[50] C.L. Nikias and A.P. Petropulu. *Higher-order Spectra Analysis*. PTR Prentice Hall, New Jersey, 1993. 30, 31

[51] J.P.J. Pinel. *Biopsychology*. Allyn and Bacon, Pearson Education Company, Needham Heights, 2000. 2

[52] E. B. Saff R. K. Nagle and A. D. Snider. *Fundamentals of differential equations and boundary value problems*. Pearson Addison Wesley, Boston, MA, 2008. 28, 29

[53] S. Ruan. Delay differential equations for single species dynamics. In M.L. Hbid O.Arino and E. Ait Dads, editors, *Delay Differential Equations and Applications*, chapter 11, pages 477–515. Springer, Dordrecht, The Netherlands, 2006. 14, 53

[54] S. Ruan and R.S. Filfil. Dynamics of a two-neuron system with discrete and distributed delays. *Physica D*, 191:323–342, 2004. 17, 127

[55] S. Ruan and G.S.K. Wolkowicz. Bifurcation analysis of a chemostat model with a distributed delay. *J. Math. Anal. Appl.*, 204:786–812, 1996. 127

[56] H.W. Stech. Hopf bifurcation calculations for functional differential equations. *J. Math. Anal. Appl.*, 109:472–491, 1985. 16, 127

[57] G. Stépán. *Retarded Dynamical Systems: Stability and Characteristic Functions*, volume 210 of *Pitman Research Notes in Mathematics*. Longman Group, Essex, 1989. 102

[58] A. Thiel, H. Schwegler, and C.W. Eurich. Complex dynamics is abolished in delay recurrent systems with distributed feedback times. *Complexity*, 8(1):102–108, 2003. 13

[59] W. Wichert, A. Wunderlin, A. Pelster, M. Oliver, and J. Groslambert. Delay induced instabilities in nonlinear feedback systems. *Phys. Rev. E*, 49:203–219, 1994. 128

[60] G.S.K. Wolkowicz, H. Xia, and S. Ruan. Competition in the chemostat: A distributed delay model and its global asymptotic behaviour. *SIAM J. Appl. Math.*, 57:1281–1310, 1997. 13

[61] G.S.K. Wolkowicz, H. Xia, and J. Wu. Global dynamics of a chemostat competition model with distributed delay. *J. Math. Biol.*, 38:285–316, 1999. 13

[62] J. Wu. *Introduction to Neural Dynamics and Signal Transmission Delay*. Series in Nonlinear Analysis and Applications. Walter de Gruyter, Berlin, 2001. 1, 2, 5

[63] P. Yan. Separate roles of the latent and infectious periods in shaping the relation between the basic reproduction number and the intrinsic growth rate of infectious disease outbreaks. *J. Theoret. Biol.*, 251:238–252, 2008. 42

[64] Y. Yuan and J. Bélair. Stability and Hopf bifurcation analysis for functional differential equations with distributed delay. *SIAM J. Appl. Dyn. Syst.*, 10(2):551–581, 2011. 14, 16, 108, 127